RESPONSE OF UNSATURATED SILTY SAND OVER A WIDER RANGE OF SUCTION STATES USING A NOVEL DOUBLE-WALLED TRIAXIAL TESTING SYSTEM

by

UJWALKUMAR DASHRATH PATIL

Presented to the Faculty of the Graduate School of

The University of Texas at Arlington

in Partial Fulfillment of the Requirements

for the Degree of

DOCTOR OF PHILOSOPHY

THE UNIVERSITY OF TEXAS AT ARLINGTON

August 2014

This work is dedicated to my parents and whole family

Acknowledgements

First and foremost, I would like to give thanks and praise to the Almighty God for giving me good mental and physical health and strength to pass through all the hurdles encountered during my dissertation work. Without his grace and blessings, this is nothing.

I would like to express my sincere gratitude to my advisor, Dr. Anand J. Puppala, for providing me with excellent facilities for conducting research, for his caring nature, invaluable remarks, motivation, and, wholehearted encouragements right from start and through the conclusion of this dissertation. His mentorship and constructive advice on my research, as well as on my career, has been priceless. I couldn't have completed my dissertation without his support, patience and guidance.

My appreciation also goes to my co-advisor, Dr. Laureano R. Hoyos, for his valuable lessons, advice and guidance during course work, the writing of research papers and in finalizing the dissertation. His special knowledge and interest in the area of unsaturated soil mechanics has been inspirational.

Furthermore, I would like to thank my committee members, Dr. Chien-Pai Han, Dr. Shih-Ho (Simon) Chao and Dr. Xinbao Yu, for their valuable advice, insightful comments and careful review of this dissertation. I also take this opportunity to thank all the staff members, especially Mrs. Ginny Bowers, all my professors from the Civil Engineering Department, and everyone who has supported this dissertation work. I would like to extend my appreciation to all my colleagues from the geotechnical and structural engineering research group for their help, friendship and support of each other during my studies at UT Arlington. The work described in this dissertation was funded by the National Science Foundation's grant # 1039356. Their financial support is gratefully acknowledged.

Finally, I would like to thank my loving parents, brother, sister-in-law, Om, Jai, and Jagdish for their selfless love, care and understanding. It is needless to say that without their love and blessings nothing can be truly said to be accomplished.

July 15, 2014

Abstract

RESPONSE OF UNSATURATED SILTY SAND OVER A WIDER RANGE OF SUCTION STATES USING A NOVEL DOUBLE-WALLED TRIAXIAL TESTING SYSTEM

Ujwalkumar D. Patil, PhD

The University of Texas at Arlington, 2014

Supervising Professor: Anand J. Puppala

Co-Supervising Professor: Laureano R. Hoyos

In recent decades, the state-of-the-art of our understanding of unsaturated soil performance has been considerably enhanced by the incorporation of novel and advanced features into the conventional testing devices such as direct shear device, ring shear device, triaxial device and true triaxial device. The novel suction-controlled triaxial system used in this research is fully automated and has enhanced features such as volume change device and double-walled cell to monitor the volume change accurately during all the stages of the unsaturated triaxial test.

Despite their sophistication, such devices can help in testing mechanical behavior of unsaturated soils only up to the matric suction (*s*) value of 1500 kPa (limitation in using axis-translation technique to control matric suction). There is limited experimental evidence of unsaturated soil response over a wider range of suction. This research was motivated by the need to investigate the influence of a wide range of soil suctions on the shear strength, as well as volume change behavior, of compacted silty sands.

A comprehensive series of drained (constant-suction) conventional triaxial compression (CTC) tests was conducted on compacted, 2.8 in (71.12 mm) diameter and

5.6 in (142.24 mm) height cylindrical specimens of silty sand (SM) under constant suction states. The specimens were statically compacted. Target matric suction levels up to 750 kPa were induced and kept constant during testing using the axis-translation technique. The specimens were consolidated at constant suction, prior to shearing, at three effective confining pressures: $\sigma_3 - u_a$ = 100, 200 and 300 kPa.

Another series of CTC drained tests was conducted in which high total suction of a magnitude of 20 MPa and 300 MPa was imposed and controlled, using automatic computer-controlled relative humidity apparatus (RH-equipment). Higher suction states (i.e. *s* = 20 MPa and 300 MPa) were imposed, using separate auto-relative humidity equipment attached with the developed novel Triaxial setup. The efficacy of using auto-RH equipment that uses the vapor equilibrium technique in combination with the triaxial test equipment to induce and control the high total suction was investigated. The effect of suction on the stiffness of the soil was indirectly monitored via stress-strain curves.

The specimens had an over-consolidated stress history, prior to shearing. An experimental investigation revealed sufficient evidence that the mechanical response of such unsaturated soils during shear was associated with stress-induced dilatancy and post-peak softening. On the other hand, the volumetric behavior was associated with the initial contraction, followed by dilation. Such responses are typical and have not been investigated adequately through experiments. Nor have they been extensively incorporated into soil modeling.

The popular models, such as the Barcelona basic model (BBM) and the Cambridge model, are efficient in simulating the shear-induced volumetric compressive behavior, as well as the strain-induced hardening type response that are typical of loose soils with normally consolidated to slightly over consolidated stress history. Experimental

results were used to calibrate and then validate the elasto-plastic, critical state-based constitutive framework, namely, the Barcelona basic model (Alonso et al., 1990).

Finally, the results from suction-controlled tests under axisymmetric conditions ($\sigma_2 = \sigma_3$) were used for a thorough calibration of the elasto-plastic, critical state-based frameworks previously postulated by the Barcelona basic model. Results from the suction-controlled conventional triaxial compression (CTC) tests were used for the validation of this model in predicting stress-strain and volume change response of compacted silty sand under 50, 250, 500 and 750 kPa of matric suction. In addition, the inability/limitation of BBM in continuous prediction of stress-strain response (i.e. the post-peak strain-induced softening) as well as its inability to link it with the corresponding volumetric response (i.e. the stress-induced dilatancy) during shear is discussed.

Table of Contents

List of Illustrations

List of Tables

Chapter 1

Introduction

1.1 Background

Soils above the ground water table are in an unsaturated state. Unsaturated soils are encountered all over the world, especially in arid and semi-arid regions (Gulhati and Satija, 1981; Fredlund and Rahardjo, 1993). Extreme environmental temperature fluctuations at the ground surface can greatly affect the degree of saturation in soils that are encountered at shallow depths, and especially on slopes. The depth at which the underground soil becomes completely saturated is referred to as the ground water table. Climatic conditions prevailing near the ground surface control the fluctuations in the location of the ground water table and, hence, the depth of the unsaturated soil zone (Fredlund and Rahardjo, 1993).

A vast majority of geotechnical infrastructure, such as earth dams, levees, natural and man-made slopes, compacted pavement subgrades, earth retaining structures, excavations, footings, and nuclear waste disposal clay liners involve soil materials that remain under unsaturated condition throughout any given year (Estabragh et al., 2004; Gallage and Uchimura, 2006; Sawangsuriya et al., 2008). Characterization of the mechanical response of these materials, such as shear strength and stiffness, plays an important role in the design of such structures. Unsaturated soil behavior is characterized by some typical features that are not observed in saturated soils. The hydro-mechanical response of unsaturated soil is rather complex and its experimental assessment calls for special treatment due to the co-existence and interaction between each of the three different phases: solid (soil particles), liquid (pore water) and gas (pore air) (Bishop et al., 1960).

The strength and deformability response is governed by externally applied loads, soil type/gradation, soil structure/fabric, initial density, water content, and negative pore-water pressure (Estabragh et al., 2004; Russell and Khalili, 2005). As the soil de-saturates from the original saturated condition, air begins partially replacing the water occupying the pore space. The surface tension created between the water and the air contributes to forming a meniscus, thus inducing a pressure difference (suction) between pore water and pore air (Kohgo et al., 1993). The numerical difference between pore air and pore water pressure across the air-water interface is known as matric suction. Increase in matric suction typically causes an increase of effective stress in the soil, culminating in the improvement in strength and moduli properties (Fredlund and Rahardjo, 1985; Rahardjo et al., 1995; Blatz et al., 2002). Consequently, saturation of unsaturated soil medium may result in softening and hence cause major geotechnical failures. Rainfall induced slope failures and landslides are prime examples of these.

The surface tension or capillarity effects dominate the mechanical behavior of unsaturated soils and hence should be given due consideration. The magnitude of such soil suction may vary from few to as large as several thousand kilopascal. Therefore, fundamental behavior of unsaturated soils can be better explained by taking into account suction as an independent variable (Jennings and Burland, 1962; Matyas and Radhakrishna, 1968).

Traditional practice in soil mechanics considers the fully saturated soil condition (voids filled with water) for most analyses and design purposes. Such an approach is rather conservative in the sense that the shear strength of fully saturated soil is lower than that of partially saturated soil for a wide range of suction values, and, as such, is not appealing from an economic point of view. Findings from research with unsaturated soils

during the past decades have highlighted the need for reassessing this traditional methodology (Lu and Likos, 2004).

Clayey soils located on slopes and embankments are typically unsaturated, and these soils can sustain the steep angles when subjected to relatively high matric suctions, which enhance shear strength of the soil (Lu and Likos, 2004; Lu, 2008; Puppala et al., 2009). However, these soils undergo desiccation cracking in high temperature environments. When rainfall infiltrates the desiccated slopes, the soil suction reduces, shear strength decreases and hence shallow slope failures occur.

Loose, collapsible soils in the unsaturated condition are held in a stable state by the presence of matric suction. When water infiltrates this soil, the matric suction is drastically reduced and, as a result, the loose soil fabric becomes unstable and then collapse. Large volume reductions take place quickly, which will cause considerable disruption and damage to the civil infrastructure (Mitchell, 1986; Katti, 2000; Perera et al., 2004).

Expansive soils with high swell-shrink potential induce high distress to infrastructure. It is well known that matric suction in field subsoils, expansive clay buffers used for nuclear waste storage, and bentonite materials, can reach thousands of kPa (close to 100,000 kPa or above, which is well above the current test suctions of 1500 kPa) based on the dry conditions in the soil (Anandarajah and Chen, 1994; Navarro and Alonso, 2000; Perera et al., 2004; Li et al., 2008; Manosuthkij et al., 2008). Such conditions followed by moisture hydration/infiltration in the soil, can lead to considerable volume changes, as well as losses of strength/stiffness properties, which eventually result in distress to civil infrastructures.

1.2 Thesis Research Objectives and Tasks

The brief background given in previous section clearly highlights the critical need for an advanced experimental test device that can be utilized to determine strength and stiffness properties of unsaturated soils at various soil suction conditions, including matric suction and high total suction range, as well as at zero-to-moderate volume changes within the soils. Such reliable property determinations will lead to substantially improved unsaturated soil characterization, which in turn will lead to better design of civil infrastructures on the unsaturated soil environments. The main objective of the present dissertation research work is to characterize the mechanical response of unsaturated silty sand over a wide range of soil suction conditions (up to 300 MPa). This will lead to improved characterization of unsaturated intermediate soils and, thereby, better the design practices of geoinfrastructure made of or resting on such soils.

Collective efforts of a research team at the University of Texas at Arlington were aimed at developing a custom-designed triaxial test setup that combines two techniques that allow for suction-controlled environments under both low-to-moderate matric suction conditions and very high soil suction conditions. The newly developed test setup also the capability of testing large size soil specimens under both static and repeated load environments, featuring internal volume change measurements via diametric measurements. Although beyond the scope of this work, this unit is also designed to accommodate bender elements that can provide stiffness property measurements along with shear strength properties.

With these novel and advanced features, the system will facilitate various research investigations related to characterization of static and dynamic behaviors of unsaturated soils, strength and stiffness properties of expansive soils under varying suctions and select volume change conditions, and evaluation of chemical and

mechanical modifications on unsaturated soil property improvements. All these studies will significantly advance the understanding of unsaturated soils and also improve current design practices on unsaturated soils. The performance of the custom designed test setup was thoroughly checked and then validated for providing repeatable results. This has been the chief motivation for the present research work.

To achieve the main objective stated above, the present research study was divided into four main tasks, as described in the following.

The first task was to set up the above mentioned custom-designed system and demonstrate its proper functioning, operation and testing capabilities, including compatibility of its process control software and data acquisition system.

Second, a comprehensive series of saturated and unsaturated consolidated drained (CD) triaxial tests on statically compacted silty sand specimens was performed. The axis-translation technique was used to impose and control matric suction in the range of 0 to 750 kPa. Three confining pressures were used: 100, 200 and 300 kPa.

Third, a custom-designed relative humidity (RH) chamber, along with an in-house fabricated Plexiglas chamber, was used to assess the soil water characteristic curve (SWCC) of the test soil in the high suction range. The same RH chamber was integrated into the new triaxial testing system and a second series of CD tests, at higher values of total suction (20 MPa and 300 MPa), were performed, under three different confining pressures: 100, 200 and 300 kPa. The efficacy of using the Auto-RH chamber with the unsat-triaxial testing equipment is discussed.

Fourth, the hydro-mechanical response observed from the experimental series performed under controlled matric suction states was used in predicting shear strength response of silty sand at critical state using the most general form of Barcelona Basic Model (BBM). The constitutive equations proposed in the model were calibrated to obtain

the best fitting parameters using test results from a matric suction range, i.e., *s* = 0 to 750 kPa. The experimental results were compared with BBM predictions.

Figure 1.1 presents a flow chart summarizing the research tasks undertaken. The convention used here to designate the specimen is $CD_{x\text{-}y}$ where "CD" denotes the consolidated drained test; "x" represents the net confining pressure $(\sigma_3\text{-}u_a)$, while "y" represents the imposed constant matric suction $(u_a\text{-}u_w)$. Both net confining pressure and matric suction are expressed in kPa. However, suction in high total suction range is expressed in MPa.

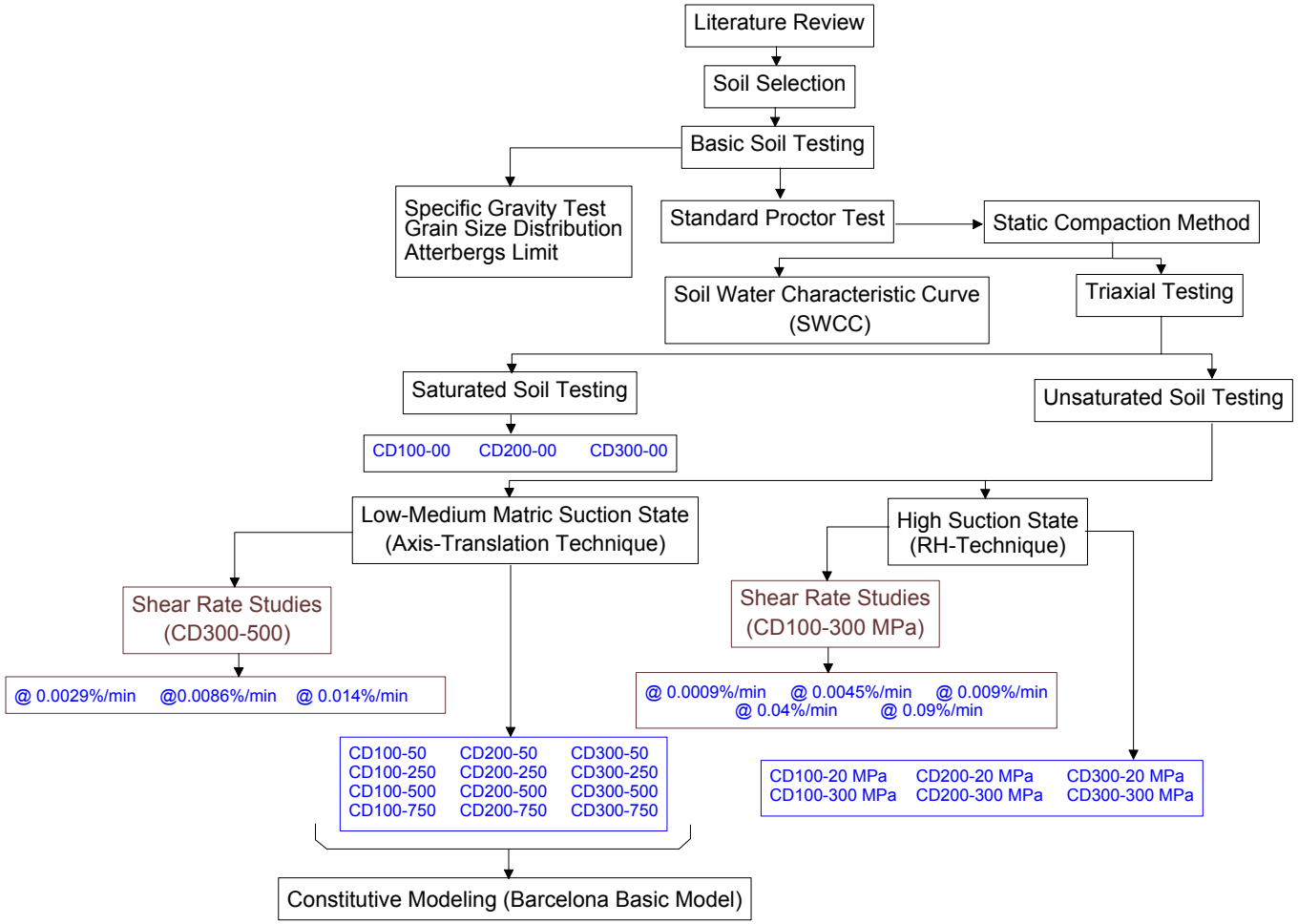

Figure 1.1 Flow chart representing research tasks

1.3 Thesis Organization

This dissertation has been organized into six chapters. A brief summary of each chapter is presented in the following:

Chapter 1 provides an introduction to the typical behavior of partially saturated soils and discusses the importance of developing an advanced triaxial system that allows for testing soils over a wider range of suction states. The primary research objectives, including the main tasks needed to achieve it, are discussed.

Chapter 2 includes an overview of the basic concepts and soil properties related to unsaturated soil mechanics. The review mainly focuses on soil suction, its relationship to gravimetric or volumetric water content, and various direct and indirect methods of assessing soil suction. It is also devoted to summarizing key information about past and recent advances in triaxial testing to determine unsaturated hydro-mechanical response of soils.

Chapter 3 provides a detailed description of basic laboratory tests conducted on the test soil, including mechanical sieve analysis, hydrometer analysis (to classify the soil), standard proctor test (to determine the dry unit weight and optimum moisture condition), selection of method of compaction to obtain identical specimens, and soil water characteristic curve (SWCC). Descriptions of the newly developed system are included, along with details of the methodology followed in performing a first series of drained (suction-controlled) conventional triaxial compression tests (CTC), using the axis-translation technique. Results from a first series of experiments performed to validate the suitability of the double-walled triaxial system to produce repeatable results, the selection of an adequate loading rate, and the effect of matric suction and confining pressure on the rate of dilation of compacted silty sand are also discussed in this chapter.

Chapter 4 describes the main features of the relative humidity (RH) chamber used and adopted to the triaxial system as a part of this research. Included are the details of a second series of tests undertaken in this work, including procedures/protocols followed, to conduct the drained (suction-controlled) conventional triaxial compression tests (CTC) in the high suction range via the RH chamber. This chapter includes all the test results from this experimental program, as well as results from tests performed to validate the dependability of the RH-apparatus in controlling and maintaining the highest total suction (300 MPa). Studies performed to evaluate the appropriate strain rates in the high total suction range are also included. It also discusses the observations made through synthesis of data from both low-to-medium and high suction range.

Chapter 5 includes a brief description of the original critical state-based, elasto-plastic framework proposed by Alonso et al. (1990), known as the Barcelona Basic Model (BBM), for unsaturated soil. The chapter describes the experimental calibration of model parameters and compares the numerical stress-strain predictions of compacted silty sand behavior from BBM, as well as the experimental results.

Chapter 6 summarizes the main conclusions of this research work and presents some recommendations for future experimental and theoretical investigations. The novelty in the experimental technique stemming from this research is discussed in brief.

Chapter 2

Fundamental Concepts and Experimental Techniques for Unsaturated Soil Testing

2.1 Introduction

Ground surface acts as a boundary across which continuous moisture movement occurs due to evaporation (high temperature/hot summers), evapotranspiration (grasses, trees and plants) and precipitation (through rainfall, snowfall or irrigation). Thus, thermal and moisture fluxes occur at ground surface and control fluid flow through the unsaturated soil zone, leading to complex spatial distribution of water within the soil matrix (Fredlund and Rahardjo, 1993; Zhang et al., 2004; Puppala et al., 2012). This poses a growing need for accurate assessment of such moisture fluxes. A net upward moisture flux produces a gradual drying, cracking and desiccation of the soil mass whereas the net downward flux tends to wet a soil mass (Fredlund et al., 1993).

In geotechnical engineering, the zone between the ground surface and the water table is referred to as the unsaturated soil zone and has gained interest due to the presence of negative pore water pressure. Just above the water table lies the zone of the capillary fringe, which is completely saturated but still possesses negative pore water pressure. The rise of water from the water table in the capillary fringe zone depends upon the pore size distribution of soil that gives rise to capillary forces. The smaller the pore size (example clayey soil), the greater is the depth of this zone (several feet), and larger the pore size (granular soils), the lesser is the depth of the capillary fringe (few inches). A more correct term for the entire zone above the water table, including the capillary fringe, is the “vadose zone” (Bouver, 1978; Fredlund et al., 2012).

Figure 2.1 illustrates the typical classification of saturated and unsaturated zones due to variation in the degree of saturation that may result as a consequence of seasonal moisture flux. The voids are fully filled with water below the ground water table,

generating positive pore water pressure. In the unsaturated soil, void spaces are filled with air and water, and the pore water pressure becomes negative relative to pore-air pressure. As the soil becomes drier above the capillary fringe, the pore water pressure becomes more negative. Tension applied by most plants to pore water can be as high as 1000-2000 kPa (Taylor and Ashcroft, 1972; Fredlund et al., 2012), and can even exceed lateral confining pressure in the soil, thus leading to the secondary mode of desaturation, i.e. cracking. Thus, the entire soil deposit is continuously subjected to shrinking and swelling due to influencing environmental changes in the proximity of the ground surface.

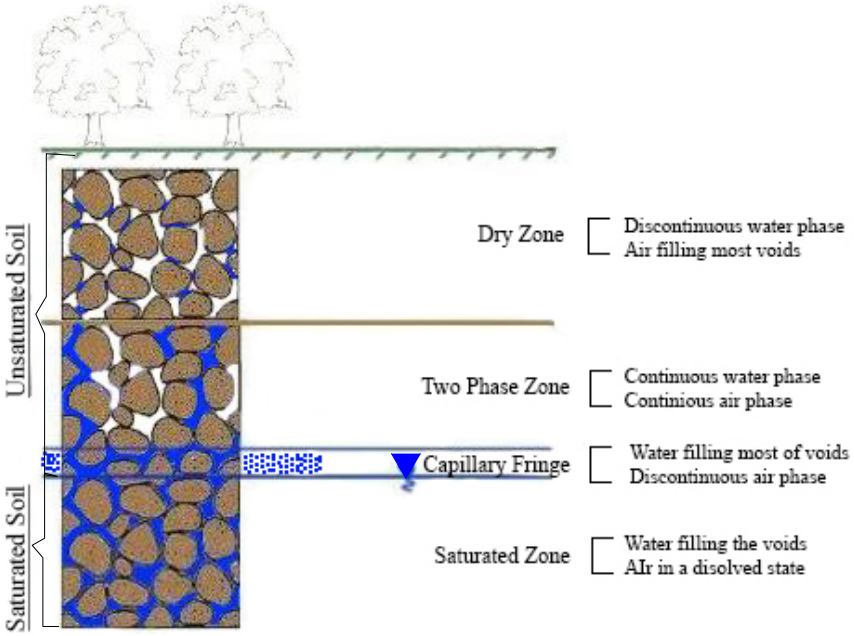

Figure 2.1 Saturated and unsaturated soil classification based on moisture flux

2.2 Unsaturated Soils

Knowledge of the typical properties of unsaturated soil forms the basis for the solution of problems related to earth pressures, slope stability and bearing capacity of foundation, to name a few. Saturated soils are considered to be a two-phase system, solids and water, while unsaturated soils are considered to be a three-phase system,

solids, water and air. However, most importantly, an additional fourth phase, i.e. the air-water interface or contractile skin, should also be considered (Fredlund and Morgenstern, 1977).

Stress state changes in the contractile skin may alter water content, overall volume and shear strength of unsaturated soil. Hence, according to Fredlund (1993), the contractile skin should be considered as part of the water phase when considering changes in the volume-mass soil properties. However, due to its ability to exert tensile pull and behave like an elastic membrane with a definite boundary surface, the contractile skin must be seen as an independent phase when describing the stress state and phenomenological behavior of unsaturated soil (Fredlund et al., 2012).

An unsaturated soil should be viewed as having two phases that flow under the influence of a stress gradient (i.e., air and water) and two phases that come to equilibrium under the impact of that stress gradient (i.e., structural arrangement of soil particles and the contractile skin forming a partition between the fluid phases) (Fredlund and Rahardjo, 1993a).

2.3 Soil Suction

Unsaturated soils possess a fundamental physical property, called soil suction, that describes the potential with which a given soil at given water content can adsorb and retain pore water (Likos and Lu, 2002). It represents a negative pressure within the void space between soil particles, which increases with decreasing moisture content and is a function of the soil particle size, shape and chemistry (Rainwater et al., 2010). The total suction is the sum of matric ($u_a - u_w$, *or* Ψ_m) and osmotic suction (π).

In unsaturated soil mechanics, the matric suction is an important parameter that governs the state of stress and represents the difference between the free energy of the water in the soil and that of pure water in a free surface condition (Sawangsuriya et al.,

2008). Matric suction is the result of adsorptive and capillary force existing in the soil matrix, whereas osmotic suction results from salt or contaminants present in the soil pore water (Krahn and Fredlund, 1972; Lu and Likos, 2004; Malaya and Sreedeep, 2012).

Matric soil suction forms a significant component of total suction in non-plastic cohesionless soils; whereas, osmotic suction may be significant in high plasticity clays having high activity due to its inherent mineralogy or due to dissolved salt concentrations (Blatz et al., 2008). It is a common practice to consider soil suctions below 1500 kPa to be measured as matric suction, and those above as total suction. Soil suction may be expressed in different units, such as kPa, Atm, pF and centibar. Schofield (1935) defined pF as the common logarithm of height in centimeters of the water column that is needed to provide the suction.

Unsaturated soils under field conditions have pore-air pressure that is atmospheric, and set to zero reference, while the pore-water pressure is negative with respect to the atmospheric pressure. This means that the matric suction (u_a - u_w), under a field condition, has positive value. For matric suction to be negative, the pore water pressure must increase to positive values while maintaining the air pressure as a constant, resulting in the saturation of soil and reductions in the matric suction value (Lu and Likos, 2004).

Drying of soil means increasing soil suction (negative pore-water pressure), resulting in a decrease in volume of soil. Such soil shrinkage process, due to imposed suction, may be referred to as suction consolidation (Kohgo et al., 1993). If the soil is dried from its initial completely saturated condition, the bulk water will be first replaced by air. As the suction is further increased, the more bulk water that is removed, the greater the amount of meniscus water associated with the soil at grain point contact will be. The

larger the pore size, the smaller is the amount of associated meniscus water, and vice versa (Fredlund and Rahardjo, 1993).

Terzaghi's effective stress principle (for saturated soils) can be applied to analyze the strength and deformation behavior of soils having suction states below air entry suction. However, the changes in the water phase of partially saturated soils (both granular as well as clayey) beyond air entry suction can alter the soil response in a non-linear fashion, which is not accounted for by Terzaghi's effective stress principle, thus making it necessary to incorporate the suction as an independent variable (Jennings and Burland, 1962).

2.4 Capillary Phenomenon

Capillary phenomenon in soil refers to the movement of water from a water table source into the continuous void spaces due to a combination of cohesion, adhesion and surface tension forces created between water molecules and surrounding soil particles. Since the capillary zone lies close to the water table source in real soils, it can be considered to be associated only with the matric suction component. The amount of rise of water depends upon the pore diameter of soil in the capillary zone. As a general rule, the finer the soil particle, the smaller is the pore diameter resulting in higher capillary rise.

Capillary tube models are a good way to understand the physical interpretation of the capillary aspect and can be further extended to estimate the air entry suction in soils (Fredlund and Rahardjo, 1993; Lu and Likos, 2003). In real soils, the air-water interface is in contact with soil solids and subjected to the pressure difference between the air and water phases, $u_a - u_w$, is very often called matric suction, with air pressure (atmospheric) being greater than pore water pressure. As a result, this curved and concave contractile membrane possesses a property called surface tension (Lu and Likos, 2003).

The radius of curvature of such meniscus and surface tension forces governs the mechanism of matric suction equilibrium. As the soil dries (i.e. matric suction increases), the radius of meniscus decreases, further exerting more pull on the adjoining soil particles and creating more normal forces at grain point contacts. Such an additional resulting stress is often referred to as suction stress. In real soils, the relationship between capillarity and suction forces becomes complex, making it difficult to analyze the capillarity mechanism without assumptions pertaining to particle shape and size, geometry of pores. Hence, the reason that the radii of curvature of the air-water interface is under study (Lu and Likos, 2003).

2.5 Soil-Water Characteristic Curves

Soil water characteristic curves (SWCC) or soil water retention curves (SWRC) describe the relationship between measured soil suction (either total suction, Ψ_t or matric suction, Ψ_m) and the corresponding amount of water present in the soil. This water can be expressed as gravimetric (w), volumetric (θ) or degree of saturation (S). Numerous properties of unsaturated soils including strength, volume change, permeation of water through the vadose zone, and solute and thermal diffusivity are dependent on the SWCC of soil (Fredlund and Rahardjo, 1993; Vanapalli et al., 1996; Malaya and Sreedeep, 2012).

It is a common practice to consider soil suctions below 1500 kPa to be measured as matric suction and those above as total suction. According to Fredlund and Rahardjo (1993), total soil suction is the amount of energy required to expel a unit volume of water from the unsaturated soil. The measured total soil suction of magnitude slightly less than 1000,000 kPa has been experimentally supported for a variety of soils (Fredlund and Xing, 1994; Vanapalli et al., 1999). This value is also supported by thermodynamic considerations (Richards, 1965).

Thus, a wide range of soil suction states can exist, depending upon soil type. The SWCC curve typically takes a sigmoidal shape relationship when suction is plotted with a logarithmic scale, as shown in Figure 2.2. The shape largely depends upon the pore size distribution and compressibility of the soil in relation to the suction that is influenced by the initial water content, soil structure, mineralogy, and the stress history (Vanapalli et al., 1999; Marinho, 2005).

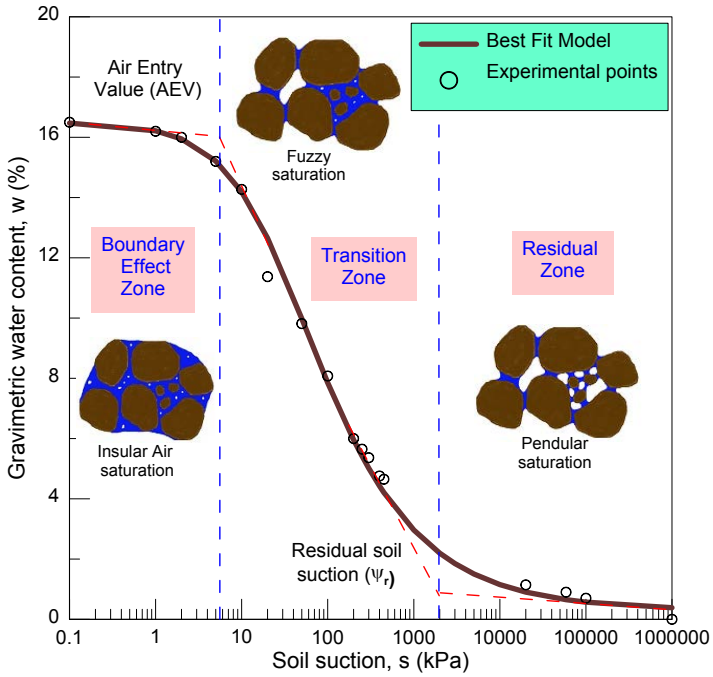

Figure 2.2 Soil water characteristic curves for the entire range of soil suction

Irrespective of the soil type, soil suction in fully saturated soil can be considered zero while for unsaturated soil in dry condition approximately 1000,000 kPa. While drying or wetting, the soil moves between these limiting conditions, and the distribution of the soil-water-air interphase relationship changes as stress state changes, thereby influencing the response (mechanical or hydraulic) of unsaturated soil (Vanapalli et al., 1998). Thus, the soil-water characteristic curve provides a conceptual and interpretative tool to better understand behavior of unsaturated soil (Vanapalli and Fredlund, 2000).

Most of the researchers have used soil-water characteristic curves as an interpretative tool, along with the saturated shear strength parameters, c' and ϕ', to predict the shear strength variation for an unsaturated soil (Vanapalli et al., 1996; Fredlund et al., 1996; Oberg and Sallfors, 1997; Khalili and Khabbaz, 1998; Bao et al., 1998). Soil water characteristic curves are sensitive to changes in compaction energy applied, as compared to the variation in water content. In general, the SWCC curve tends to shift to the right, as a result of the increase in compaction effort for the same type of soil (Miller et al., 2002).

2.5.1 Air-Entry Value of Soils (AEV)

Air-entry suction or bubbling pressure (ψ_b) refers to the value of matric suction at or beyond which air starts receding into the pore space thereby replacing the pore water. During de-saturation, water from large size pores will be first emptied. As shown in Figure 2.2, AEV marks the distinction between the boundary effect zone and the transition zone. The permeability of unsaturated soil in this zone is dependent upon the movement of the liquid phase through interconnected voids.

Soil with matric suction below air entry value may be treated as fully saturated soil. As suction is further increased beyond its air entry value, the water content reduces dramatically up to residual suction, causing greater influence on the mechanical and hydraulic response of soil. The air entry value is estimated as the value of suction corresponding to a point on SWCC that can be found by the intersection of the extension of the constant slope portion of the SWCC and the line on the portion of the curve for suction at 100% saturation, as shown in Figure 2.2.

The compaction energy applied during the preparation of the specimen also affects the air entry value of the specimen (Marinho and Stuermer, 2000; Leong and Rahardjo, 2002). The increase in compaction effort applied causes closer/denser packing

of the soil particles, causing a reduction in pore size. This increases the water retention capacity of the soil and, hence, increases in the air entry value.

2.5.2 Residual Soil Suction

Residual soil suction is the boundary between the transition zone and the residual zone, as shown in Figure 2.2. In the residual zone, a large increase in suction is associated with relatively small changes in water content. According to Vanapalli et al. (1998), residual soil suction is defined as the suction corresponding to water content (residual water content) on the soil-water characteristic curve at which the soil suction phase goes from being held primarily by the capillary action force to being held in the soil primarily by adsorption force.

The water phase becomes discontinuous and isolated with thin films of water surrounding the soil particles and air, making it difficult to remove water from the soil with further increase in suction. The permeability will, therefore, be influenced by the combined flow of liquid and vapor phase. Identifying residual suction along with air entry suction is necessary to obtain the best fitting parameters that can be used in numerical models for prediction of the coefficient of permeability (Brooks and Corey, 1964; van Genutchen, 1980) and shear strength (Fredlund et al., 1996; Vanapalli et al., 1996).

Wilting point of most of the plants may be considered as residual suction (Van Genutchen, 1980). If the complete soil-water characteristic curve is available, then it can be graphically obtained as suction, corresponding to a point located by the intersection of the tangent line through the inflection point, on the central straight part of the soil-water characteristic curve, and the line extending from 1000 MPa tangent to the final portion of the curve (Vanapalli and Fredlund, 2000). In some cases, such as clean sandy soils, the strength of soil may decrease beyond residual suction.

2.5.3 Possible Pore Water States in Unsaturated Soils

It is a conventional and conservative approach to consider soil voids as a single fluid phase (either air or water), especially with well-established knowledge that the shear strength of fully saturated soils is lower than its unsaturated counterpart.

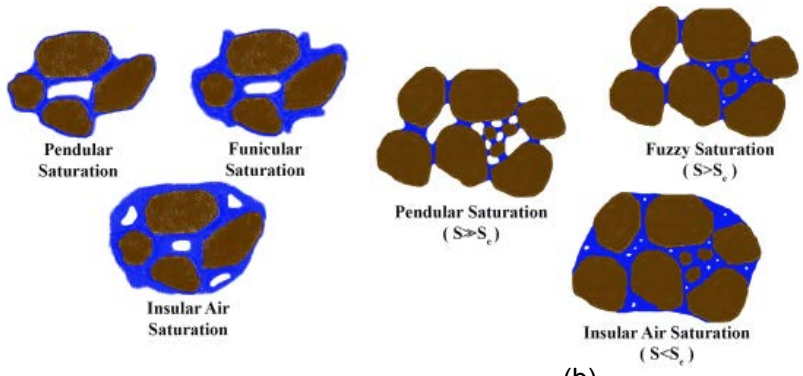

Figure 2.3 Possible pore water saturation states in saturated and unsaturated soils a) Theoretical possible water saturation states and b) Possible saturation conditions in real soils (modified from Kohgo et al., 1993)

Bear (1979) explained the possible pore water states in soil. At a very low saturation, also referred to as pendular saturation, as shown in Figure 2.3a, water is retained in meniscus created around the grain point contact without forming a continuous water phase. As the water saturation increases, a continuous water phase is formed, and the resulting saturation condition is called funicular saturation (Figure 2.3a), where both the water and air phases are continuous. Suction forces, dominated by capillarity effects in pendular and funicular saturation phases, greatly affect the shear induced mechanical response.

With additional increase in saturation, the pore air loses its continuity, and at high degree of saturation, some part of the air will remain as air bubbles surrounded by water. Such a condition is referred to as insular (occluded) air saturation. However, Kohgo et al.

(1993) suggests that real soils have non-uniform pore sizes that influence the retentive situations of pore water and, hence, all the three possible saturation conditions may co-exist (such a condition is also called fuzzy saturation) except at very extremely high suctions and suction states below air entry suction (Figure 2.3b).

In addition to the effective stresses that are transferred through the grain-to-grain contact, certain physicochemical forces exist, such as van der Waals attraction, the electrical double-layer repulsion, and the net attraction arising from the chemical cementation at the grain contacts. These are influenced by mineralogy, surface area, and pore-water chemistry (Lu and Likos, 2006). Van der Waals forces are additive in nature and result from short-range electromagnetic field interactions between adjacent atoms of approaching surfaces that may result in considerable attraction for large molecules. Van der Waals attraction decreases exponentially with an increase in the degree of saturation and increases to its upper bound of about 1,000 kPa at zero saturation (Lu and Likos, 2006).

Cementation between particles results from covalent or ionic bonds formed between the cementing agent and soil particles, and the magnitude of such cohesive forces varies from zero in clean sand to an upper bound of about 300 kPa (Ingles, 1962; Lu and Likos, 2006).

Hydrogen bonding results from dipole-dipole interaction where hydrogen atoms serve as a bridge between two electronegative atoms. These forces are stronger than van der Waals forces but weaker than ionic bonds (Cresser et al., 1993). A strong field of interaction between water and soil particles may result from hydrogen and van der Waal's forces, due to which water molecules are strongly adsorbed, forming a film covering the soil particles (Suzuki, 2000).

Electrical double-layer forces are strong in saturated clay soils, due to a charge deficiency within the soil solid (clay mineral) crystalline lattice, and are essentially absent in coarse-grained soils. They decrease in magnitude with desaturation. These may result in repulsive interparticle stress, with a face-to-face or edge-to-edge arrangement of clay particles, while edge-to-face interparticle interaction may result in small attractive interactions. Van Olphen (1991) reported its magnitude up to 1,000 kPa.

2.5.4 Hydraulic Hysteresis

Drying a soil from full saturation and wetting a soil from its low water content follow two different paths, also known as main branches of retention curves (Fleureau et al., 1993). Such a property is called a hydraulic hysteresis and is primarily due to non-uniform pore size distribution. There are several explanations, such as, the “rain drop effect,” and the “ink-bottle effect.” The rain drop effect is due to the contact angle between the air-water interface and soil particles during the wetting and drying process. The “ink-bottle effect” is due to an increase in local pressure, which is required during wetting when water re-enters narrow channels, resulting in an unstable condition that does not allow the waterfront to further enter the pores until the surrounding pores are completely filled with water (Bear, 1979).

Experimental results have verified such nonbijective relationship between suction and degree of saturation (Sun et al., 2007a; Geiser et al., 2006). Different degrees of saturation at the same matric suction may exist along these two distinct paths. Higher matric suction is required to achieve a similar degree of saturation on the main drying path, as compared to the main wetting path as illustrated in Figure 2.4. They coincide at full saturation and beyond residual suctions.

If the soil undergoes suction reversal along these main paths, it leaves the original main path and follows the “scanning curve” (with slope less than main curves),

joins the other main path and stays on it as long as there is no further suction reversal, as shown in Figure 2.4. Suction reversal along the “scanning curve” reverses the direction of travelling, but does not change the slope (Morvan et al., 2011).

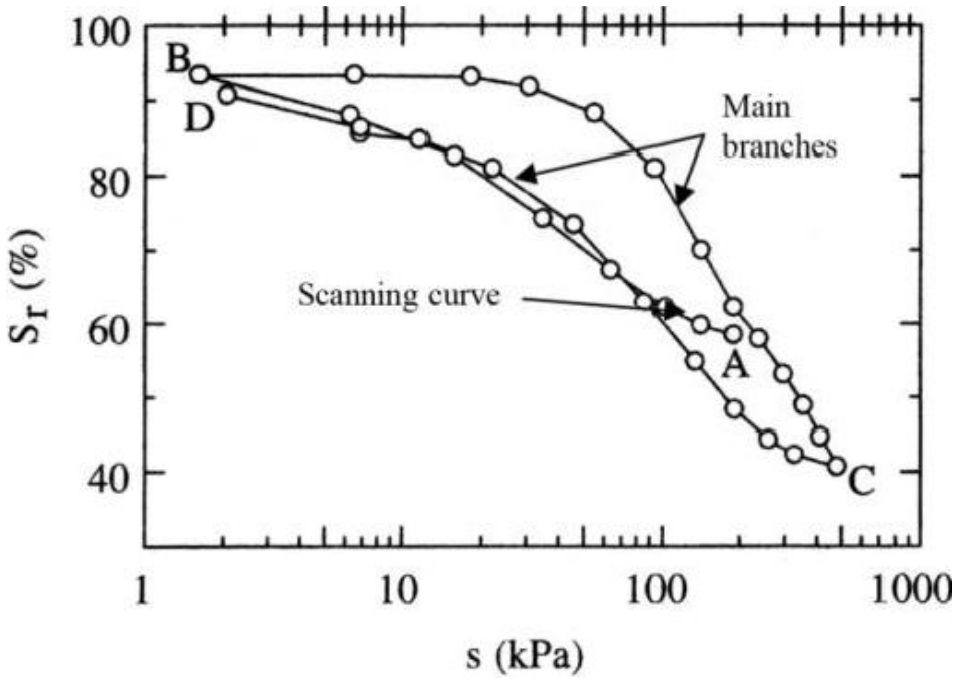

Figure 2.4 Hydraulic hysteresis in unsaturated soils illustrated via experimental drying and wetting path (modified from Sun et al., 2007a; Morvan et al., 2011)

2.6 Suction Measurement Methods

Soil suction can be measured directly or indirectly in the laboratory or field, depending on the range and suction required (Rainwater et al., 2012). Field instrumentation is needed to monitor the moisture/matric suction fluctuations in subsoil to understand how the environment affects the performance of engineering structures built on it (for example pavement) and how they impact soil moisture and suction parameters (Sawangsuriya et al., 2008; Puppala et al., 2012).

Direct measurement of matric suction of soils involves measuring negative pore water pressure and includes tensiometers, null-type pressure plate devices, pressure

membranes, thermocouple psychrometers, hygrometers and suction probes (Fredlund and Rahardjo, 1993).

An indirect method measures a variable other than negative pore-water pressure such as thermal or electrical properties of sensor material in contact with or in close vicinity of the soil.

These properties are then correlated with suction via proper calibration. Such indirect methods include the filter paper method, electrical conductivity sensors and thermal conductivity sensors. Both direct and indirect methods are summarized in the Table 2.1. Actual suction/moisture data obtained from field monitoring over a considerable period of time is of utmost importance because it suggests more appropriate values of suction to be applied and controlled during laboratory tests used to characterize the unsaturated soil.

2.6.1 Filter Paper Technique

The filter paper method was first presented by Gardner (1937) and has been used since then by numerous researchers to measure total as well as matric suction as documented in Table 2.1 (Reference: Fawcett and Collis-George, 1967; McQueen and Miller, 1968; Al-Khafaf and Hanks, 1974; Hamblin, 1981; van der Raat, 1987; Houston et al., 1994; Likos and Lu, 2002; Rainwater et al., 2011; Puppala et al., 2011). Total suction is determined by the non-contact filter paper technique, while matric suction is determined by the contact filter method (Fredlund and Rahardjo, 1993).

In the contact filter method, filters are placed in direct contact with soil specimens that are sealed in a closed environment allowing moisture exchange to take place by capillary and particle surface adsorption forces which are the result of matric suction in specimen, thus indirectly allowing its measurement.

In the non-contact method, filter papers are suspended in the headspace above the soil specimens.

Table 2.1 Direct and indirect methods for measuring total, matric and osmotic suction

Device	Suction Measured	Range (kPa)	Principal Constraints
Tensiometers	Matric	0 to 90	Range is limited by the air-entry value of ceramic. Requires daily maintenance.
Thermistor Psychrometer	Total	100 to 10,000	Poor sensitivity in the low suction range. Frequent re-calibration required.
Transistor psychrometer	Total	200 to 18,000	Accuracy is very user-dependent. Highly effected by temperature changes in the surrounding environment.
Thermocouple psychrometer	Total	100 to 7,500	Affected by temperature fluctuations and gradients. Sensitivity deteriorates with time.
Filter paper (non-contact)	Total	3000 to 100,000	Calibration is sensitive to the equilibrium time.
Filter paper (in-contact)	Matric	Entire range	Automation of the procedure is difficult.
Null type pressure plate (Axis translation technique)	Matric	0-1500	Range of suction is limited by the air-entry value of plate. Long equilibration time for clay.
Thermal conductivity sensors	Matric	0 to ~1500	High failure rate. Fragile ceramic. Long-term problems associated with drift and deterioration with time.
Pore fluid squeezer	Osmotic	Entire range	Used in conjunction with psychrometer or electrical conductivity measurement.
Relative humidity equipment	Total	7000-700,000	Only high suction range possible.

The moisture exchange occurs via a vapor phase until equilibrium is attained and is a function of the pore water relative humidity, thus indirectly measuring both capillary and osmotic suction components that together make total suction (Likos and Lu, 2002).

In both techniques, the water content of the filter paper at equilibrium is theoretically related to the matric/total suction through appropriate calibration curves (Houston et al., 1994). A more detailed procedure is described by Houston et al. (1994) and Likos and Lu (2002).

Table 2.2 Filter paper calibration equations published for Whatman 42 filter paper (from Rainwater et al., 2011)

Researcher	Calibration equation	Moisture content or Suction Range
Fawcett and Collis-George (1967)	$log\psi = 4.777 - 0.0600\ W_{fp}$ $log\psi = 2.271 - 0.0230\ W_{fp}$	$W_{fp} < 43\%$ $W_{fp} > 43\%$
Hamblin (1981)	$log\psi = 8.022 - 3.683\ log\ (W_{fp})$	Less than 3 MPa
Greacen et al. (1987a)	$log\ \psi = 5.327 - 0.0780\ W_{fp}$ $log\ \psi = 2.413 - 0.0135\ W_{fp}$	$W_{fp} < 45.3\%$ $W_{fp} > 45.3\ \%$
Chandler et al. 1992	$log\ \psi = 4.842 - 0.0622\ W_{fp}$	$W_{fp} < 47\ \%$; Matric suction ≥ 80 kPa
Chandler et al. 1992	$log\ \psi = 6.050 - 2.48\ log\ W_{fp}$	$W_{fp} \geq 47\ \%$; Matric suction ≤ 80 kPa
Houston et al. (1994)	$log\ W_{fp} = 3.63 - 0.483\ \psi$	Higher suction range
Likos and Lu (2003)	$\Psi = -0.138\ W_{fp} + 5.48$	Higher suction range
ASTM D5298-03(2007)	$log\ \psi = 5.327 - 0.00779\ W_{fp}$	< 45.3 % ; Total and matric suction
	$log\ \psi = 2.412 - 0.0135\ W_{fp}$	≥ 45.3 % ; Total and matric suction

2.6.1.1 Calibration equations for filter paper technique

Proper calibration of filter paper plays a vital role in the reliability of the method adopted in measuring suction. Some of the types of filter papers used for suction testing include Whatman # 42, Schleicher and Schuell # 589 White Ribbon, and Fisher 9-790A (Likos and Lu, 2002). Salt solutions of different known concentrations can be used to generate and control relative humidity in sealed chambers where filter papers are kept in headspace. The water content of filter paper (at least with 0.0001 g. accuracy) is measured at equilibrium as quickly as possible, and is then correlated to the suction to prepare calibration curves for the entire range of suction.

Such a calibration curve prepared for a porous filter paper is similar to its soil water retention curve (Marinho and Oliveira, 2005). ASTM D5298 provides relationships between concentration and relative humidity for several concentrations of sodium chloride and potassium chloride solutions. Table 2.2 summarizes a few published calibration equations (Rainwater et al., 2011).

2.6.2 Pressure Plate Device

The pressure plate device is made of a steel pressure vessel, with a high-air-entry ceramic plate/cellulose membrane that acts as a separator between several unsaturated soil specimens (with the same initial conditions placed on top of it) and a small water reservoir formed beneath the plate using an internal screen and a neoprene diaphragm. The water reservoir beneath the ceramic plate is kept open to the atmosphere via aseparate flexible outflow tube; hence, the pore water pressure is controlled independently at atmospheric pressure.

Air pressure is separately/independently applied and controlled at the top of specimen through an opening on the side of the pressure chamber. Target matric suction is imposed to soil specimens by elevating and maintaining the desired air pressure. The

outflow of water through the bottom reservoir is monitored, and when the equilibrium is established (no water flow condition), one specimen is removed and it's water content is determined. This moisture content along with matric suction provides one point on the SWCC plot. This process is repeated with different soil suction values, and at each soil suction value, the moisture content is determined. All these points will be used to establish SWCC plots.

2.6.3 Fredlund's Soil Water Characteristic Device

The pressure plate apparatus is incapable of obtaining continuous water or volume changes that simulate the overburden stress condition in the field without disassembling the apparatus (Padilla et al., 2005). Fredlunds SWCC apparatus is a pressure plate device that removes that limitation. The overburden pressure can be simulated via vertical loads that are kept on top of the specimen. It uses the axis-translation technique and has a matric suction measurement range of 0-1500 kPa. The entire range of SWCC can be obtained by combining these results with the filter paper method or osmotic method results.

The schematic details are shown in Figure 2.5. The soil specimen rests on the previously saturated ceramic disk (air entry value up to 1500 kPa) that is fitted inside the water filled recess, with water beneath the bottom of disk. The water leaving or absorbed by the specimen is continuously monitored through two graduated volume indicator tubes on the pressure panel that are connected, by flexible plastic tubing, to the bottom chamber below the ceramic disk.

A special air pump is designed to flush any diffused air bubbles from the bottom chamber at least once in a day. The overall volume change of the specimen can be obtained by monitoring the movement of the load plate on top of the specimen, using a dial gauge or an LVDT. The desorption curve is obtained by starting the test with a fully

saturated specimen and applying air pressure in increments. Each air pressure increment is maintained until equilibrium is reached. Similarly, the wetting curve is obtained by decreasing air pressure. Some researchers prefer only one specimen to produce both wetting and drying curves (and hence are able to study hysteresis) while some prefer getting one point on the retention curve from one test.

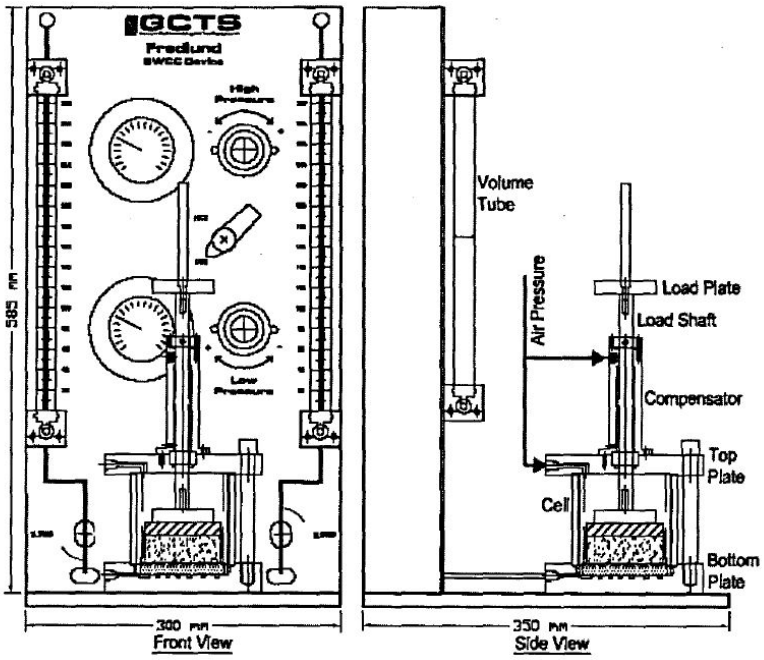

Figure 2.5 Fredlund soil water characteristic curve device (from Padilla et al., 2005)

2.7 Mathematical Models for Soil-Water Characteristic Curve

Direct measurement of suction and corresponding water content data points over the entire range of soil suction is not possible due to the costs and complexities associated with sampling, transporting, and preparing laboratory specimens, as well as installing, maintaining and monitoring field instrumentation (Lu and Likos, 2004). Very often, these limitations lead to measurements limited to a narrow range. Mathematical models in the form of equations are the alternative to direct techniques and help in the continuous prediction of SWCC over the entire range of soil suction.

These mathematical models use different parameters of soil, such as air entry suction, residual suction, volumetric water content at full saturation, or at residual suction, and degree of saturation, as well as empirical or semi-empirical fitting constants that are chosen to best fit/capture the general shape of SWCC (Fredlund and Rahardjo, 1993). Numerous researchers have proposed mathematical functions to best fit the limited available experimental discrete data points on SWCC and for prediction of the soil-water characteristic curve (Brooks and Corey, 1964; van Genutchen, 1980; Fredlund and Xing, 1994; Kosugi, 1997; Leong and Rahardjo, 1997a; Singh, 1997; Sillers et al., 2001; Gitirana and Fredlund, 2004; Sreedeep and Singh, 2006; Rahardjo et al., 2012).

Reliable estimates of hydraulic conductivity of unsaturated soil can be made to simulate the transport of fluids (van Genuchten, 1980; Lappala et al., 1987; Tindall and Kundell, 1999). Studies have also been done to evaluate the effect of cement or lime stabilizers on SWCC of problematic soils such as expansive soil (Khattab and Al-Taie., 2006; Puppala et al., 2006; Hoyos et al., 2007). Gap-graded soils exhibit bimodal grain-size and pore-size distribution. Zhang et al. (2005) presented a theoretical continuum method for the determination of soil-water characteristic curves for soils with a bimodal or multimodal pore-size distribution.

Among these models, the ones proposed by Brooks and Corey (1964), van Genuchten (1980) and Fredlund and Xing (1994) are popular mathematical models used for simulating SWCCs. These are described in the following section.

Θ is defined as the dimensionless water content variable obtained by normalizing volumetric water content with its saturated and residual values as given in equation 2.1.

$$\Theta = \frac{\theta - \theta_r}{\theta_s - \theta_r} \tag{2.1}$$

Where, Θ = normalized volumetric water content

θ = volumetric water content (any)

θ_s = saturated volumetric water content

θ_r = residual volumetric water content

The normalized water content Θ is equal to the degree of saturation S if the residual water content θ_r is equal to zero.

S_e is called as the effective degree of saturation and may be normalized by the fully saturated condition (S = *1*) and the residual saturation S_r as given by equation 2.2.

$$S_e = \frac{S - S_r}{1 - S_r} \tag{2.2}$$

Where, $$\Theta = S_e \tag{2.3}$$

The effective degree of saturation S_e becomes equal to the degree of saturation S if the residual saturation S_r is equal to zero.

The effective water content can also be expressed in terms of gravimetric water content as

$$S_e = \frac{w - w_r}{w_s - w_r} \tag{2.4}$$

Where, w = Gravimetric water content of soil

w_s = Gravimetric water content at complete saturation

w_r = Residual gravimetric water content

2.7.1 Volumetric Variables

Soil, in its natural condition, is a porous material, with a large portion of its volume being voids. The voids may be filled with water or partially filled with water and air. In areas where ground water is contaminated, voids may also be filled with different fluids, such as oil and, gas, and various chemicals. Such soils, upon loading, may undergo considerable change in volume, with a significant part of deformation very often

being irreversible. Hence, it is essential to explain the saturated, as well as unsaturated, soil response in terms of volumetric changes, as shown in Figure 2.6.

Dry and saturated soil is a two-phase system. Saturated soil has solid and water phases, while dry soil possesses solid and air phases. On the other hand, unsaturated soil is a three phase system (soil solids, pore water and pore air phase) with $0 < S < 100$ condition. Unsaturated soils are further subdivided, depending upon whether the air phase is continuous (in general the degree of saturation is less than 80%) or occluded (in general the degree of saturation greater than 90%). The transition zone between these two phases occurs when $80\% < S < 90\%$ (Fredlund et al., 2012).

The water content, w, is defined as the ratio of the mass of water to the mass of solids in any given volume of soil. The voids ratio, e, is defined as the ratio of the volume of voids to the volume of soil solids. One can calculate the voids ratio, e, of the given soil provided that the specific gravity of the soil solids, G_s and degree of saturation S through relation, is known

$$e = \frac{wG_s}{S} \tag{2.5}$$

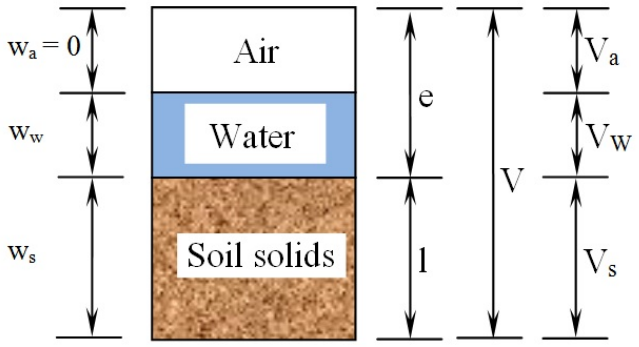

Figure 2.6 Volumetric state variables for unsaturated soil in terms of three phase system

In unsaturated soils the SWCC relationship is often expressed using volumetric water content, θ_w that can be calculated in terms of w, S, and G_s, as shown in equation 2.6.

$$\theta_w = \frac{SwG_s}{S + wG_s} \tag{2.6}$$

Another important parameter is the specific volume, v, which is used to express the volume change behavior of soil during the consolidation and shearing phases. It is defined as the volume composed of a unit volume of solids, with its surrounding void expressed as,

$$v = 1 + e \tag{2.7}$$

Some soil scientists, such as Wheeler and Sivakumar (1995), proposed using the term "specific water volume," (V_w) instead of "water content," (w), which is the volume composed of a unit volume of solids, with its surrounding voids filled with water. It is expressed by equation 2.8.

$$v_w = 1 + G_s \tag{2.8}$$

Inclusion of the variation of specific water volume under different loading paths helps to model and explain the hydro-mechanical response of unsaturated soils.

2.7.2 Brooks and Corey Model (1964)

Brooks and Corey (1964) were among the first to propose a mathematical equation for modeling the soil-water characteristic curve using a two-part power law relationship, with the help of fitting parameter, λ as shown in equation 2.9.

$$\Theta = S_e = \begin{cases} 1, & \psi < \psi_b \\ \left(\frac{\psi_b}{\psi}\right)^{\lambda}, & \psi \geq \psi_b \end{cases} \tag{2.9}$$

Where, Θ = S_e = Normalized volumetric water content as described by Equation (2.9).

Ψ = soil suction

Ψ_b = air-entry suction value of soil

λ = Pore size distribution index that varies with type of soil and its texture

2.7.3 van Genuchten Model (1980)

Van Genuchten (1980) proposed a smooth, closed-form, three-parameter, continuous mathematical expression to define the soil-water characteristic curve, as given by equation 2.10.

$$\Theta = S_e = \left[\frac{1}{1 + \left(\frac{\psi}{\alpha}\right)^n}\right]^m \tag{2.10}$$

Where, α, n and m are the fitting parameters and

$$m = 1 - \frac{1}{n}$$

The parameter, α is related to air-entry suction, the parameter m is related to the overall symmetry of the SWCC curve, and the parameter n is related to the pore size distribution of soil.

2.7.4 Fredlund and Xing Model (1990)

Fredlund and Xing (1994) proposed a model based on pore size distribution in a form similar to van Genuchten's model, as shown in equation 2.11.

$$\theta = C(\psi)\theta_s \left[\frac{1}{ln\left[e + \left(\frac{\psi}{a}\right)^n\right]}\right]^m \tag{2.11}$$

Where ψ = suction

θ_s = saturated volumetric water content

a, n, m are the fitting parameters

e = the natural logarithmic constant

$C(\psi)$ = correction factor that forces the model through a prescribed suction value of 10^6 kPa suction at zero water content.

Also,

$$C(\psi) = \left[1 - \frac{ln\left[1 + \frac{\psi}{\psi_r}\right]}{ln\left[1 + \frac{10^6}{\psi_r}\right]}\right] \tag{2.12}$$

Where, Ψ = soil suction

Ψ_r is the estimated residual suction.

2.8 Stress Tensor Representation

2.8.1 Stress State Tensor in Saturated Soil

Effective stress state is a variable for a saturated soil and is expressed as.

$$\sigma' = \sigma - u_w \tag{2.13}$$

Where σ represents the total stress and u_w is the isotropic pore water pressure or neutral stress. According to the effective stress concept, the mechanical behavior of saturated soil is governed by the effective stresses and shear stresses in each of the three Cartesian coordinate directions. Complete understanding of the stress state for a saturated soil can be achieved by adding the three effective (normal) stress variables, along with six shear stress components that arise from consideration of moment equilibrium for each of the three orthogonal directions in the form of a 3 x 3 stress tensor, as shown in the equation,

$$\sigma_{ij} - u_w\delta_{ij} = \begin{bmatrix} \sigma_x - u_w & \tau_{yx} & \tau_{zx} \\ \tau_{xy} & \sigma_y - u_w & \tau_{zy} \\ \tau_{xz} & \tau_{yz} & \sigma_z - u_w \end{bmatrix} \tag{2.14}$$

Where, $\sigma_{ij} - u_w\delta_{ij}$ is the net normal stress and δ_{ij} is the Kronecker delta. Variation in the effective stress (i.e. a change in pore-water pressure or a change in total stresses) will change the equilibrium state of the saturated soil (causing the soil matrix to compress, distort or change its shearing resistance).

2.8.2 Stress State Tensor in Dry Soil

The suction may no longer affect the mechanical behavior of extremely dry soil except when there is a change of suction leading to volume increase/swelling. The normal effective stress element $\sigma - u_a$ is the one that most affects the strength and volume change behavior (Fredlund and Rahardjo, 1993). The stress tensor may be written as

$$\sigma_{ij} - u_a\delta_{ij} = \begin{bmatrix} \sigma_x - u_a & \tau_{yx} & \tau_{zx} \\ \tau_{xy} & \sigma_y - u_a & \tau_{zy} \\ \tau_{xz} & \tau_{yz} & \sigma_z - u_a \end{bmatrix} \quad (2.15)$$

Where, $\sigma_{ij} - u_a\delta_{ij}$ is the net normal stress and δ_{ij} is the Kronecker delta.

2.8.3 Stress State Tensor in Unsaturated Soil

In unsaturated soils, contractile skin may be considered as a fourth phase as it allows for equilibrium conditions to be maintained between the air and water phases. It also maintains a constant degree of saturation in unsaturated soil when in equilibrium as well as allows air and water to flow in an independent manner (Fredlund et al., 2012). The three stress state variables that can be taken from the equilibrium equations for the soil structure are $\sigma - u_a$, $u_a - u_w$, and u_a. The stress variable u_a may be neglected considering that the soil particles are incompressible.

The stress variables controlling the equilibrium of soil structure are the same as those controlling the equilibrium of the contractile skin (Fredlund and Morgenstern, 1977). Contractile skin is only few molecular layers thick, yet its ability to exert surface tension (T_s) can alter the equilibrium conditions in an unsaturated soil and hence is considered as a fourth phase (Fredlund et al., 2012). Following the continuum mechanics methodology, each of these independent stress variables can be expressed in the form of two independent stress tensors in three-dimensional space, as below:

$$\sigma_{ij} - u_a\delta_{ij} = \begin{bmatrix} \sigma_x - u_a & \tau_{yx} & \tau_{zx} \\ \tau_{xy} & \sigma_y - u_a & \tau_{zy} \\ \tau_{xz} & \tau_{yz} & \sigma_z - u_a \end{bmatrix} \quad (2.16)$$

And

$$(u_a - u_w)\delta_{ij} = \begin{bmatrix} u_a - u_w & o & 0 \\ 0 & u_a - u_w & 0 \\ 0 & 0 & u_a - u_w \end{bmatrix} \quad (2.17)$$

Where, $\sigma_{ij} - u_a\delta_{ij}$ is the net normal stress tensor, $u_a - u_w\delta_{ij}$ is the matric suction tensor and δ_{ij} is the Kronecker delta (Lu and Likos, 2004). Even though, the pore-air pressure appears in both the stress tensor, it is the difference between stress components that allows the two tensors to qualify as independent stress state variables (Fredlund and Rahardjo, 1993).

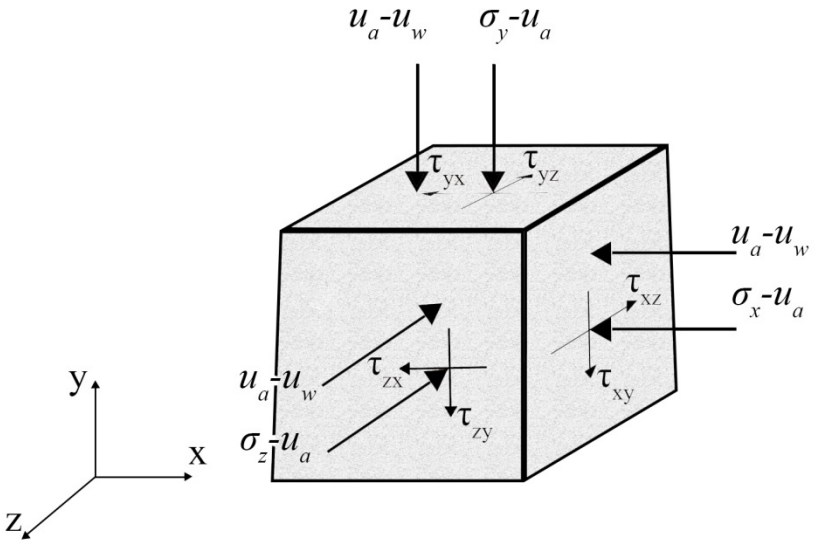

Figure 2.7 Three-dimensional stress state at a point in an unsaturated soil (from: Fredlund et al., 2012).

In order to maintain stable equilibrium, It is very important that the total stress value is greatest with the pore-air pressure value being greater than or equal to the pore

water pressure, i.e., the following condition being always maintained (Lu and Likos, 2004),

$$\sigma \geq u_a \geq u_w \tag{2.18}$$

2.9 Axis Translation Technique

Hilf (1956) was the first to demonstrate the suitability of using the axis-translation technique to measure and control matric soil suction. Unsaturated soils are associated with negative pore water pressure with respect to the atmosphere (u_w < 0). One limitation associated with measurement of large negative pore water pressure is that large water cavities are formed as gauge pressure approaches -101 kPa and less. As air accumulates below the disk inside water compartment, it causes erroneous pore pressure and volume measurements. Such a limitation can be removed by employing axis-translation technique. This technique is similar to the pressure membrane method described by Crooney et al. (1952).

2.9.1 High-Air-Entry Ceramic Disk and its Installation

The high-air-entry ceramic disk is made of ceramic material such as sintered kaolin and has small pores of relatively uniform size (Fredlund and Rahardjo, 1993). It is installed into the recess at the base pedestal/steel holder. The ceramic disk acts as a separation between the air and water mediums. High air entry value means that air pressure when applied to this value on one face of the ceramic disk, will not allow air to recede into its largest diameter pore, as long as the disk remains saturated from the other side.

The difference between air pressure and pore water pressure ($u_a - u_w$) across this contractile membrane is termed as matric suction applied. The ability of the ceramic disk to prevent the passage of free air through it is related to the surface tension T_s developed

across the contractile skin. The contractile skin acts as a membrane, joining the small pores of radius R_s on the surface of the ceramic disk.

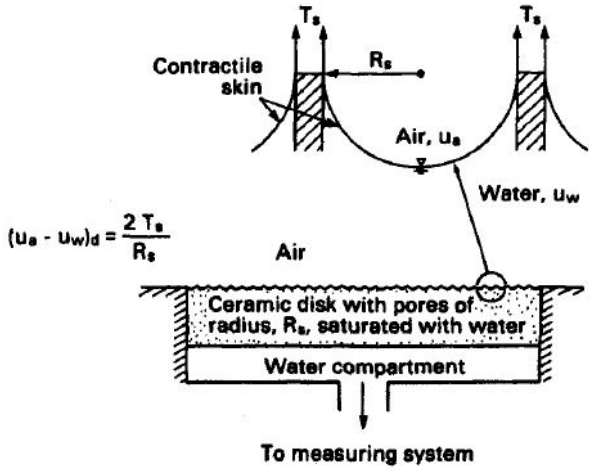

Figure 2.8 Operating principle of high-air-entry ceramic disk (from Fredlund and Rahardjo, 1993)

The maximum matric suction that the ceramic disk can withstand is called the air-entry value $(u_a - u_w)_d$ of the disk and is expressed as in equation 2.26. The air-entry value of the disk is controlled by the radius of curvature R_s of the largest pore size available in disk.

$$(u_a - u_w)_d = \frac{2T_s}{R_s} \tag{2.26}$$

The ceramic disk can be accommodated into the base pedestal of the triaxial cell or any other testing equipment. High strength glue such as Araldite or epoxy seal can be used to affix the disk into the stainless steel holder, as shown in Figure 2.9 (Murray and Sivakumar, 2010). Any excess glue should be wiped off, and care should be taken to prevent any contact of glue with the top surface of the disk. A tight seal between the ceramic disk and the base (the holder or pedestal) ensures that air will not leak through it when in use (Fredlund and Rahardjo, 1993).

2.9.2 Saturation of Ceramic Disk

The pressure chamber assembly to implement the axis-translation technique is shown in Figure 2.10. The ceramic disk of appropriate AEV is installed in the grooved recess of the base pedestal. Water is flushed through the bottom compartment and kept saturated all the time. One end of the compartment is connected to a burette that is open to the atmosphere or to the back water pressure system.

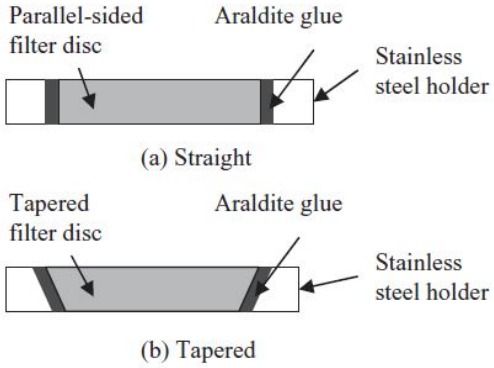

Figure 2.9 High air entry filter disc holder arrangements (After Brown, 2009; Sivakumar and Murray, 2010)

The chamber is then assembled and closed, then filled with water up to a few centimeters (2.5 cm) above the ceramic disk, to submerge it completely. Air pressure of magnitude less than the AEV of the ceramic disk is applied inside the chamber from the top. The ceramic disk is hydrophilic in nature; hence water can pass through it, but free air cannot flow through it unless a limiting air-entry value is exceeded. Despite the limiting air-entry value being not exceeded, it is still possible for the air to dissolve in the water in a ceramic disk and then slowly diffuse through the water in the disk, causing erroneous pore water measurements. The air pressure is kept applied for about one hour, during which the valve connecting the water compartment to the measuring system is closed.

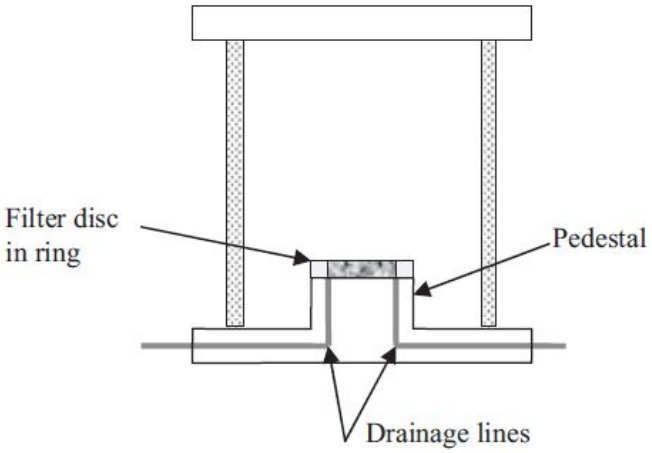

Figure 2.10 Chamber for saturating high air entry ceramic disc.

Following this, the valve is opened for approximately 10 minutes to allow the water from the disk to flow into the compartment, from where the air bubbles are flushed via a flushing operation. Such procedure is repeated several times until the bottom compartment becomes free from diffused air. Hence periodic flushing is required to flush the air accumulated in the bottom compartment (Fredlund and Rahardjo, 1993). Once the disk is completely saturated, the air pressure is released slowly to ensure that the dissolved air is not released back into the ceramic disk by diffusion.

The chamber is dissembled, and the unsaturated soil specimen is kept quickly on the ceramic disk with good contact. The difference in the pore water pressure of the soil specimen and saturated ceramic disk causes the specimen to draw water immediately from the saturated ceramic disk (provided good contact is established) and register a negative value of pore water pressure via the pressure transducer connected in line with the bottom compartment. This flow of water also helps to establish continuity of the water phase between the soil and the ceramic disk. Further, the water in the ceramic disk provides continuity between the pore water in unsaturated soil and the water in the measuring system.

The chamber is quickly reassembled, and positive air pressure of a magnitude equal to the negative pore water pressure measured earlier is applied to bring it to zero or atmospheric pressure. Thus, the process involves translation of the reference pore-air pressure, so as to translate the pore-water pressure to a positive value, hence, the technique being named axis-translation technique. It relies on the continuity of the air phase, within the soil specimen, as well as the continuity between the water in the soil specimen, the water in the ceramic disk, and the water in the compartment below the ceramic disk in order to obtain the reliable results.

The pore-air pressure is subsequently elevated above the atmospheric pressure, thereby also elevating the pore-water pressure to become positive, yet maintaining the same matric suction relative to the atmosphere in the specimen (Hilf, 1956; Bishop et al., 1961; Fredlund and Rahardjo, 1993). Depending upon the applied matric suction and the initial matric suction within the specimen, the soil specimen will either release or absorb water until equilibrium (no water flow condition) is reached.

The numerical difference between the pore air pressure and pore water pressure is termed as matric soil suction. If the pore water pressure is kept at atmospheric pressure, then the matric suction will be equal to the applied air pressure. After sufficient time is allowed, the flow of water through the ceramic disk under the influence of air pressure u_a and pore water pressure, u_w (usually atmospheric i.e. zero) will come into equilibrium finally maintaining a no-flow condition. Continuity of the water phase plays an important role in the hydro-mechanical response of the soil.

Even though, the matric suction may be equilibrated, the water phase may lack continuity at the high matric suction imposed. Tripathy et al. (2011) verified experimentally via the null-type axis-translation technique, that an increase in the degree of saturation due to an increase in water content created a better continuity in the water

phase between the water in the soil specimens, the water in a ceramic disk, and the water in the compartment beneath the ceramic disk.

The matric suction applied to the specimen $(u_a - u_w)$ should not exceed the air entry value of the disk; otherwise, air will enter into the compartment below disk, get filled with air bubbles, and eliminate the continuity between the pore water in the specimen and the water in the measuring system (Fredlund and Rahardjo, 1993; Ho and Fredlund, 1982). A series of null tests verified that the translation of pore water pressure to a positive value by elevating the pore air pressure by an equal amount, does not appear to affect the measured shear strength of unsaturated soils (Fredlund and Rahardjo, 1993).

Numerous factors affect the suction equilibration time and, hence, the reliability of test results. These include the thickness and the air-entry value of the ceramic disk, defects in the ceramic disk and methods of mounting the disk, deflection of the membrane of the pore pressure transducer used, air-diffusion through the ceramic disk, contact between soil specimen and the saturated ceramic disk, expansion of the water compartment below the ceramic disk, and compressibility of the air-water mixture in the water compartment (Fredlund and Rahardjo, 1993; Tripathy et al., 2011).

Bocking and Fredlund (1980) reported some issues associated with using the axis-translation technique. Air pressure increase on unsaturated soils will cause compression of the air-water mixture that, in turn, tends to decrease the volume of the pore fluid. This causes a decrease in the size of the air-water interface, leading to overestimation of the actual suction. Another issue is due to air diffusion through the ceramic disk, causing an increase in air volume in the bottom compartment. As illustrated in Figure 2.11c, the air will replace the water in the compartment and may push water back into the soil through the ceramic disk.

The diffused air eventually comes out of the solution beneath the ceramic disk and obstructs the water phase continuity between the water in the ceramic disk and the water in the compartment below the ceramic disk.

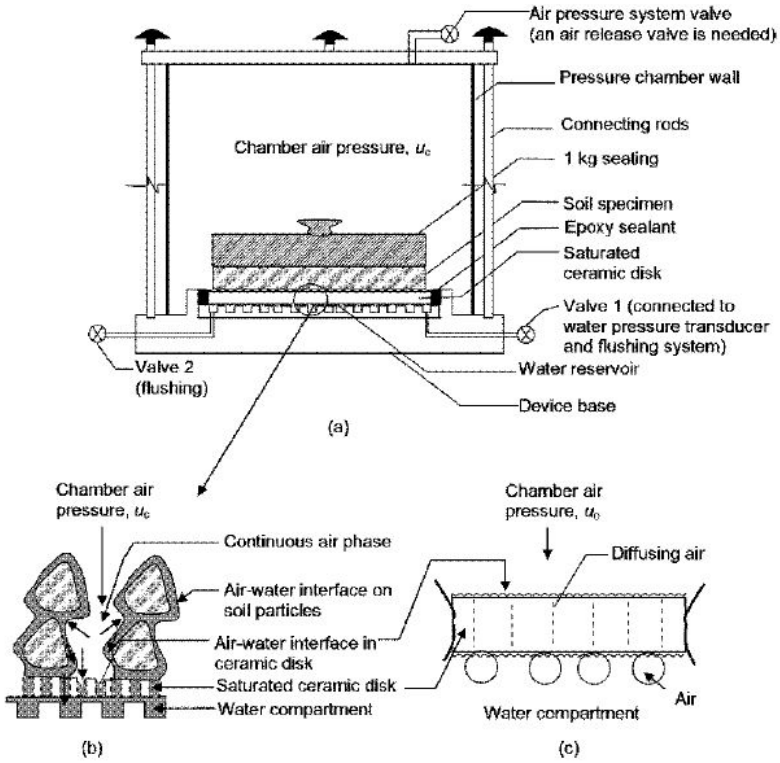

Figure 2.11 a) Null-type axis-translation device, b) water phase continuity requirement, and c) air diffusion through saturated ceramic disk (from Tripathy et al., 2011).

This may underestimate the actual matric suction of the soil, as well as delay the suction equilibration time (Fredlund, 1975).

2.10 Other Techniques to Impose Soil Suction

2.10.1 Introduction

In this section, a brief literature review related to various techniques, including osmotic and vapor pressure techniques is presented. Both of the techniques have been proven to be reliable in controlling relative humidity, and, hence, suction in the soil,

enabling it to impose both drying and wetting stress paths for evaluating strength, deformation and flow characteristics of unsaturated soils (Blatz et al., 2008). The major distinction between the two techniques is that the total suction is controlled within vapor pressure techniques, while the matric suction is controlled with the osmotic technique. Neither method measures the suction directly in the specimen.

2.10.2 Osmotic Technique

The osmotic technique uses the principle of osmosis for controlling suction in the soil specimen. Most of the osmotic techniques use a semi-permeable membrane and solutes, such as polyethylene glycol (PEG) to produce a solution that needs to be calibrated appropriately so that its concentration can be related to osmotic pressures. Williams and Shaykewich (1969) provided such calibrations (PEG 6,000 and 20,000) that covered range of 0 to 1.5 MPa while Delage et al. (1998) extended it up to 10 MPa. Because the air pressure around a soil specimen remains atmospheric, the field stress path is better simulated by using the osmotic technique (Ng et al., 2007).

Referring to Figure 2.12, the soil specimen is wrapped in a semi-permeable membrane, around which an aqueous solution of large or small size sized polyethylene glycol (PEG) molecules is circulated using a magnetic stirrer. Due to the difference in concentration, a gradient is generated across the membrane between a solution and the pore water in the soil. Water molecules can permeate the membrane; whereas, PEG molecules cannot, thereby imposing an osmotic pressure (suction) to the soil specimen that increases with the PEG concentration.

Equilibrium is reached when the drop in free energy, generated by the addition of a solute, is balanced by the rise in free energy generated by the increase in the osmotic pressure (Boso et al., 2005). Since water transfer takes place in the liquid phase and ions

can cross the semi-permeable membrane freely, the osmotic technique controls the matric suction of soil and not the osmotic suction (Blatz et al., 2008).

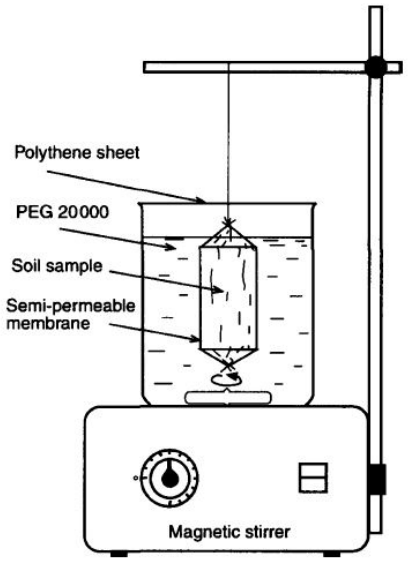

Figure 2.12 Osmotic techniques to impose suction in soil specimen (after Cui and Delage 1996)

The osmotic technique was first adopted by biologists in kidney bean experiments, where they used Polyethylene glycol as an agent to control the osmotic pressure of plant nutrient solutions (Legerwerff et al., 1961). However, Zur (1966) was the first soil scientist to apply the osmotic technique to create the gravimetric soil water characteristic curve for a sandy loam and clay type soil, as well as to compare the results obtained with those from the axis-translation technique. Good agreement was found between both techniques for sandy loam. However, Zur (1966), as well as Williams and Shaykewich (1969), concluded through their experiments that, for clay, the equilibrium water content obtained when using the axis-translation technique was higher than when using the osmotic technique, under same applied nominal suction.

The osmotic technique has also been successfully coupled with the conventional oedometer to understand the consolidation and/swelling behavior of unsaturated soils (Kassif and Shalom, 1971; Delage et al., 1992; Dineen and Burland, 1995; Tarantino and Mongiovi, 2000a), direct shear test apparatus (Boso et al., 2005) as well as in a triaxial apparatus (Delage et al., 1987; Cui and Delage, 1996, Ng et al., 2007). Most of these researchers confirmed the established suction equilibrium via an independent suction probe/tensiometer.

Ng et al. (2007), were among the first to investigate the possible differences in using the axis-translation and osmotic techniques in triaxial shear testing of compacted expansive clays with applied suction ranging between 0 to 165 kPa (low-to-moderate range) and the net confining pressure from 25 to 100 kPa. Their comparison of the test results, based on the extended Mohr-Coulomb shear strength formulation, showed that the value of φ' was unaffected, but the value of φ^b, using the axis-translation technique, was slightly greater than that of those using the osmotic technique from 3 to 4 deg. The larger values of φ^b were attributed to lower specific volume and higher inter-particle contact forces, (because of high degree of saturation), transmitted through the soil skeleton of the specimens tested using the axis-translation technique.

2.10.3 Vapor Pressure Technique

The vapor pressure technique can be divided into two types. One type uses salt solutions, or ionic solutions, with the target suction value to manipulate the air's relative humidity in and around the specimen. The second type relies on mixing adequate proportions (mass/volume) of wet and dry air flow to circulate the saturated air of particular relative humidity around and inside the pore space of specimens under controlled temperature to create high total soil suction. The second method is described

later in section 2.11.3.9, and explains its use with triaxial testing. Both of the methods use the principle of vapor equilibrium.

2.10.3.1 Vapor pressure technique using salt solutions

Relative humidity conditions in soil specimens can be controlled using different salt solutions in a temperature controlled environment to achieve a constant soil suction.

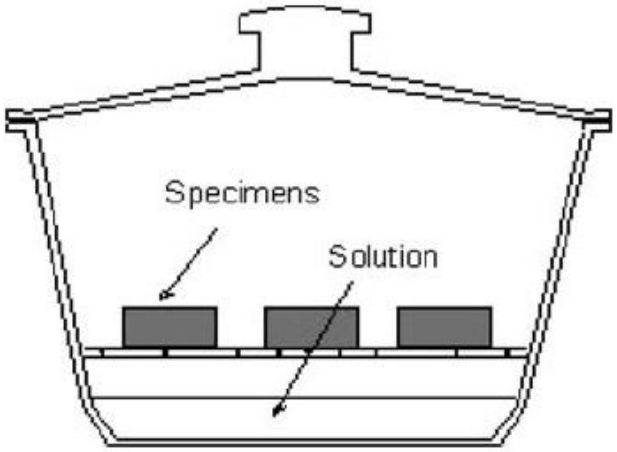

Figure 2.13 Soil specimens in constant suction environment (after Tang et al., 1998)

The osmotic potential of chemical solutions is used to create known partial vapor pressures in the sealed environment (Figure 2.13) that alter the suction in the specimens suspended over salt solutions through moisture transfer between the soil and surrounding head space (Blatz et al., 2002). The soil specimens achieve equilibrium conditions with respect to their moisture content over a considerable period of time. However, strict control of temperature is essential, as any fluctuation will dramatically alter the applied suction (Tang and Cui, 2005).

Saturated salt solutions, (usually a mixture of sodium and potassium chloride), with a limited lower range of approximately 0-10 MPa, and unsaturated acid solutions with a higher range up to about 150 MPa are used (Blatz et al., 2008). Using salt solutions is more beneficial than unsaturated acid solutions because, that when using the

former, the concentration of an osmotic solution does not alter as water exchange takes place between specimens and the vapor environment.

This technique has been used, in combination with lab equipment, to establish points on soil water characteristic curves in the high suction range (Fredlund and Rahardjo, 1993; Vanapalli et al., 1999), for assessment of unconfined compression strength and volume change of silty soil (Nishimura et al., 2008), triaxial strength and stiffness assessment of sand-bentonite mixtures (Blatz and Graham, 2000; Blatz et al., 2002), and direct shear strength analysis of silty soil (Nishimura et al., 2010).

2.11 Shear Strength Measurement Devices

2.11.1 Triaxial Testing Systems

2.11.1.1 Introduction

In its most basic form the traditional triaxial test is used to measure shear strength, stress-strain behavior (hardening or softening), volume change response (contractive or dilative), and pore pressure response (positive or negative) of soils (dry as well as saturated), under an axisymmetric state of stress and controlled drainage conditions.

Shear strength of soil is not a unique property, and its determination in the laboratory depends on factors that are related to natural conditions beyond our control but that can be assessed by field observations, such as mineralogy of grains, particle shape, size distribution, configuration, voids ratio, water content, previous stress history, existing stresses in-situ; factors that depend upon the quality of sampling such as stress changes imposed during sampling, the initial state of the sample/test specimen, stresses applied prior to the test; factors that depend upon testing method adopted such as strain rate during loading, drainage conditions, pore pressure conditions and criterion adopted for determining shear strength (Head, 1998).

2.11.2 Traditional Traixial Testing System for Saturated Soil Testing

The triaxial test is conducted on a cylindrical soil specimen encased inside a latex rubber membrane, mounted inside a cell, subjected to an all-round confining pressure by pressurizing the water-filled cell, and then loading it axially until failure is reached. In saturated soil testing, the soil specimen with porous stones placed at the top and bottom is sealed inside the rubber membrane to allow the passage of water to and from the specimen allowing control of drainage conditions. Since the soil is saturated, the change in its volume can be monitored through the measurement of water going inside or out of the specimen. The principal stresses along all three directions are known and can be controlled; hence, the name “Triaxial” test.

A minimum of three specimens, each tested under varying confining pressures, are tested to establish a relation between shear strength and normal stress. The test conditions give a realistic representation of field stress conditions on soil specimens and are, therefore, more reliable than the other tests, such as the direct shear test. Triaxial equipment and testing procedures have been described in detail by Bishop and Henkel (1962); Bardet (1997), and Head (1998). The various protocol/procedures to be followed have been explained through ASTM D7181-11 standards depending upon drainage conditions during triaxial testing of saturated soils.

2.11.3 Modified Unsaturated Soil Triaxial Testing Systems

The traditional triaxial testing setup has been modified by researchers, over the last four decades or so, to facilitate the unsaturated triaxial testing. Major modifications include arrangement to allow independent control and measurement of pore-air and pore-water pressures (and hence matric suction), via the axis-translation technique and other techniques that would allow tracking volume change measurements of both the air and water phases in soil specimens.

In addition, the problems associated with the axis-translation technique, such as accumulation of diffused air in the water compartment beneath the ceramic disk and providing an arrangement to flush air, as and when required, need to be taken care of for accurate assessment of strength and volume change measurements (Bishop and Donald, 1961; Alonso et al., 1990; Fredlund and Rahardjo, 1993; Sivakumar, 1993; Rampino et al., 1999).

The ASTM has not yet standardized the unsaturated soil triaxial testing methodology. However, the unsaturated soil triaxial testing procedures are well documented elsewhere in the literature (Fredlund and Rahardjo, 1993; Fredlund et al., 2012; Lu and Likos, 2004; Murray and Sivakumar, 2010). Modern day developments in computer technology, sensors and equipment have made it possible to adopt these modifications easily, with improved precision. Some of these modifications are discussed in the next section.

2.11.3.1 Air-Water Pressure Control

The conventional triaxial device was first modified by Bishop and Donald (1961) to allow control of both pore air, u_a, and pore water pressure, u_w, by installing a porous stone in the top cap and a high-air-entry ceramic disk in the base pedestal to allow control of the matric suction. The volume change was measured by monitoring the rise or fall of the mercury level in the unstressed inner cell, via cathetometer.

Soon, Fredlund and Rahardjo (1993) made modifications and replaced mercury, which was used as cell fluid, with water and employed the axis-translation technique to control the matric suction. The volume change measurement was done via a more precise volume change controller, along with a double-wall cell mechanism. Thu et al. (2007) further modified it to accommodate the NTU mini suction probe at the center of the specimen and to monitor matric suction throughout the testing as shown in Figure 2.14.

Simultaneous application of u_a and u_w, at both ends of the specimen, is possible by installing a peripheral annular coarse porous stone and an internal HAE disk in the top cap and bottom pedestal that allows double drainage (Romero, 1999; Barrera, 2002; Rojas et al., 2008) as shown in Figure 2.15.

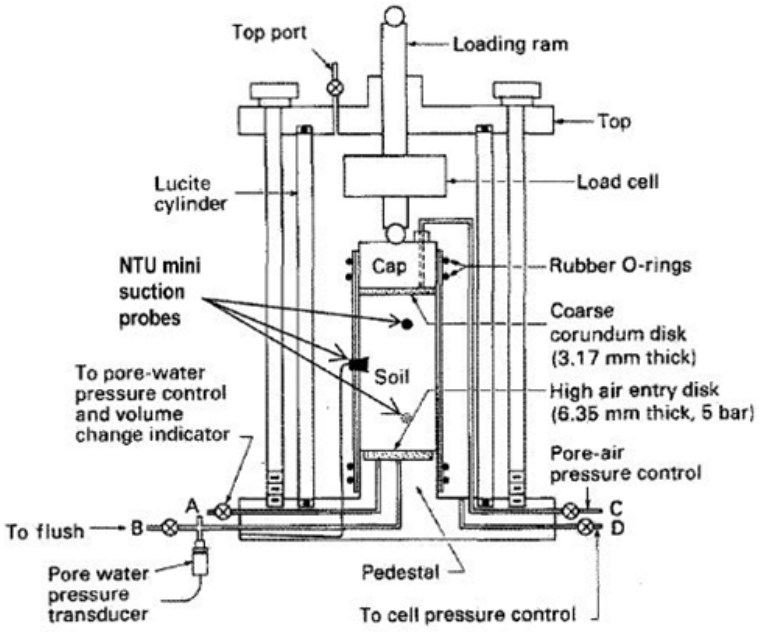

Figure 2.14 Triaxial cell modified to accommodate unsaturated soil testing (modified from Fredlund and Rahardjo, 1993; Thu et al., 2007)

Sharma et al. (1998) used a HAE disk at both the ends, with a porous stone only at one end, thus, allowing control of pore water pressure at both the ends while air pressure was applied and controlled only at one end. Both the techniques help reduce the suction equilibrium time by a considerable amount. One limitation of such method is that the air bubble might get trapped in the middle of the specimen due to the two water front's moving toward the middle from the opposite direction. Maatouk (1993) removed this problem by supplying u_a at the middle of specimen at the sacrifice of being not able to measure the specimen volume change.

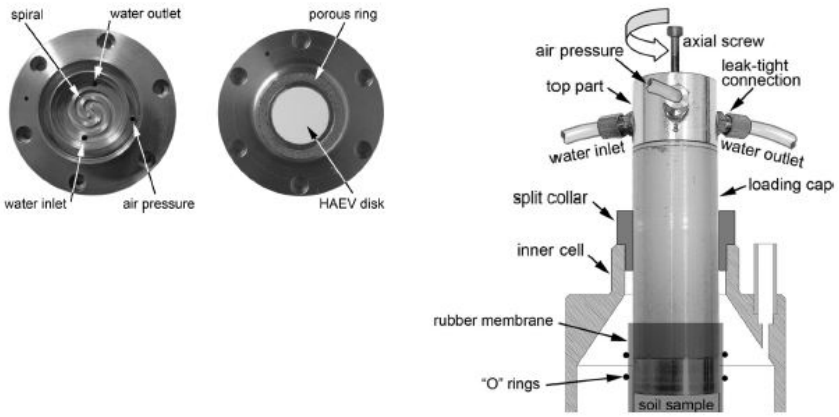

Figure 2.15 Modifications to top cap and base pedestal to allow pore-air and pore-water drainage through both ends of triaxial specimen (from Rojas et al., 2008)

Ishikawa et al. (2012) proposed a novel medium-sized triaxial apparatus to study the water retention characteristic curves and the deformation-strength characteristics of unsaturated granular base course materials by replacing the ceramic disk with hydrophilic microporous membrane filters. The pore water pressure was applied to the specimen through a versapor membrane filter attached to the water plumbing path while the pore air pressure was applied through a hydrophobic polyflon filter attached to the air supply path in the cap and pedestal as illustrated in Figure 2.16. The test results from this novel technique were found to be consistent with those from previous research.

2.11.3.2 Water sub-pressure and air over-pressure technique

Barrera (2002) used an air over-pressure technique by imposing a target suction in the soil specimen by changing u_w, while u_a was kept constant. The initial value of u_w applied needs to be high in order to reduce it in later stages to impose the desired suction. High u_w also ensures that the air remains in a dissolved state in the back water drainage system. Such technique is beneficial while applying low suction, especially close to the saturation/air entry value of soil.

The water sub-pressure technique, deals with simultaneous change in σ and u_a, that may cause instantaneous soil deformation due to bedding error (Rampino et al., 1999; Vassallo, 2003). Apart from minimizing leakages, a low value of u_w also allows investigating a wider $(\sigma - u_a)$ range under given suction state, facilitating, for instance, a better definition of the compression curve during triaxial testing (Hoyos et al., 2008). Both the techniques are discussed in detail by Romero (2001).

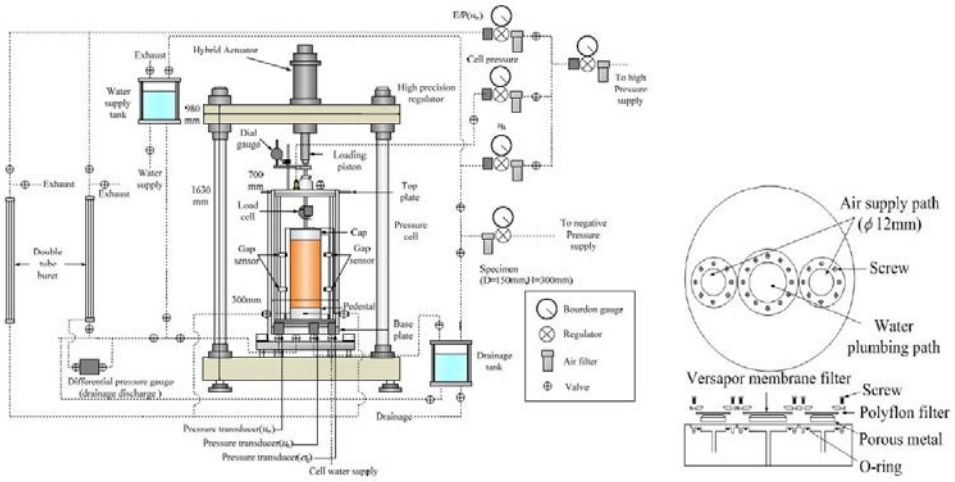

Figure 2.16 Medium-size triaxial apparatus with microporous membrane filter instead of ceramic disk to control pore air and pore water pressure (from Ishikawa et al., 2012)

2.11.3.3 Volume change measurement

The volume change in saturated soil can be monitored by measuring the amount of water drained through the soil. Such a conventional technique cannot be used on unsaturated soil. Volume change in unsaturated soils is associated with compression of the air phase as well as drainage. Bishop and Henkel (1962) and Matyas (1967) developed a procedure to monitor volume changes in both fluid phases using two burettes. However, due to the effect of compressibility and capillarity in the air bubbles, it fails to produce accurate results.

Several techniques have been developed by numerous researchers over the years to improve the capability of measuring unsaturated soil volume changes during triaxial testing. Laloui et al. (2006) summarized these techniques broadly into three categories; cell liquid measurements, direct air-volume/water-volume measurements and direct measurements on the specimen.

2.11.3.4 Cell liquid measurements

2.11.3.4.1 Single-walled triaxial cell

The specimen volume is obtained via monitoring volume changes in confined cell liquid used in a single-walled cell that is filled completely with water or other fluids such as mercury. Certain corrections are applied such as for piston intrusion into the cell and for expansion of the plexiglass cell due to cell pressure increase, which involve appropriate calibration methods to ensure accuracy. Cell volume change may also be affected by temperature fluctuations, stiffness of cell material (Leong et al., 2004), and numerous other factors as discussed by Head (1986). Thus, despite offering simplicity, the single-walled cell is not preferred in unsaturated soil triaxial testing.

2.11.3.4.2 Inner cylinder technique

In order to enhance the volume change measurement, Bishop and Donald (1961) proposed to add an inner cell that was sealed to the outer cell base to minimize the actual liquid volume used to measure volume change. They used mercury as the inner cell fluid, while water was used in the outer cell. Equal pressure was applied on both sides of the inner cell and, hence, any change in the fluid level in the inner cell that was measured via the cathetometer would measure the overall volume change thereby improving the quality of volume change measurement. Such a system was automated subsequently by Josa et al. (1987).

Following the advent of the inner cylinder technique, Cui and Delage (1996) modified the technique by replacing mercury (that can be hazardous from a safety point of view) with water and recorded volume changes via high-precision cathetometer-based readings. Ng et al. (2002) replaced cathetometer with a high accuracy differential pressure transducer that could track the differential pressure between the water inside the open-ended inner cell and water inside a reference reservoir, as shown in Figure 2.17.

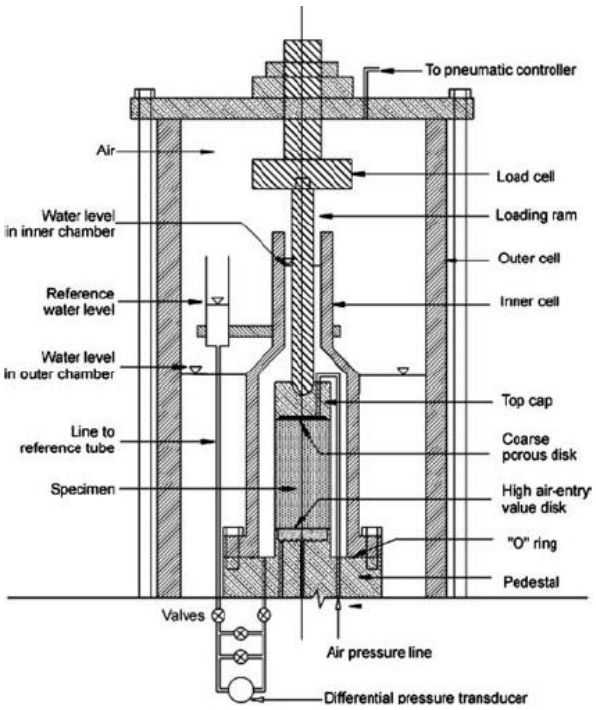

Figure 2.17 Inner cylinder technique to monitor overall volume change (from Ng. et al., 2002)

Some researchers (Wheeler, 1988; Sivakumar, 1993; Houston et al., 2008), have preferred to use a double-walled cell that has an inner cylinder sealed to both the top and base of the cell. Such a refined system removes most of the possible errors discussed by Head (1986) and has been used in the current research, in conjunction with a high

precision volume change device to improve the overall performance. This will be discussed in detail in Chapter 3.

2.11.3.5 Direct air-volume and water-volume measurements

In this method, both volume changes of air and water entering or leaving the pore spaces are monitored by separating draining pore-water from the pore-air using porous stones and HAE ceramics, respectively, and then independently measuring each by pressure-volume controllers. It can be used simultaneously with the axis-translation technique. Adams et al. (1996) satisfactorily evaluated the suitability by using a digital pressure-volume controller under the effects of temperature, confined volume and pre-compression of the measurement medium.

This device was further improved by changes in temperature and atmospheric pressure effects by Geiser et al. (1999) using a mixed air and water controller that allowed reduction of air volume to the tubing only. Laudahn et al. (2005) described another method to monitor pore-air volume changes in drained tests under atmospheric conditions. A U-tube filled with ethanol, whose level was monitored via a photoelectric sensor, was connected to the GDS volume controller to track any excess pore air pressure generation during the drained test. The detected change in levels could then be reversed by the GDS controller to keep the pore-air at atmospheric pressure.

2.11.3.6 Direct measurements on the specimen

In this approach, any associated deformations are calculated by direct measurements of the radial and axial movements of the specimen. Such method can be split into three distinct approaches. In the first approach, local displacement sensors, such as miniature LVDTs (Costa-Filho, 1982; Klotz and Coop, 2002), Hall- effect transducers (Clayton and Khatrush, 1986; Clayton et al., 1989), strain gauges (Kolymbas

and Wu, 1989; Lo Presti et al., 1995) are attached directly onto the specimen to measure axial, as well as radial, deformations during the test.

In addition, non-contacting transducers were also proposed (Cole, 1978; Khan and Hoag, 1979). Oka et al. (2010) proposed a modified triaxial equipment, with direct axial strain measurement via non-contacting proximity transducer for low levels of axial strain of less than 0.1% and a local vertical deformation transducer (LVDT) for medium-to-high levels of strains with a differential pressure transducer to measure changes in volume of pore water. In addition, the volume change was calculated by measuring the lateral displacements of the two sides of the specimen with four proximity transducers that had aluminum foil as a target, as illustrated in Figure 2.18.

The major advantage of such method is that the proximity transducers can be controlled from outside the triaxial cell, and, hence, the volume changes can be evaluated without any contact with the specimen.

A major disadvantage is the delicacy required when placing the sensors, as a slight mistake in placement can cause errors in experimental measurements. Also, volume change measurement becomes meaningless if a shear plane/irregular bulging forms across the specimen during shear.

The second approach is a non-contact method and is more promising, but involves costly long-range, electro-optical lasers and sophisticated installation procedures, as shown in Figure 2.19 (Romero et al., 1997). A laser is swept across the entire height of the specimen, from diametrically opposite sides, that allows for accurate determination of the specimen volume and identifies any non-uniformities and localized deformations. Hird and Haji (1995) employed a similar technique, using a proximeter transducer sealed in a housing and mounted on a rigid tube around the sample, facilitating an output voltage proportional to the distance of a lightweight conductive target

placed on the specimen. Extreme care is required on the part of the operator in making sure that the target is aligned with the sensor all of the time.

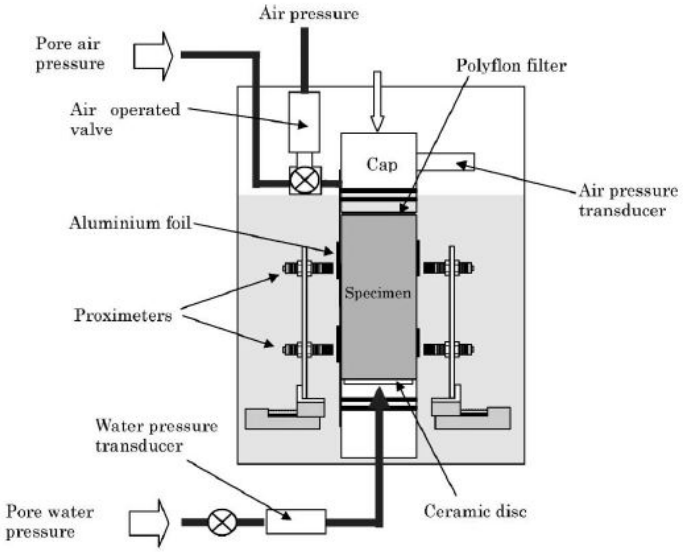

Figure 2.18 Direct volume change measurement via non-contact proximity transducers in triaxial cell (from Oka et al., 2010)

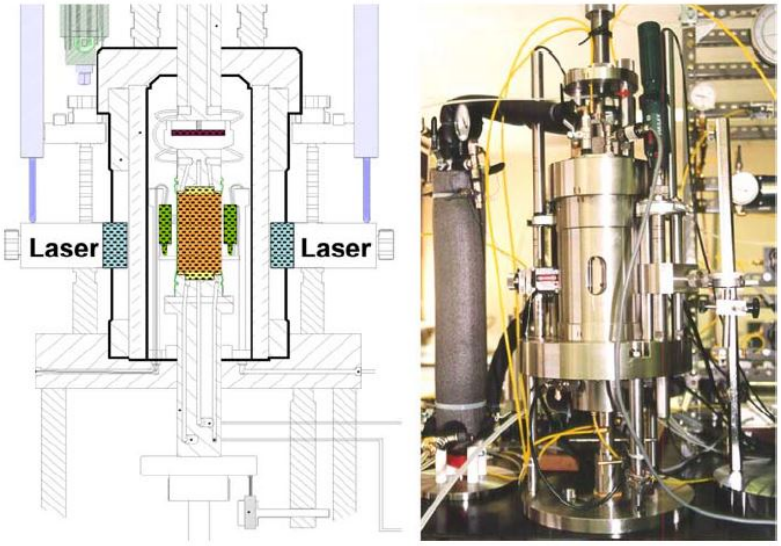

Figure 2.19 Direct volume change measurement via electro-optical laser technique (from Romero et al, 1997)

The third approach is the image process technique and involves taking photographs through the plexiglass cell during testing and later analyzing them to obtain the specimen profile and volume changes (Macari et al., 1997; Gachet, 2003). Rifai et al. (2002) used a digital computer-controlled camera fixed at a constant distance from the cell, as illustrated in Figure 2.20. Optical distortions are corrected by conducting proper calibration prior to testing.

Reasonably good agreements in volume change measurements were found while using a mixed air/water controller and image processing techniques by Laloui et al. (2006). They tested unsaturated sandy silt with volume change measurements during the shearing stage under controlled suction of 100 kPa up to 12% axial strain, after which strain localization occurred.

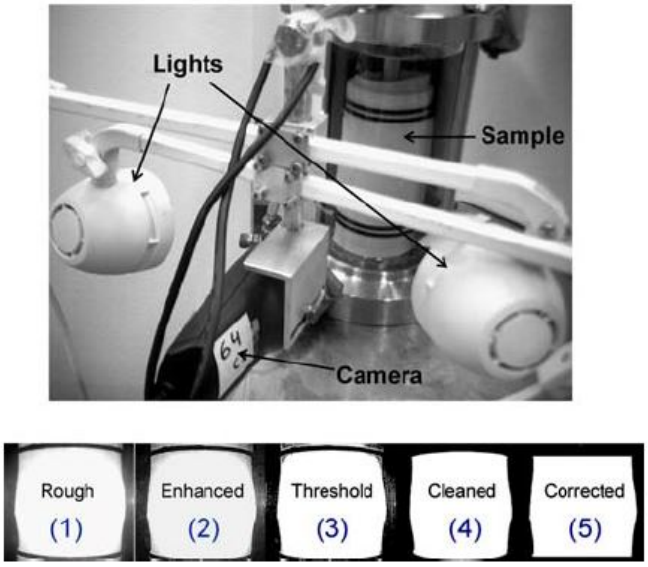

Figure 2.20 Image processing technique for volume change measurement (from Rifae et al, 2002)

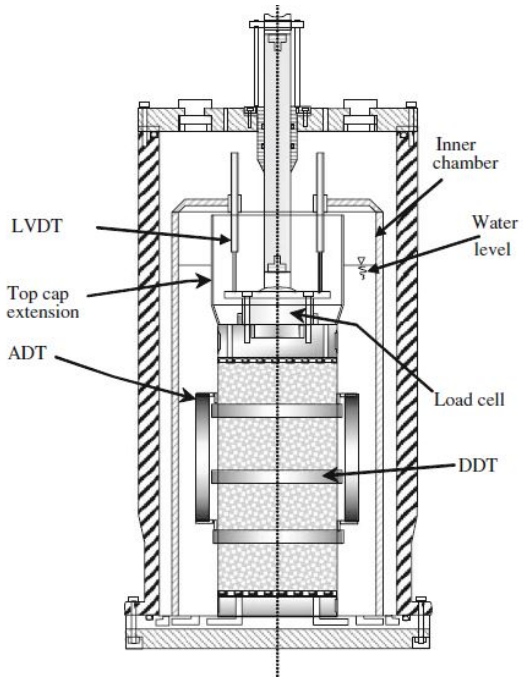

Figure 2.21 Volume change measurement via inner chamber liquid measurement and direct measurement using displacement transducers (from Chavez et al., 2005)

Chavez et al. (2005) proposed a new triaxial cell that enables global measurements of specimen volume changes by a combination of the liquid measurement technique and direct measurement techniques. The liquid measurement technique method was employed by recording the differential pressures between the water levels in the inner chamber and that of the reference tube using a differential pressure transducer. The direct measurement technique was employed, by installing three internal LVDTs, to monitor axial displacement and radial deformation, as shown in Figure 2.21.

2.11.3.7 Bender element-based triaxial cell system

Recently, Cabarkapa and Cuccovillo (2006) proposed a sophisticated system by combining the bender element set-up with features such as monitoring volume change measurement via a full set of internal LVDTs including a radial strain belt for volume change measurements, as illustrated in Figure 2.22.

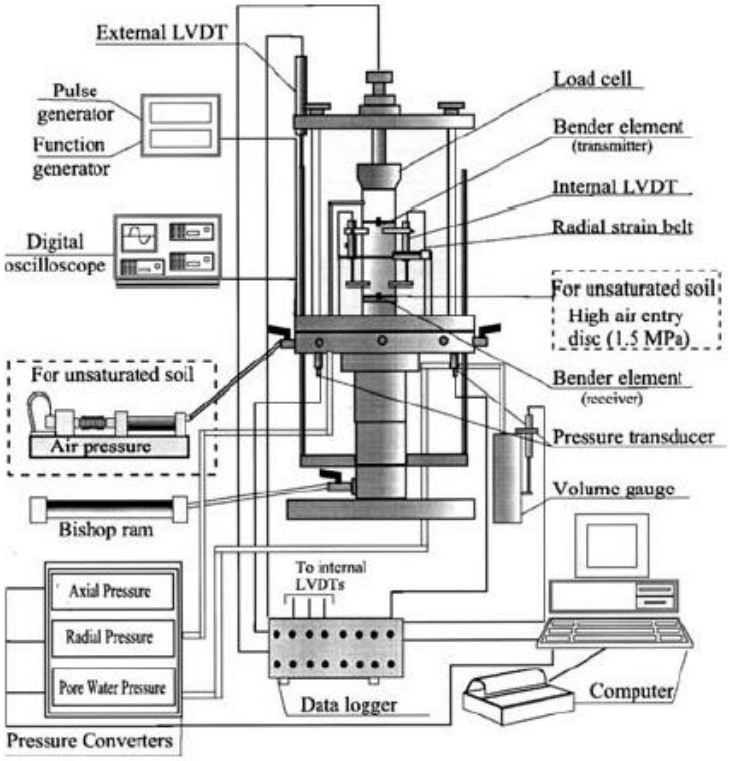

Figure 2.22 Triaxial cell featuring LVDTs for direct volume change measurements along with Bender element set (from Cabarkapa and Cuccovillo, 2006)

2.11.3.8 Osmotic technique in triaxial equipment

The osmotic technique was combined with triaxial equipment by Delage et al. (1987) and Cui and Delage (1996). A semipermeable membrane was kept in contact with the top and bottom of the triaxial specimen, and PEG 2000 solution was circulated at the top and bottom via an independent reservoir, as shown in Figure 2.23. Depending upon the concentration of the PEG solution, the exchange of water molecules takes place across the membrane, between the soil pore water and the PEG solution, until equilibrium is achieved. The pore air pressure was kept atmospheric by providing an air vent in the bottom pedestal, that was connected to anti-evaporation system to neutralize water evaporation from the specimen.

One benefit of using the osmotic method over the vapor equilibrium method is the reduction in equilibrium time due to the direct exchange of liquid water. Vicol (1990) reported equilibrium time as little as four days to be sufficient to impose suction of several hundreds of kilopascals to a silty soil prepared from slurry.

Major concerns associated with the osmotic technique are the weakness of the semi-permeable membrane, a possible attack of bacteria, and tear of the membrane by any traction (especially in triaxial testing where the membrane is subjected to shear stress). The performance and life of the membrane can be improved by the addition of penicillin to the PEG solution (Blatz et al., 2008).

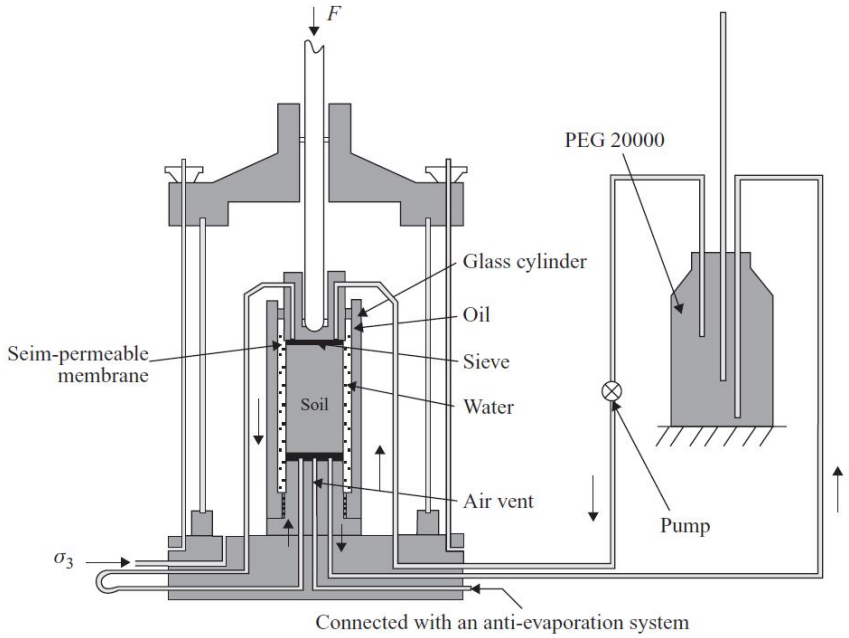

Figure 2.23 Triaxial equipment integrated with osmotic technique (after Cui and Delage 1996)

2.11.3.9 Vapor equilibrium technique in triaxial equipment

Blatz and Graham (2000) efficiently modified their original triaxial cell to accommodate the vapor equilibrium system to control high suction in the specimen.

Schematic details of such equipment are shown in Figure 2.24. The vapors created in the desiccator, from an ionic solution, were pumped through the bottom to the top of the specimen, and then back to desiccator, thus forming a closed circulation system. The water exchange took place between the specimen and vapor, depending upon the suction gradient between the ionic solution and the specimen.

The suction imposed inside the specimen, via the vapor exchange, was measured independently through psychrometers installed in the top cap and at mid-height of the specimen. Volume changes were monitored via linear variable displacement transducers to record the change in height and diameter. The vapor flow process was expedited by installing geotextile strips along the length of the specimen as well as covering the top and bottom porous stones, thus providing continuous passage for vapor flow.

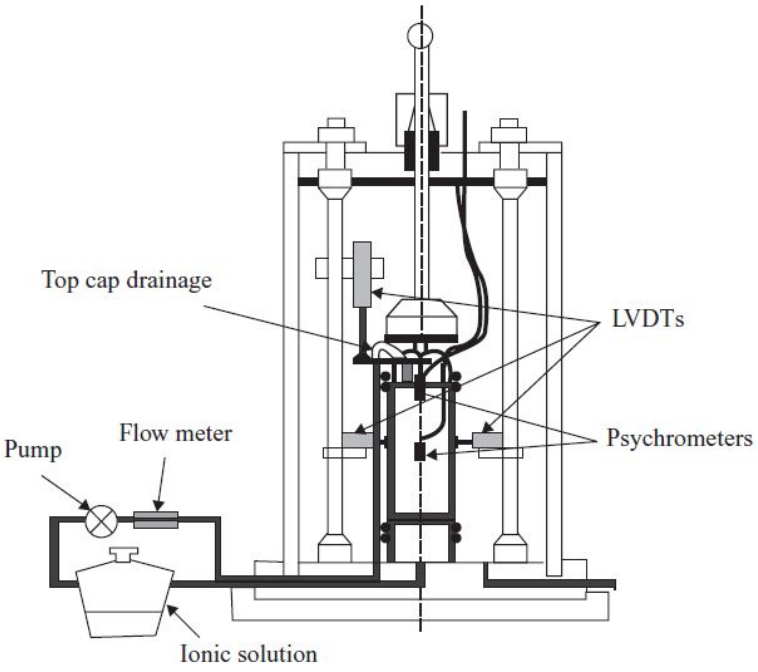

Figure 2.24 Suction control in triaxial apparatus via vapor equilibrium technique (after Blatz et al., 2000)

Cunningham et al. (2003) integrated a technique of controlling suction in a triaxial cell by means of air circulation through a porous stone at the bottom pedestal, in combination with independent suction measurement via suction probes. Non-oven geotextile strips were placed along the length of specimen to facilitate vapor circulation around the specimen. One issue with such methodology, adopted both by Blatz and Graham (2000), as well as Cunningham et al. (2003), is the presence of sensors inside the specimen, as well as the geotextile at the boundary of specimen, that may have a possible influence on overall mechanical response of the specimen.

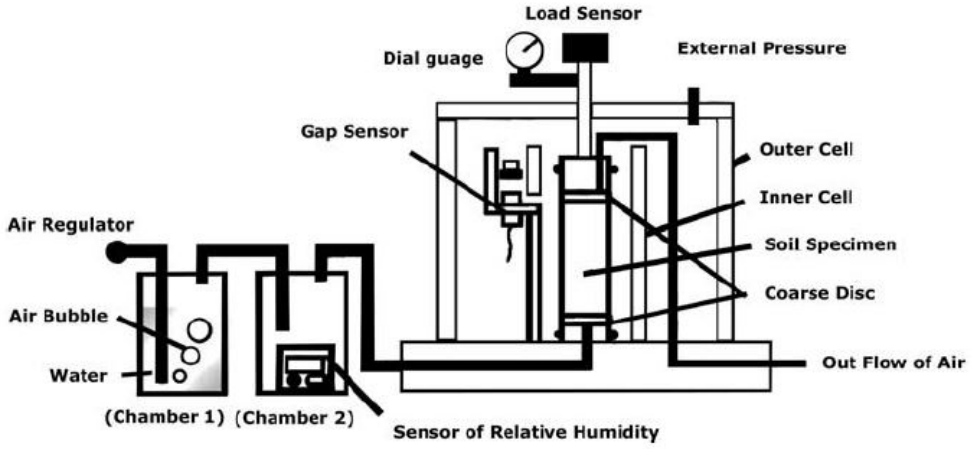

Figure 2.25 Triaxial equipment integrated with vapor equilibrium technique (after Nishimura and Fredlund, 2003)

Nishimura and Fredlund (2003), and later Nishimura and Vanapalli (2005) described the design details of the new triaxial equipment in which they controlled the relative humidity by using an air regulator and air bubbler system (Figure 2.25), along with an independent relative humidity sensor embedded in the circulation system, thus eliminating the limitations from the systems used by Blatz and Graham (2000) and Cunningham et al. (2003). Relative humidity inside the actual specimen was not directly

measured, but was dependent on the one measured from the influent stream. The authors did not mention the equilibration time in either of the references.

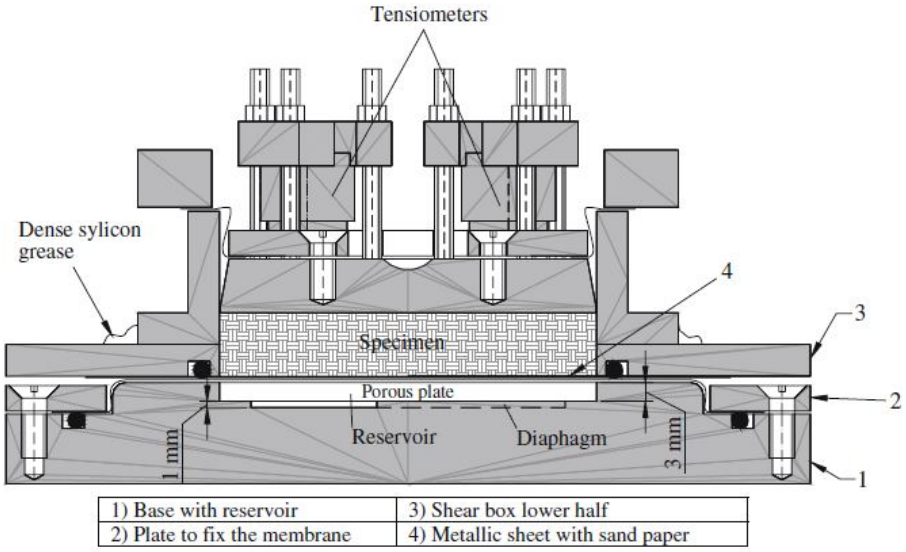

Figure 2.26 Direct shear apparatus modified to accommodate osmotic technique (after Boso.et al., 2005)

Boso et al. (2005) developed an alternative for investigation of unsaturated soils by modifying a conventional direct shear box to conduct suction controlled shear tests, using an osmotic technique under atmospheric pressure. The shear box was designed independently to measure as well as control suction. The details are shown in Figure 2.26. Suction was independently measured via two tensiometers fixed with small top caps clamped to the loading pad by means of three screws. The PEG solution was circulated from an independent reservoir to the specimen (with a semipermeable membrane separating solution and specimen), using two flexible tubes connected to shear box.

Hossain and Yin (2010) studied the dilative characteristics of an unsaturated compacted granite soil in direct shear test apparatus modified to apply and control matric

suction. They noticed that there existed some frictional resistance between the soil and side walls of the large shear box, causing reduction in dilation of soil, and, thereby, lowering the values of the measured dilation angles. These experimental dilation angles were further used to predict analytical shear strength response.

Hence, the analytical shear strength is lower than the experimental values, with the effect getting more pronounced with high suction and high net normal stress applied. The triaxial test equipment used in this research does not suffer from such limitations. The specimen has freedom to dilate isotropically/anisotropically in all directions, without boundary restrictions, giving more realistic dilation angles.

2.11.3.10 Strain rate selection for CD tests on unsaturated soils

The importance of assessment of a suitable loading rate during the shearing stage (henceforth called as shear rate), has long been well recognized, as it affects the strength, stiffness and volume change behavior of unsaturated soil specimens during triaxial testing. Effective strength parameters in geotechnical design are usually obtained via consolidated drained (CD) or consolidated undrained (CU) tests. Due to the growing evidence of the increase in strength due to matric suction, there is a need to modify the conventional triaxial test apparatus to accommodate both the unsaturated and saturated soil testing.

In unsaturated soil triaxial testing, the pore air and pore water pressures are controlled independently. CD tests are run at lower shear rate than the constant water content test (CW), CU or UU tests. These shearing rates should ensure proper equalization of pore pressure in the CW tests, while sufficient dissipation of pore water and pore air pressure is necessary for CD tests (Satija and Gulhati, 1979). Gibson and Henkel (1954) were among the first to extend the one-dimensional consolidation theory to the isotropic consolidation of saturated triaxial test and arrive at a theoretical model to

find the time to reach the failure in a CD test. However, applying these theories to the unsaturated soil is complicated because the permeability of the ceramic disk is low and, at the same time, the compressibility behavior of unsaturated soil involves compression of water, as well as the air phase.

The growing interest in the mechanical characterization of the unsaturated soil testing has encouraged the researchers to propose numerous approaches to determine the appropriate shear rate. Bishop et al. (1960) recommended that the procedure for selecting the shear rate for saturated soils be used for unsaturated soils too. However, the value of the coefficient of consolidation C_v should be obtained from the actual constant-suction isotropic consolidation of the specimen, with a ceramic disk, at the bottom, separating the pore water and pore air pressures via the axis-translation technique.

They also recommended that such a shear rate should be reduced by half for specimens with a low degree of saturation. The high air entry ceramic disk has low permeability and, hence, may impede the flow or dissipation of pore pressures, thereby governing the shear rate. Ho and Fredlund (1982) correlated the problem of impeded drainage due to the presence of the ceramic disk from an unsaturated soil with the impedance type factor given as below:

$$\lambda = \frac{(k_d h')}{(k_w h_d)} \tag{2.27}$$

Where λ = impedance factor; h' = length of the drainage path; k_d = coefficient of permeability of high air entry disk.

Also,

$$k_w = k_{sat} \left[\frac{(S - S_r)}{(1.0 - S_r)}\right]^4 \times 100 \tag{2.28}$$

where, k_w = coefficient of permeability with respect to the water phase at any degree of saturation; S = degree of saturation; S_r = residual degree of saturation; and k_{sat} = saturated coefficient of permeability.

Major highlights of the parametric study of Ho and Fredlund (1982) include, first, the decrease in the coefficient of permeability by three to four orders of magnitude and the corresponding reduction in the coefficient of consolidation due to desaturation i.e. imposing of matric suction. The second is the dominant influence of reduced coefficient of permeability of the ceramic disk on time to reach failure and some delay in testing time, with an increase in thickness of ceramic disk.

Nonetheless, the available literature does not undermine the importance of testing actual soil empirically to arrive at the suitable strain-rate that could further reduce the testing times, and ensure the adequate dissipation of pore air and pore water pressure, thus minimizing its influence on shear-induced stress-strain and volume change behavior. Separate studies were performed in this research to determine the appropriate shear rate for CD unsaturated soil triaxial testing.

2.11.4 Shear Strength Equations

2.11.4.1 Effective stress approach

2.11.4.1.1 Effective stress for saturated soil

The total normal stress on any plane may be decomposed into two components; the stress carried by the solid particles and the pressure of the fluid in the void space. The shear stresses are carried only by the skeleton of solid particles, except at very high rates of strain (Bishop et al., 1960). Effective stress represents that part of the total stress which produces measurable effects, such as compaction, or an increase in shearing resistance (Terzaghi, 1943). Hence, the concept of effective stress is the most significant principle in geotechnical engineering (Head, 1998).

For saturated soils, it can be expressed mathematically as the difference between total stress σ and pore-water pressure u_w (Terzaghi, 1936). Such an effective stress (Equation 2.29), suitably captures the macroscopic stresses defined at the boundary, treating the soil-water system as an equivalent continuum medium (Lu and Likos, 2006).

$$\sigma' = \sigma - u_w \tag{2.29}$$

The shear strength can be expressed by classical Mohr-Coulomb Equation 2.30.

$$\tau_f = c' + \sigma' tan\varphi' \tag{2.30}$$

Where c' = effective cohesion intercept; and ϕ' = effective angle of internal friction.

2.11.4.1.2 Effective stress for unsaturated soil

Early classical studies on unsaturated soils have revealed that the definition of effective stress should also incorporate the effect of capillary forces (Bishop, 1959; Lambe and Whitman, 1969; Mitchell, 1976). There are three macroscopic approaches for describing the state of stress in unsaturated soil: The modified effective stress approach (Bishop, 1959), the independent stress state variable approach (Fredlund and Morgenstern, 1977), and modified stress-variable approaches adopted by numerous researchers for stress-strain analysis (Matyas and Radhakrishna, 1968; Alonso et al., 1990; Gallipoli et al., 2003; Houlsby, 1997; Lu and Likos, 2006).

2.11.4.2 Bishop's effective stress approach

Bishop suggested that special treatment be given to the definition for effective stress in unsaturated soils due to the presence of two fluids (i.e. water and air) in the pore space, which may be, in equilibrium, at a pressure which differs considerably due to surface tension (Bishop et al., 1960). It is also called a single stress state approach. Bishop (1959) modified effective stress from its original form (Terzaghi, 1936) by using

the independent state variable that combined net normal stress, $\sigma - u_a$ and matric suction, $u_a - u_w$ and introduced one material variable, "the effective stress parameter," χ, as shown by Equation 2.31 to account for capillary forces.

$$\sigma' = (\sigma - u_a) + \chi(u_a - u_w)_f \tag{2.31}$$

χ is considered to vary between zero (representing completely dry state) and unity (representing full saturation state) as a function of degree of saturation. The term $\chi(u_a - u_w)$ represents the contribution of matric suction to effective stress. Under completely saturated conditions, Equation 2.31 reduces to Equation 2.29, thus describing the macroscopic behavior of unsaturated soil within the established framework of saturated soil mechanics. The classical Mohr-Coulomb failure criterion can be now extended to express shear strength by Equation 2.32.

$$\tau_f = c' + \left[(\sigma - u_a)_f + \chi_f(u_a - u_w)_f\right] tan\varphi' \tag{2.32}$$

Where c' = effective cohesion intercept; and ϕ' = effective angle of internal friction.

In typical UNSAT triaxial test conditions, χ can be expressed, after few manipulations by Equation 2.33.

$$\chi_f = \frac{(\sigma_1 - u_a)_f - (\sigma_3 - u_a)_f tan^2\left(\frac{\pi}{4} + \frac{\varphi'}{2}\right) - 2c'\tan\left(\frac{\pi}{4} + \frac{\varphi'}{2}\right)}{2(u_a - u_w)_f \tan\left(\frac{\pi}{4} + \frac{\varphi'}{2}\right) tan\varphi'} \tag{2.33}$$

Jennings and Burland (1962) studied the effective stresses in partly saturated soils via experiments and pointed out that Equation 2.31 fails to explain the volume change behavior due to the wetting-induced collapse phenomenon. They demonstrated that suction within the pore water and external stress applied to the boundary of a soil element act in qualitatively different ways within the soil skeleton.

Matyas and Radhakrishna (1968) confirmed these findings through a series of suction-controlled consolidation tests. Hence, it would be inappropriate to combine both external stress and matric suction into a single effective stress to assess the volume change behavior of unsaturated soils. It was also realized that values of χ are different when determined for shear strength and volume change (Jennings and Burland, 1962). Furthermore, the experimental verification of non-uniqueness of $\chi = f(S)$, as well as the difficulties associated with experimental or theoretical determination of the effective stress parameter χ, have limited Bishop's approach applicability in research and practice (Lu and Likos, 2006).

2.11.4.3 Independent two-stress-state variable approach

The limitations encountered in Bishop's single stress state approach paved the way to consider a two-stress-state variable approach to treat net normal stress $(\sigma - u_a)$ and matric suction $(u_a - u_w)$ as independent stress state variables in assessment of their role in the mechanical response of unsaturated soil (Fredlund and Morgenstern, 1977). The independent stress-state variable separates the effect due to changes in normal stress from those due to change in pore-water pressure. They express the shear strength by formulating extended Mohr's-Coulomb criteria as given in Equation 2.34.

$$\tau_f = c' + (\sigma - u_a)_f tan\varphi' + (u_a - u_w)_f tan\varphi^b \quad (2.34)$$

Where τ_f = shear strength at failure, c', is the effective cohesion, and it represents the shearing resistance arising from interparticle physicochemical forces such as van der Waals attraction, φ' is the effective friction angle associated with net normal stress $(\sigma - u_a)_f$ on the failure plane at failure, respectively.

φ^b is an additional friction angle that captures the contribution of matric suction to shear strength. Initially, Fredlund et al. (1987) treated φ^b as constant (due to limited published literature) for a particular soil, which means that, with an increase in suction,

the strength of soil increases infinitely. Subsequently, it became clear, through further experiments conducted over a large range of suction values, that the value of φ^b tends to decrease with an increase in suction (Escario and Saez, 1986; Gan et al., 1988). It was observed that the value of φ^b is equal to ϕ' up to the air entry value; thereafter, it starts to decrease. Equation 2.34 can further be modified as Equation 2.35.

$$\tau_f = c' + c'' + (\sigma - u_a)tan\varphi' \tag{2.35}$$

c'' is defined as the capillary cohesion describing shearing resistance arising from capillarity effects given by equation 2.36.

$$\tau_{us} = c^{''} = (u_a - u_w)_f tan\varphi^b \tag{2.36}$$

$$Thus, c_1 = Total\ apparent\ cohesion = c' + c'' \tag{2.37}$$

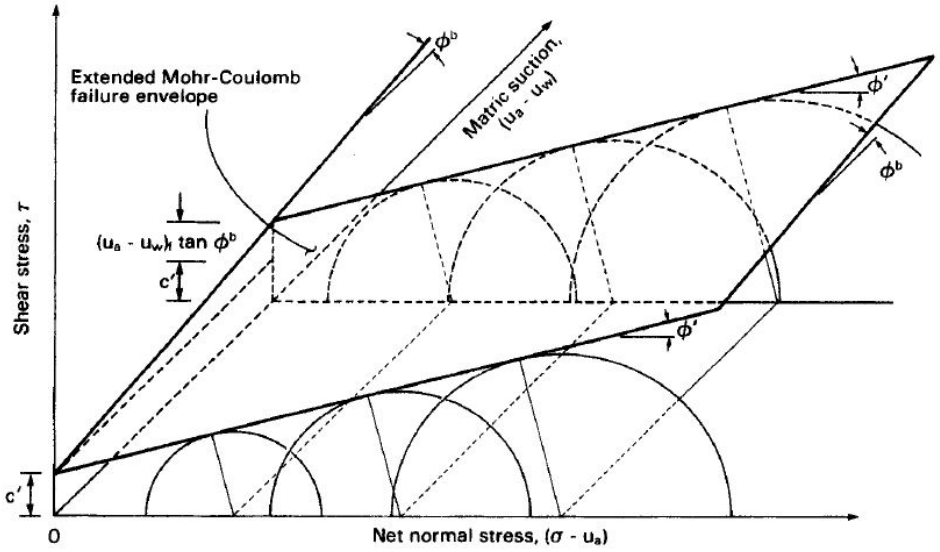

Figure 2.27 Mohr-Coulomb failure envelope extended to unsaturated soils using independent two-stress-state variable theory (After Fredlund and Morgenstern, 1977; Fredlund and Rahardjo, 1993)

Figure 2.27 clearly illustrates the translation of Mohr's circle along the suction axis, accompanied by an increase in size for unsaturated soils as compared to saturated

soils. Also, the intersection of the failure plane with the shear stress axis gives intercept (apparent cohesion), that tend to increase as soil becomes unsaturated from its initial saturated state. If a series of suction-controlled tests are conducted at different matric suction levels, one can obtain the failure envelope and its evolution.

2.11.4.4 Alternative stress strain approaches in soil modeling

Following the theoretical frameworks proposed by Bishop (1959), as well as Fredlund and Morgenstern (1977), numerous researchers have tried alternative approaches to analyzing unsaturated soil behavior using modified stress variables, especially in developing elasto-plastic models that could incorporate suction effects separately in calculating volumetric strains (Alonso et al., 1990; Wheeler and Sivakumar, 1995; Houlsby, 1997; Gallipoli et al., 2003; Datcheva and Schanz, 2003; Khalili et al., 2005; Russell and Khalili, 2006; Yang et al., 2008; Morvan, 2010).

Lu and Likos (2006) conceptually lumped the van der Waals forces, electrical double-layer forces, cementation forces, surface tension forces, and forces arising from negative pore water pressure, into a macroscopic stress referred to as “suction stress” to demonstrate the suitability of using the suction stress characteristic curve (SSCC) for unsaturated soil. Some of these approaches will be discussed in Chapter 5 while dealing with soil modeling.

2.11.5 Shear Strength based on SWCC Models

The framework proposed by Bishop (1959) and Fredlund and Morgenstern (1977) require expensive, time consuming experimental studies to determine the shear strength of unsaturated soils. In an effort to make the process cost-effective, several researchers used SWCC as an interpretative tool, along with the saturated shear strength parameters, c' and ϕ' to develop predictive shear strength equations or models (Vanapalli et al., 1996; Fredlund et al., 1996; Oberg and Sallfors, 1997; Khalili and Khabbaz, 1998

and Bao et al., 1998). As the matric suction increases, the wetted area of contact between soil particles decreases, and vice versa. There exists a non-linear relationship between the soil-water characteristic curves and the shear strength of soil as it changes its phase from saturated to unsaturated state (Vanapalli et al., 1996).

2.11.5.1 Shear strength model by Vanapalli and Fredlund (1996)

Vanapalli and Fredlund (1996) proposed a nonlinear function for predicting the shear strength of unsaturated soil, utilizing the entire soil-water characteristic curve with suction between 0 to 1000,000 kPa along with saturated shear strength parameters, c' and ϕ', as shown in Equation 2.38. They also suggested the use of Fredlund's and Xing's (1994) equation to plot the best fitting SWCC curve through experimental points.

$$\tau_f = c' + (\sigma - u_a)\, tan\varphi' + [(u_a - u_w)\, \{(\Theta^{\kappa})(tan\varphi')\}] \quad (2.38)$$

Where, κ = fitting parameter used for obtaining best-fit between the measured and predicted values.

Θ = normalized water content = θ_w/θ_s

Second part of the Equation 2.38 represents the shear strength contribution, τ_{us}.

$$\tau_{us} = [(u_a - u_w)\, \{(\Theta^{\kappa})(tan\varphi')\}] \quad (2.39)$$

Equation 2.38 also yields the same results if written in terms of degree of saturation, S, or gravimetric water content, w, to predict the shear strength. A comparison was made with solutions from Equation 2.38 by Fredlund and Morgenstern (1977) using experimental values of φ^b obtained for three types of soils such as Madrid gray clay, red silty clay and Madrid clay sand. It was observed that the shear strength in the boundary effect zone was similar to the saturated soil since $tan\phi'$ is same as $tan\ \varphi^b$ in this zone, thus allowing the soil to be treated as saturated in the boundary effect zone. In the transition zone, the contribution of $tan\ \varphi^b$ was less than $tan\phi'$; hence, the shear strength

variation was non-linear in the transition zone. The shear strength dropped gradually as suction was further increased in the residual suction zone.

2.11.5.1 Shear strength model by Vanapalli et al. (1996)

Vanapalli et al. (1996) proposed the predictive model, eliminating the use of a fitting parameter κ as given by Equation 2.40.

$$\tau_f = c' + (\sigma_n - u_a)tan\varphi' + (u_a - u_w)\left[\left(\frac{\theta_w - \theta_r}{\theta_s - \theta_r}\right)tan\emptyset'\right] \quad (2.40)$$

Where, θ_w = volumetric water content, θ_w = saturated volumetric water content and θ_r = residual volumetric water content that can be estimated from the soil water characteristic curve, using the graphical method, as explained in Section 2.5. Similar results were obtained while using the degree of saturation (S) or gravimetric water content instead of volumetric water content in Equation 2.40. Both Equation 2.38 and 2.40 are consistent with the stress-state variable approach and satisfy the continuum mechanics concept.

2.11.5.2 Shear strength model by Oberg and Sallfors (1997)

Oberg and Sallfors (1997) suggested a one-to-one relationship between the degree of saturation (S) and the area of water contact along the shear plane in the soil. They expressed shear strength of non-clayey soils such as sands and silts, through Equation 2.41.

$$\tau_f = c' + (\sigma_n - u_a)tan\varphi' + (u_a - u_w)[(S)tan\emptyset'] \quad (2.41)$$

Although Equation 2.41 was not verified experimentally by Oberg and Sallfors (1997), it was later verified by Vanapalli and Fredlund (2000).

2.11.5.3 Shear Strength Model by Khalili and Khabbaz (1998)

Khalili and Khabbaz (1998) extended Bishop's (1959) equation by introducing an empirical constant χ as expressed in Equation 2.42.

$$\chi = \left[\frac{(u_a - u_w)_f}{(u_a - u_w)_b}\right]^{-0.55} \quad (2.42)$$

Where, $(u_a - u_w)_f$ = matric suction in the specimen at failure condition, $(u_a - u_w)_b$ = air entry value suction of soil. Published data, based on 13 soils, indicates that, the value of -0.55 best fits the equation over a wider range. In addition, the air entry suction value is needed along with saturated strength parameters to predict the shear strength using Equation 2.43.

$$\tau_f = c' + (\sigma_n - u_a)tan\varphi' + (u_a - u_w)\left[\left\{\frac{(u_a - u_w)_f}{(u_a - u_w)_b}\right\}^{-0.55} tan\emptyset'\right] \quad (2.43)$$

2.11.5.4 Shear strength model by Bao et al. (1998)

Bao et al. (1998) predicted shear strength of unsaturated soil by introducing parameters ξ and ζ along with saturated strength parameters using extension of Fredlund's and Morgenstern's (1977) approach, as expressed by Equation 2.44.

$$\tau_f = c' + (\sigma_n - u_a)tan\varphi' + (u_a - u_w)[\xi - \zeta \log(u_a - u_w)]tan\emptyset'] \quad (2.44)$$

Where,

$$\xi = \frac{\log(u_a - u_w)}{\log(u_a - u_w)_r - \log(u_a - u_w)_b}\ ; \qquad \zeta = \frac{1}{\log(u_a - u_w)_r - \log(u_a - u_w)_b} \quad (2.45)$$

The parameter, ξ, represents the intercept, and the parameter, ζ represents the slope of the linear part of the soil-water characteristic curve, respectively. Bao et al. (1998) suggested the use of Equation 2.46 to fit the soil-water characteristic curve data.

$$\left(\frac{\theta_w - \theta_s}{\theta_s - \theta_r}\right) = \xi - \zeta \log(u_a - u_w) \quad (2.46)$$

2.12 Summary

This chapter presents properties related to unsaturated soils. In general, the importance of appreciating the role of soil suction, capillarity, soil water characteristic

curves, air entry value of soil, residual soil suction, possible pore water states and the hydraulic hysteresis in characterization of unsaturated soil is discussed.

Also, discussed are several direct suction measurement methods, several mathematical models that help in the continuous prediction of SWCC over the entire range of soil suction, methods to impose matric suction (i.e. axis-translation technique), methods to impose total suction (i.e. osmotic and vapor pressure techniques), a review pertaining to the role of appropriate shear rate selection for CD tests on unsaturated soils, various shear strength equations, and models based on SWCC to predict shear strength. This chapter is also devoted to providing a summary of recent, as well as past, advances in triaxial test equipment for the purpose of studying the behavior of unsaturated soil's hydro-mechanical response.

Chapter 3

Triaxial Test Results at Low to Medium Matric Suction States

3.1 Introduction and General Properties of Test Soil

This chapter describes the experimental program undertaken to characterize the unsaturated silty sand in low-to-medium matric suction range used in this research. It also presents an analysis of the test results. Basic soil tests, such as mechanical sieve and hydrometer analysis, were first performed. The test soil was classified as silty sand (SM) as per the Unified Soil Classification system (USCS). The grain size distribution curve for the silty sand is shown in Figure 3.1. The specific gravity test was conducted to obtain the specific gravity of the soil solids. Atterberg limit tests conducted on the passing # 4 fraction classified the soil as non-plastic. The results of the standard proctor test (see Figure 3.2) on the soil indicated a maximum dry density of 1.87 g/cm^3 at an optimum water content of 12.2%. Basic soil properties are summarized in Table 3.1.

Table 3.1 Soil properties and grain sizes of silty sand

Sand (%)	55
Silt (%)	37
Clay (%)	8
Specific gravity, G_s	2.67
USCS classification	Silty sand (SM)
Maximum dry unit weight, ρ_{dmax} (g/cm^3)	1.87
Optimum moisture content, w (%)	12.2

3.2 Specimen Preparation

Undisturbed field samples that represent better in-situ conditions may be obtained for triaxial testing, using sampling tubes trimmed to the required size, or remolded specimens that can be prepared in the laboratory. Difficulties arise with procuring undisturbed samples because they may shrink upon loss of moisture, may have stones/vegetative cover and may be heterogeneous in nature. These conditions

may result in uneven stress distributions and pore pressures within the soil specimen while testing, thereby altering the triaxial response. Wulfsohn et al. (1998) pointed out that remolded specimens are used for fundamental, theoretically-based investigations into the nature of soil behavior, while undisturbed specimens are used when comparing model predictions with field data, or when evaluating the natural variability of soil properties.

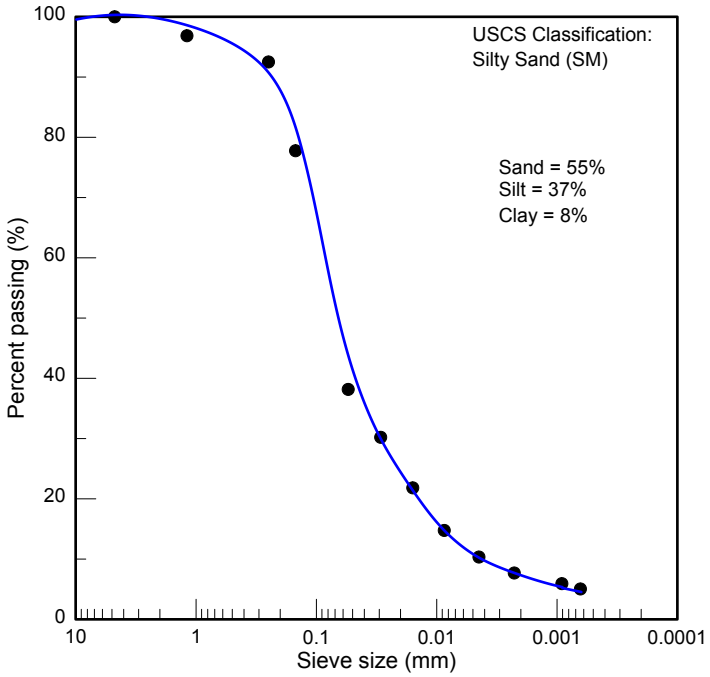

Figure 3.1 Particle size distribution curve of test soil

The laboratory method of compaction influences the soil fabric, and, therefore, the test response. Remolded specimens can be prepared by compaction of a soil sample by mixing it with the desired moisture content to its target density by static, dynamic or tamping (kneading) compaction methods, depending upon the soil type, purpose of the test, and desired initial structure. Compaction induces complex structure and stress history to the soil specimen and, therefore, makes it difficult to isolate the fundamental behavior affecting the shear strength component related to matric suction, as well as

identify whether a true critical state has been reached upon shearing (Wheeler and Sivakumar, 1995; Mancuso et al., 2000; Wang et al., 2001).

The applied compaction effort/energy produces specimens with different pore sizes, and, hence, creates different structures. Thus, the suction behavior of the same soil with differently applied energy will vary (Vanapalli et al., 1999; Miller et al., 2002). One way to produce specimens with simple soil fabric and the least complex stress history is to prepare them by gradually consolidating an initially slurried soil. Wang et al. (2001) used such soil specimens to perform suction-controlled triaxial shear tests on unsaturated "Botkin silt" to study the unsaturated soil response. The specimens should be "identical" in order to obtain the shear strength parameters or compare the shear/consolidation test results. "Identical" specimens mean they are compacted at the same initial water content and bulk density, using the same compaction method.

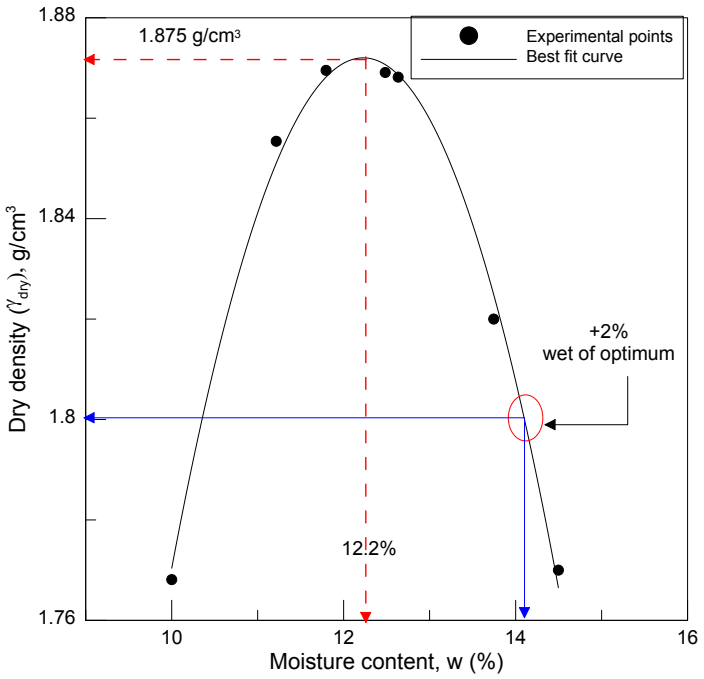

Figure 3.2 Standard proctor curve for test soil (silty sand)

3.2.1 Specimen Dimensions

The specimen should be prepared of appropriate size. The diameter and height should be chosen such that the experimental stress-strain and volume change obtained reflects the true representation of soil behavior. ASTM D7181-11 standard calls for minimum diameter to be 33 mm (1.3 in.), the average height to average diameter ratio be between 2 and 2.5, and the largest particle size to be smaller than 1/6 the specimen diameter.

3.2.1.1 Specimen diameter

Usually, the specimen diameter (D) is related to the maximum size of the particle d_{max} of the soil. Researchers in the past have studied the effect of the ratio $D/D/d_{max}$, either by changing the specimen diameter for one soil gradation or by changing d_{max} and keeping D constant, and finding the minimum D/d_{max} ratio at which the change in strength is negligible. Based on his studies, Holtz and Gibbs (1956) proposed $D/D/d_{max}$ to be 4.3 or more for soils containing 20% gravel, and 8.0 or more for soils containing 50% gravel. The soil used in this research had maximum particle soil size as that of sand (2 mm). The diameter chosen was 71.12 mm (2.8 in.), and therefore the D/d_{max} was far greater than 6.0, as recommended by ASTM D7181-11. Considering the suggestion by Holtz and Gibbs (1956) and ASTM D7181-11, the chosen diameter of specimen is considered to be appropriate.

3.2.1.2 Specimen height

The restriction imposed on the length-to diameter ratio (L/D) is usually imposed to minimize the end effects due to the end platens of the apparatus and to reduce the likelihood of buckling during testing (Bishop and Green, 1965; Scott and Ko, 1970). End effects are due to friction developed between the ends of the soil specimen and the top cap and base pedestal. They prevent the soil from freely moving outwards and induce a

shear stress on the ends of the specimen. Thus, the stress conditions and strains developed are no longer uniform and cause errors in interpretation of test results.

During the shear stage, the silty sand used in this study tended to form barrel-shape shear bands/bulging due to the formation of dilating and dead zones similar to the one proposed by Kirkpatrick and Younger (1970) and Salman (1995), as illustrated in Figure 3.3; therefore, it showed non-uniform deformations along its height. Figure 3.3 shows shear zones formed due to the non-uniform (barrel shape) deformation caused by shear-induced dilation. Figure 3.3a shows a photograph of an actual specimen with dilating shear bands, with localized dilation at about the center (after test) due to the end effect (from CD100-250 test). Figure 3.3b shows theoretical shear bands at failure as explained by Kirkpatrick and Younger (1970) and Salman (1995).

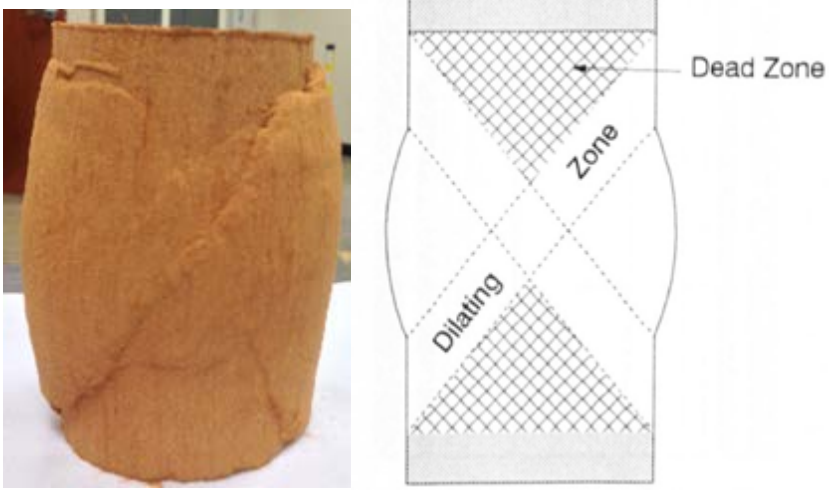

Figure 3.3 Distinct shear zones: a) actual specimen showing shear bands with localized dilation b) Theoretical shear bands at failure (Kirkpatrick and Younger, 1970; Salman, 1995)

The specimens in their studies were subjected to deform uniformly by providing one or multiple layers of the rubber membrane disc with silicon grease in between.

However, such method was avoided in this study as it might affect the peak strength and volume change (as recommended through CD triaxial test studies by Bishop and Green, 1965; Lee, 1978). It was thought that the silicon grease might ooze into porous soil during long term unsaturated soil testing, hinder air pressure application through top cap, introduce bedding errors between the specimen and the top cap and the base pedestal, and may even induce the slip in the lubricant.

Despite efforts being made by researchers, it is practically impossible to impose boundary conditions that might result in perfectly uniform stress-strain during experiments. Some studies indicate that the end effects can be minimized by keeping the specimen height to diameter ratio greater than two (2). As suggested by ASTM D7181-11, the average height-to-average diameter ratio was selected to be two (2) throughout the testing program, with height as 142.24 mm (5.6 in.) and diameter as 71.12 mm (2.8 in.).

3.2.2 Specimen Preparation Technique

According to Sivakumar and Wheeler (2000), the use of various compaction procedures produces entirely different soil fabrics and, hence, impact its subsequent mechanical behavior, so that some or all of the soil constants in an elasto-plastic model (such as slope of the normal compression line (λ_s), and elastic swelling index (κ) as proposed by Alonso et al., 1995) take different values, depending on the compaction method. Therefore it is crucial to mention the compaction method used to prepare the test specimen. Different methods of compaction are used by various researchers such as static, dynamic, moist tamping, and dry/wet depositional method. The static compaction procedure followed in this research is explained as below:

The soil was first thoroughly dry mixed and later hand-mixed with distilled water at a slightly high water content of 14.2% (2% more than the optimum water content as

determined by the standard compaction test). It was then sealed in airtight ziplock bags in nine equal parts. These nine sealed bags were then sealed in a plastic container and kept in a 100% humidity chamber for at least 24 hours (see Figure 3.4a and b).

All specimens (both for saturated, as well as unsaturated triaxial tests) were prepared by static compaction, using the stress-based approach, as explained by Cui and Delage (1996). They noted that the stress-based criterion is more consistent with the field compaction conditions where a constant compaction effort is applied regardless of strains that are induced. Its importance in better understanding compaction stresses and, hence, the yield stress generated during static compaction is well acknowledged by several authors (Blatz et al., 2002, Estabragh et al., 2004).

The preparation of an identical test specimen is crucial for comparison of stress-strain and volume change curves at different speeds. Toll (1990, 2000 and 2003) explained the importance of compaction of the specimens on the wet side of optimum (high degree of saturation). Compacting soil specimens on the dry side of optimum, results in an aggregated fabric (especially when silt is present in appreciable amount) that can be maintained during shearing due to the suction that provides additional strength to the aggregations. This affects the critical state behavior, as the particles, instead of sliding tend to roll up over each other, exhibiting a dilational behavior. However, the samples compacted on the wet side of the optimum, i.e. high degree of saturation are not expected to have aggregated fabric.

Attempts were made to prepare specimens by statically compacting them in one, three, eight and nine equal layers in a compaction mold at a displacement rate of 1.5 mm/min as well as 1 mm/min, and subjecting each layer to a maximum vertical total stress of 1200, 1400 and 1600 kPa, using a 50 kN triaxial frame. The test results showed that the target dry density was achieved only when the specimen was prepared in nine

layers, each layer compressed at 1 mm/min and subjected to total vertical stress of 1600 kpa.

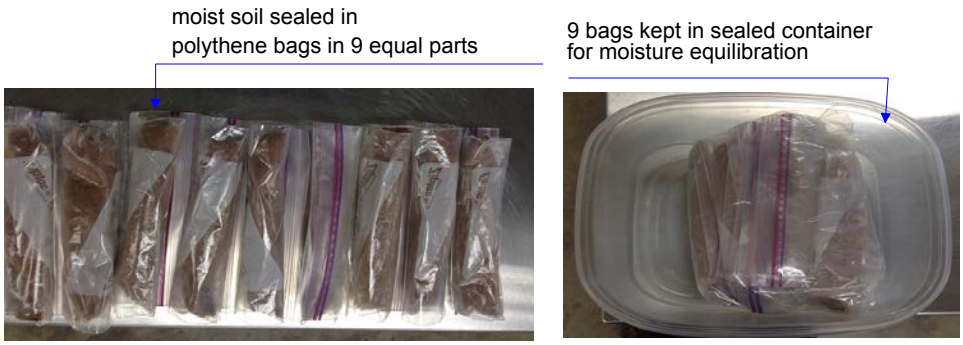

Figure 3.4 Soil storage for moisture equilibration prior to compaction

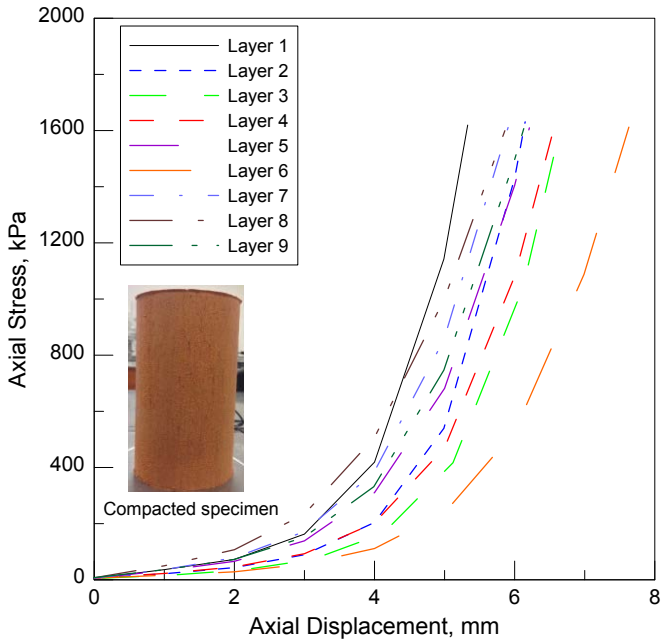

Figure 3.5 Compression curves for each of the 9 layers during static compaction

The matric suction obtained from the soil-water characteristic curve (see Figure 3.7) corresponding to the water content at “as compacted condition” is approximately 10 kPa (just beyond the air entry value of soil), with a degree of saturation about 81%. The

specimens yielded an initial voids ratio between 0.46 to 0.49. The convention used here to designate the specimen is $CD_{x\text{-}y}$ where "CD" denotes the consolidated drained test; "x" represents the net confining pressure $(\sigma_3\text{-}u_a)$, while "y" represents the imposed constant matric suction $(u_a\text{-}u_w)$.

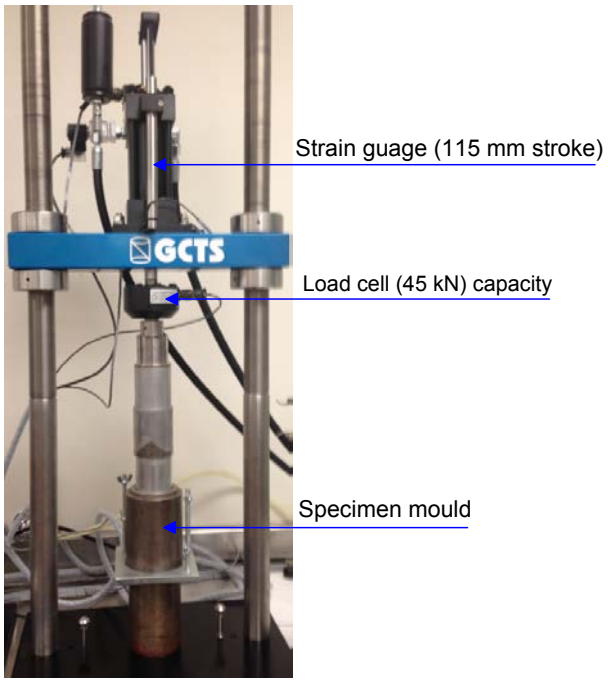

Figure 3.6 Static compaction set up

3.2.3 Soil-Water Characteristic Curve

The Fredlund's device, also called "Tempe-cell," was used to prepare the soil water characteristic curve up to 500 kPa of matric suction. Dry silty sand soil was mixed with 14.2% of distilled water (+2% on the wet of optimum moisture content) to produce a specimen of appropriate size (2 in. diameter and 1 in. height) encased in a ring by a static compaction method in one lift to produce the target density (1.87 g/cm^3). The specimen, along with a ring, was mounted inside the small mold with a set of porous stones at the top and bottom.

The entire assembly was then slowly submerged in a small reservoir filled with distilled water. The specimen was allowed to take in water through a porous stone at its bottom to upside so that no air remained trapped inside the specimen. Finally, the specimen was submerged completely in water and allowed to get soaked for at least 24 hours. The specimen was then removed from the assembly and weighed as quickly as possible.

Figure 3.7 Fredlund's device (Tempe cell) for SWCC measurements

The ceramic disk (5 bar capacity) was initially submerged in distilled water and quickly installed in a recess at the bottom of the device that was already filled with distilled and de-aired water. The fully saturated specimen was mounted on the saturated ceramic disk with good contact, and the Tempe cell was re-assembled. The water reservoir beneath the ceramic disk was connected with two graduated burettes that were open to the atmosphere, as shown in Figure 3.7.

Appropriate air pressure was applied, through a regulator, inside the tempe cell and, therefore, to the top of the specimen. Since the pore-water inside the specimen and

the water in the reservoir were connected through saturated ceramic disk, the pore water pressure inside the specimen was atmospheric. Any applied air pressure corresponded to the matric suction i.e. $u_a - u_w$, imposed inside the specimen. Thus, the Axis-translation technique was used to measure and control the matric suction. A photograph of the actual setup is shown in Figure 3.7

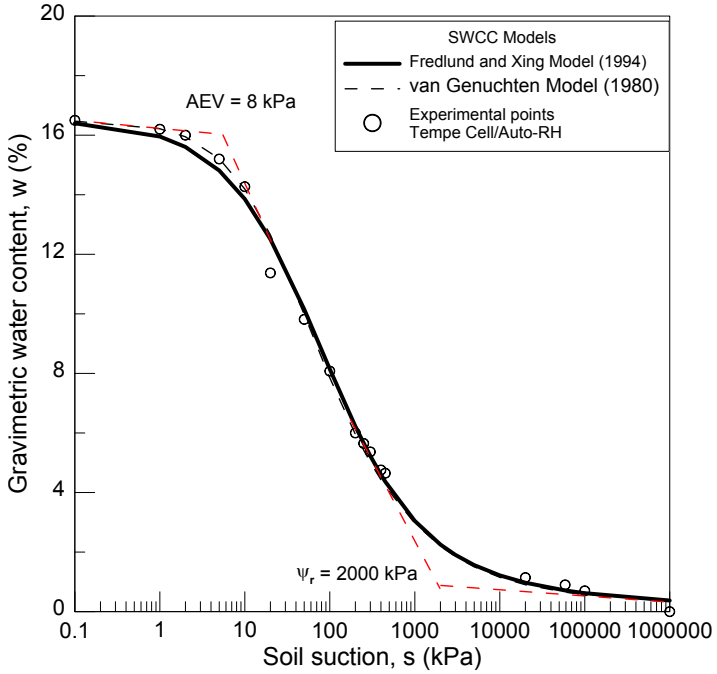

Figure 3.8 Soil-water characteristic curve for silty sand (SM)

As the specimen de-saturated, the water level in the burette was monitored periodically until equilibrium (i.e. no water flow condition), was reached to calculate the water content corresponding to the matric suction applied. Subsequently, the matric suction was increased, and the procedure was repeated to complete the curve up to the potential of the ceramic disk.

In this research, the specimen was removed after equilibrium at each matric suction applied, and its water content was determined. The next level of matric suction was then applied using new specimen that had same initial conditions. Thus, one point

on the SWCC represents one test. The soil water characteristic curve obtained is as shown in Figure 3.8. The total suction points in the high suction range were obtained by using a relative-humidity apparatus that is described and explained later in Chapter 4.

Table 3.2 Fitted parameters for selected SWCC functions

Van Genuchten (1980) Equation 2.7	Fredlund and Xing (1994) Equation 2.8
$\alpha = 0.036$	$\alpha = 55$
$n = 1$	$n = 0.75$
$m = 0.5$	$m = 1.9$
$\theta_r = 0.3$	$\theta_s = 16.5$
$\theta_s = 16.5$	$\Psi_r = 2000$ kPa

Popular SWCC models such as Fredlund and Xing (1994) and van Genuchten (1980) were used to best fit the experimental points in order to complete the characteristic curve over the entire range from 0-10,000 MPa soil suction. The best fitting parameters are summarized in Table 3.2.

3.3 Triaxial Testing Equipment Setup

3.3.1 Modifications to Conventional Apparatus

The conventional triaxial test set up needed to be modified to accommodate unsaturated soil testing. This included modifications to the base pedestal, attachment of flushing assembly, and the air pressure supply arrangement. These are explained in the following sections.

3.3.1.1 Base-pedestal modifications to implement axis-translation technique

Imposing negative pore water pressures in excess of 100 kpa causes cavitation issues and, hence, errors in measurement of matric suction. To avoid this, the axis-translation technique, as suggested by Hilf (1956) is widely used in modified triaxial test apparatus to control matric suction in laboratory soil specimens. Figure 3.9 shows the

modifications made to the base plate of the triaxial cell. It includes three high air entry value ceramic disks installed in the base pedestal while three low air entry value porous stones were installed in the top cap independently to control the pore water and pore-air pressures respectively.

The axis-translation technique consists of elevating the pore air pressure, u_a, above the atmospheric pressure to increase the pore water pressure, u_w, to be positive, thereby preventing cavitation and making the matric suction easily measurable (positive).

3.3.1.2 Saturation of ceramic disk

Saturation of the ceramic disk prior to using it is crucial. As illustrated in Figure 3.10, the cell was assembled and filled with water up to 2-3 cm above the top of ceramic disk.

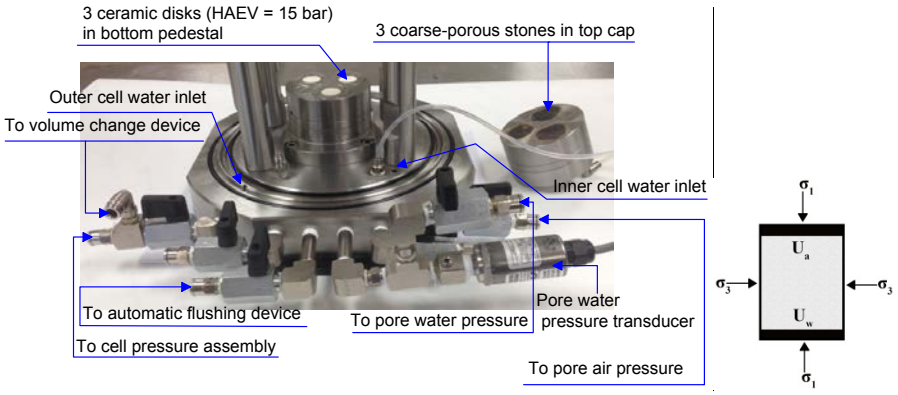

Figure 3.9 Base plate of triaxial cell modified to apply axis-translation technique

An air pressure of about 50 kPa was applied through the top for at least one day, and water was allowed to flow into the burette attached to the reservoir below ceramic disk.The burette was open to the atmosphere, so the water pressure was atmospheric. The permeability of the ceramic disk can also be calculated by measuring the volume of water with time under the differential pressure i.e. $u_a - u_w$. The dissolved air, if any, will diffuse through the disk into the bottom compartment. The accumulated air was flushed

using a syringe filled with distilled de-aired water into the burette, as shown in Figure 3.10. The ceramic disk was kept submerged under water until the specimen was ready to be mounted for the suction equalization stage.

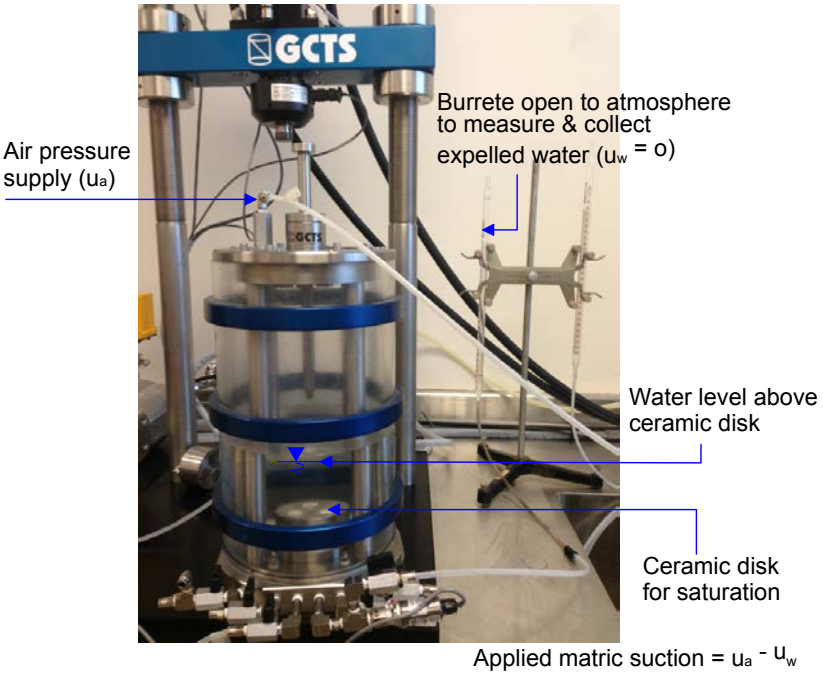

Figure 3.10 Set up for saturation of high air entry ceramic disk in triaxial cell prior to suction equalization.

The total suction is defined as the sum of matric suction (ψ_m) and osmotic suction ($\psi_{osmotic}$). The osmotic suction is affected by the changes in pore fluid salt concentration. The water used in lab testing was de-aired and distilled water; hence, the osmotic suction was fairly constant. Thus, any change in mechanical behavior of soil during testing was considered to be associated with matric suction variation alone (i.e. desaturation of specimen).

3.3.1.3 Double-walled triaxial cell and automatic volume change device

Single-walled triaxial cells have several disadvantages associated with cell liquid measurements such as the hysteresis exhibited by acrylic cell, immediate expansion of

cell wall due to pressure increase, Plexiglas creeps under constant stress and possible water leakage. If proper corrections are not applied (which involve careful calibration procedures), these errors may give misleading volume change measurements of the specimen.

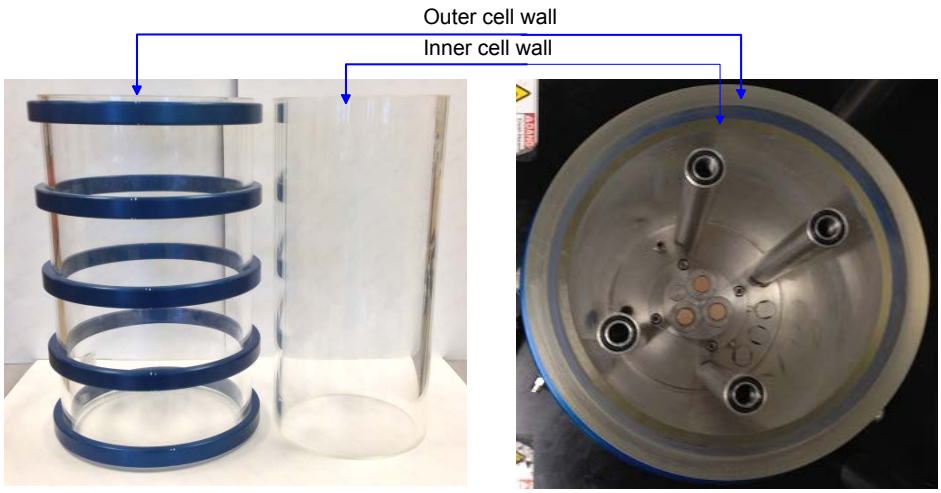

Figure 3.11 Double-walled triaxial cell

The double-walled triaxial cell system used in the current research, as shown in Figure 3.11, featured an inner cell wall subjected to identical internal and external pressures, thus avoiding the differential pressures and minimizing cell expansion and leakage problems. The pressure and flow of water to the cell was controlled by a cell pressure volume controller system. The total volume change of the specimen inside the inner cell was equivalent to the amount of water that moved to and from the inner cell into the outside chamber.

The total volume change of the specimen was monitored by a volume change device with a rolling diaphragm to minimize the sliding friction that occurs in conventional volume change devices. The overall combination of double-wall cell with volume change measuring device makes it a more sophisticated unit than a single walled triaxial cell. Precaution was taken to condition the inner cell by always keeping it submerged in water

tank when it wasn't in use to make sure that there was no further absorption of water from the cell during testing.

3.3.1.4 Flushing device

Even though, the ceramic disk is initially saturated, air diffuses through it into the reservoir beneath it in response to an air concentration gradient (Fredlund and Rahardjo, 1993). A concentration gradient is created due to the difference in density between free air and the dissolved air in the water that causes diffusion of air through water. Similarly, when the high air entry value ceramic disks are used, the air dissolves in water in the disk and eventually comes out of solution causing diffusion of air.

This diffused air accumulates in the water compartment beneath the disk (Padilla et al., 2006). This hinders the equilibrating water flow to and from the specimen, reduces the hydraulic conductivity of the ceramic disk causing delay in suction equalization time during drained test, and induces errors in volume change measurements. Air diffusion through the ceramic disk can even exceed the total volume of water in the specimen, especially due to long-term testing conditions during drained triaxial testing (Fredlund and Rahardjo, 1993).

Similarly, during undrained tests, the accumulation of diffused air, in an appreciable amount, beneath the ceramic disk may give misleading pore-water pressure measurements, hence errors in matric suction measurement. Due to these reasons, it becomes essential to flush the accumulated air completely and periodically from beneath the water reservoir connected to the saturated back water pressure line.

A diffused-air flushing device was used in this research for flushing purposes. The device has differential pressure transducer, computer-controlled ball valve and water reservoir with level sensor. The differential pressure transducer has a range of 7 kPa with an accuracy of 0.08 cm of water and is used to measure the height of water in the

reservoir while compensating for any barometric pressure change. The water reservoir is built with a 10 mm inside diameter measuring shaft and a 65 mm inside diameter overflow shaft.

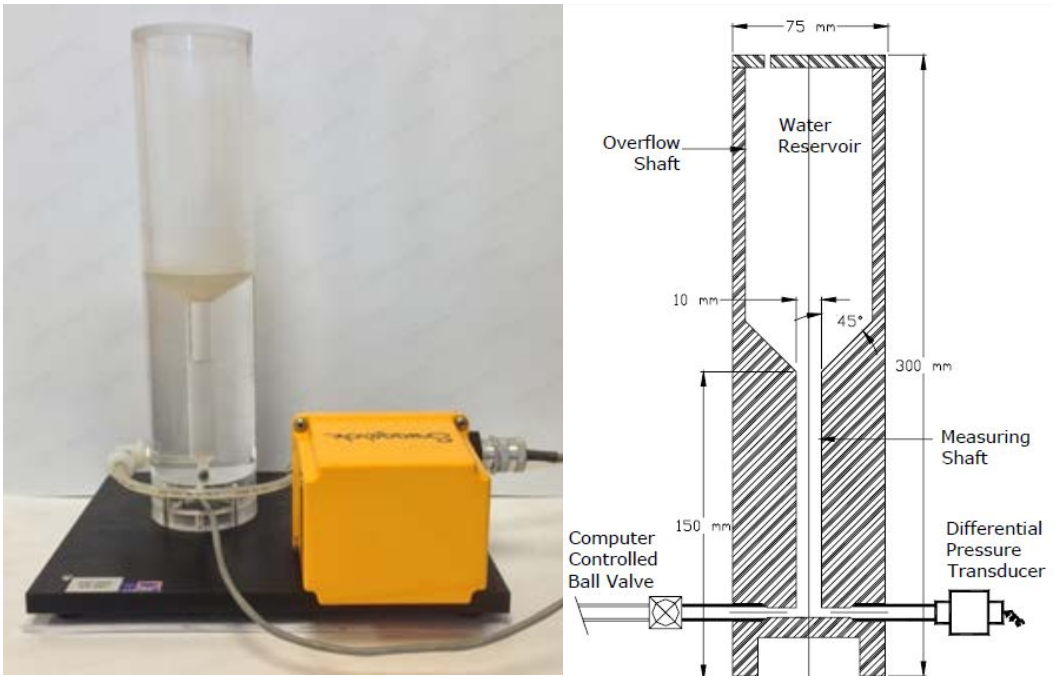

Figure 3.12 Schematic and actual photograph of automatic flushing device (from GCTS 2010)

Further details of the water reservoir and procedure to calculate its volume capacity are discussed thoroughly in the GCTS (2010) manual. The pressure transducer port and the specimen pore-water port are welded into the bottom of the flushing device to avoid pipe threads where air bubbles could adhere. This device is hydraulically connected in line to the bottom of the high-entry ceramic disk from the triaxial base via a computer-controlled ball valve that has zero volume change upon actuation, as shown in Figure 3.12.

3.3.1.5 Flushing procedure

A pressure volume controller is required to be connected, along with the flushing device, to the pore water pressure line at the bottom of the ceramic disk to flush the diffused air automatically. Each device is connected to opposite sides of a spiral groove in the high air entry disk compartment, as shown in Figure 3.13.

Diffused air flushing is performed by opening the ball valve and moving a sufficient amount of water from the pressure volume controller (that draws water from independent reservoir) under displacement control mode thereby flushing the accumulated air bubbles from lower compartment into the flushing tube that is open to the atmosphere. The water level in the reservoir is then brought back to the original position via the pressure volume controller by reversing the flow.

The appropriate volume of flushing water and rates are chosen to ensure complete removal of air from the water reservoir beneath the ceramic disk. The rate with which the water is pushed into the flushing tube is kept higher than the rate at which water is brought back to its original level to prevent any air bubbles from being carried back into the system. These values may vary depending upon the matric suction applied, and the stage of testing, and should be decided through trials and visual examination.

Fredlund and Rahardjo (1993) suggested adding a few drops of “Fantastik” or similar commercial surface cleaner to the water in the flushing device to reduce the surface tension, thereby promoting the upward movement of air bubbles in the device. We followed this suggestion, and it improved the flushing operation.

Flushing frequencies were recommended by Padilla et al. (2006), based on their studies on the accumulation of diffused air with 1, 3, 5 and 15 bar ceramic disks; however, they recommended that it should be adjusted by observing actual air diffusion

during a test. The complete process can be automated by setting up the flushing device within the software provided with the equipment by GCTS.

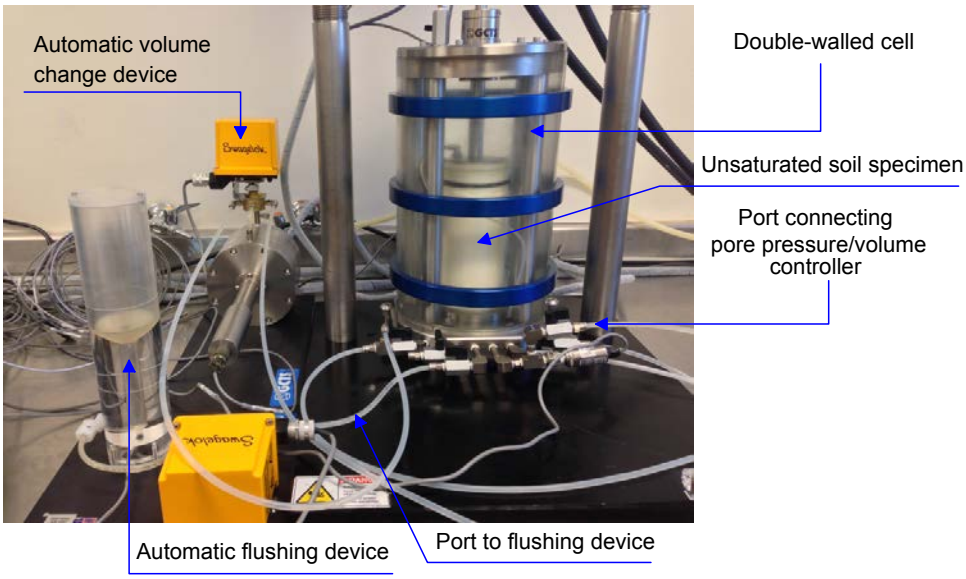

Figure 3.13 Triaxial base with independent ports for connecting the flushing device and pressure volume controller in line from opposite sides

The software calculates the amount of diffused air flushed during each iteration, making it possible to correct the pore water volume change by deducting the diffused air flushed from the volume change measured by the back pressure controller before flushing. Unsaturated triaxial testing may last for days to months and, as such, the automation of periodic flushing process comes in as handy for the operator.

3.3.1.6 Volume change device

Specimen volume change is measured via a “frictionless” volume change device (accuracy of 0.01 cm^3) by measuring the volume of fluid entering or leaving the inner confining pressure cell to compensate for the change in volume of the specimen, as shown in Figure 3.14.

Any differential pressure created across the inner and outer cells can result in significant compliance error. This has been prevented by the device utilizing a rolling diaphragm with essential zero differential pressure. The device has an infinite volume measurement capacity due to the computer-controlled flow reversal valve (GCTS, 2010).

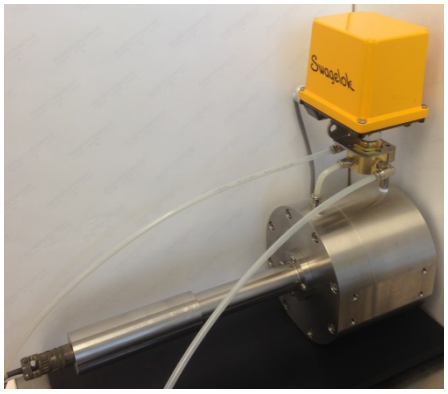

Figure 3.14 Automatic volume change device

3.3.1.7 Piston friction

The triaxial equipment used in this research is built to offer essentially zero frictional resistance to piston movement. Hence, the load measured by the load cell does not need to be corrected for any additional frictional load sensed (GCTS, 2010).

3.3.1.8 Membrane and filter paper corrections

The membrane that encases the specimen and filter paper cage placed along the sides of the specimen makes a small contribution to the resistance offered against compression. Henkel and Gilbert (1952) gave expression for applying it to correct the deviator stress.

$$\Delta(\sigma_1 - \sigma_3)_{rm} = \frac{4M\varepsilon(1-\varepsilon)}{D_s} \tag{3.1}$$

Where, $\Delta(\sigma_1 - \sigma_3)_{rm}$ is the membrane correction to be subtracted from measured deviator stress, M is the rubber modulus, ε is the axial strain, D_s is the initial diameter of the specimen.

Filter paper strips are used in saturated soil testing to facilitate the saturation procedure. Bishop and Henkel (1962) provided an equation for contribution of resistance by filter paper strips. However, no filter paper strips were used in this research.

3.3.1.9 Membrane penetration

In conventional triaxial compression tests, the effect of the membrane penetrating the specimen surface and affecting the volumetric measurements is rarely a problem. However, in a test where the radial stress is varied, the membrane penetration, which is dependent on the cell pressure, may have a significant influence on the volume change measurements, particularly in coarse-grained soils (Ali et al., 1995).

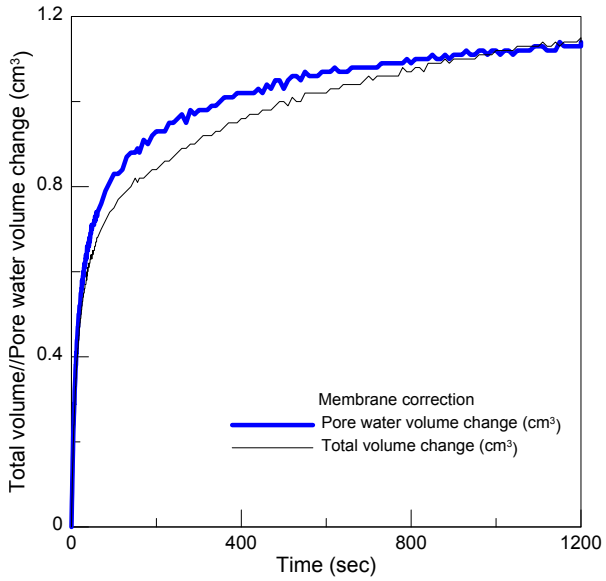

Figure 3.15 Total and pore water volume change during isotropic consolidation of saturated soil specimen

Analytical equations have been proposed to calculate the corrected volume, which mainly depends upon the diameter of the specimen, thickness and Young's modulus of the membrane, mean particle size of 50% material passing, and cell pressure applied (Molenkamp and Luger, 1981; Baldi and Nova, 1984; Kramer et al., 1990; Ali et

al., 1995; ASTM D7181-11). They can also be experimentally determined by measuring the difference between the total water volume expelled out of the sample and the volume change of the saturated soil skeleton under constant confining cell pressure (Garga and Zhang, 1997).

The volume of water expelled, as well as the total volume change of the specimen during the consolidation stage of the saturated triaxial test, was monitored. The volumes were almost same at the end of the consolidation time (Figure 3.17). Hence, the membrane penetration effects were not addressed in these studies. No filter paper strips were added to facilitate side drainage during saturated/unsaturated triaxial testing.

3.3.1.10 Uplift forces acting on loading piston

The loading piston is screwed into the top cap/platen causing the confining pressure to be applied only partially to the top platen and, hence, to the specimen, resulting in an anisotropic stress state. This can be avoided by applying an axial load equal to the confining pressure times the piston area. Also if the piston is not screwed into the top platen, an uplift component equal to the confining pressure times the piston cross-sectional area will be sensed by the load cell. The software is programmed to calculate both these stresses and applies them automatically, as the test progresses, to maintain the isotropic stress state during all stages of triaxial testing.

3.4 Saturated Soil Triaxial Testing

An actual photograph of the Triaxial test set-up capable of conducting static, as well as cyclic triaxial testing on unsaturated soils along a wide variety of stress paths installed at UT-Arlington's geotechnical engineering laboratory, is shown in Figure 3.15, along with a sketch of the entire setup, as shown in Figure 3.16.

The "as compacted specimen" properties are given in Table 3.3. Once the specimen is prepared by the static compaction method, it is mounted on the triaxial base

with saturated porous stone and filter paper on it. The average initial height and diameter are calculated from measurements taken by a digital caliper along three different positions of the specimen. Saturated filter paper is also placed on top of the specimen to prevent migration of fines into saturated water lines. The top cap, with a porous stone inside it, is placed on top of the specimen.

Table 3.3 As compacted properties of unsaturated soil specimen

Dry unit weight, ρ_d (g/cm^3)	1.8
Moisture content, w (%)	14.2
Matric suction (kPa)	10
Degree of Saturation (%)	81

The specimen is then enclosed inside a membrane with the aid of a membrane stretcher, and the whole assembly enclosed in the membrane is then sealed at the top cap and bottom pedestal with three O-rings to isolate it from chamber cell pressure. It is noteworthy to mention here that the application of one or two coats of silicon vacuum grease between the membrane and top cap, as well as bottom pedestal, helps to form a perfect seal and prevents leakages of cell water into the specimen during the saturation stage when the high cell, as well as high back pressures, are encountered.

3.4.1 Back Pressure Saturation

After mounting the specimen as explained above, the triaxial cell is then assembled with double-walled cell arrangement, and the cell is filled with low water pressure of about 10 kPa through a cell water pressure system.

After filling the cell, the pore water pressure line is saturated, and a back water pressure of 5 kPa is applied at the bottom of the specimen while the cell pressure is increased simultaneously from 10 kPa to 15 kPa, thus maintaining an effective stress of 10 kPa in the specimen all the time.

The first stage in triaxial testing is that of saturating the specimen. Bishop and Henkel (1957) described a back pressure procedure for saturation of test specimens. The back pressure is applied to the pore water of the test specimen in a triaxial machine, along with the addition of an equal amount of chamber pressure. A pore pressure transducer placed near the bottom pedestal is used to monitor the pore-water pressure. Both the increments are applied slowly to allow the adjustment of the water content under each increment before the next one applied, thus ensuring that the back pressure acts as a neutral pressure, with no significant effect on the soil skeleton.

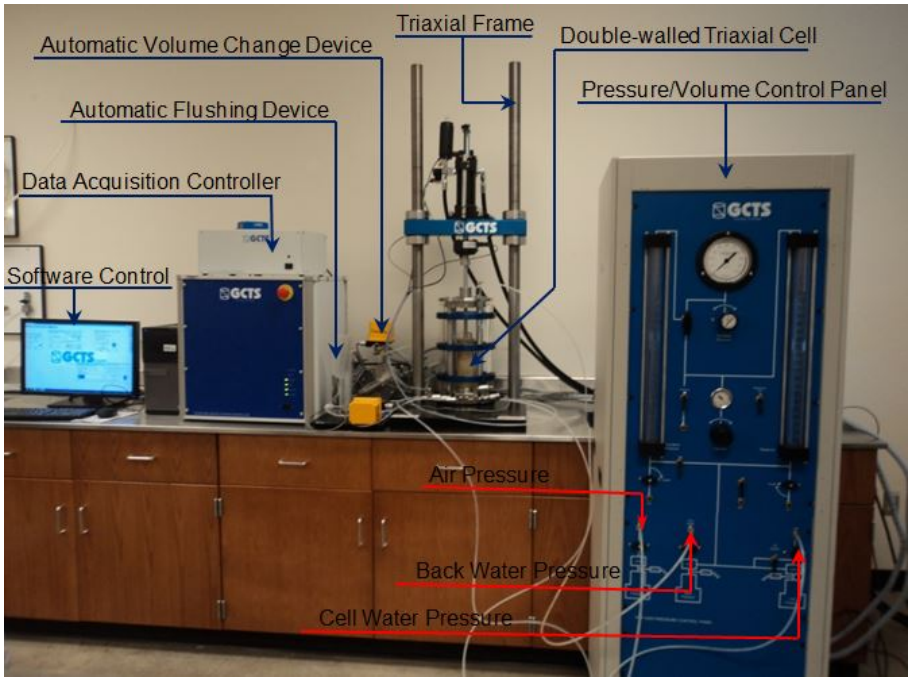

Figure 3.16 Unsaturated soil Triaxial testing set-up installed at UT-Arlington's geo-mechanics lab

Few soils tend to dilate upon shearing and, therefore, develop less than atmospheric pore water pressures during undrained shear. Elevating the backwater pressures well above atmospheric during saturation procedures will ensure that the pore water pressure during undrained shear does not fall below atmospheric (Lowe et al.,

1960). Such a back pressure saturation procedure was followed, by constantly maintaining the effective stress inside specimen of 10 kPa.

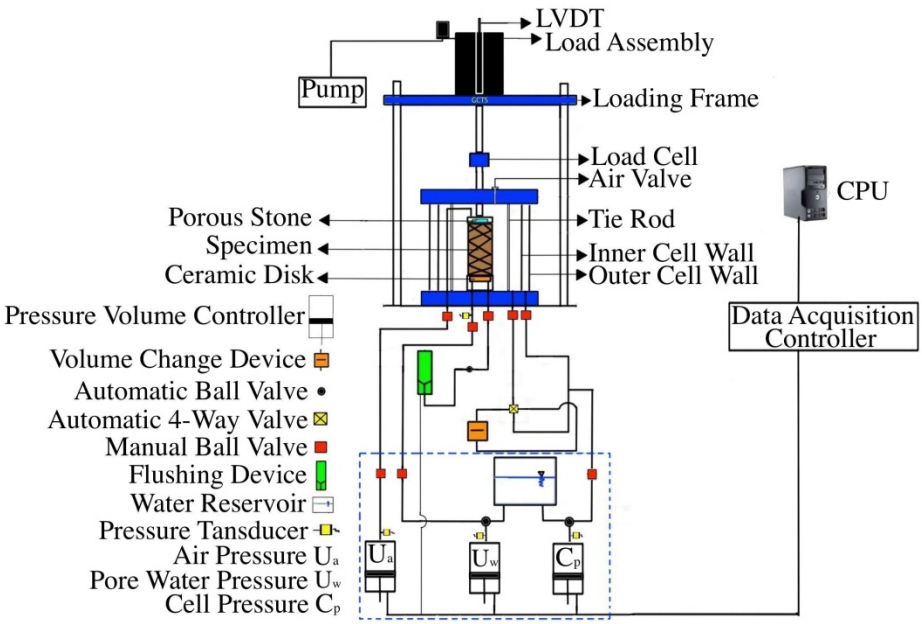

Figure 3.17 Sketch of entire unsaturated soil triaxial testing set-up

High backwater pressures also ensure that the air, if any, in void spaces is forced into, ensuring complete saturation. After each load increment, the pressures were kept as is for at least one day to allow water to flow into specimen and equalize throughout its height under the pressure increment before performing the check for B-value. To ensure complete saturation, the B-value check was performed. The pore-pressure parameter B is defined by the following equation:

$$\mathrm{B-value} = \frac{\Delta u}{\Delta \sigma_3} \tag{3.2}$$

To check B value, the back pressure drainage valve was closed, and the cell pressure was increased by 15 kPa. The excess pore water pressure (Δu) generated under the incremental cell pressure $(\Delta \sigma_3)$ was recorded, and B value was calculated using Equation 3.2. Complete saturation was considered when the B value of 0.95 or greater

was achieved (ASTM D7181-11). If the target B value was not reached, then the pore water drainage valve was opened, and the effective consolidation pressure was brought to the same value as before the B value check by increasing the back water pressure by an amount equal to $\Delta\sigma_3$.

The saturation procedure was further repeated by applying the next increment of cell pressure, as well as back water pressure, followed by a B value check, as explained earlier. The theoretical additional back pressure Δu required to increase the degree of saturation from an initial value S_o to a final value S was given by Lowe and Johnson (1960) as below

$$\Delta u = [Po]\frac{(S - So)(1 - H)}{1 - S(1 - H)} \tag{3.3}$$

Where H is Henry's coefficient of solubility. The specimen used had 81% of initial degree of saturation. Although the effective stress of 15 kPa was always maintained inside the specimen, cell pressures as high as 1000 kPa and back pore water pressures of about 985 kPa were required for complete saturation in these studies. These experimental values are consistent with the theoretical values of pressures required for complete saturation using Equation 3.3.

3.4.2 Isotropic Consolidation Stage

Following saturation, the consolidation stage was performed to allow the specimen to reach equilibrium under the target effective consolidation stress. The effective stress required for the consolidation stage is equal to the difference between the confining/cell pressure and the pore water pressure at the end of consolidation. Three effective confining pressures were used in this research; 100, 200, and 300 kPa. Consolidation was performed by ramping the cell pressure to the final value within 30 seconds under undrained conditions.

The drainage valve was then opened, and the total volume change, as well as pore water volume change, of the specimen were monitored. If the specimen was completely saturated during a saturation procedure, both the volumes measured should be same at the end of consolidation stage which can be confirmed from the plot shown in Figure 3.17. The specimen was allowed to consolidate, holding the cell pressure and back water pressure constant until the excess pore water pressure generated dissipates completely. It can be observed from Figure 3.17 that at the end of 20 minutes after applying the consolidation pressure, both the total volume change and pore water volume change coincides indicating that the membrane penetration effects are not affecting the volume change measurements.

3.4.3 Shearing Stage

Following the consolidation of the specimen under target effective confining pressure, the specimen was ready to be sheared under drained condition. For a consolidated drained test, the chamber pressure was kept constant, while the specimen was axially loaded under constant strain rate (strain controlled) or under constant axial stress rate (stress controlled). In this research, all the tests performed were strain-controlled tests. The strain rate should be slow enough that no excess pore water pressures are generated during shearing. The specimen was sheared at a constant shearing strain rate of 0.2%/min until about 20% axial strain was reached, during which it was confirmed that no excess pore pressures were generated. After the test, the cell pressure and back water pressure were slowly released to zero, and the specimen was removed quickly for water content determination.

All three specimens tested during shear failed without any distinct shear plane by bulging at the center. They all showed compressive type behavior during shear failure, as shown in Figure 3.18b. The stress-strain curve showed a strain-induced hardening type

failure as shown in the figure 3.18a. The three drained stress paths followed 1:3 slopes in p-q space, as shown in figure 3.19b.

The slope of the critical state line in p-q space is 1.42 as shown in Figure 3.19b. The Mohr's circles, at failure condition, were drawn for three confining pressures, as shown in Figure 3.19a. The Mohr-Coulomb analysis performed by the GCTS software is shown in Figure 3.20. The shear strength parameters, such as cohesion intercept obtained, was zero $(c' = 0)$, and the effective frictional angle at critical state was 35 degrees $(\phi' = 35^o)$, as illustrated in Figure 3.19 and Figure 3.20.

The procedures, including saturation, consolidation, and shear can be automated by proper selection of templates and by programming the appropriate begining and end of various stages. After each stage, the dimensions of the specimen are corrected based on the volume change measurement and axial deformation recorded during the prior stage so that new specimen dimensions may be entered in the software before starting the next stage.

If all the stages are programmed to run one sequence after another, then the software tracks the volume changes based on the user's input of initial dimensions and corrects the specimen dimensions automatically. Figure 3.20 shows the screen shot of the software window that can be used to plot the Mohr's stress circle at critical or peak failures and also gives best fit strength parameters. However, such facilities are not available with current software for unsaturated soil testing, and one has to plot the Mohr's stress circles at failure independently to obtain the related unsaturated strength parameters.

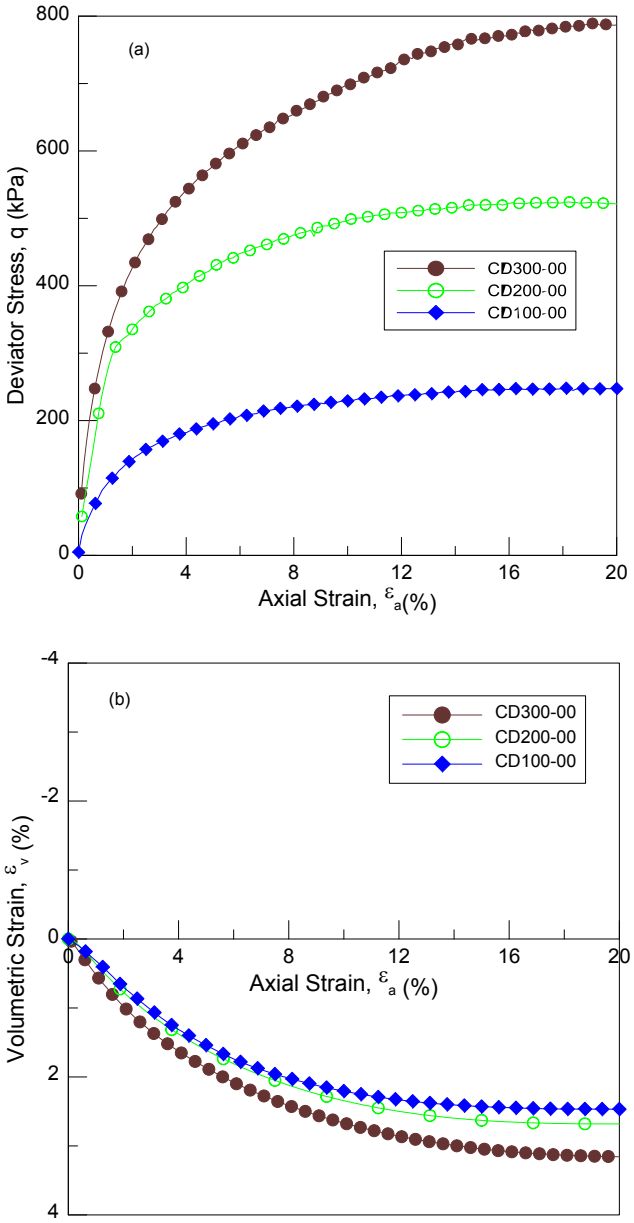

Figure 3.18 Fully saturated soil response for silty sand at three net confining pressures of 100, 200 and 300 kPa (a) Deviatoric stress against axial strain curves, (b) volumetric strain against axial strain curves

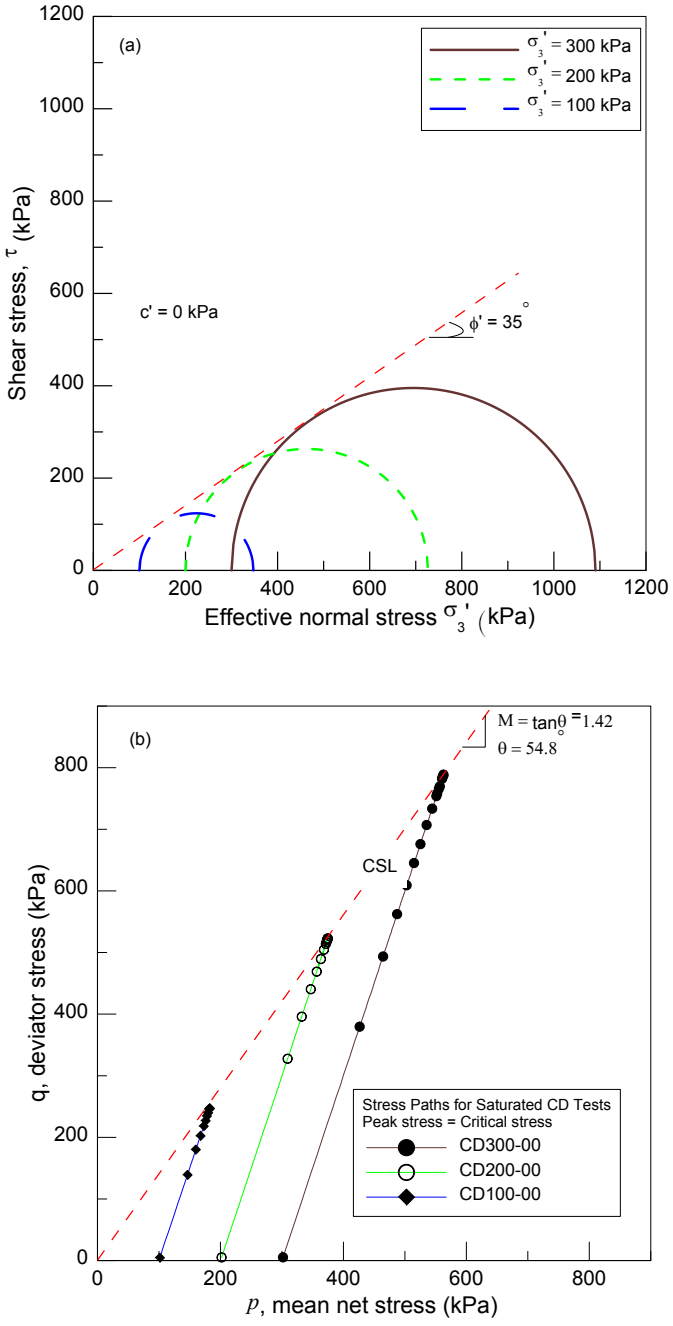

Figure 3.19 Fully saturated soil response a) Mohr's stress circle at three effective confining pressures 100, 200 and 300 kPa, b) Conventional triaxial stress path in p-q space

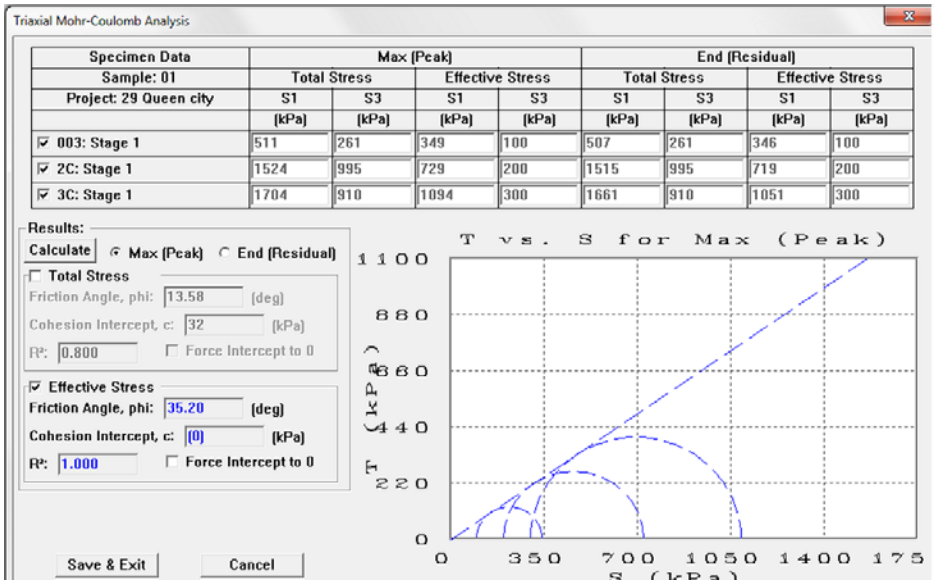

Figure 3.20 Software window showing Mohr's circles for saturated soil response

3.5 Unsaturated Soil Triaxial Testing

The conventional/traditional triaxial test systems that were performed manually are now being replaced by advanced computer-controlled automatic test systems. Unsaturated soil triaxial testing requires several test accessories that usually need to be operated simultaneously, such as a cell pressure/volume controller, back pressure/volume controller, air pressure/volume controller, the axial actuator system often accompanied by a pump, the flushing device, and the volume change device.

Considerable advancements in computer technology and its applications to civil engineering laboratory equipment have made it possible to program computers through compatible software program, and thus control the various stages involved in saturated as well as unsaturated triaxial soil testing. This has made it possible for experimentalists to simulate more realistic stress paths experienced by soils in actual field situations.

Such accurate and more realistic testing methodology will certainly result in improved design quality. However, incorporating such enhanced capabilities requires a

significant capital investment in the research and development of related compatible software programs (GCTS, 2008). Figure 3.21 illustrates the modifications made to the triaxial cell apparatus to accommodate the unsaturated soil testing.

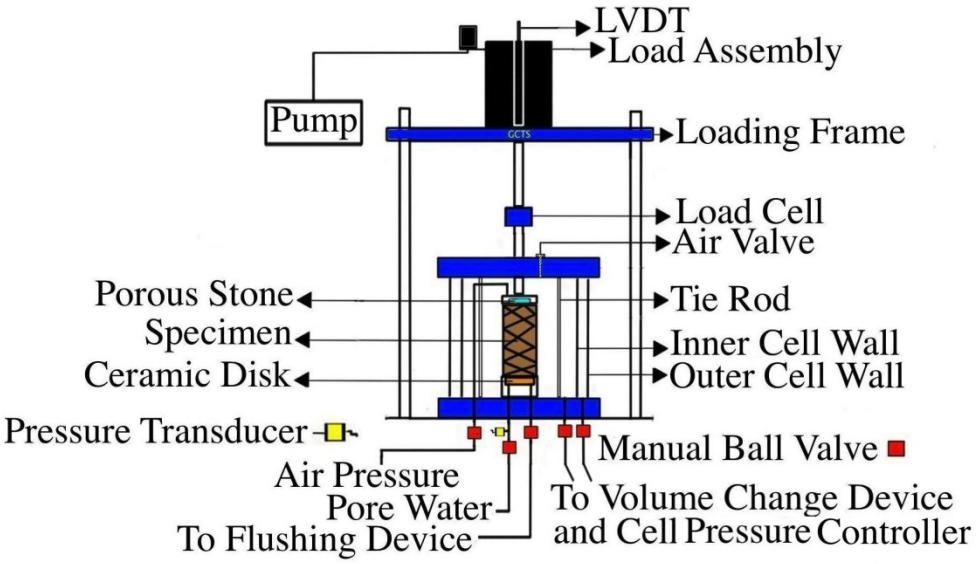

Figure 3.21 Modified triaxial set up to accommodate unsaturated soil testing

3.5.1 Stress Variables

For axisymmetric conditions (triaxial test condition), three stress parameters are required to explain the behavior of unsaturated soils, and these are usually chosen as mean net stress *(p)*, deviator stress *(q),* and suction *(s)*, as defined by the following expressions:

$$p = \frac{\sigma_1 + 2\sigma_3}{3} - u_a \tag{3.4}$$

$$q = \sigma_1 - \sigma_3 \tag{3.5}$$

and,

$$s = u_a - u_w \tag{3.6}$$

Where σ_1 and σ_3 are the axial and radial total stresses respectively; u_a and u_w are the pore-air and pore-water pressures respectively; s is matric suction, and q is the deviator stress.

3.5.2 Matric Suction Equalization

Two methods were employed in this research to induce the desired matric suction in the specimen. Method I was used for CD50-xx and CD250-xx tests, as explained below, while method II, as explained later, was used for CD500-xx and CD750-xx tests.

3.5.2.1 Suction equalization method I

Matric suction is the potential energy of soil water created by capillary tension between soil particles and pore water and surface adsorptive forces (Sawangsuriya et al., 2008). The suction equalization stage is necessary to create the desired matric suction inside the specimen by allowing the pore-air and pore-water pressure to equalize to the applied air pressure and back pressure, respectively. During the equalization, the suction in the specimen is changed gradually from its initial value after compaction (approximately 10 kPa) to the desired value.

The as-compacted properties of the specimen are the same as discussed in Section for the saturated soil test. After the initial preparation, the specimen was immediately mounted on the triaxial base that had a previously saturated ceramic disk of appropriate air-entry value installed inside its recess. The double-walled triaxial cell was assembled and filled with water under 15 kPa of cell pressure, after which, the tubes connecting the back water pressure line, volume change device, as well as the flushing device, to the triaxial cell were saturated by flushing with de-aired water to remove any air trapped in the system.

The effective stress acting inside the specimen at this point was 15 kPa, with the negative pore water pressure of u_w = 10 kPa and air pressure ($u_a = 0$) equal atmospheric or zero reference, thus producing positive matric suction (u_a-u_w) of 10 kPa. The system was designed so that in order for the flushing device to function automatically, backwater pressure of minimum 5 kPa value needs to be maintained. Hence the backwater pressure was increased from zero to a value of 5 kPa.

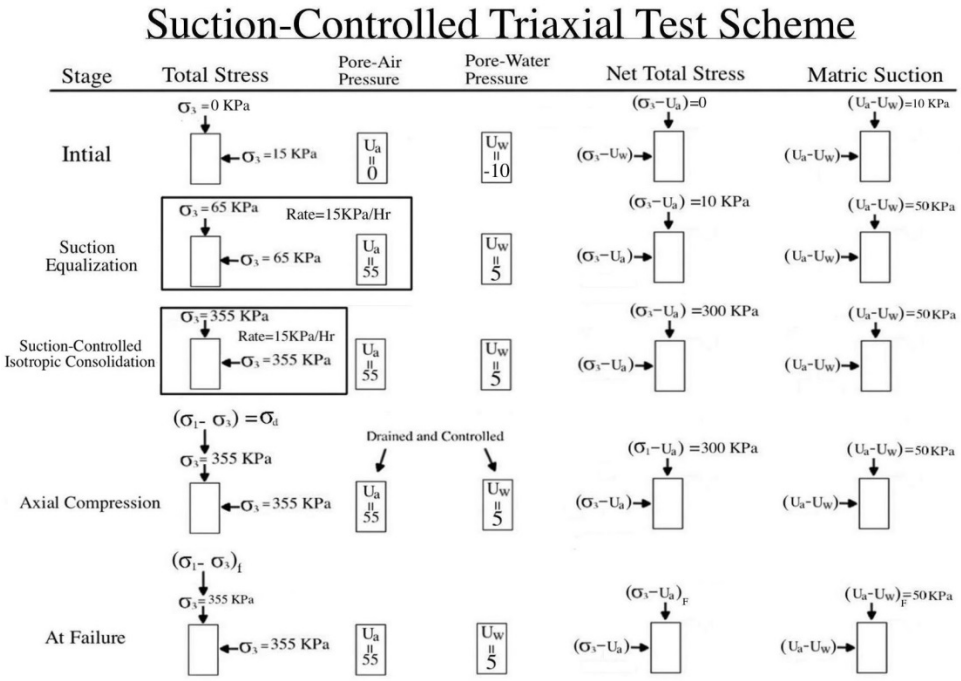

Figure 3.22 Suction-controlled triaxial test scheme adopted in this research explained for CD300-50

The desired final matric suction was achieved by elevating the cell pressure and the air pressure by equal increments, while keeping the back water pressure constant at a nominal value of 5 kPa, as illustrated in Figure 3.22 for CD300-50 test. The target values of cell pressure (σ_3 =70 kPa), air pressure (u_a = 55 kPa) and pore water pressure

(u_w = 5 kPa) were selected and entered into the computer program, based upon the value of matric suction desired (u_a - u_w = 50 kPa).

A ramping procedure was used to reach the target values at a rate of 10 kPa/hr. The volume of water flow to and from the specimen was monitored, and equalization was assumed to be completed when there was no flow of water to and from the specimen or at least when the flow of water decreased to less than 0.1 cm^3/day (Zakaria, 1994; Sharma, 1998; Estabragh et al., 2004). The equalization time depends upon the value of the target suction but usually took 5 days for s = 50 kPa, 10-12 days for 250 kpa.

At the end of the suction equalization stage, the mean net stress acting on the specimen was $p = \sigma_3$ - u_a while the matric suction was $u_a - u_w$. Figure 3.22 shows the sequence of the various stages followed.

3.5.2.2 Matric suction equalization method II

For CDxx-500 and CDxx-750 tests that involved testing soils at medium-to-high matric suction, another procedure (method II), also called the “preconditioning stage” was adopted to induce matric suction in order to reduce the testing times. The preconditioning stage avoids the errors caused due to delays in testing times while dealing with the unsaturated soil. The test specimens were brought close to the desired matric suction outside the test chamber before being mounted on the triaxial cell for actual testing.

The specimen was enclosed in a membrane and was dried by rolling back the membrane during the day. At night, the membrane was rolled back, and the specimen was allowed to equilibrate. Continuous monitoring of the specimen weight, as well as use of drying soil water characteristic curve (SWCC), was done to check if it reached water content close to the corresponding desired matric suction. This technique is similar to the one described by Houston et al. (2008).

After the preconditioning stage, the specimen was mounted on the base pedestal, with the pre-saturated ceramic disk inside the triaxial cell. The specimen dimensions were measured to correct any change in the initial volume during the preconditioning stage. The desired matric suction was then imposed, using the axis-translation technique. The tube or lines connected to the backpressure system were saturated, and the base pedestal was flushed thoroughly to remove any entrapped air. The suction equalization stage was necessary to ensure that the desired matric suction level was induced in the specimen and that enough time was allowed for the equalization of the pore-air pressure and pore-water pressure to the applied air pressure and back pressure, respectively.

The sample was subjected to a predetermined level of matric suction (for e.g. s = 500 kPa) by equally increasing the cell pressure and air pressure at a constant rate of 10 kPa/hr, maintaining cell and air pressure difference of 10 kPa (to prevent specimen from accidental swelling). Thus, the net confining pressure σ_3- u_a was always kept at 10 kPa. The slow rate of 10 kPa/hr was chosen so that the suction could be applied gradually and, at the same time, the volume change during the suction application was minimized.

The equalization stage was considered to be complete when the outflow of water through the specimen reduced to 0.04% per day (Sivakumar, 1993). After initial preconditioning, an additional 3-4 days were required to achieve the desired 500 kPa matric suction in the triaxial chamber.

3.5.2.3 Suction-controlled isotropic consolidation

Application of an external load to an unsaturated soil specimen results in the generation of excess pore-air and pore-water pressures which will eventually dissipate with time, depending upon the permeability of the soil and the drainage conditions available. This will cause a decrease in volume of soil and the process is referred to as

consolidation (Fredlund and Rahardjo, 1993). Although, in the field, the anisotropic conditions are likely to be possible, the type of consolidation studies done in this research is limited to isotropic conditions.

The suction is controlled and measured using the axis-translation technique, and each specimen is compressed isotropically to a virgin state by increasing the mean net stress (p), while holding the suction (s) constant. There are two methods commonly used to apply consolidation stress, namely, step loading and ramping procedures. During incremental step loading, excess pore-air pressure that is generated will be dissipated quickly due to a relatively high value of air permeability (k_a), allowing the mean net stress (p) to rise to its final value throughout the entire specimen (Ho and Fredlund, 1982).

On the other hand, excess pore-water pressure will take significant time to dissipate to the back water pressure value owing to the relatively low value of water permeability (k_w). This means that matric suction u_a - u_w will gradually increase over the period of consolidation (Estabragh et al., 2004). Cui and Delage (1996) suggested that step loading should not be used in compressibility studies of unsaturated soils as this procedure overestimates the coefficient of compressibility $\lambda(s)$ and underestimates the value of the yield stress (σ_{yield}).

The excess pore-water pressure generated at the top portion of the specimen can be minimized by applying an external load slowly by ramping the cell pressure at a rate low enough to keep it within the acceptable limits (Sivakumar, 1993). The ramping procedure also helps to obtain a continuous plot of specific volume (v) against mean net stress (p) under constant suction, which can be further utilized to locate the yield stress (required for loading-collapse studies) and slope of the normal compression and reloading lines (required for constitutive modeling).

The ramped consolidation procedure (see Figure 3.23) was followed in this research for e.g. for CD300-50, by increasing the cell pressure to a target value (σ_3 = 355 kPa) that corresponded to the prescribed mean net stress (p = 300 kPa) at a rate of 10 kPa/hr while holding the air (u_a = 55 kPa) and back water pressure (u_w = 5 kPa) at constant values, thus maintaining constant suction (u_a - u_w = 50 kPa) throughout the consolidation process via the computer program.

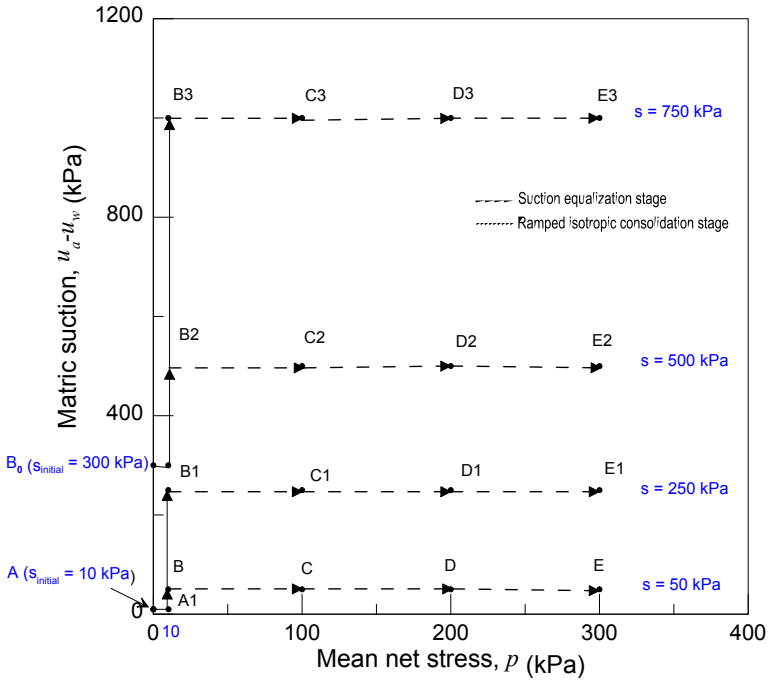

Figure 3.23 Stress paths during the matric suction equalization/consolidation process

The volume change of specimen, and pore water volume changes, were recorded. Following each consolidation stage, the target pressures were maintained for at least 24 hours to allow for complete dissipation of excess pore-water/pore-air pressures and to ensure that each sample was consolidated to a virgin state. The plot of specific volume ($v = 1+e$) plotted against mean net stress (p) on a logarithmic scale indicated that the virgin state was achieved at the end of the consolidation stage.

3.6 Mechanical Response Under Suction-Controlled Isotropic Loading

Following the suction equalization stage, the suction-controlled isotropic consolidation stage was performed in the same way as that described in method I. Figure 3.24 shows the test results of isotropic consolidation under controlled-suction conditions at s = 50, 250, 500 and 750 kPa.

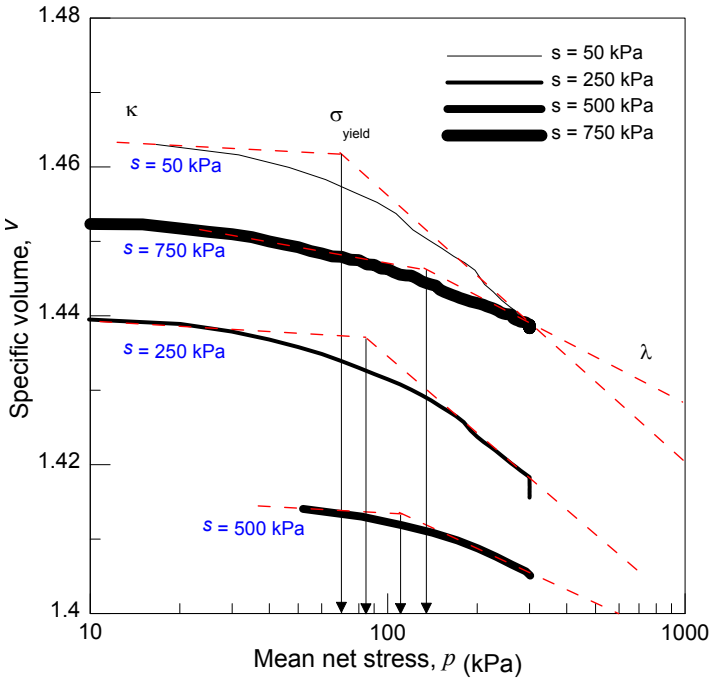

Figure 3.24 Suction-controlled isotropic consolidation at *s* = 50, 250, 500 and 750 kPa

Yielding was observed during isotropic compression loading. Yield stresses were significantly influenced by suction level. Continuous increase in the mean net stress caused the specimen to yield at some point. In general, the yield stress increased with an increase in matric suction and resulted in a maximum value for highest matric suction s = 750 kPa. The procedure and values obtained for parameters essential to constitutive modeling using BBM such as yield stresses, $p_o(s)$, slope $\lambda(s)$ and κ are explained in detail in Chapter 5. These studies are also necessary for corroboration of the existence of loading collapse (LC) locus.

3.7 Shearing Stage

Following the isotropic consolidation, each sample was sheared under constant net confining pressure under drained conditions by axial loading at a constant rate of strain, thus following a CTC (conventional triaxial compression) drained stress path at a constant strain rate of 0.0086%/min. During the shearing, the valves for both the air and water pressure lines were opened and controlled at the required pressures (i.e., they were kept at the same magnitude as those acquired at the end of equalization stage). The specimens were sheared until the axial strain reached 20%. All specimens showed distinct failure plane or constant deviator stress between 12 to 20 % axial strain. The appropriate shear rate was decided based on following independent research studies.

3.8 Independent Shear Rate Studies Pertaining to Axis-Translation Technique

3.8.1 Introduction

Selection of an appropriate shear rate is crucial in the accurate determination of shear-induced volume changes in the specimen, and in making sure that there is no bifurcation of the target effective stress path from the measured stress path. However, in triaxial testing of unsaturated soils (UNSAT testing) at constant suction values, the axial shear rate should also be slow enough to maintain equilibrium of matric suction, and uniformity in water content of the soil specimen throughout the shearing stage.

In this case, the shear rate was controlled primarily by the high-air-entry ceramic disk. The maximum suction to be applied during the test program, at a highest confining pressure, had to be chosen to quantify this rate. In a medium-to-dense silty sands, with a tendency to dilate upon shearing, it was necessary to have shear rates slow enough to permit upward flow of water into the specimen through the low-permeability ceramic disk.

The suitable shear rate was determined empirically through a series of strain-controlled UNSAT Triaxial CD tests at three axial shear rates (0.014%/min, 0.0086%/min

and 0.0029%/min), with highest suction applied via the axis-translation technique. The most suitable shear rate would be the maximum rate for which the specimen was subjected to constant matric suction throughout the test, with induced axial strains similar to those induced at lower shear rates.

3.8.2 Experimental Program for Shear Strain Rate Studies

Initially, s = 500 kPa was thought to be the maximum suction to be used in this research. Hence, three tests, namely, CD500-300 were conducted on three identical specimens prepared by using Method II, as explained in Section 3.2.4. All the procedures, including the preconditioning stage, matric suction equalization, and isotropic consolidation were performed as per the procedure explained above. Following the isotropic consolidation stage, each sample was sheared under constant net confining pressure by axial loading at a constant rate of strain, thus following a CTC (conventional triaxial compression) drained stress path.

Three rates of strains were chosen; namely, 0.0029%/min (low), 0.0086%/min (medium) and 0.014%/min (fast) based on previous studies by Satija and Gulhati (1979). The water volume change was measured by the back pressure volume controller, while the total volume change of specimens was recorded by a new volume change device, as discussed earlier. The deviatoric stress was measured using the load cell of 10,000lbf capacity while the axial deformation was recorded by strain gage mounted on the loading frame.

The complete process, including suction equalization, isotropic consolidation under constant suction, and the shearing stage was accomplished using an automated software program developed by GCTS. A negative sign was used for the dilating volume change, while a positive sign was used for compressive type behavior.

3.8.3 Results and Discussions Related to Shearing Strain Studies

3.8.3.1 Interpretation based on deviator stress criteria

To achieve completely drained shearing stress path, u_a and u_w were kept constant (constant matric suction), while the deviatoric stress ($q=\sigma_1-\sigma_3$) was increased monotonously at a fixed rate. Irrespective of the rate of loading, all the stress-strain curves showed strain softening at higher axial strains (above 7%). The shearing was continued until the critical state was reached. All the specimens showed failure by bulging. Post-consolidation, the specimen, had an over consolidated stress history with OCR ~ 5.

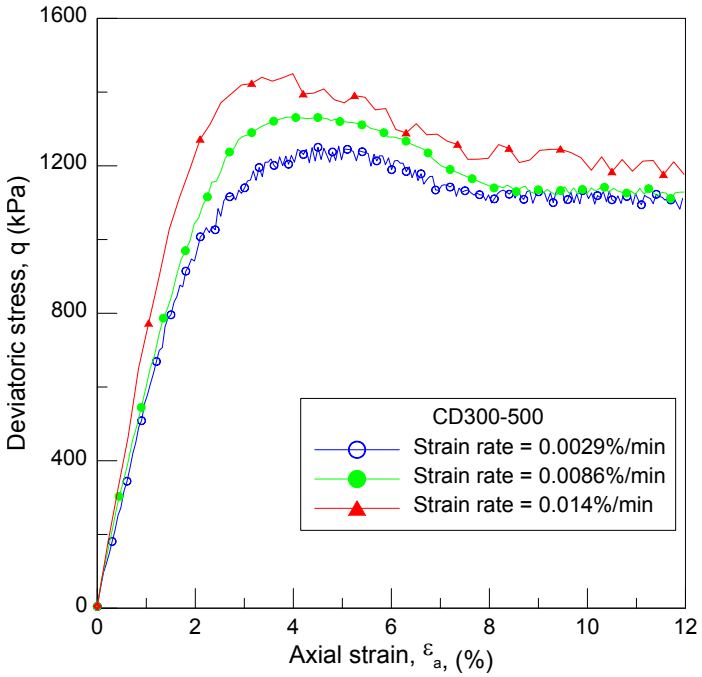

Figure 3.25 Deviatoric stress variations with axial strain for CD300-500 at various shear rates

Its impact was clearly seen in the form of, first, a peak failure, followed by the post-peak softening stress-strain response, and, secondly, in the form of a dilating type of volume change response during the shearing stage (Figure 3.25 and Figure 3.26). A

close examination of the stress-strain curve (Figure 3.25) indicated that the peak was reached faster as the axial shear rate was increased. This is in agreement with previous research results by Satija and Gulhati (1979).

One notable observation is the large difference in the peak stresses at various rates of loading. The peak stress at the fastest shear rate differed from the lowest by 197 kPa (16%), while the peak stress at the medium and the lowest shear rates differed by 79 kPa (6%). The current findings differ from previous researchers (Satija and Gulhati, 1979) who observed differences as minimal as 50 kPa between their lowest and fastest shear rate.

Satija and Gulhati (1979) performed similar triaxial CD tests on compacted Dhanauri clay specimens having an initial dry density between 15.2-15.4 kN/m^3 with induced matric suction between 50-60 kPa and net confining stress, σ_3 - u_a = 392.3 kPa. They used a shear rate of 0.016%/min, 0.008%/min and 0.004%/min. Based on their experimental evidence, it was suggested that deviator stress is a relatively insensitive parameter to use in assessing the influence of shear rate. Current research results seem to contradict this observation.

Thus, if peak response is important for the design, then one should choose the lowest shear rate. The applied matric suction in this research was 500 kPa (much higher than 50-60 kPa), and the soil used in this research was silty sand. Satija and Gulhati (1979) also mentioned that for samples at different degrees of saturation, the appropriate rate of strain would be different, and the rate would decrease as the degree of saturation reduces. For 500 kPa suction (low degree of saturation), a low or medium rate seems appropriate. Thus, deviator stress does seem to be an influencing factor in this case.

Usually, geotechnical researchers are interested in the critical state condition parameters for modeling soil shear behavior. It can be observed that the critical state is

reached almost at the same axial strain (9-10%) irrespective of the rate of loading. The reason for this may be that by the time the specimen reaches critical state, the time allowed is sufficient enough to allow the complete dissipation of excess pore air and pore water pressures.

However, the critical stress is higher at the fastest rate of loading (0.014%/min), while it almost coincides for medium (0.0086%/min) and low shear rate (0.0029%/min). Based on the three loading rates adopted, the shearing stage would take about 0.6, 1 and 3 days for a shear rate of 0.014%/min, 0.0086%/min, and 0.0029%/min, respectively, to reach axial strain of about 12% (critical state). This finding indicates that if stress-strain curves are used to judge the appropriate shear strain rate, one should choose the medium shear strain rate that happens to produce almost identical critical stress at failure (same as a low shear strain rate). It also reduces the testing times by more than half.

3.8.3.2 Interpretation based on shear-induced total volume change

The deviator stress response versus strain provides an idea of the failure conditions but fails to provide direct information about complete dissipation of pore water and pore air pressures. Also, the volumetric strain response during shearing is important for assessing or predicting the likely field settlements. Hence, the monitoring of volume changes during shearing becomes crucial. All the test specimens showed an initial compression, followed by dilation by the increase in applied axial strains (Figure 3.26).

The axial strain against the volumetric strain plots (Figure 3.26) at shear rates of 0.0029%/min and 0.0089%/min are almost identical. The specimen loaded at fastest shear rate (0.014%/min) tends to exhibit much higher volumetric changes throughout shearing than other two chosen lower ones, indirect evidence that full dissipation of pore air and pore water pressure is not occurring at 0.014%/min of shear rate.

At about 12% axial strain, the volumetric changes are almost the same for low and medium shear rates. At this point, the critical state is almost established. The current study is more focused on obtaining critical state parameters and, therefore, based on the above discussion, the medium shear rate is most suitable.

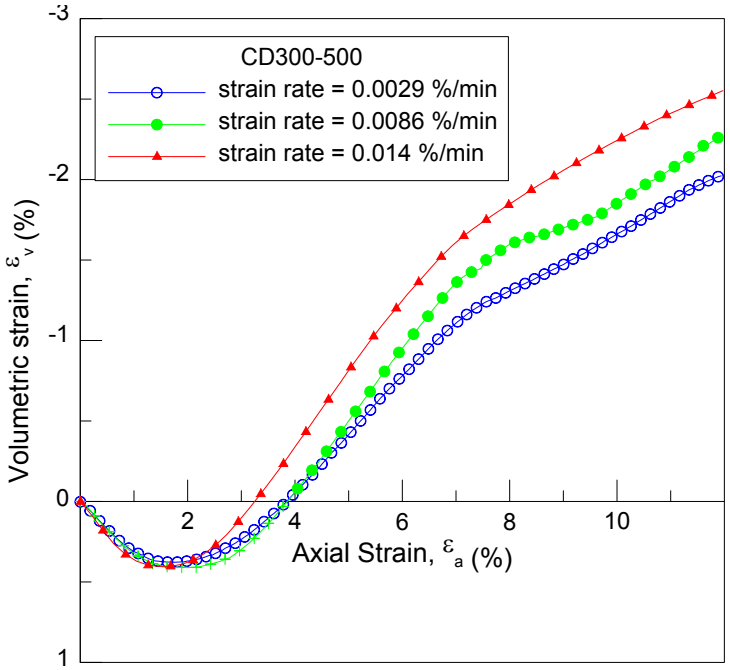

Figure 3.26 Volumetric strain variations with axial strain for CD300-500 at various shear rates

3.8.3.3 Interpretation Based on Change in Water Content Criteria

The changes in water content during shearing may be considered in judging the shear rate for CD tests. If the specimen is too stiff (aggregated fabric) due to the induced matric suction of 500 kPa during shearing, it exhibits a tendency to dilate (particles tend to ride up over each other rather than shearing). At such a high level of matric suction (500 kPa), the corresponding water content is too low (about 4.5%) to allow the proper exchange of water between the specimen and the water reservoir below the ceramic disk.

The water retained in the specimen pores is in the form of meniscus, and the water phase is not expected to be continuous (pendular saturation). Most of the volume change is due to air volume compression or expansion rather than the water exchange. The exchange of water is not observed during shear, as there is no continuity of the water phase. Thus, one can conclude that at this level of suction, the overall volume changes and, hence, volumetric strains are more important than the water content changes.

3.8.4 Modified Theoretical Approach

Geiser et al. (2006) extended the classical Gibson and Henkel (1954) method used for saturated soil so that it could be used for unsaturated soils. According to this approach, complete equalization of pore water pressure throughout the specimen is possible if the time required to fail the sample is set to:

$$t_f = \frac{H^2}{\eta c_v (1 - U_f)} \tag{3.7}$$

Where, t_f = 7075 min = time required for the sample to fail,

H = Half height of the sample (141.24/2 mm)

η = 0.75 = numerical factor that depends upon the extent and location of the drainage boundary.

U_f = Average degree of dissipation of the induced pore water pressures at failure = 0.95 for 95% dissipation of pore pressures.

c_v = 19.06 mm^2/min = coefficient of consolidation determined by using Head (1986) equation as follows

$$c_v = \frac{T_{90}(2H)^2}{t_{90}} \tag{3.8}$$

Where, t_{90} = 900 min = time at which soil reaches 90% of its consolidation for a given load. The time was determined from an actual suction–controlled isotropic

consolidation test and using a graphical approach (Head, 1986) as shown in Figure 3.27. Assuming that the failure occurs at an axial strain of approximately 5%, the shear rate calculated will be given as below

$$Shearing\ rate = \frac{strain\ at\ failure\ (\varepsilon_f)}{time\ required\ for\ failure\ (t_f)} = \frac{0.0010mm}{min} = 0.00070\%/\min \quad (3.9)$$

The theoretical shear speed seems to be at least 10 times greater than the one found by the trial and error experimental speed.

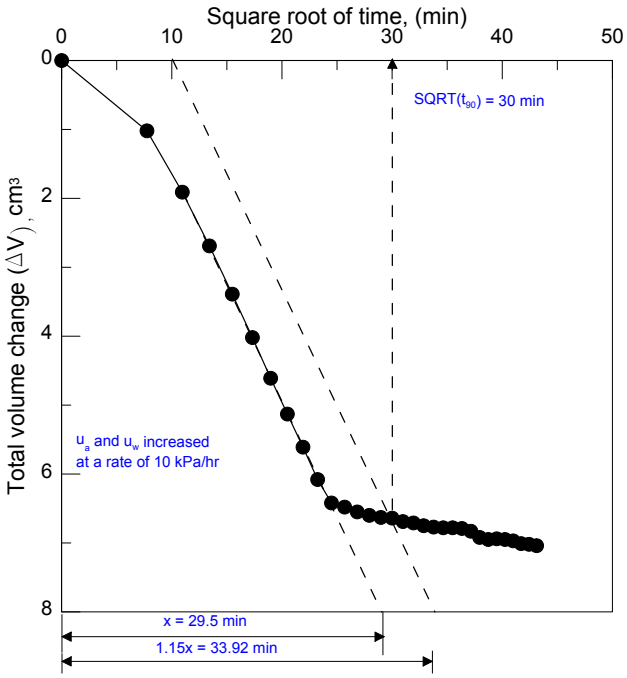

Figure 3.27 Suction-controlled isotropic consolidation curve at *s* = 500 kPa

3.8.5 Conclusions from Strain Rate Studies

Three CD triaxial tests were conducted on unsaturated silty sand specimens prepared by the static compaction method. The appropriate shear strain rate was chosen based on observations from deviator stress, total volume change, and water content changes during the shearing stage. Comparison of volumetric strain changes against axial strain plots at three different shear rates, i.e., 0.0029%/min (low), 0.0086%/min

(medium) and 0.014%/min (fastest), for CD300-500 showed that the low and medium shear rates produced almost identical plots.

The fastest shear strain rate produced a much higher volumetric strains at all times while shearing thus indirectly indicating that adequate dissipation of pore air and pore water is not possible at such a fast shear rate. Comparison of stress strain plots showed significant influence of shear rate on peak deviator stress. The comparison showed that the low and medium shear rates produce almost same deviator stress at a critical state, while, at peak, it varied by 6%.

The peak deviator stress at the fastest shear rate is about 16% greater than the lowest at peak, indicating inadequate dissipation of pore pressures (indirectly). To sum up the test results, the shear rate of 0.014%/min is insufficient for producing completely drained conditions at matric suction of 500 kPa and net effective confining pressure of 300 kPa.

Performing these tests also confirmed the proper functionality of the created software, along with the overall developed new test equipment. The theoretical shear speed found by using a modified approach by Geiser et al. (2006), based on the extension of the classic Gibson and Henkel (1954) method, seems to be at least 10 times slower than the one found by trial and error experimental speed. Thus, the shear speed, 0.0086%/min, was chosen for all the CD tests using the axis-translation technique on unsaturated soils in this research.

3.9 Mechanical Response under Suction-Controlled Shear Loading

3.9.1 Effect of Confining Pressure at Constant Matric Suction

The stress-strain curves provide an idea of the strength and deformability of the test soil material. The complex stress-strain behavior of unsaturated soil is influenced by many factors, including externally applied stress (σ_3 - u_a), soil type, structure, density, and

suction ($u_a - u_w$), arising from surface tension across the air-water interface within the soil (Russell and Khalili 2006). The results of deviatoric stress and volumetric strain response against axial strain obtained from the CD triaxial shear tests under three net confining stresses of 100, 200 and 300 kPa but at the same matric suction of 50 kPa, 250 kPa, 500 kPa and 750 kPa are presented in Figures 3.29a, b, 3.30a, b, 3.31a, b and 3.32a, b.

The specimen's sign convention and designation used were the same as those explained in section 3.2.4. All stress-strain curves clearly indicate that an increase in initial and overall stiffness (i.e. initial and subsequent tangent modulus) as well as the brittleness with increase in confinement. The peak deviatoric stress increased with an increase in confining pressure followed by a slight decrease for *s* = 50 kPa until it reached a critical state.

The post-peak reduction in stress, with a large amount of deformation, is known as strain-softening type behavior. The peak strength is attributed to the effect of the increase in interlocking due to the increase in confinement. The critical strength represents the strength of soil after such interlocking arrangement has been broken down, and large amounts of deformation have occurred.

Figures 3.29b, 3.30b, 3.31b, and 3.32b clearly manifest the change in shear-induced volumetric response from compressive to dilational type when the soil saturation state changed from saturated to unsaturated state with the introduction of matric suction of magnitude as low as 50 kPa. Volume changes can occur during shearing due to particle re-arrangement because of particle sliding (slippage) and rolling that can cause better interlocking resulting in compression.

On the other hand, particles can ride over one another resulting in an increase in volume, as illustrated in Figure 3.28. All the unsaturated soil specimens showed initial compression followed by stress-induced dilatancy type response. Continued shearing

causes the onset of shear localization thereby causing breakdown of interlocking, and is accompanied by an increase in volume (dilatancy).

Increase in confinement pressure causes higher compression of the specimen and, hence, should suppress the amount of dilation. This is clearly manifested in Figures 3.29b, 3.30b, 3.31b and 3.32b, where dilation is suppressed with increased in confining pressure from 100 to 300 kPa as expected. Such type of stress-strain and volumetric response are typical of dense or over consolidated soils, especially, silty sands.

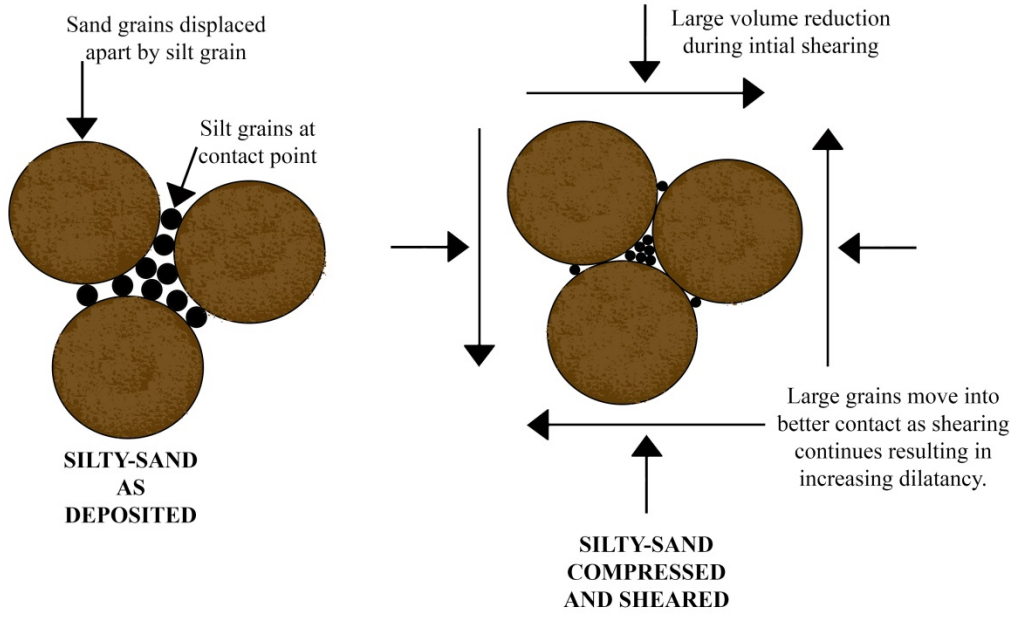

Figure 3.28 Particle structure before and during shearing (from Yamamuro and Lade, 1997)

One can observe that an increase in the matric suction causes an increase in rate of shear strength for *s* = 50 kPa to *s* = 500 kPa at σ_3- u_a = 100 to σ_3- u_a = 200, but at *s* = 750 kPa, the rate of increase in strength from σ_3- u_a = 200 to σ_3- u_a = 300 is suppressed. This occurs because, at a high level of confinement, there will be bond breakage during continued shearing. This may result in the lower rate of increase in suction-induced

strength. Thus, bond damage may not be dominated at low stress level, but may have dominated the influence at a high stress level, thereby putting a limit to the increase in shear strength response at high suction and high stress level.

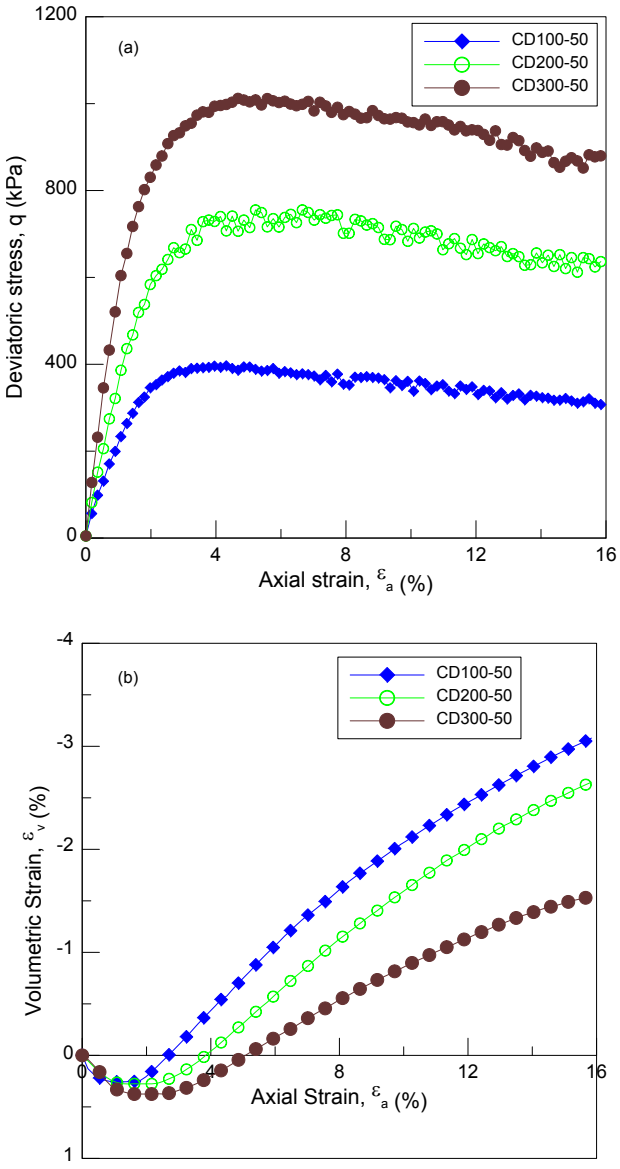

Figure 3.29 (a) Deviatoric stress against axial strain curves, (b) volumetric strain against axial strain curves at three net confining pressures of 100, 200 and 300 kPa but at same matric suction of 50 kPa

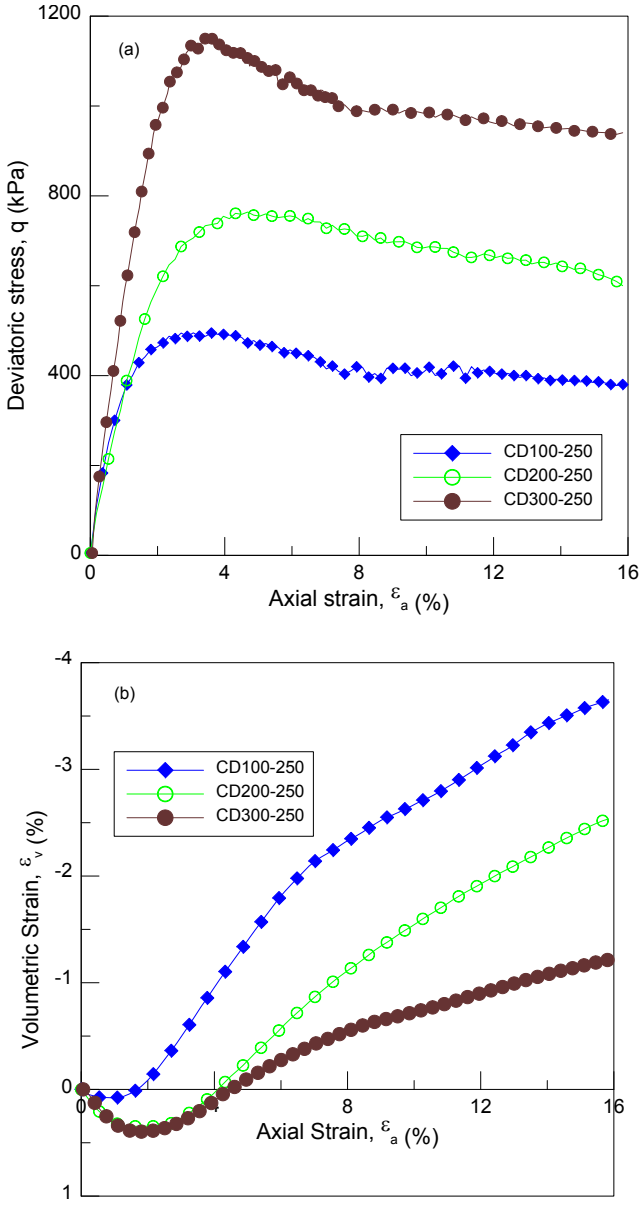

Figure 3.30 (a) Deviatoric stress against axial strain curves, (b) volumetric strain against axial strain curves at three net confining pressures of 100, 200 and 300 kPa but at same matric suction of 250 kPa

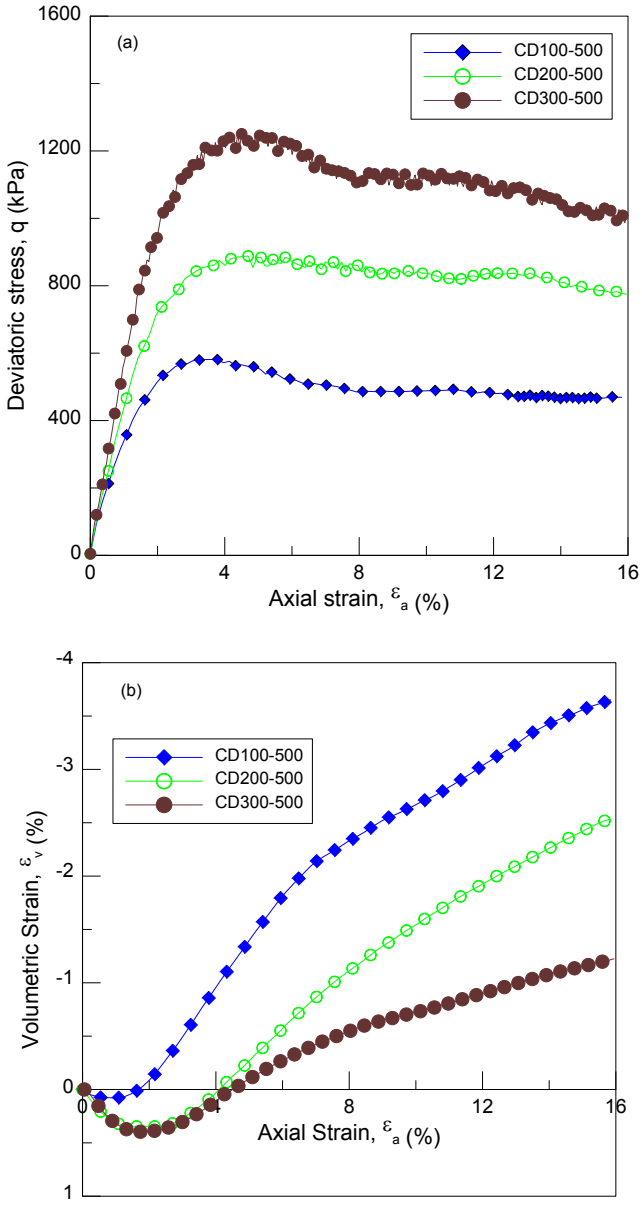

Figure 3.31(a) Deviatoric stress against axial strain curves, (b) volumetric strain against axial strain curves at three net confining pressures of 100, 200 and 300 kPa but at same matric suction of 500 kPa

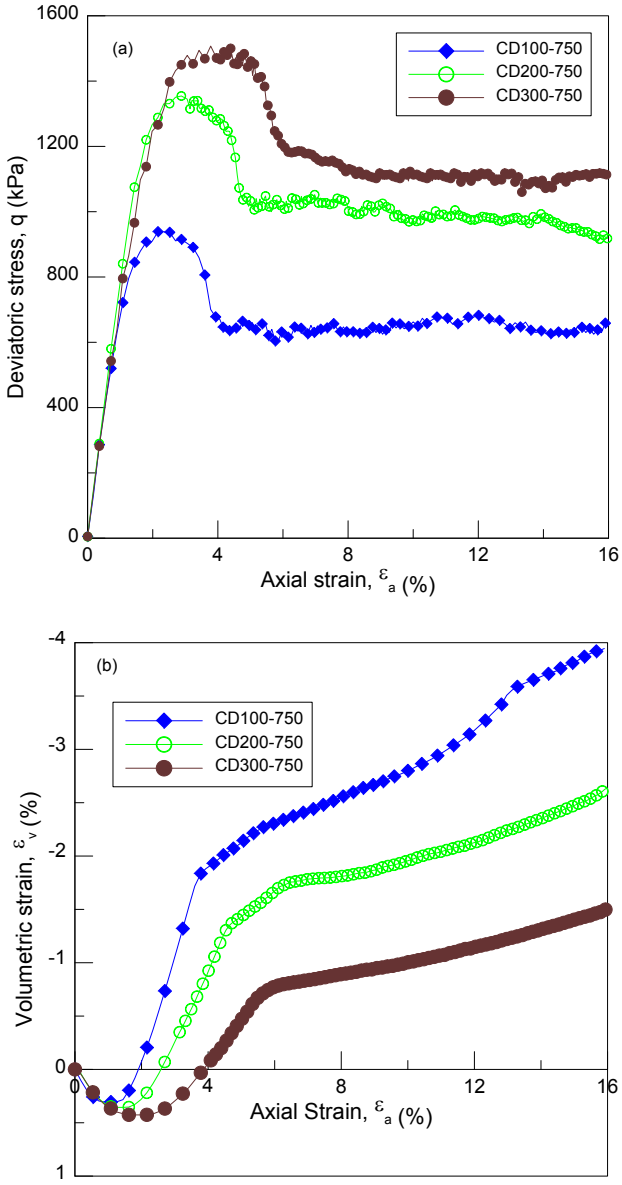

Figure 3.32(a) Deviatoric stress against axial strain curves, (b) volumetric strain against axial strain curves at three net confining pressures of 100, 200 and 300 kPa but at same matric suction of 750 kPa

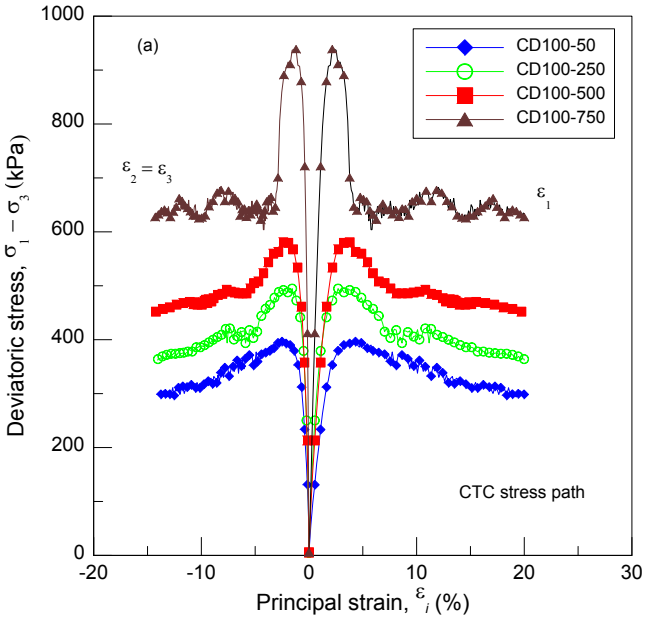

Figure 3.33 Experimental deviatoric stress – principal strain response for CTC stress path of CD tests at *s* = 50 kPa, 250 kPa, 500 kPa and 750 kPa; a) $P_{initial}$ = 100 kPa

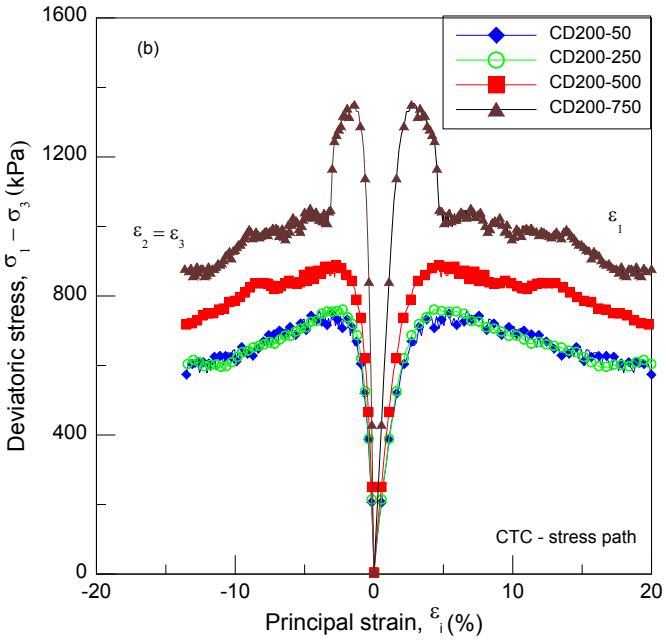

Figure 3.34 Experimental deviatoric stress – principal strain response for CTC stress path of CD tests at *s* = 50 kPa, 250 kPa, 500 kPa and 750 kPa; b) $P_{initial}$ = 200 kPa

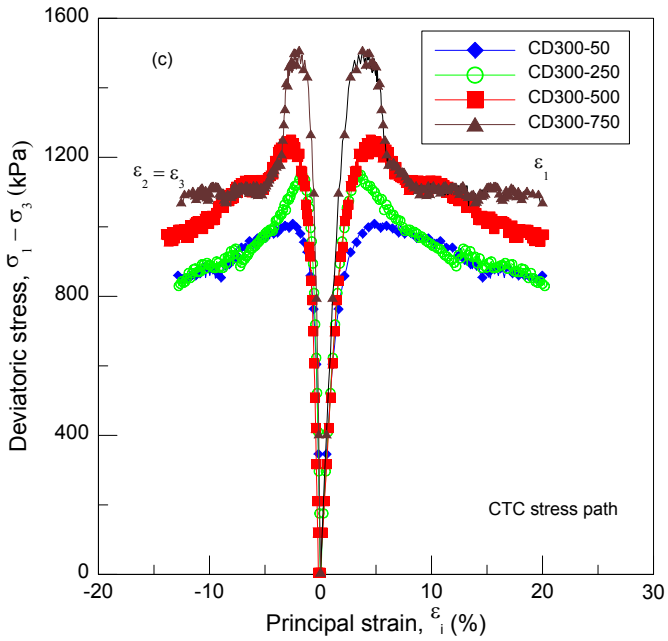

Figure 3.35 Experimental deviatoric stress – principal strain response for CTC stress path of CD tests at *s* = 50 kPa, 250 kPa, 500 kPa and 750 kPa; c) $P_{initial}$ = 300 kPa

Figures 3.36a, 3.37a, 3.38a, 3.39a show the three Mohr's circle plotted at different confining pressures for varying matric suctions of 50 kPa, 250 kPa, 500 kPa and 750 kPa. These Mohr's circles can be used to find the apparent cohesion intercept as well as the angle of internal friction ϕ^b. Figures 3.36b, 3.37b, 3.38b, and 3.39b show the stress path followed by specimens tested at 100, 200 and 300 kPa of mean net pressure in p-q space, along with the critical state line.

Each Mohr-Coulomb failure envelope was plotted, based on three tests each at different net confining pressures (i.e., 100, 200 and 300 kPa), but at same matric suction (i.e., 50 kPa), at critical state failure conditions. A tangent drawn to these three Mohr's circles will intersect the y-axis, yielding the total apparent cohesion intercept, c." The tangent makes an angle of approximately 35 deg., with respect to a horizontal indicating that the saturated effective friction angle does not change with suction. This confirms the

assumption made in the classic Barcelona basic model that the critical state line slope is independent of matric suction.

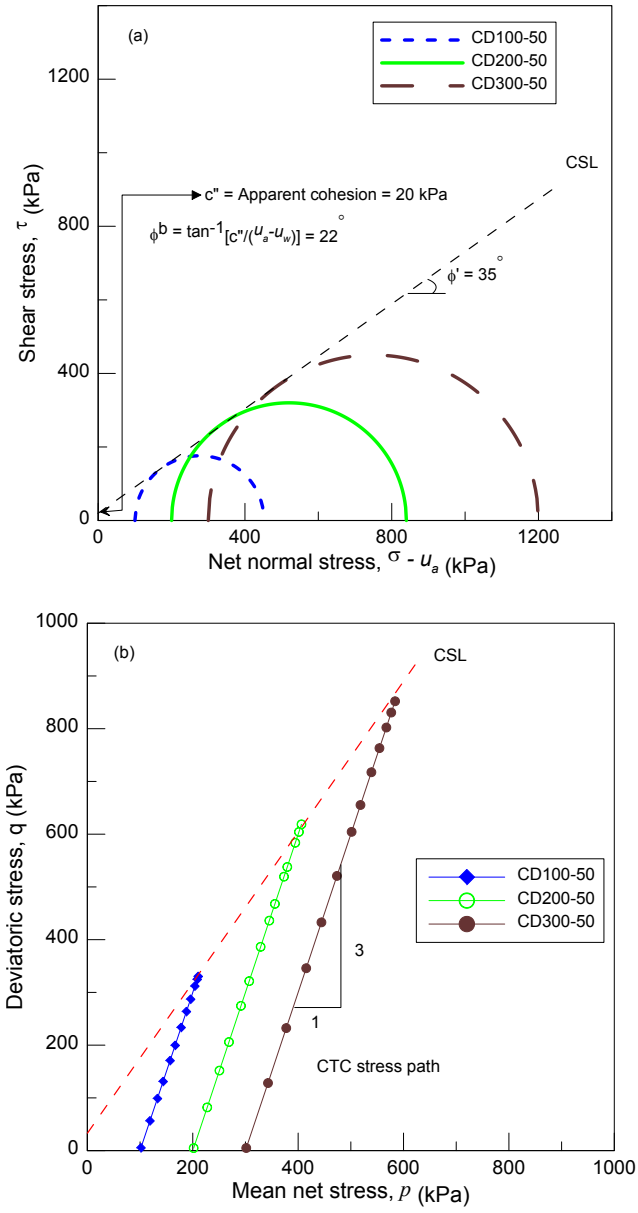

Figure 3.36 a) Mohr's stress circle at three effective confining pressures 100, 200 and 300 kPa and at *s* = 50 kPa, b) Conventional triaxial stress path in p-q space at *s* = 50 kPa

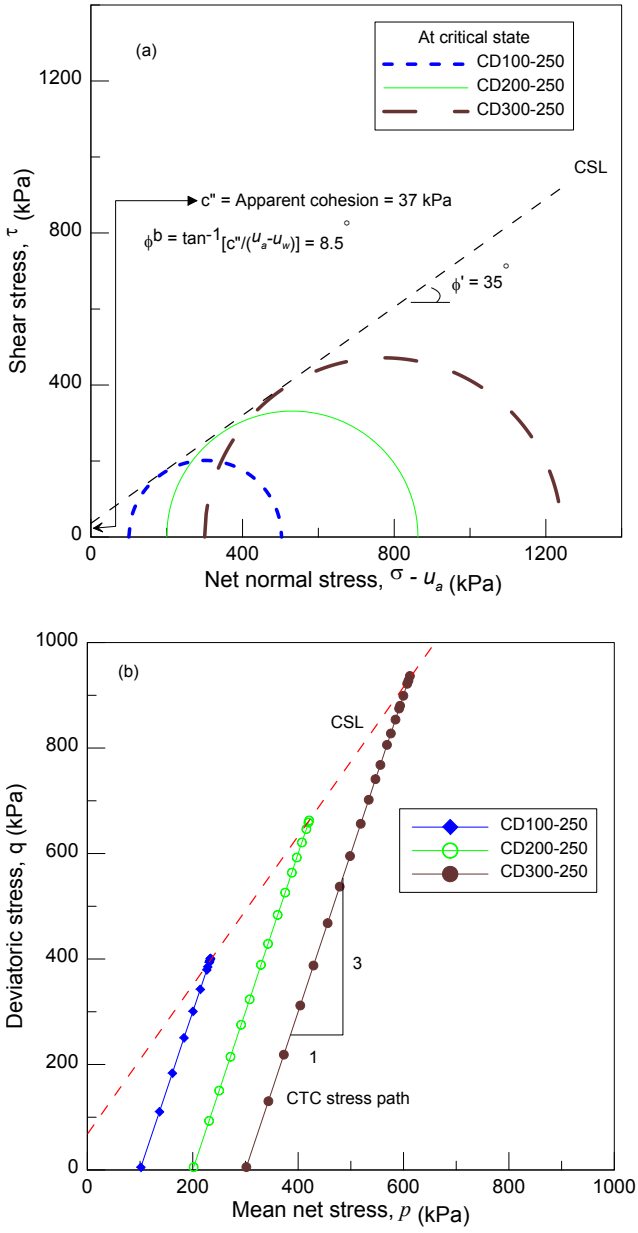

Figure 3.37 a) Mohr's stress circle at three effective confining pressures 100, 200 and 300 kPa and at *s* = 250 kPa, b) Conventional triaxial stress path in p-q space at *s* = 250 kPa

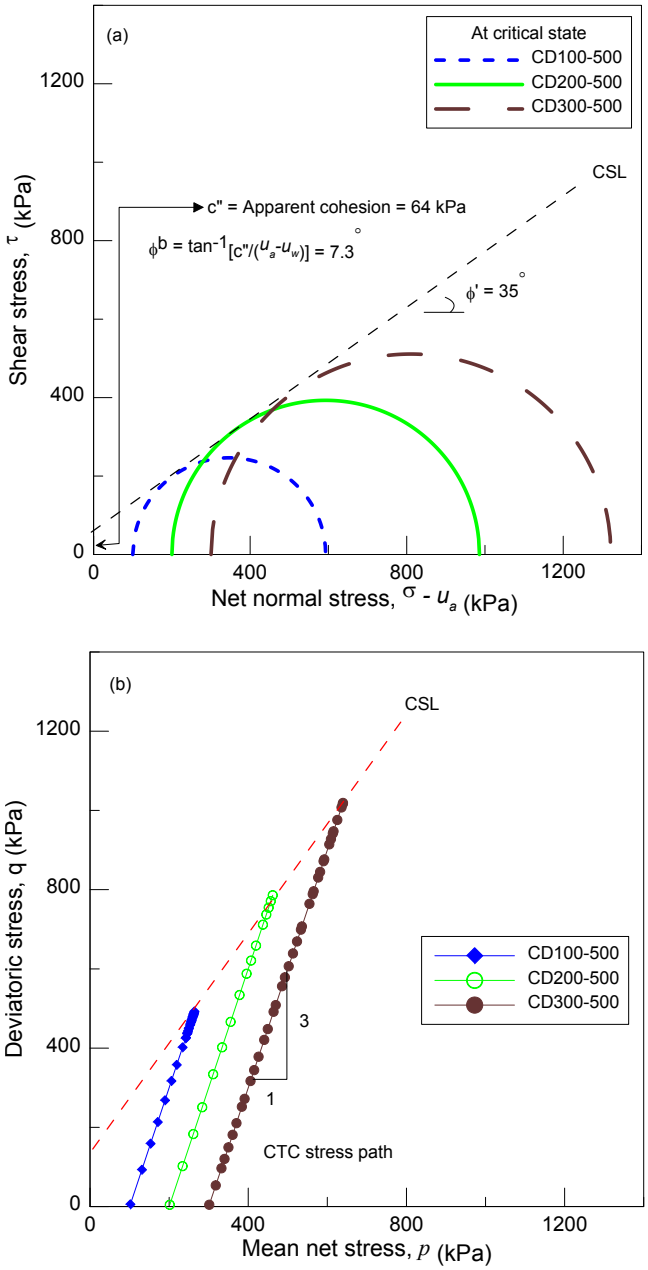

Figure 3.38 a) Mohr's stress circle at three effective confining pressures 100, 200 and 300 kPa and at *s* = 500 kPa, b) Conventional triaxial stress path in p-q space at *s* = 500 kPa

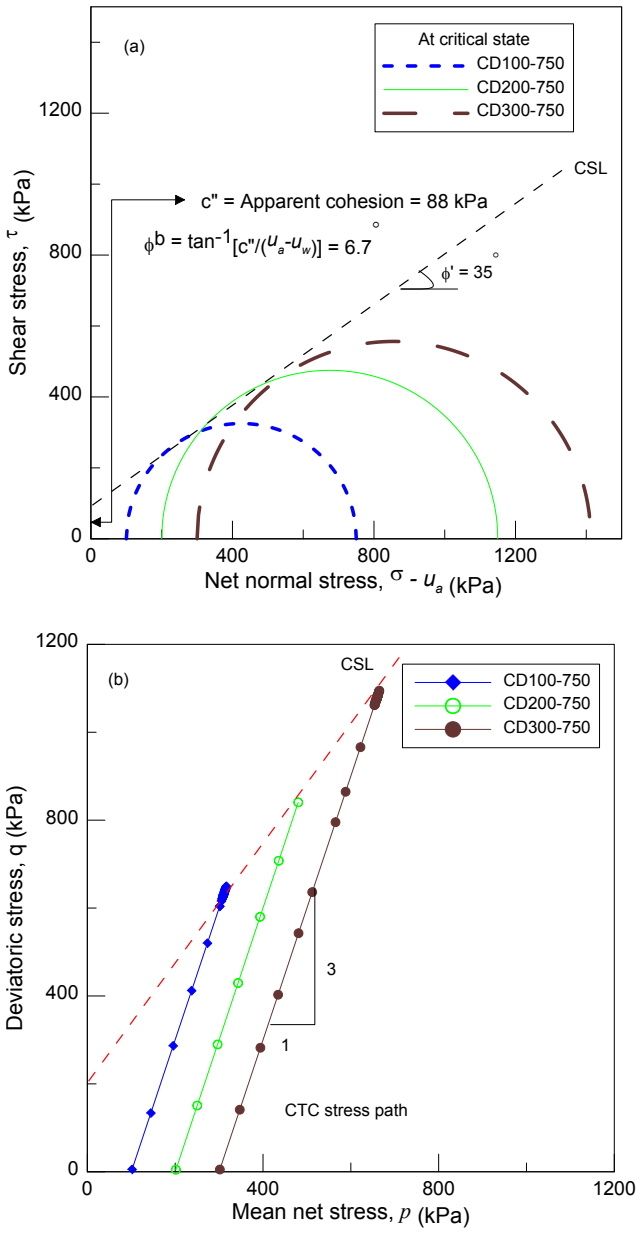

Figure 3.39 a) Mohr's stress circle at three effective confining pressures 100, 200 and 300 kPa and at *s* = 750 kPa, b) Conventional triaxial stress path in p-q space at *s* = 750 kPa

3.9.2 Effect of Matric Suction at same Confining Pressure

The results of deviatoric stress and volumetric strain response against axial strain, obtained from the CD triaxial shear tests under different matric suctions of 0 kPa, 50 kPa, 250 kPa, 500 kPa and 750 kPa but at constant net confining stresses of 100, 200 and 300 kPa are presented in Figures 3.40a,b; 3.41a,b; and 3.42a,b. The specimen sign convention and designation used were the same as those explained in section 3.2.4.

Figure 3.40a clearly indicates an augmentation in initial and overall stiffness (i.e. initial and subsequent tangent modulus), as well as the brittleness with increase in matric suction. The peak deviator stress increased with an increase in matric suction, followed by a decrease in deviator stress for s = 50 kPa until it reached a critical state. The part of stress-strain curve that shows a reduction in stress, after reaching the peak is known as post-peak strain-softening.

The strain-hardening, as seen in saturated soil, was replaced by the strain-softening type response due to the introduction of matric suction into all unsaturated specimens. The magnitude of strain-softening was more pronounced with an increase in matric suction. The specimen failed at lower axial strain, while taking less axial strain to reach a critical state, with an increase in matric suction.

All the specimens were sheared until they softened back to critical state, at which they were expected to exhibit only shear deformations (plastic flow), without further change in strength or volume. The critical state strength increased by about 3 times, while the peak strength increased by 4.5 times when the matric suction was increased to 750 kPa.

Figures 3.40b, 3.41b and 3.42b clearly manifest the change in shear-induced volumetric responses from compressive to dilational types when the soil saturation state changed from saturated to unsaturated state with the introduction of matric suction of a

magnitude as low as 50 kPa. All the specimens showed initial compression, followed by a stress-induced dilatancy-type response that increased with an increase in suction induced.

Such type of stress-strain and volumetric responses are typical of dense or soils with an overconsolidated stress history. Clearly an increase in matric suction also tends to enhance interlocking between particles; which, upon continued shearing results in particles to ride over each other, leads to dilation. Such behavior of increase in volume, with continued shearing, is highly inelastic, and it accompanies the strain-softening behavior. The shearing was continued until the critical state was reached. All the specimens showed failure by bulging.

3.9.3 Impact of Overconsolidation Stress History

The soil used in this work was made of 55% sand, 37% silt, and 8% non-plastic clay; hence, it can be considered an “intermediate” material. The soil was subjected to overconsolidated stress history prior to loading. Post-consolidation, the specimen had an over-consolidated stress history (OCR ~ 16 for CD100-*xx*, ~ 8 for CD200-*xx* and ~ 5 for CD300-*xx*). The impact of over consolidated stress history and suction imposed was clearly seen in the form of a peak failure, followed by the post-peak softening type of stress-strain response, and a dilating-type of volume change response during the shearing stage (Figures 3.40a and b).

It was expected that the test specimen, CD100-750, would dilate to the highest volumetric strain. A close look at the volumetric strain against the axial strain plot indicated that the initial rate of dilation was the highest for the CD100-750 test. At this stage, the peak shear strength had already been crossed and the specimen, while undergoing strain-softening, reached towards its critical state.

All the test specimens were loaded with a shear strain rate of 0.0086%/min except the CD300-750, which was sheared with 0.0086%/min up to peak load and, thereafter, was sheared with a lower shear strain rate of 0.0026%/min until the completion of the test.

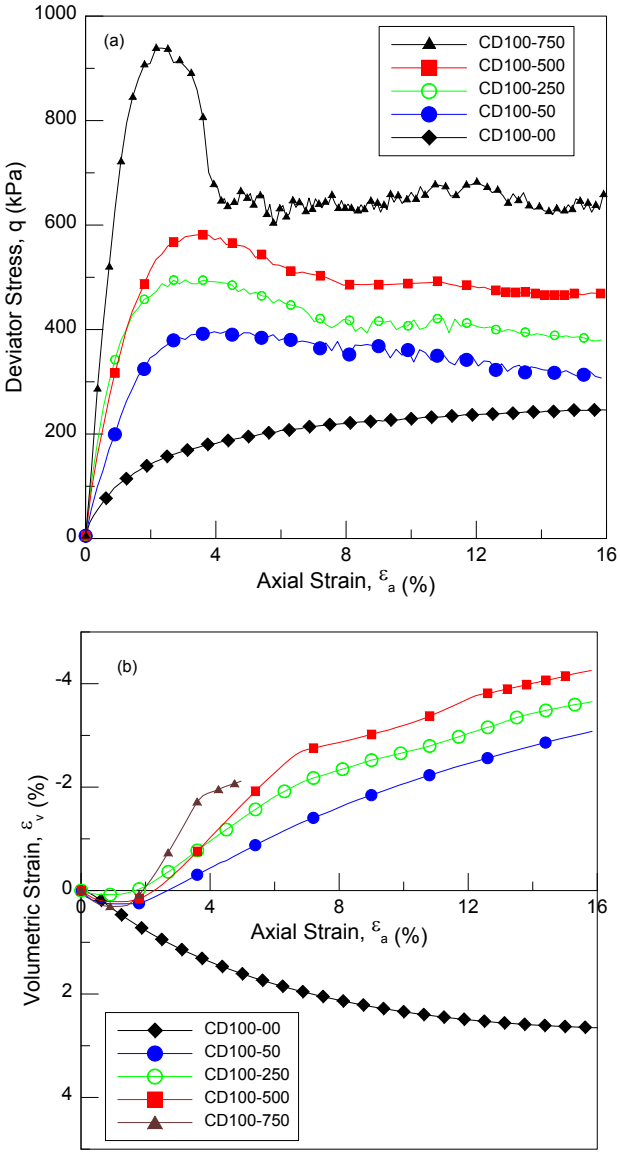

Figure 3.40 Response of compacted silty sand from suction-controlled CD tests at 100-kPa net confining pressure: (a) stress-strain response, (b) volumetric change response

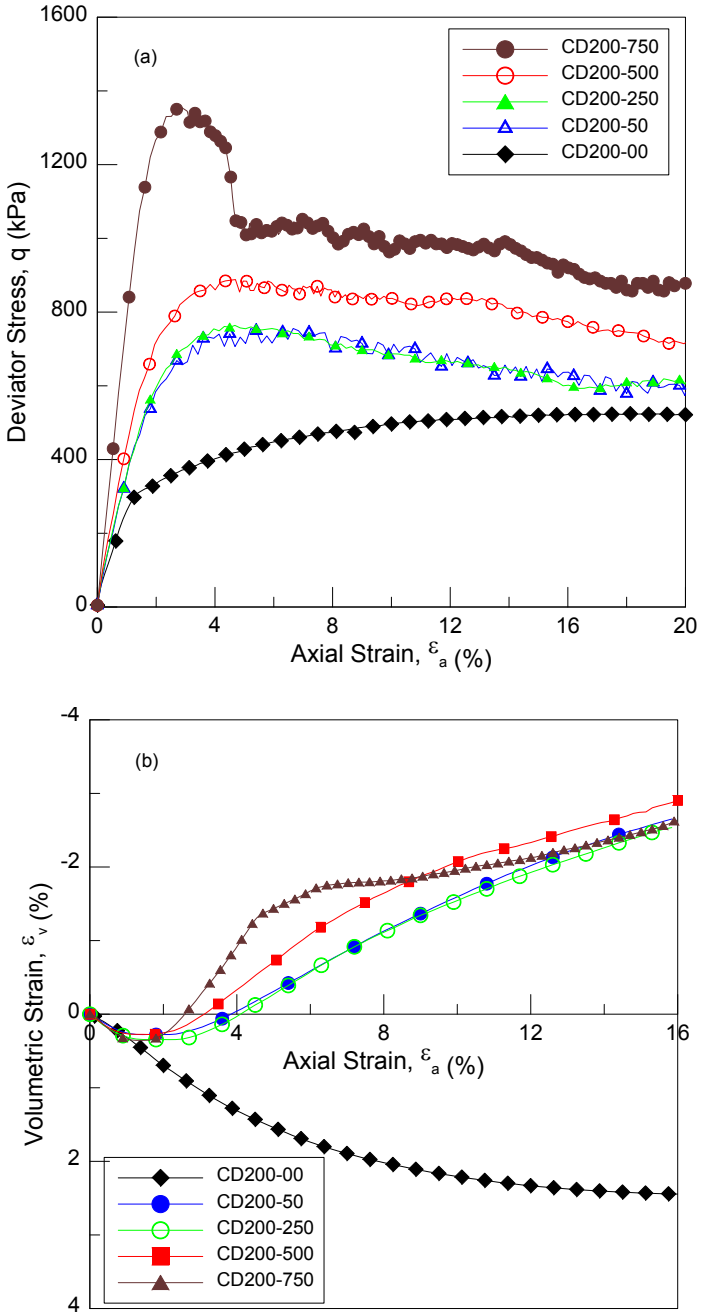

Figure 3.41 Response of compacted silty sand from suction-controlled CD tests at 200-kPa net confining pressure: (a) stress-strain response, (b) volumetric change response

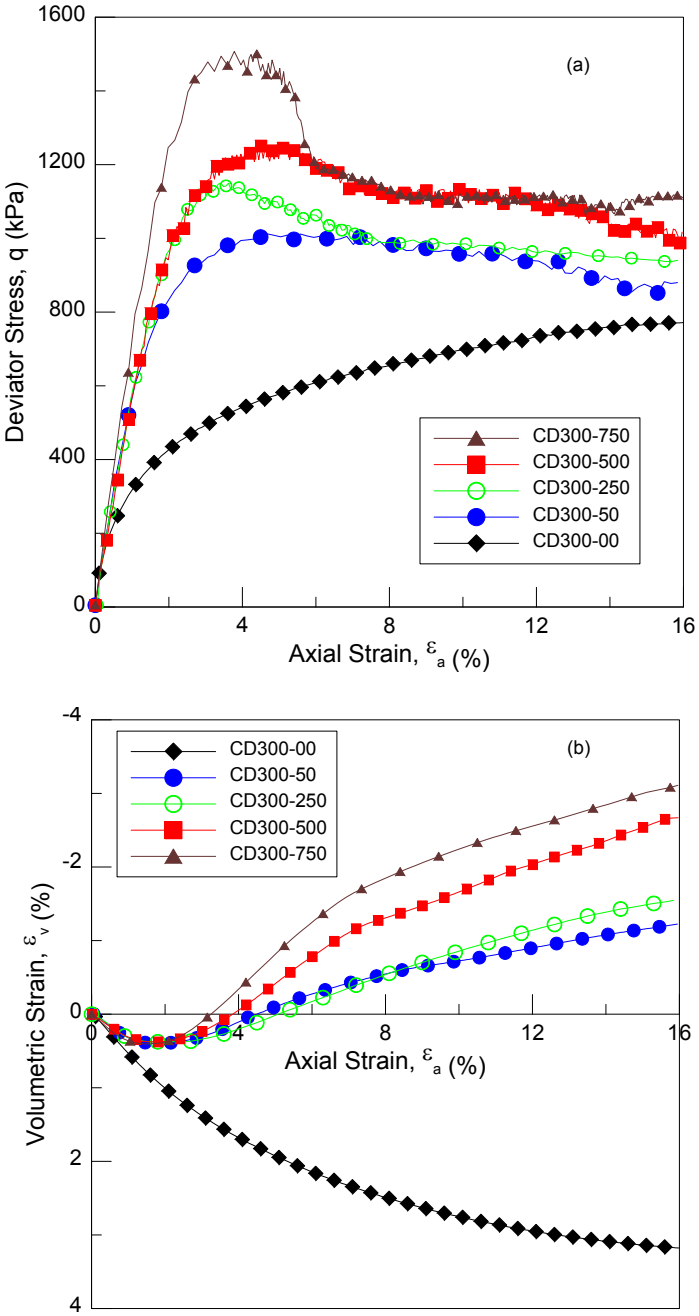

Figure 3.42 Response of compacted silty sand from suction-controlled CD tests at 300-kPa net confining pressure: (a) stress-strain response, (b) volumetric change response

Figure 3.43 indicates the influence of matric soil suction (from *s* = 0 to 750 kPa) on the deviator stress. The deviatoric stress is increased and follows a linear trend for different mean net stress values, varying from p = 100 kPa to 700 kPa.

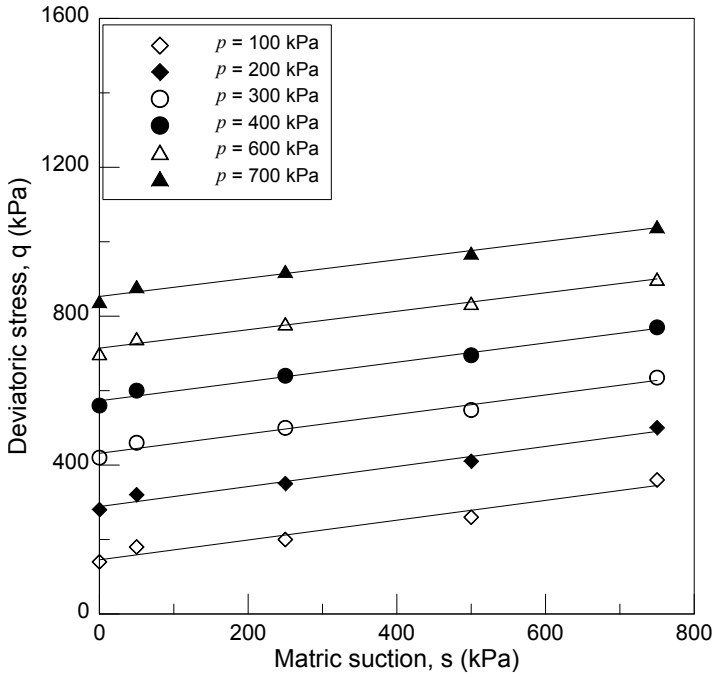

Figure 3.43 Variation of deviator stress with matric suction at varying mean net stress

The CD100-750 and CD200-750 specimen showed an increasing initial rate of dilation, as expected, but the final amount of dilation was lower than their previous counterparts (CD100-500, and CD200-500).

Clearly, the shear rate was not slow enough for these specimens, at *s* = 750 kPa, to allow them to dilate to their maximum (see Figure 3.42b). It is worth mentioning here that it is almost impossible for the dilation to be isotropic due to the end restraints offered, resulting in restriction of movement of the specimen away from base /top support, especially when suction as high as 750 kPa is induced.

3.9.4 Effect of Suction on Secant Stiffness Modulus

Three definitions for stiffness modulus have been used in this program. First, the secant modulus $E_{1\%}$, measured from the beginning of shearing strain to 1% strain. Second, the secant modulus E_{peak}, measured from the beginning of shearing to strain at peak strength, and the third is the secant modulus $E_{critical}$, measured from the beginning of shearing up to strain (about 12-18%) at critical strength.

All the above three stiffness modulus are obtained from stress-strain curves for all three confining pressures $\sigma_3 - u_a$ = 100, 200 and 300 kPa, and are plotted as a function of matric suction, s = 50, 250, 500 and 750 kPa as shown in Figures 3.43, 3.44 and 3.45.

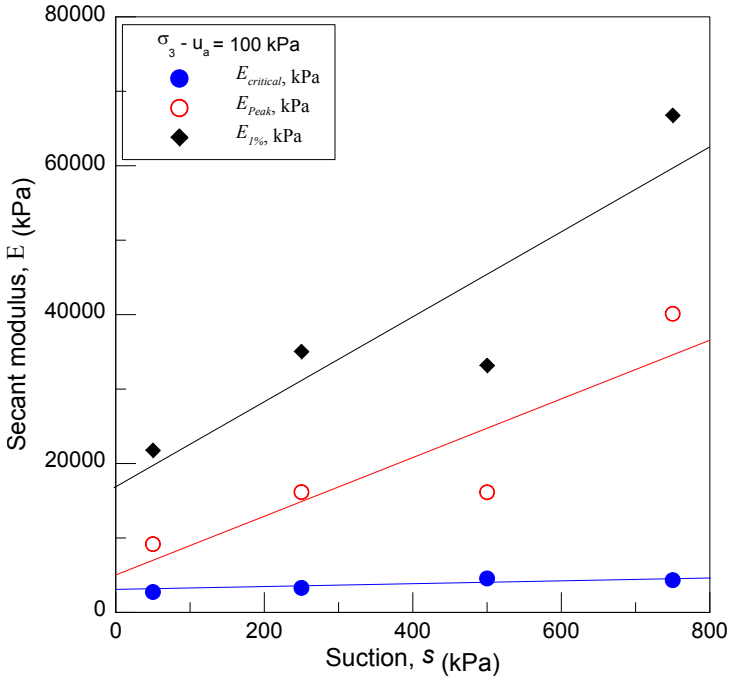

Figure 3.44 Secant stiffness modulus $E_{critical}$, $E_{1\%}$ and E_{peak} variation at $\sigma_3 - u_a$ = 100 kPa

As shown in Figures 3.44, 3.45 and 3.46, all the three secant modulus tend to increase with an increase in matric suction. The secant modulus $E_{critical}$ increases almost linearly and shows a small increase in its value with an increase in matric suction; thus, indicating less influence of matric suction on secant modulus at critical strength ($E_{critical}$).

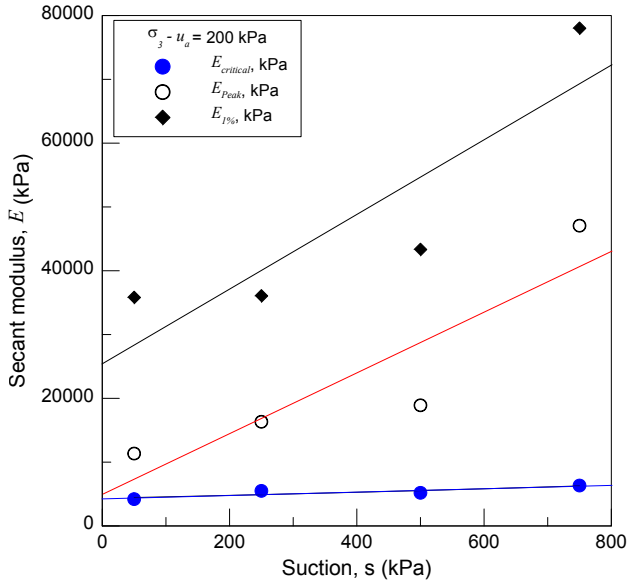

Figure 3.45 $E_{critical}$, $E_{1\%}$ and E_{peak} modulus variation at $\sigma_3 - u_a$ = 200 kPa

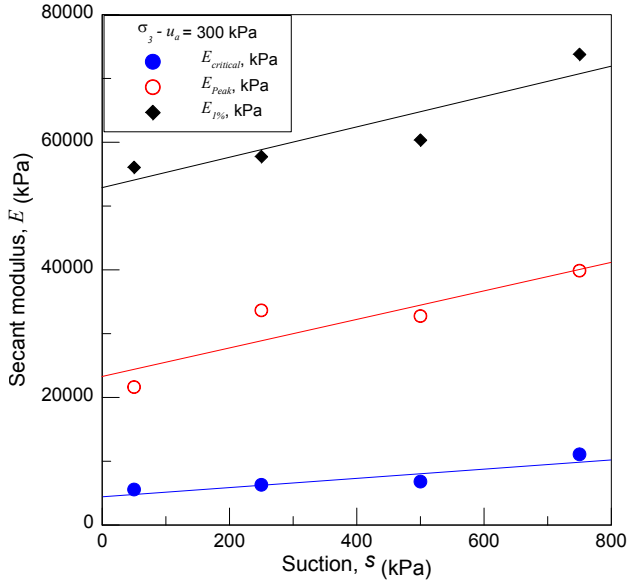

Figure 3.46 $E_{critical}$, $E_{1\%}$ and E_{peak} modulus variation at σ_3 - u_a = 300 kPa

However, the $E_{1\%}$ and E_{peak} shows a large increase in its value with an increase in matric suction, indicating greater influence of matric suction on small strain stiffness modulus ($E_{1\%}$). Similar results are seen at all values of $\sigma_3 - u_a$ = 100, 200 and 300 kPa. It

should be noted that the relationship is linear at all confining pressures between matric suction and small strain modulus. On the other hand, for $E_{1\%}$ and E_{peak}, it is highly non-linear (exponential form), indicating a rapid increase in its magnitude with an increase in suction for $\sigma_3 - u_a$ = 100 and 200 kPa.

However, it becomes more of the linear form at $\sigma_3 - u_a$ = 300 kPa. It also indicates that the rate of increase of small strain modulus ($E_{1\%}$), with an increase in matric suction, will be suppressed if the confining pressure is increased hereafter.

3.9.5 Effect of Confining Pressure on Secant Stiffness Modulus for Varying Suction

Figure 3.47 shows the effect of confining pressure $(\sigma_3 - u_a)$ on small strain modulus ($E_{1\%}$). The plot suggests that a small strain modulus, in general increases, with an increase in external confinement ($\sigma_3 - u_a$) at all values of matric suction; however, the rate of increase in small strain modulus tends to decrease at *s* = 750 kPa, with an increase in confining pressures from $\sigma_3 - u_a$ = 100 to 300 kPa.

As shown in Figure 3.48, large strain modulus ($E_{critical}$) increases linearly and shows a small increase in its value, with an increase in matric suction for $\sigma_3 - u_a$ = 100 and 200 kPa. However at $\sigma_3 - u_a$ = 300 kPa, it shows an appreciable increase at *s* = 750 kPa, indicating less influence of matric suction on large strain modulus ($E_{critical}$) at low confinement, but an appreciable increase with highest suction (i.e., *s* = 750 kPa) at highest confinement (i.e., $\sigma_3 - u_a$ = 300 kPa).

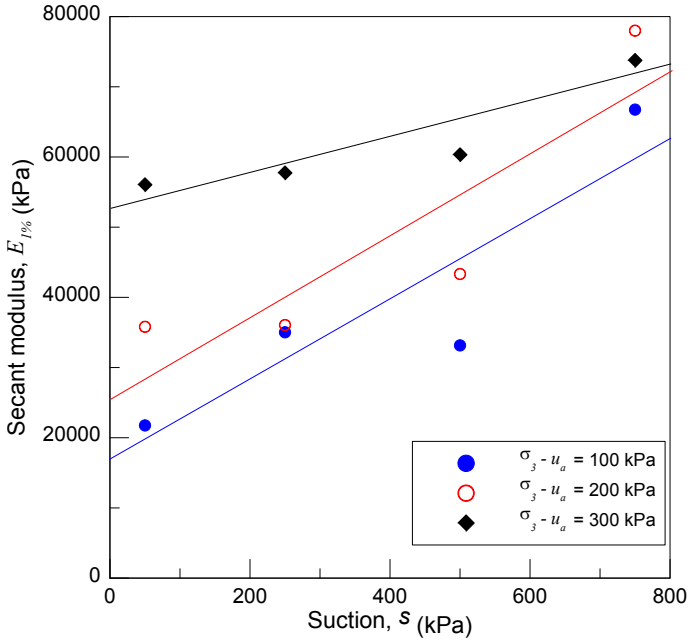

Figure 3.47 Effect of confining pressure, $\sigma_3 - u_a$ on $E_{1\%}$ modulus at different values of matric suction from *s* = 50 to 750 kPa

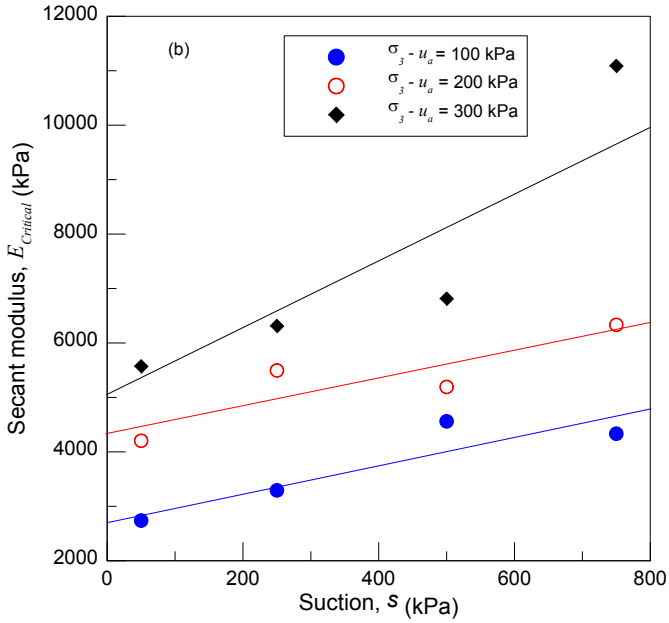

Figure 3.48 Effect of confining pressure, $\sigma_3 - u_a$ on $E_{critical}$ modulus at different values of matric suction from *s* = 50 to 750 kPa

3.9.6 Analysis at Peak Stress

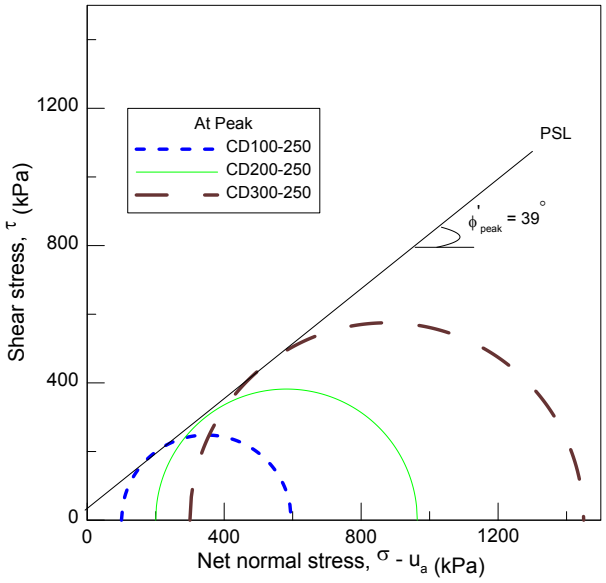

Figure 3.49 Mohr's stress circle at peak failure corresponding to effective confining pressures $\sigma_3 - u_a$ = 100, 200 and 300 kPa at *s* = 250 kPa

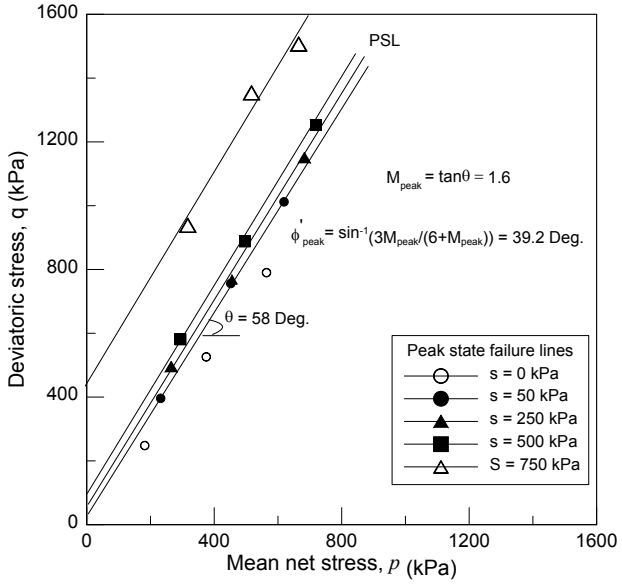

Figure 3.50 Peak state lines in the *p*-*q* plane from the saturated and unsaturated soil CD triaxial tests

The angle of internal friction at peak failure was analyzed to be 39 degrees, by drawing three Mohr's stress circles at peak failure, corresponding to effective confining pressures $\sigma_3 - u_a$ = 100, 200 and 300 kPa at *s* = 250 kPa, as illustrated in Figure 3.49.

The line joining the peak failure stress, corresponding to *s* = 50, 250, 500 and 750 kPa at three confining pressures of 100, 200 and 300 kPa drawn in p-q space, yielded the peak state line slope of 1.6 (M_{peak} = 1.6), as shown in Figure 3.50. Similar to the critical state lines in p-q space, there was not much change in the slope, but an upward shift in the peak state line was observed due to an increase in suction.

3.9.7 Effect of Matric Suction on Cohesion Intercept

The shear strength variation was primarily due to the cohesion intercept variation with suction. Vilar (2006) and Reis et al. (2010) proposed the hyperbolic equation that considers an increase in matric suction contributing to an increase in shear strength by an increase in cohesion. This model was used to predict the shear strength/cohesion intercept, based on following hyperbolic mathematical equation (3.10).

$$c(\psi) = c' + \frac{\psi}{(a + b\psi)} \tag{3.10}$$

Where $c(\psi)$ is the cohesion intercept function of the soil suction, $\psi = u_a - u_w$, c' = effective soil cohesion (at ψ = 0). a and b are curve-fitting parameters obtained from best-fit analysis, by plotting $\psi/(c(\psi) - c')$ versus $\psi > 0$ and fitting the experimental points by a straight line given by the least square method as shown in Figures 3.51a, 3.52a and 3.53a. Figures 3.51b, 3.52b and 3.53b show the variation of cohesion intercept using the Vilar (2006, 2010) model, along with the experimental points.

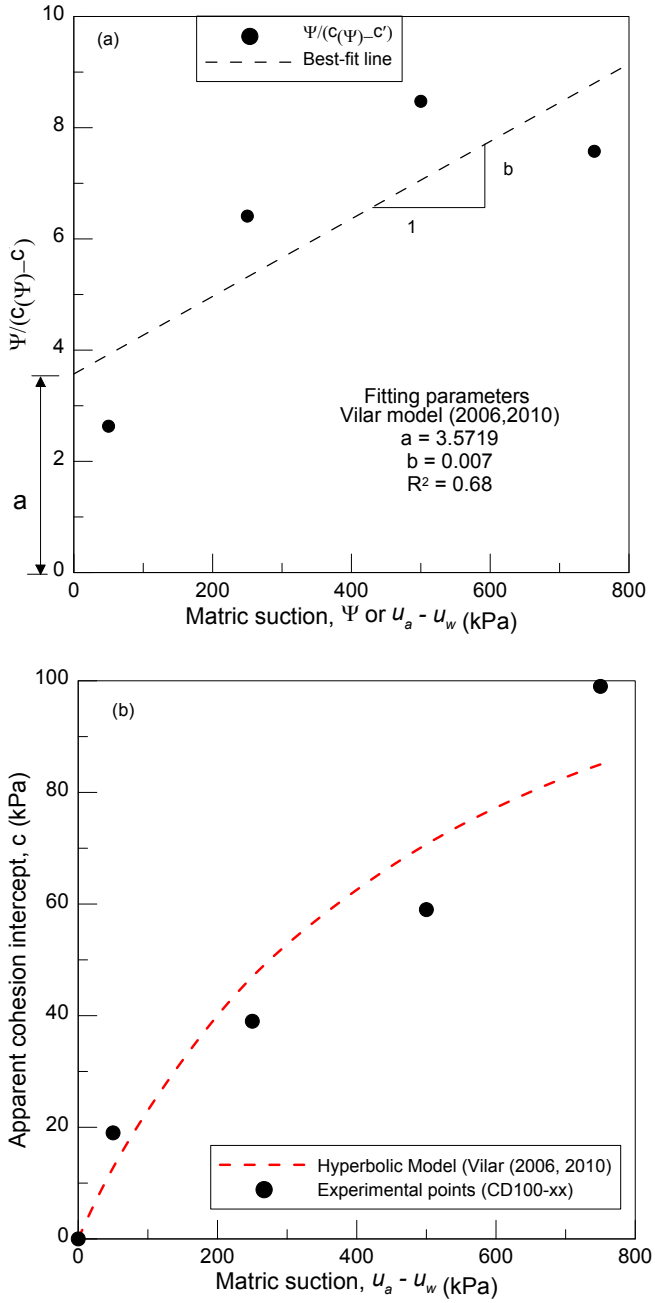

Figure 3.51 a) Evaluation of best-fitting parameters, b) Variation of the cohesion intercept with matric suction (Vilar 2006, 2010) from CD100-xx

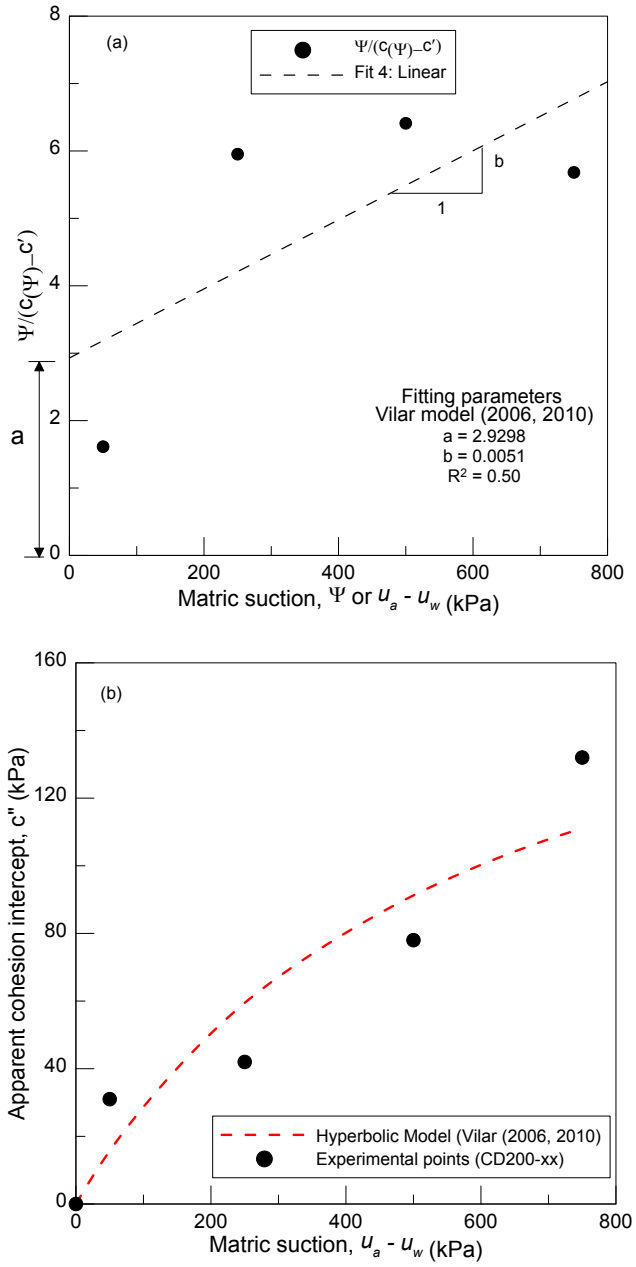

Figure 3.52 a) Evaluation of best-fitting parameters, b) Variation of the cohesion intercept with matric suction (Vilar 2006, 2010) from CD200-xx

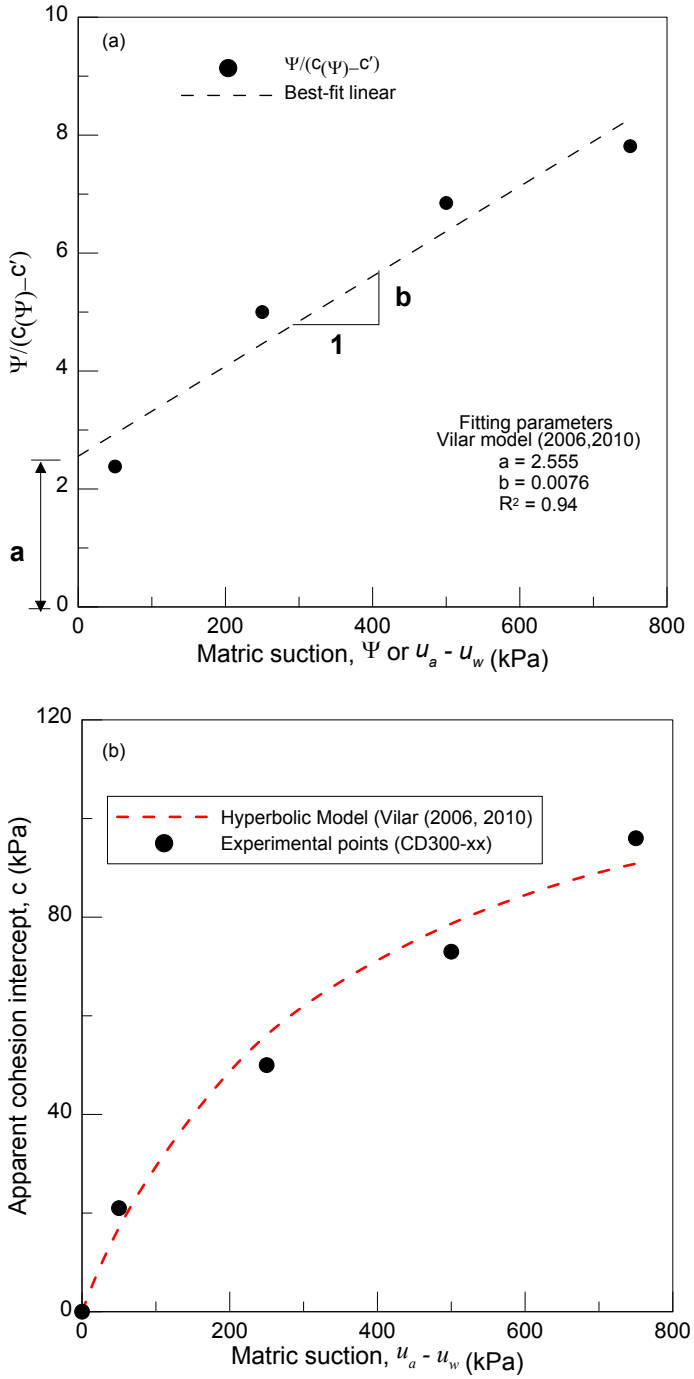

Figure 3.53 a) Evaluation of best-fitting parameters, b) Variation of the cohesion intercept with matric suction (Vilar 2006, 2010) from CD300-xx

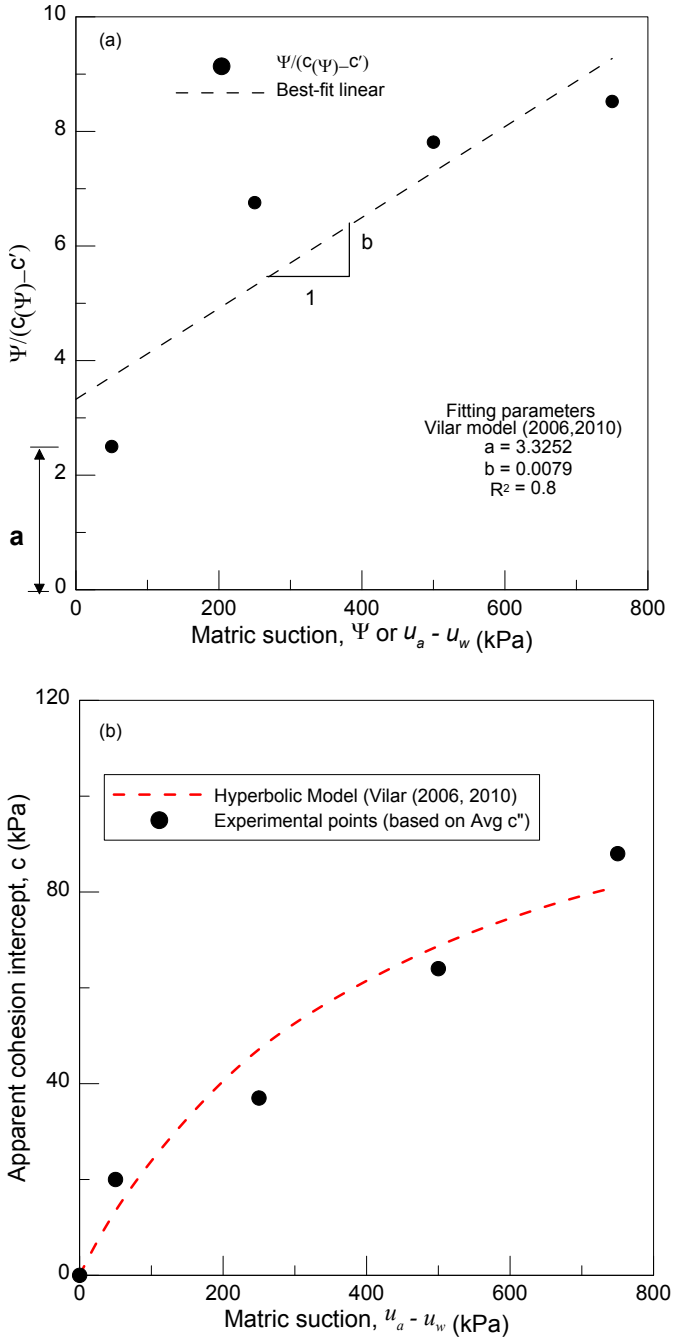

Figure 3.54 a) Evaluation of best-fitting parameters, b) Variation of the cohesion intercept with matric suction (Vilar 2006, 2010) from average value of *c"* at same suction but different confining pressures

3.9.8 Hyperbolic Fit to the Angle of Friction with Respect to Matric Suction

Houston et al. 2008 proposed a hyperbolic equation (3.11) to best fit the experimental data.

$$\emptyset^b = \emptyset' - \left[\frac{\psi^*}{(a + b\psi^*}\right] \; and \; \psi^* = (u_a - u_w) - AEV \tag{3.11}$$

The above equation can be used to determine the unsaturated soil shear strength/friction angle, with respect to cohesion, for different values of matric suction, provided that, the air entry value of soil (AEV) is known, along with the saturated soil effective stress parameters. The parameters a and b are obtained by plotting ψ^* against $\psi^*/(\phi'\text{-}\phi^b)$. Figures 3.56a & b and 3.57a & b show the variation of ϕ^b plotted against matric suction, using the Houston et al.'s (2008) model.

3.9.9 Matric Suction Variation During Shearing

It is very important to ensure completely drained conditions for pore pressures during shear. The variation of matric suction during the shearing stage, as shown in Figure 3.55, is well within ± 0.5 kPa.

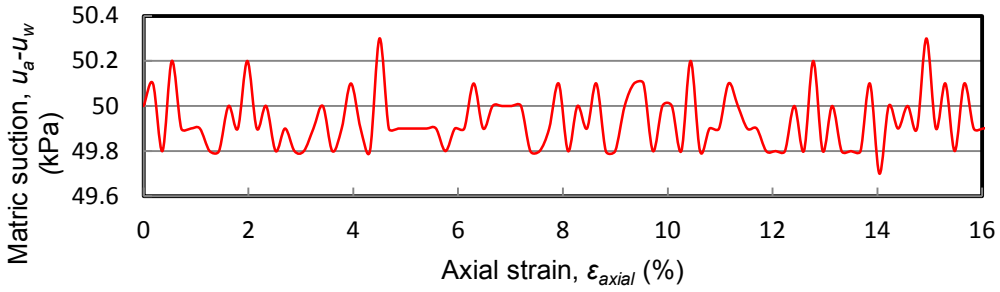

Figure 3.55 Variation of matric suction with axial strain during shearing for CD100-50

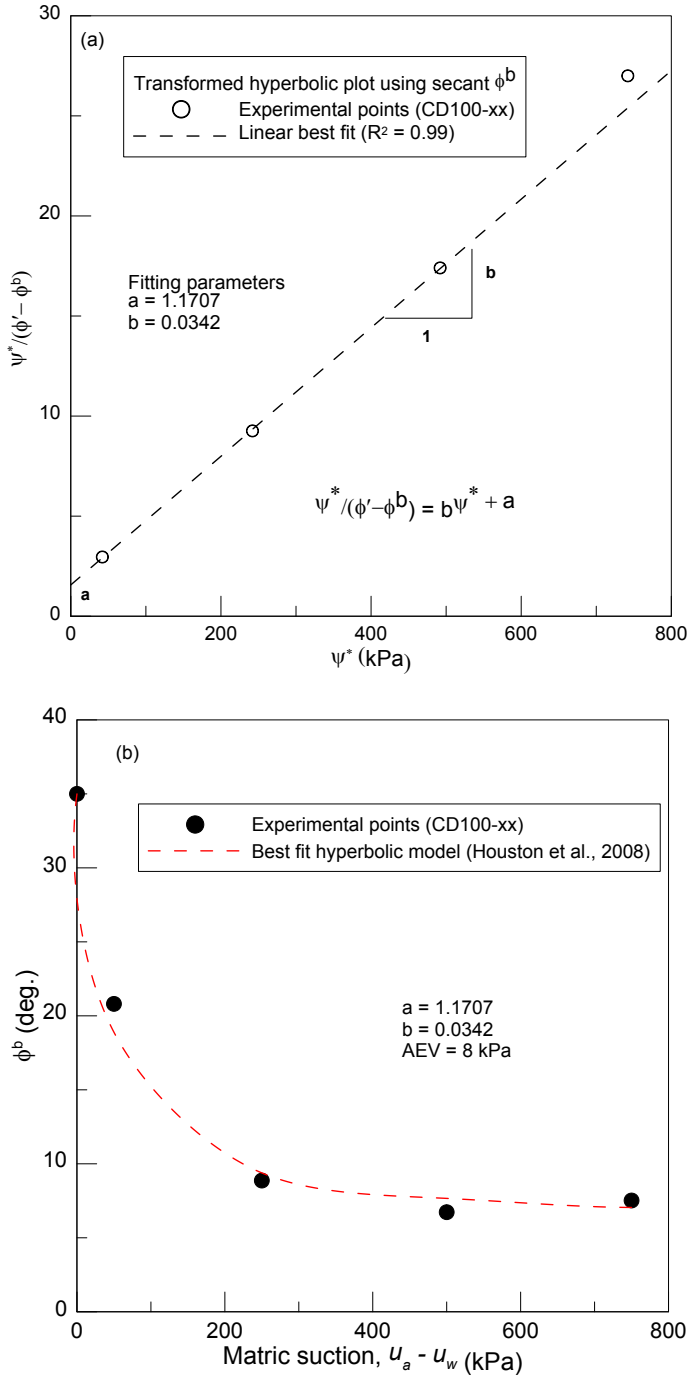

Figure 3.56 a) Evaluation of best-fitting parameters, b) Variation of the cohesion intercept with matric suction (Houston et al., 2008) from CD100-xx

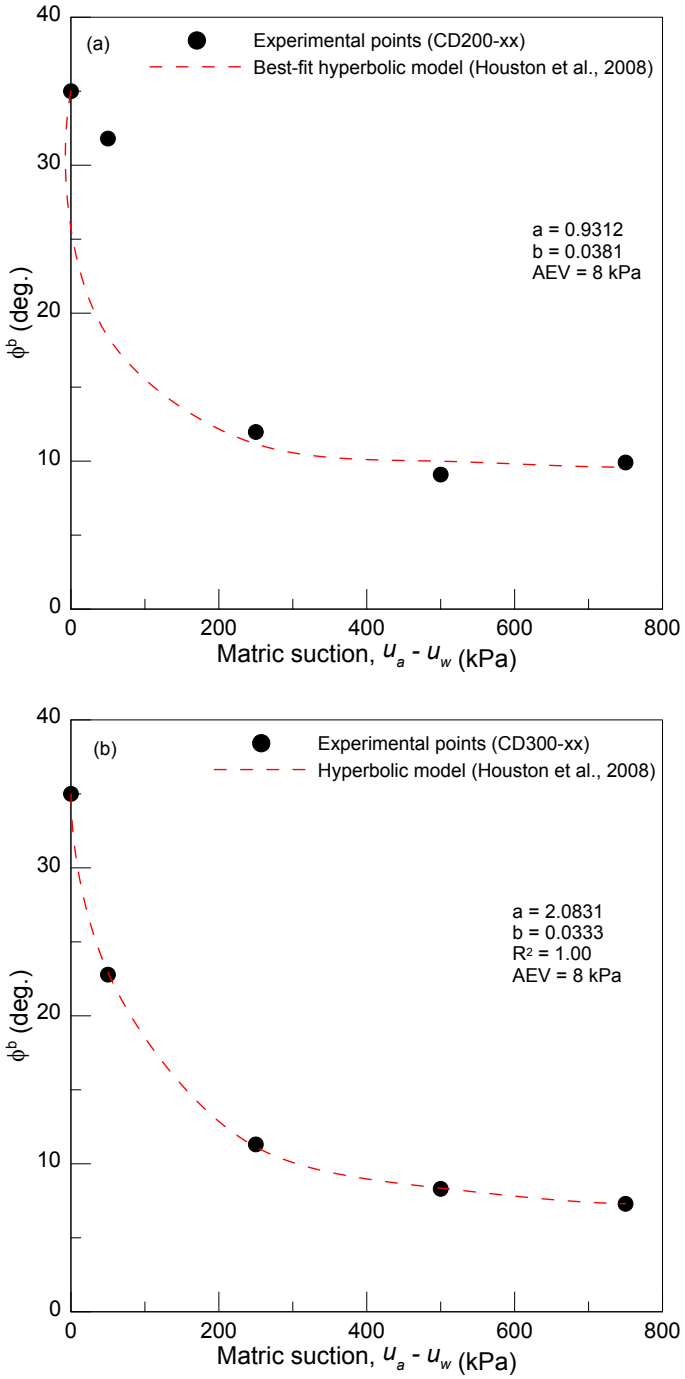

Figure 3.57 a) Variation of the cohesion intercept with matric suction (Houston et al., 2008) from CD200-xx and b) from CD300-xx

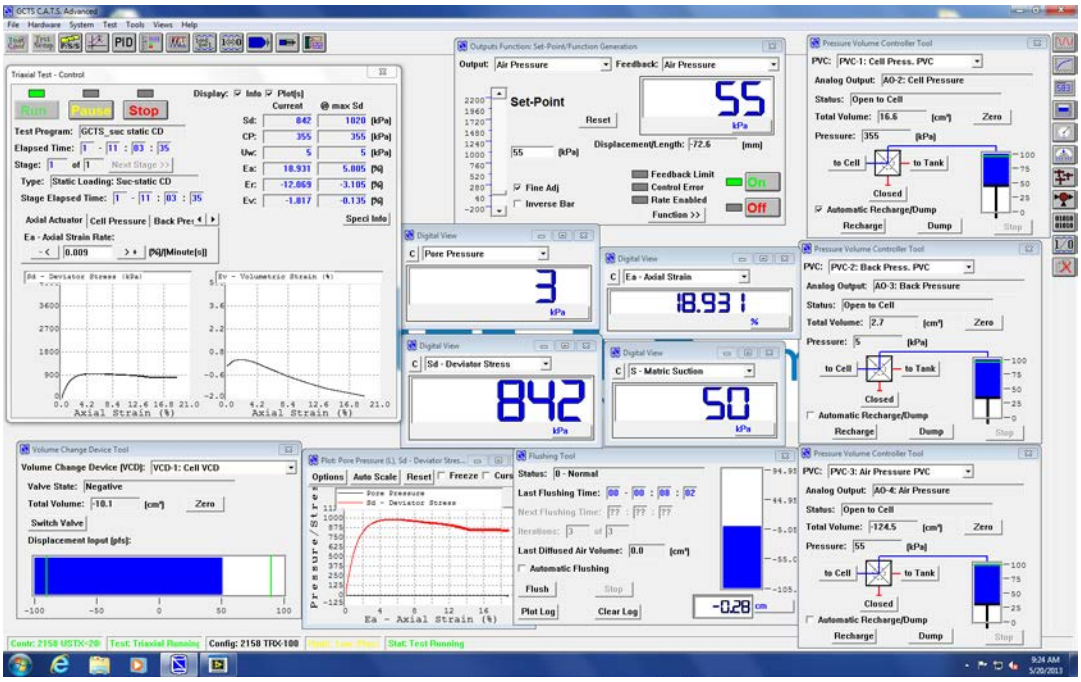

Figure 3.58 Screen shot of software window for CD300-50 triaxial test during shearing

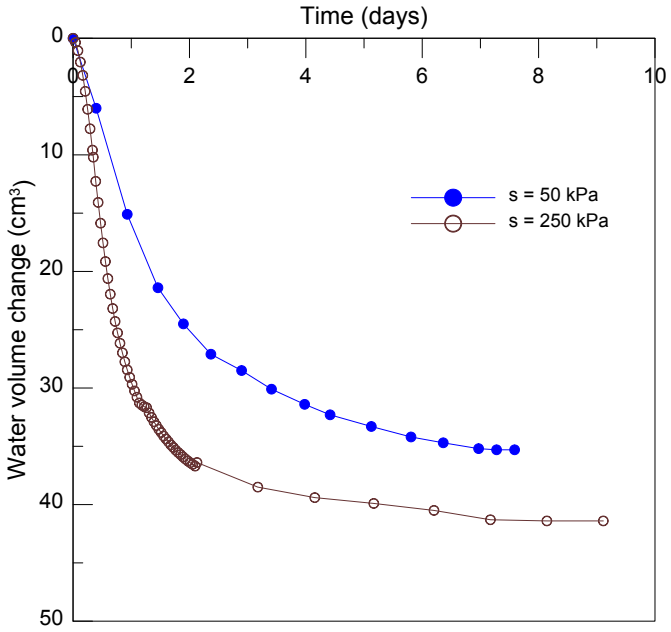

Figure 3.59 Water volume change as observed during suction equalization for *s* = 50 and 250 kPa with respect to time in days

Figure 3.58 shows the screen shot of the software window. Figure 3.59 shows the water volume change, as observed during suction equalization, using the axis-translation technique for *s* = 50 and 250 kPa with respect to time in days. Both specimens were subjected to suction equalization from "as compacted" condition, with a degree of saturation approximately 81% under the net confinement of 10 kPa. It took 8-9 days for suction equalization, depending upon the suction level.

3.9.10 Shear Strength Prediction Based on SWCC Parameters

Prediction of shear strength properties, using at least five different models, based on key model parameters from the soil-water characteristic curve, are presented and compared with experimental values assessed from suction-controlled CD triaxial tests, as shown in Figures 3.60, 3.61, 3.62, 3.63 and 3.64. These methods were already discussed in detail in Chapter 2.

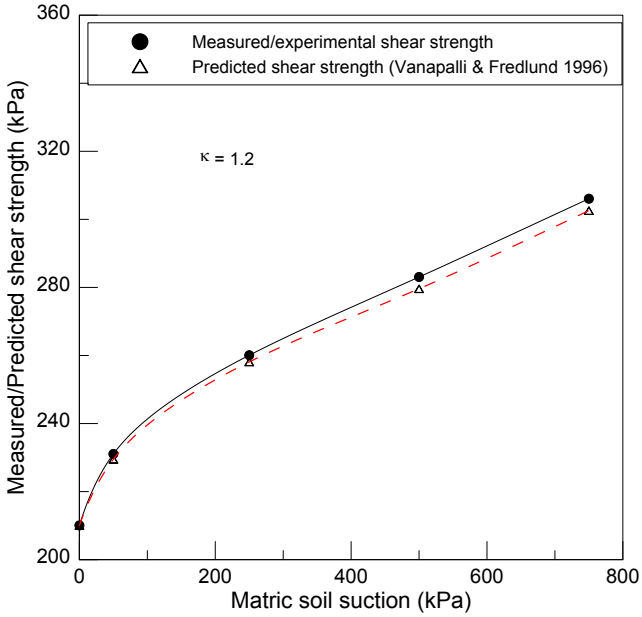

Figure 3.60 Experimental and predicted shear strength (Vanapalli and Fredlund, 1996)

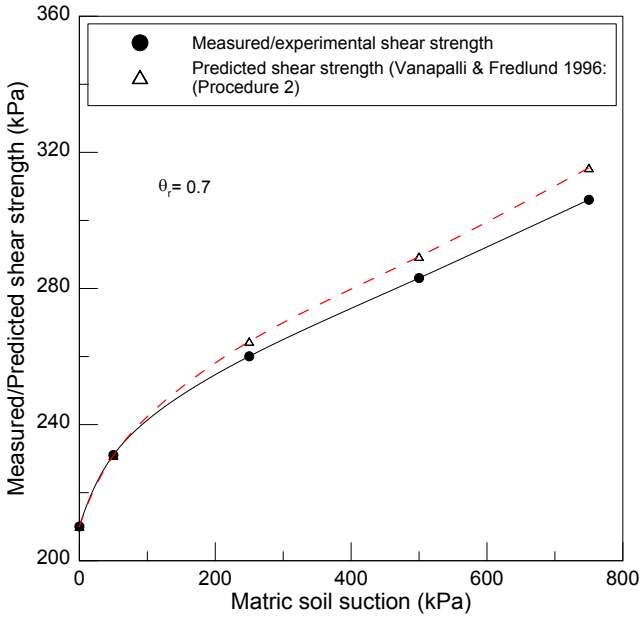

Figure 3.61 Experimental and predicted shear strength (Procedure II)

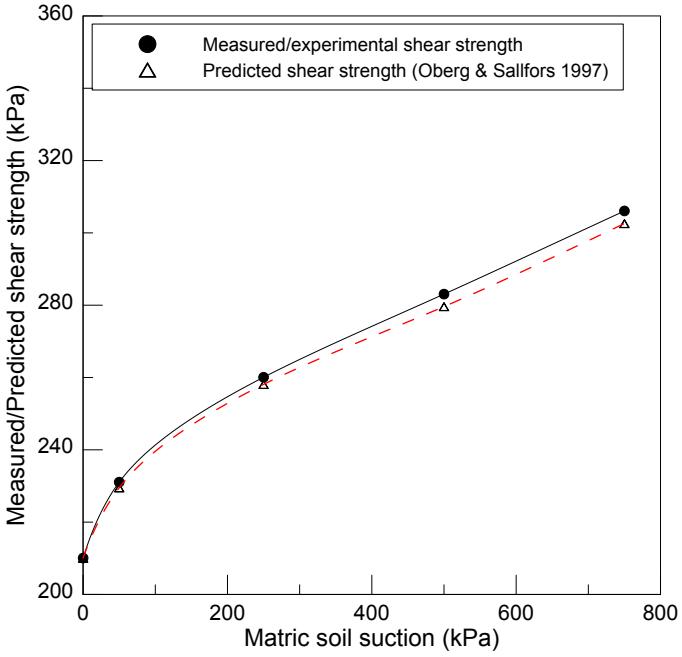

Figure 3.62 Experimental and predicted shear strength (Oberg and Sallfor's, 1997)

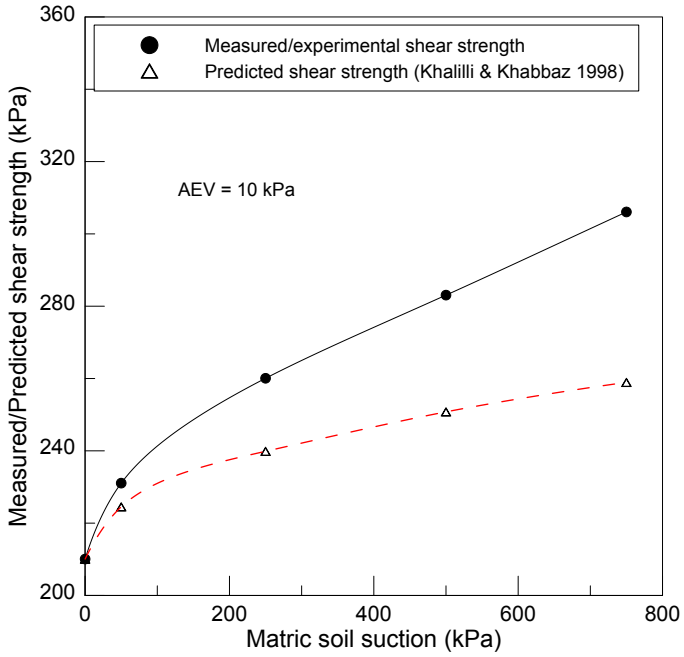

Figure 3.63 Experimental and predicted shear strength (Khallili and Khabbaz, 1998)

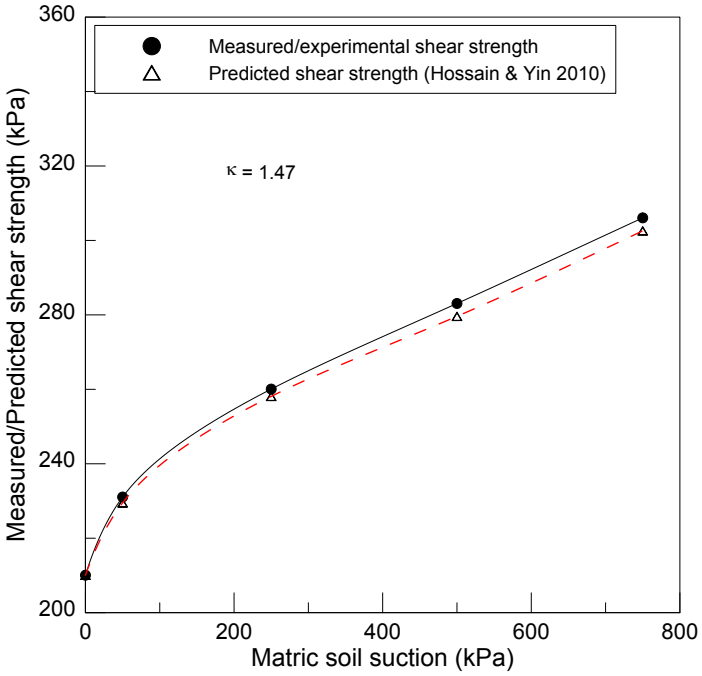

Figure 3.64 Experimental and predicted shear strength (Hossain and Yin, 2010)

The model's proposed by Vanapalli (1996), Fredlund and Vanapalli (1996), Khalili and Khabbaz (1997) and Hossain and Yin (2010) were able to predict the shear strength, in close agreement with measured shear strength at a wider range of soil suction from 50 kPa to 20 MPa. Oberg's and Sallfor's-1997 procedure yielded better predictions, up to 750 kPa matric suction, while the predictions were not in agreement at total suction of 20 MPa.

3.9.11 Soil Dilatancy and Suction in Triaxial test

One of the advantages of using triaxial test equipment over direct shear test is that the specimen has freedom to dilate isotropically/anisotropically in all directions, without boundary restrictions, giving more realistic dilation angles. Shear deformation of geomaterials, such as sands and gravel, during triaxial testing, induces dilatancy; that is, an increase in volume of specimen, and affects the strength of soil. Therefore, dilatancy becomes an essential component in elasto-plastic modelling of saturated, as well as unsaturated, soils.

Chui and Ng (2003) presented an elasto-plastic model with the inclusion of a dilatancy parameter. However, very limited reliable experimental evidence is available for verifying assumptions and calibrating such constitutive relationships for unsaturated soils (Ng and Zhou, 2005). Rowe (1962) defined the dilatancy rate *as* $-d\varepsilon_v/d\varepsilon_1$, where $d\varepsilon_v$ is the volumetric compressive strain and $d\varepsilon_1$ is the major principal compressive strain. He developed his stress-dilatancy relationship as:

$$\frac{\sigma_1'}{\sigma_3'} = tan^2\left(45^o - \frac{\varphi_f}{2}\right)\left(1 - \frac{d\varepsilon_v}{d\varepsilon_1}\right) \tag{3.12}$$

Where, ϕ_f is a function of the density of the sand and lies between the true, particle friction angle, ϕ_μ and the critical state friction angle ϕ_{cv}. Dilatancy is characterized

by a dilation angle, ψ, which can be experimentally determined via direct shear test or triaxial test.

Bolton (1984) gave following expression for plain-strain compression for saturated sandy soils:

$$\emptyset_p - \emptyset_c = 0.8(\psi_p) \tag{3.13}$$

Where ϕ_p and ϕ_c are the peak and critical state friction angle and ψ_p is the peak dilation angle.

For triaxial compression, the following expression, is used, based on best-fitting data obtained from triaxial tests on saturated sands at various confining pressures.

$$\emptyset_p - \emptyset_c = 0.5(\psi_p) \tag{3.14}$$

Due to longer duration and complex procedures that need to be accommodated to perform unsaturated triaxial tests, limited data is available to improve understanding of the effect of suction on the dilation behavior of soils. Also, the dilative type of volumetric soil behavior at critical state has been scantily analyzed. The dilative behavior of granular soils influences its shear strength response.

In most cases, the granular soils reach their maximum volume change at their peak strength stage, and start to exhibit plastic flow from there onwards (Chen et al., 2003). Various formulae are available in the literature to calculate the angle of dilatancy or dilatancy rate. Dilatancy of granular soils may be defined as the need for volume change, while shear loading and its direct assessment is possible via Equation 1. This will be called Method I.

$$tan\psi = -\frac{(\delta\varepsilon_v)}{(\delta\gamma)} \tag{3.15}$$

Where ψ = dilation angle; ε_v = volumetric strain, and γ = shear strain. The dilation angles of granular soils are not only affected by relative density, but are also sensitive to

grain angularity, and confining pressure (Chen and Lin, 2003). Ignorance of such behavior may significantly lead to errors in predicting ultimate bearing stresses, deformation or stability of geotechnical structures.

Tatsuoka (1987) suggested an equation for calculating the dilation angle for triaxial condition, based on triaxial test data, covering a wide range of relative density and confining pressure, as given by Equation 3.16. This will be called as Method II.

$$sin\psi_{max} = \left[-\frac{\frac{d\varepsilon_1}{2} + d\varepsilon_3}{\frac{d\varepsilon_1}{2} - d\varepsilon_3} \right]_{max} \tag{3.16}$$

Where, ψ = dilation angle, ε_1 = axial strain, and ε_3 = lateral strain.

The soils dilation angle can also be directly assessed by measuring the peak slope angles of the linear portion of the volumetric strain, versus the axial strain curve of the consolidated drained (CD) triaxial tests, with volume change measurements (Method III). For saturated, as well as unsaturated soils, the initial slope of this plot that represents the compression of specimen corresponds to the elastic regime, while the slope, used to assess the dilation angle corresponds to the plastic regime (Salgado, 2006). Thus, dilatancy represents the plastic behavior of soil.

The point on the stress-strain curve, at which the volumetric response shows the transition from contraction to diatant nature, is referred as “characteristic state.” The maximum dilatancy seems to occur well before the peak strength condition and persists until the critical state is mobilized. The slope or angle of dilatancy reduces considerably towards critical state.

The dilatancy angle (ψ) can also be calculated from the triaxial test, provided that the volumetric strain and maximum shear strain increments are known, using the expression given in Equation 3.17 (Bolton, 1984; Salgado, 2006; Houlsby, 1991; Vaid and Sasitharan, 1992). This will be referred to as Method IV.

$$sin\psi = -\frac{d\varepsilon_v}{|d\gamma_{max}|} \quad or \quad tan\psi = -\frac{d\varepsilon_v}{|d\gamma_{max}|} = -\left[\frac{volumetric\ strain}{shear\ strain}\right] \tag{3.17}$$

3.9.11.1 Experimental results pertaining to dilational angle

Even though, analysis of test results in this research was done at a critical state, the rate of dilation was maximum at peak failure; hence, the dilation angles, or dilation rates were analyzed at peak failure. Table 3.4 documents the dilation angles determined from a series of suction-controlled triaxial tests, using the expression given by Methods I, II, III and IV. Clearly, the dilation angle decreased with an increase in external confinement, but increased with an increase in matric suction.

Table 3.4 Experimental values of peak dilation angles

σ_3-u_a (kPa)	s (kPa)	Method I (deg.)	Method II (deg.)	Method III (deg.)	Method IV (deg.)
100	50	7.1	9.1	17.8	7.2
	250	10.3	9.7	23	10.5
	500	12.9	10.8	30	13.2
	750	15.4	11.9	40	16
200	50	5.9	8.7	14	5.9
	250	5.6	8.5	12.8	5.7
	500	7.2	8.98	19.4	7.3
	750	9.9	8.85	30.4	10
300	50	3.5	7.2	10	3.5
	250	2.8	7.4	10.5	3.7
	500	5.8	9	22	5.8
	750	4.6	6.5	17.2	4.7

The measured dilatancy (Method IV) increased with an increase in matric suction for net confining stress, σ_3 - u_a = 100 and 200 kPa; while for net confining stress, σ_3 - u_a = 300 kPa, it stabilized beyond *s* = 500 kPa. The analytical methods I and II show an initial increase in dilatancy up to 500 kPa, beyond which it stabilized for the entire range of net confining stress, σ_3 - u_a = 100, 200 and 300 kPa. Apart from several factors such as soil type, density, grain size distribution, confining pressure, matric suction, and shape of particles, the dilation angles also depended upon whether soil particles were crushed or

not before they overrode the other particles. Theoretical solutions based on triaxial conditions i.e., Methods I, II and IV tended to yield lower values, as compared to the actual dilation angle measured, using Method III.

Figures 3.65, 3.66 and 3.67 show the general trend of increase in dilation angles at constant net confining stress. Most of the geotechnical engineering software uses the values suggested by the previous work of researchers, such as Vermeer and de Borst (1984) for saturated soils. These values are between 10-20 degrees for various geological materials, including sand and clays, tested under saturated conditions. Very limited real values of dilation angle are reported in the literature for unsaturated soils. Inclusion of real dilation angles is expected to improve the numerical prediction of stress-strain relationships of granular soils.

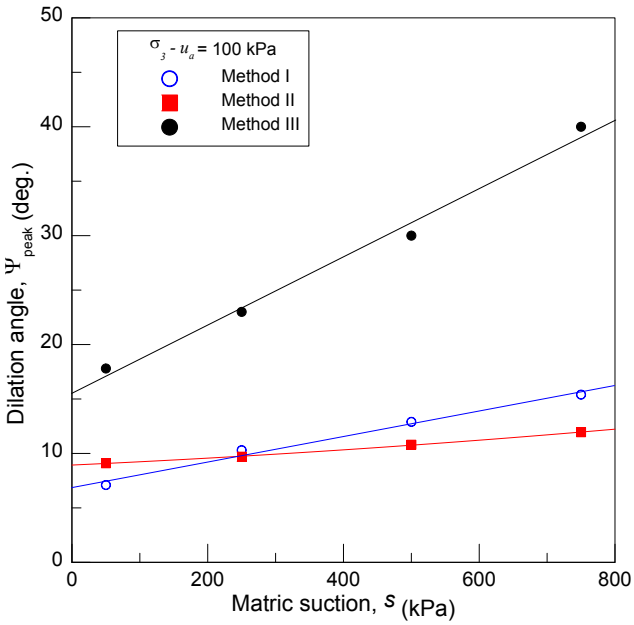

Figure 3.65 Effect of matric suction on dilation angles at net confining stress, σ_3 - u_a = 100 kPa

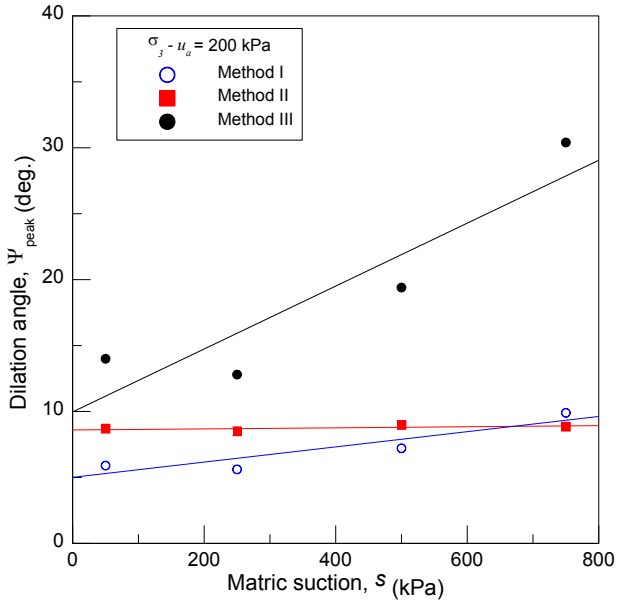

Figure 3.66 Effect of matric suction on dilation angle at net confining stress, σ_3 - u_a = 200 kPa

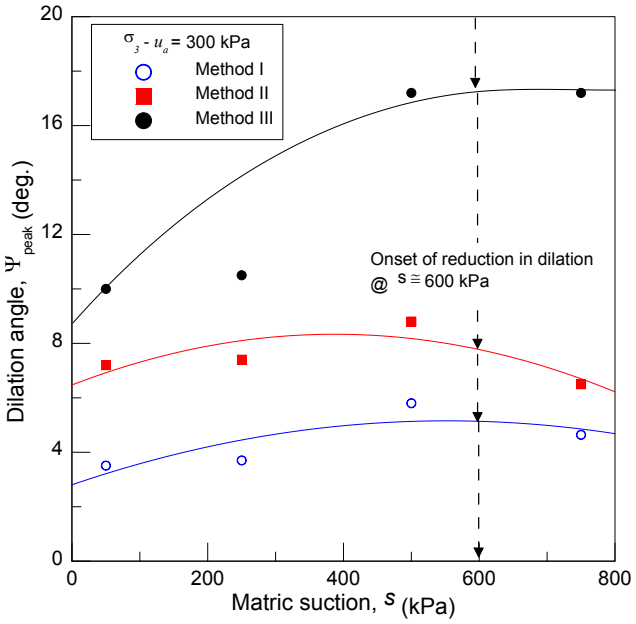

Figure 3.67 Effect of matric suction on dilation angle at net confining stress, σ_3 - u_a = 300 kPa

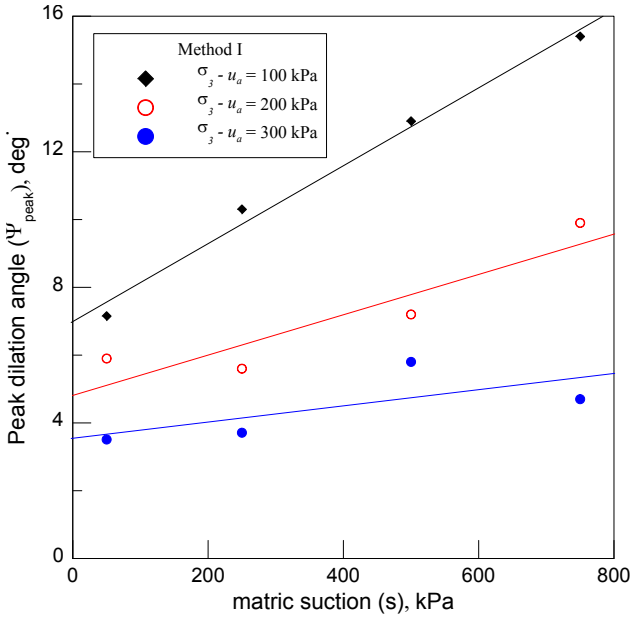

Figure 3.68 Effect of net confining stress, σ_3 - u_a on dilation angles using analytical Method I

Furthermore, the continuous incremental ratio $d\varepsilon_v^p/d\varepsilon_s^p$ (incremental volumetric plastic strain to volumetric shear strain), also termed as dilatancy, obtained during suction-controlled CD triaxial tests from this research, could be helpful to assess the dependency of the appropriate flow rule (associated/nonassociated) on the suction (Cui and Delage 1996). It is anticipated that this will be helpful to future soil modelers in predicting response of dilating soils, using existing or new soil models.

The values obtained via theoretical equations (Methods I, III and IV) seem to have values within a 10 to 20 degree range. However, the actual measured dilation angles (Method III) yielded very high dilation angles (almost 40 deg. At *s* = 750 kPa).

Figure 3.68 shows the effect of an increase in net confining stress, σ_3 - u_a on dilation angles, using Method I. The general trend was that the dilation angle was suppressed with an increase in external confinement. Also, the measured dilatancy was

enhanced with an increase in suction. The relationship between maximum dilatancy and suction is non-linear.

Matric suction may be considered to be contributing to the shear strength of soil via two different mechanisms: the contribution of capillary force on inter-particle normal stress, and the effect of suction on dilatancy. The first mechanism increases the effective stress at grain point contacts, increasing the overall stiffness/strength of a specimen. The effect of suction contributes more to the peak strength than to the critical or post-failure strength, and it is due to the result of the second type of mechanism, i.e., suction-induced dilatancy.

3.10 Summary

Laboratory test results from classifying the soil, determining specific gravity, optimum moisture content, and maximum dry density; selecting the appropriate compaction method to obtain identical specimen; and, soil water characteristic curve (SWCC) are presented. Description of a novel triaxial equipment acquired, as part of this research is detailed, along with the methodology adopted to perform the first series of experimental programs undertaken to conduct the suction-controlled consolidated drained (CD) conventional triaxial compression test (CTC), using an axis translation technique.

Test results confirmed dependability of the double-walled triaxial test equipment for producing repeatable results. An appropriate shear rate of 0.0086%/min was selected, based on independent studies on three silty sand specimens, to further test specimens in the matric suction range of s = 50 to 750 kPa. A total of 15 tests were conducted (3 saturated and 12 unsaturated, statically-compacted specimens) to study suction-controlled isotropic consolidation, shear strength, volume change behavior, small and large strain stiffness, and the dilation angle/rate of dilation variation during shearing, due

to the effect of at least four matric suction (i.e., *s* = 50, 250, 500 and 750 kPa) at three constant net confining pressure ($\sigma_3 - u_a$ = 100, 200 and 300 kPa).

Consolidated drained triaxial tests following the CTC stress path showed evidence of an increase in the shear strength and stiffness modulus, due to evolution of apparent tensile strength/apparent cohesion, and yielded stress, with an increase in matric suction. In addition, various models/equations were used to best fit experimentally obtained shear strength and related parameters with popular predicting equations proposed in the literature.

Chapter 4

Triaxial Test Results at High Suction States

4.1 Introduction

The use of the axis-translation technique to impose high soil suction is limited by the air-entry value of the ceramic disk. This normally narrows down the testing limitations up to a maximum suction value of 1500 kPa. Changes in moisture content in unsaturated soil specimens at suction greater than approximately 3,000 kPa can be controlled using vapor phase equilibrium (Nishimura et al., 2008). This method has been used to measure triaxial shear strength and volume change behavior of an unsaturated, non-plastic, silty soil at high suction range, via a controlled relative humidity environment, by regulating the inflow rate of air (Nishimura and Fredlund, 2003; Nishimura and Vanapalli, 2005). A substantial portion of the data available on unsaturated soil behavior has been obtained using the axis-translation technique (i.e. low-to- medium suction range). However, research using osmotic/vapor pressure techniques in the high suction range (i.e. above residual suction range, is very limited). This study is one of the few attempts made on high suction-based soil strength tests as it pertains to intermediate geomaterials.

This Chapter provides description of the test procedures followed. Later sections describe test results and analyses of test results.

4.2 Vapor Pressure Technique Using Auto-RH Equipment

The Auto-RH system, designed by Likos and Lu (2003), is capable of automatic control of relative humidity (RH) between ~ 1% RH and 99% RH. This corresponds to a total suction range of 600 MPa to 1.4 MPa. The thermodynamic relationship between relative humidity of pore water vapor and total suction Ψ_t (kPa) is given by Kelvin's equation (4.1).

$$\text{Total suction} = \psi_t = -\frac{RT}{v_{wo}\,\omega_v}\ln\left(\frac{u_v}{u_{vo}}\right) = -\frac{RT}{v_{wo}\,\omega_v}\ln(\text{RH}) \qquad (4.1)$$

Where u_v is partial pressure of water (e.g., soil pore-water) vapor (kPa), u_{vo} = saturation pressure of pure water vapor (kPa), R = Universal gas constant (8.31432 J mol^{-1} K^{-1}), T = Absolute temperature (K), v_{wo} = Specific volume of water (i.e. reciprocal of density, m^3/kg), ω_v = Molecular mass of water vapor (18.016 kg/kmol).

4.2.1 Operating Principle

This equipment relies on computer-proportioned mixing of vapor saturated, or "wet" gas (air), and desiccated or "dry" air, in a closed environmental chamber, to control the relative humidity. The configuration of various components on the hardware control panel is outlined in Figure 4.4.

High pressure air (from the laboratory source) is regulated using a dial gauge and a regulator to low (~ 5 psi) pressure. It is then passed through a column of granular drying agent. The drying agent loses its ability to act as a drying agent once its color changes from blue to pink. The drying agent can be recharged by removing it and placing it in the oven at a temperature between 50ºC - 100ºC) for 24 hrs. The air stream is split through two computer-controlled mass/flow (M/F) valves to regulate the flow rate of each air stream between zero and 500 cm^3/min (sccm), based on an electronic control signal from the control PC.

One of the air streams is vapor saturated (RH near 100%) by bubbling it through a gas-washing bottle filled with water (preferably, distilled water). The bubbler needs to be refilled periodically during the long testing times. The vapor saturated (or "wet") and dessicated (or "dry") gas streams are then reintroduced in a mixing chamber at a user-defined combined (total) flow rate (in this case, 200 cm^3/min). The effluent air stream has RH that is a direct function of the "wet" to "dry" (w/d) gas flow ratio or wet to total (w/t)

flow ratio maintained by the control PC. The low-pressure humid gas stream is routed into a test chamber, where RH and temperature are continuously monitored with a capacitance-film humidity/temperature probe.

Signals from the humidity probe form a feedback loop, with the control PC for automated regulation of the two mass-flow controllers. The measured RH and temperature will correspond to the target total suction desired that is calculated by the software using, Kelvin's equation. The humidity probe has to be calibrated from time to time. An acrylic chamber (Figure 4.3) is used with the Auto-RH equipment to form a closed-loop system for calibration.

4.2.2 Calibration of the RH Probe

Experimental studies by Lu and Likos (2003) have confirmed the insensitivity of RH equipment to temperature fluctuations. The lab environment is usually temperature controlled, and, hence, should not cause temperature fluctuations. A calibration chamber, (as shown in Figure 4.3), is used to perform checks for the accuracy of calibrations of RH/Temp probe. If required, re-calibration of the probe can be performed using appropriate salt solutions (Likos, 2012).

The target relative humidity is generated in the calibration chamber (approximately 6 cm in diameter and 6 cm in height) by filling it with any chosen saturated salt solution or its combination. The RH probe, when fitted with a stainless-steel compression fitting, can be easily inserted through top cap of the chamber which then forms a feedback loop with the computer via the appropriate program, thus enabling the operator to perform calibrations throughout any desired range of relative humidity.

4.2.3 Software Control

Continuous data acquisition and system control is possible through an executable (.exe) file, along with associated drivers acquired with the equipment. Figure

4.1 shows a screen shot of how the program window looks once it starts executing. The software can be automatically, as well as manually, controlled with the help of a switch on the control panel. The control panel screen is divided into four major sections: Flow controller, relative humidity readout, temperature readout and data logging control.

The control panel contains inputs such as total flow rate, target RH %, increment (%), increment time step (hr.), data logging interval (min), and a note to data file (if desired). It also includes automatic outputs such as relative humidity (%), and temperature (ºC). Also, displayed on the screen is the total suction calculated, based on the current RH and temperature readout, using Kelvin's equation 4.1. A continuous RH and temperature chart is also displayed. Thus, the software control is user friendly and easily operational. Further more details can be found in the Auto-RH manual, as described by Likos (2003).

Figure 4.1 Screen shot of the software program that controls the RH-system

4.3 Auto-RH Configuration for Soil Water Characteristic Curves

Figure 4.2 shows the photograph of the integrated set up. A similar set up has been successfully used and described by Lu and Likos (2003). An acrylic box, 10 x 10 x 18 cm, was fabricated and used in this research. It housed the balance that recorded the specimen weight. The chamber was sealed with a rubber gasket at the bottom to prevent any moisture leakage. An effluent air vent of 0.5 mm was provided at the top of acrylic box. Also, an inlet was provided for saturated air to enter into the box from RH-apparatus. A RH/Temp probe was inserted into the box, using a steel fitting arrangement.

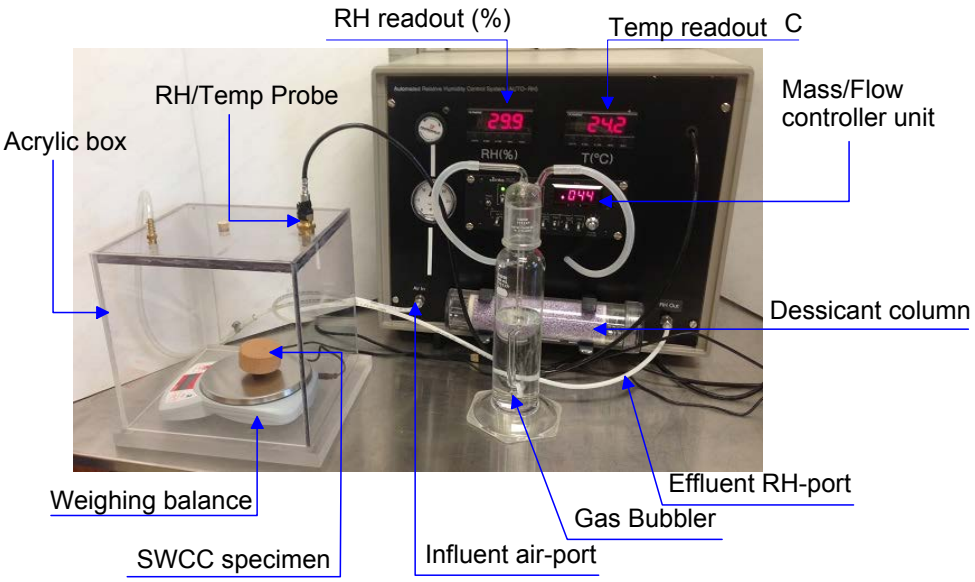

Figure 4.2 RH-equipment combined with fabricated chamber to create SWCC points

In order to control the process automatically, the target relative humidity was entered into the control panel of the software to create vapor saturated air that represented desired total suction. Vapor saturated air was then supplied via ¼ in. nylon tubing into the test chamber. If the control was desired manually, then the RH was incrementally stepped up/down by proportioning the wet to dry gas flow under feedback from the humidity probe. The water content was periodically monitored, via balance, as

the water vapor was adsorbed or desorbed by the soil specimen at each step in the RH chamber. Upon reaching equilibrium (constant mass) between the relative humidity of the pore water phase in specimen voids and that of the environmental chamber, the water content was recorded. Later, the humidity supplied to the chamber was stepped in increments (usually 10%), if required, to achieve the targeted moisture content.

Figure 4.3 shows the SWCC points obtained in the high suction range that closely match the best fit equations by Fredlund and Xing (1994) and van Genuchten (1980).

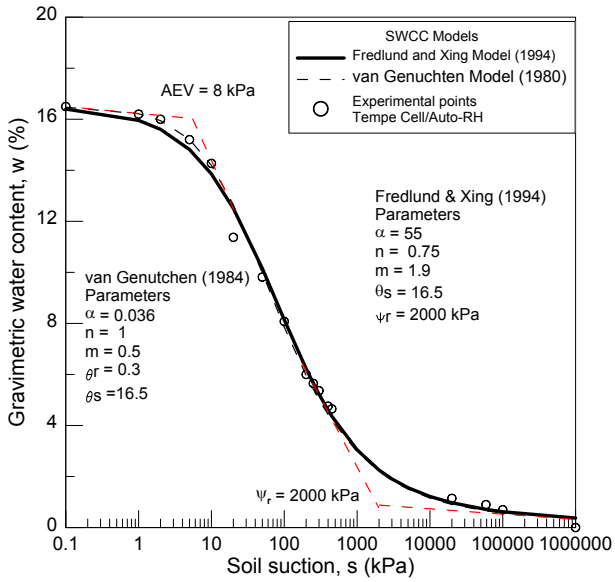

Figure 4.3 Soil-water characteristic curve points via RH equipment for silty sand (SM)

4.4 Automated Humidity Triaxial Equipment

4.4.1 Introduction

This section presents the design details and methodology adopted in combining a novel double-walled triaxial shear apparatus with automatic RH equipment for measuring the volume change and shear strength behavior of unsaturated soil in the high suction range. Soils subjected to a high suction range, and especially the silty sand type,

above their residual suction may be referred to as desiccated soils. The assessment of soil shear strength and stiffness behaviors in the high suction range has gained more attention in recent years in order to get insight into the soil behavior over a large suction range (Mahalinga-Iyer and Williams, 1985; Vanapalli and Fredlund, 2000; Blatz et al., 2002; Nishimura and Vanapalli, 2005). As compared to oedometer and direct shear tests, the triaxial testing facilitates soil testing along a wide variety of stress paths, thereby simulating different field conditions encountered in the geotechnical practice (Blatz et al., 2002).

An attempt has been made to develop a new apparatus by accommodating the RH triaxial equipment, in conjunction with the triaxial device, to directly control the relative humidity inside the specimen, as shown in the schematic Figure 4.4.

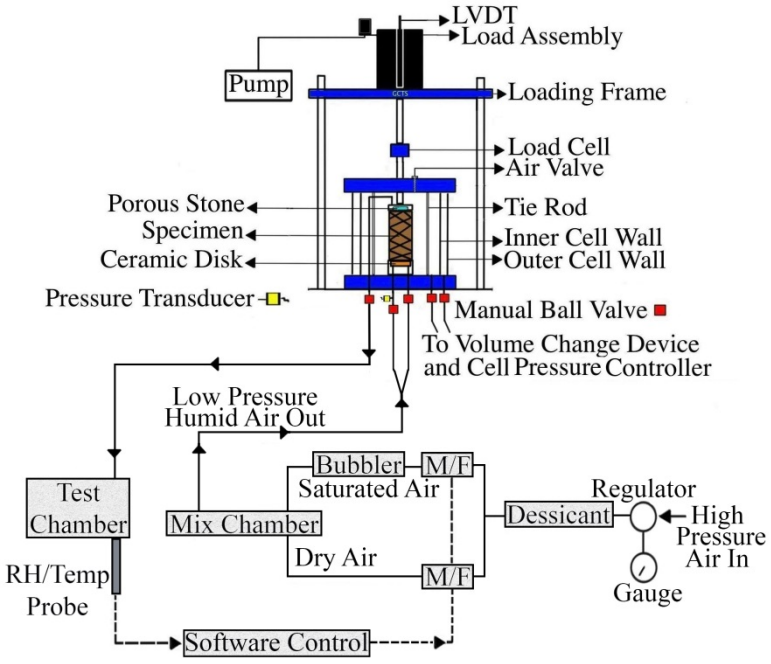

Figure 4.4 Schematic diagram of the automated-humidity system along with triaxial system for testing soils under high total suction

4.4.2 Specimen Preparation and Total Suction Equalization

The soil specimen was prepared in the same way as explained for the axis-translation technique in Chapter 3. Post-preparation, the specimen was allowed to dry in the temperature-controlled laboratory environment, and its weight was monitored periodically. The desired minimum total suction in this testing program was 20 MPa, and the corresponding water content was found, from SWCC tests on small size specimens, to be approximately 1.25%. The water content for other total suction levels was found in the same way. Visual inspection of the desiccated soil specimens showed no sign of cracks or damage due to the drying process (at lab temperature).

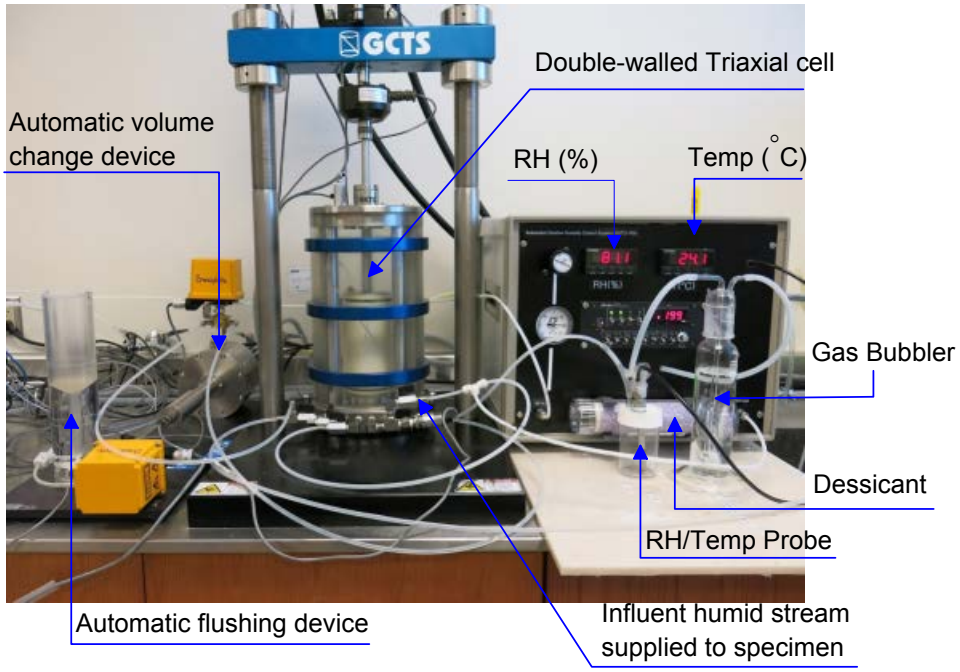

Figure 4.5 Actual photograph of triaxial set up combined with relative humidity system

The specimen was dried in the laboratory atmosphere until its water content came close to the desired value at high suction (which took between 4-5 days). The specimen was then mounted on the triaxial pedestal and enclosed/sealed in the membrane with O-rings at top and bottom in the same manner, as explained in the axis-

translation technique. A vapor-saturated air, that represents target total suction at constant laboratory temperature, was created by adjusting the wet-to-dry flow ratio. It was then passed directly through the bottom of the specimen, using ¼" nylon tubing.

The vapor-saturated air flowed, under atmospheric pressure, through the bottom of the unsaturated/dessicated soil specimen and came out of the specimen through the top cap, via 1/8" nylon, semi-rigid tubing, into the small chamber, which was housed with RH/Temp probe, as shown in Figure 4.5. Thus, the RH of the outflow was measured. The signal from RH/Temp probe was sent to computer. The software then adjusted the wet/dry flow ratio through mass/flow controllers. The arrangement used previously, by Fredlund and Nishimura, measured the RH of the influent stream that supplied the gas, while, in this research, we measured the RH of the effluent stream. The specimen was sealed in the membrane that helped the specimen to equilibrate with the relative humidity applied.

Trial tests were conducted, prior to the actual test, by keeping the specimen on a balance inside the fabricated chamber that was used for creating SWCC points. The time required by triaxial specimens for achieving constant weight, and, hence equilibrate under the required total suction, was monitored. It took around 8-10 days for the desiccated specimen to attain the equilibrium at high target total suction (between 10 MPa to 300 MPa), irrespective of its magnitude. The specimen was supplied with saturated vapor directly at the bottom through two openings beneath the porous stone under low air pressure; therefore, it was expected to equilibrate much faster. Figure 4.6 shows the desiccated specimen without any visible cracks or interfaces at s = 300 MPa. The specimen after being mounted in triaxial assembly was also allowed to equilibrate with the applied relative humidity for at least 15 days to ensure the equilibrium.

Figure 4.6 Desiccated specimen after RH application (s = 300 MPa)

The convention used to designate the specimen is $CD_{x\text{-}y}$ where "CD" denotes the consolidated drained test using relative humidity apparatus to impose desired high total suction; "x" represents the net confining pressure (σ_3-u_a) in kPa, while "y" represents the imposed constant total high suction (ψ_t) in MPa. The specimen/tests performed with Auto-RH equipment will be referred to as RHCD specimens henceforth.

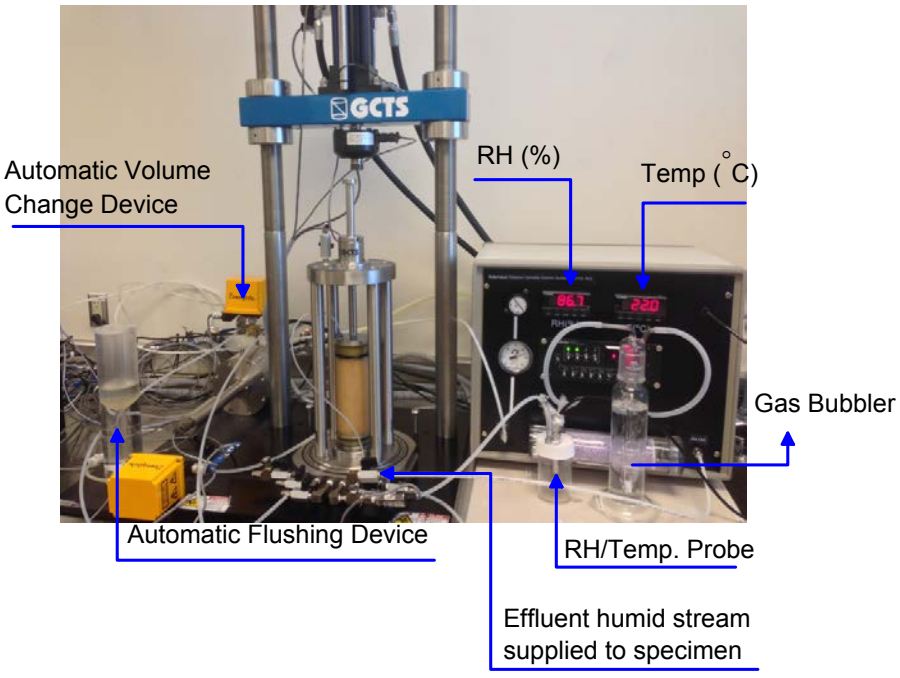

Figure 4.7 Triaxial specimen mounted for high total suction equalization

4.4.3 Suction-Controlled Isotropic Consolidation

Isotropic consolidation and shear behavior of silty sands were studied, using the newly developed triaxial device that controls relative humidity via an automatic relative humidity apparatus. Upon reaching equilibrium, the triaxial double-walled cell was assembled and filled with water under a water pressure of 10 kPa. The RH/Temp and the related total suction was continuously monitored from the suction equalization stage until shearing. This monitoring provided an indirect knowledge of total suction inside specimen. While filling the cell with water, it was observed that the initial total suction altered slightly as the specimen membrane came in contact with water. For instance, during the CD200-300MPa test, the initial relative humidity measured was 10.9% (s ≈ 300 MPa). That changed to 12% (s ≈ 286 MPa) after the cell was completely filled with water, which took ~ 45 minutes. The specimen was allowed to get back to initial target total suction (s ≈ 300 MPa), as well as undergo volume change under 10 kPa confinements, which took about 1-2 hours. The volume change of the specimen during filling of the triaxial cell with water was recorded, and corrected dimensions of the specimens were entered in the software program before starting the consolidation stage.

The next stage was isotropic consolidation under controlled suction. This was done by increasing the cell pressure at the rate of 5 kPa/hr., while keeping the circulation of relative humidity from bottom to top of the specimen. It should be noted that the bottom of the specimen was connected to the RH equipment; hence, no water back pressure was applied. The top of specimen was connected to the chamber with a RH probe that had a vent open to the atmosphere for the effluent. Thus, the air pressure in the specimen was at atmospheric pressure (or reference zero). Depending upon the final consolidation pressure (σ_3 - u_a = 100, 200 and 300 kPa), the application of desired isotropic consolidation pressure took 18, 38, and 58 hrs., respectively. Each specimen

was kept for at least 24 hours after the consolidation pressure was applied to ensure complete dissipation of pore air pressure (no change in volume of specimen).

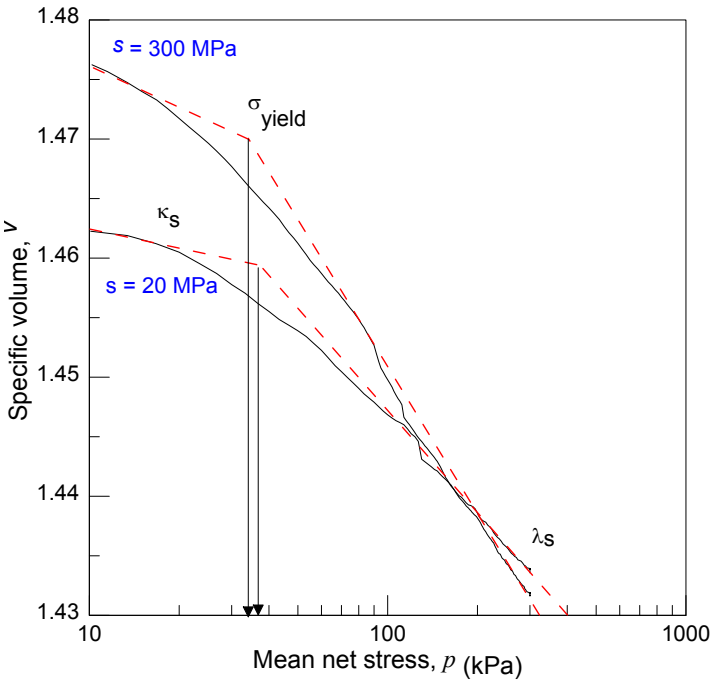

Figure 4.8 Suction-controlled isotropic consolidation at *s* = 20 and 300 MPa

Figure 4.8 shows the test results of isotropic consolidation under controlled-total suction conditions at *s* = 20 and 300 MPa. The values of yield stresses were estimated by the method of intersection of the two linear segments of the consolidation curve, as proposed by Cui and Delage (1996) and Sharma (1998). Figure 4.8 illustrates the graphical determination of the preconsolidation pressure.

For ramped consolidation tests conducted under constant-suction states, *s* = 20 and 300 MPa, the approximate values for the corresponding preconsolidation pressures, p_o(20,000) = 36 kPa, p_o(300,000) = 34 kPa were obtained. This pattern indicates that the yield stress tends to decrease at high suction values beyond residual suction values. The volumetric stiffness parameter $\lambda(s)$ was determined graphically and these are, $\lambda(20{,}000)$ =

0.012 and $\lambda(300,000)$ = 0.016. The elastic rebound index $\kappa(s)$ were found to be $\kappa(20,000)$ = 0.0021, and $\kappa(300,000)$ = 0.0047.

The BBM formulation postulates a monotonic decrease in $\lambda(s)$ with increasing matric suction. However, at high suction, the experimental evidence reflected an increase in $\lambda(s)$ with increasing total suction (i.e., beyond residual suction). This finding also corroborates the fact that there cannot be an infinite increase in the yield strength of a soil with an increase in suction. A panoramic view of the entire setup is shown in Figure 4.9.

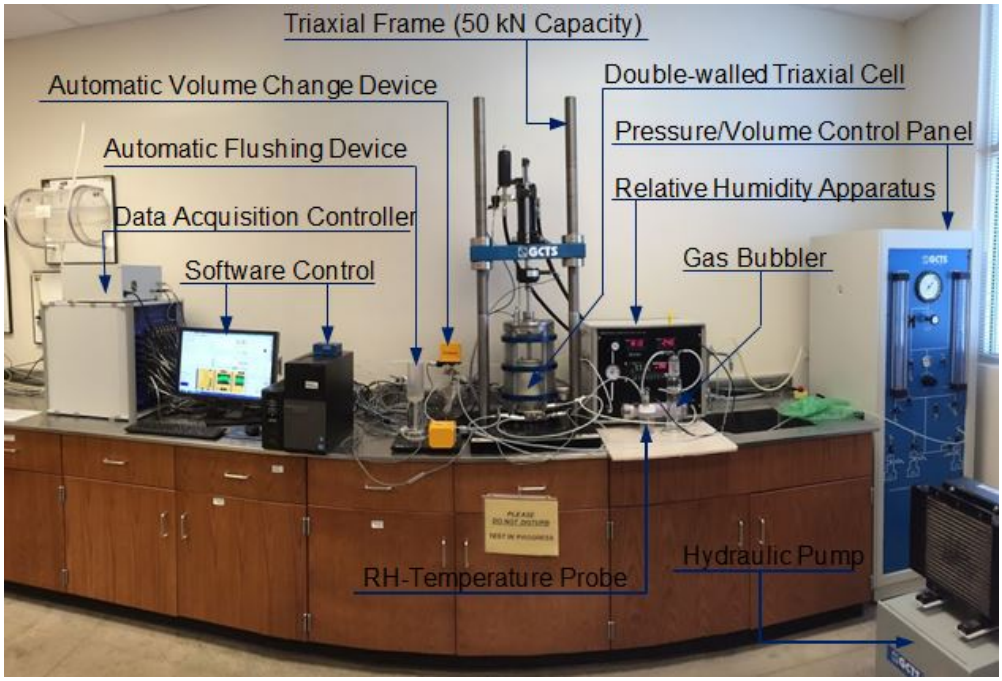

Figure 4.9 Panoramic view of entire RH-Triaxial setup

A close observation of these curves indicates that the peak shear strength was greatly affected by the shearing rate and increases with an increase in shearing rate.

4.4.4 Shearing Stage

The next stage was suction-controlled shearing at a constant axial strain rate. Appropriate shearing rate was chosen after separate studies, as discussed below.

4.5 Shearing Strain Rate Studies for CD Triaxial Tests at High Total Suction

To our best knowledge, there are no published studies available in the literature on response of “intermediate” unsaturated silty sand that show a very high magnitude of post-peak softening at high suction value when sheared over a wider range of shearing rates. A trial and error process was used to identify a suitable shearing strain rate.

Five identical specimens with the same initial compaction conditions, were prepared, equalibrated for desired total suction (300 MPa), and isotropically consolidated in the same manner as explained in the above section. These samples were then sheared under drained condition at three different shearing strain rates: 0.0009%/min, 0.005%/min, 0.009%/min, 0.05%/min and 0.9%/min, and both stress-strain and total volume change responses were monitored, as shown in Figures 4.10a and b.

A close observation of these curves indicated that the peak shear strength was greatly affected by the shearing rate and increased with an increase in the shearing rate. On the other hand, the critical state was not much affected. These observations are similar to ones from other studies, but at comparatively lower matric suction state, using axis-translation studies, as explained in Chapter 3.

On the other hand, the observed volumetric response indicated an increase in the dilation for specimens sheared at a lower shearing strain rate. This observation contradicts the shearing rate studies done using the axis-translation technique, as explained in Chapter 3, in which the specimens showed reduction in dilation while shearing with lower shearing strain rates. The specimens failed, showing brittle-type failure in all the CDRH tests.

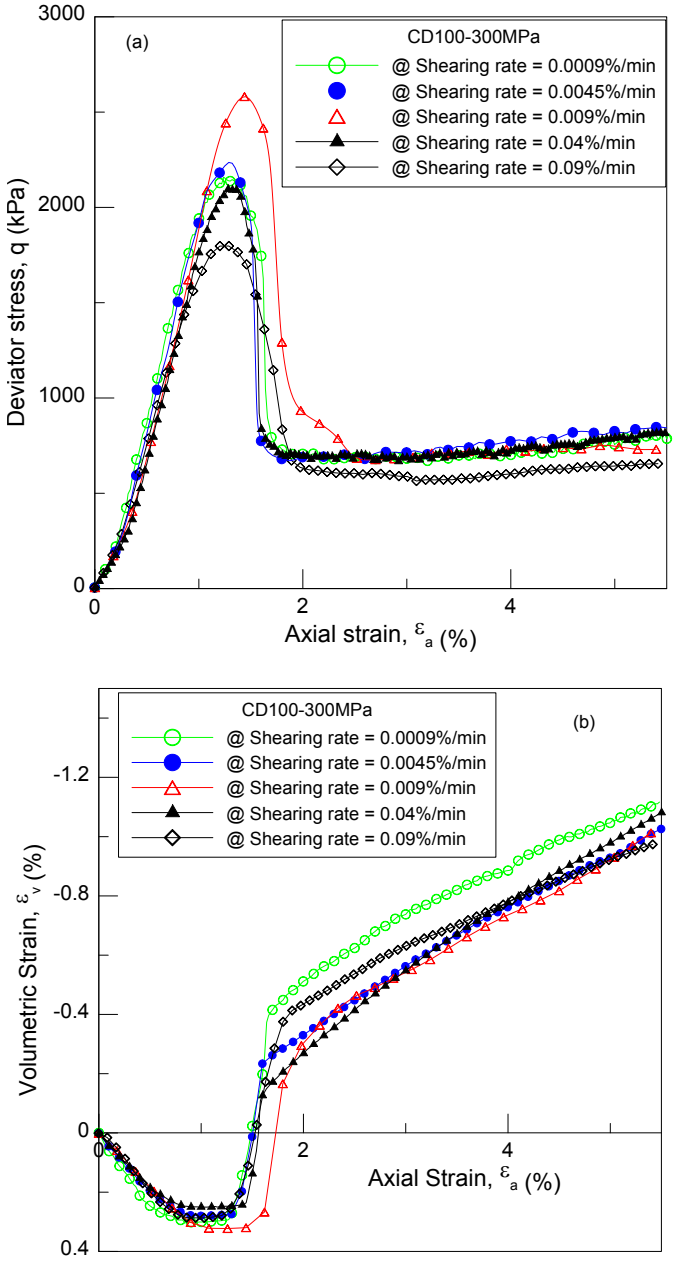

Figure 4.10 Effect of shearing rate on a) stress-strain curve and b) volumetric strain from CD triaxial test at *s* = 300 MPa and net mean confining pressure, σ_3 - u_a = 100 kPa

4.5.1 Particle Breakage and Dilatancy

Previous research on saturated granular soil has demonstrated particle crushing at elevated pressures, thereby reducing the maximum angle of dilation for given initial density (Vesic and Clough, 1968; Billiam, 1972; Bishop, 1972). Bolton, 1984 argued that "in order to achieve a given angle of dilatancy, the particle structure should both be dense and not so highly stressed that asperities should fracture in preference to over-riding." These studies were with reference to triaxial testing of saturated soils, and high stresses were due to the high magnitude of cell pressures. In the case of unsaturated soils, the stresses acting are due to suction and the cell pressures applied. If suction is very high and external stress is medium, still there are chances of particle crushing, due to high stress from high magnitude of total suction, is possible.

The amount of dilation observed in specimens using the relative humidity technique was less, as compared to those obtained from the axis translation technique even though the matric suction imposed, using the latter technique were less, as compared to the high total suction imposed using the former technique. One possible explanation for this is that at high suction, the magnitude of effective stress owing to high suction of soil is considerably large (even though the cell pressures varies between 100 to 300 kPa range), and while shearing, the particles may crush even before they over-ride, thereby prohibiting further dilation. Since the shear failure was across a well-defined single failure plane, the particle crushing may be associated only with grains along failure plane.

Post-shearing, the RHCD specimen showed visible particle crushing across the clear failure plane, with the soil specimen split into two pieces across a single clear shear failure band, as shown in the photograph in Figure 4.14. Chen and Lin, 2003 demonstrated, through their experiments, that the dilation angles of granular soils are not

only affected by relative density, but are also sensitive to grain angularity and confining pressure; hence, not considering such behavior may significantly lead to errors in predicting ultimate bearing stresses, deformation or stability of geotechnical structures. The simplest way to find the particle crushing is to perform a grain size distribution analysis on failed soil specimens during post-shearing. The grain size distribution conducted on soils obtained from specimens post-shearing confirmed the particle size breakage.

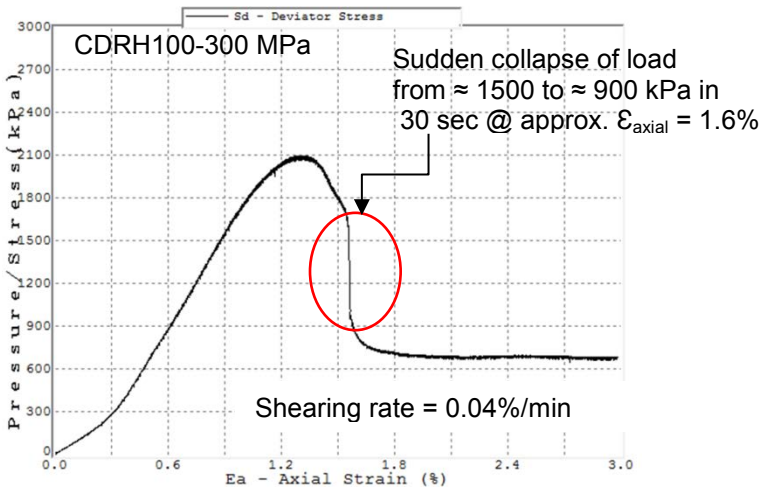

Figure 4.11 Sudden collapse of load during shear-induced softening

On the other hand, the specimens tested using the axis-translation technique had low-medium matric suction imposed and, comparatively, the magnitude of effective stress at grain-point contacts was low to medium (as compared to RHCD specimens). Hence, the particle crushing may not have been ample across the failure shear bands, thereby allowing the particles to over-ride and show higher progressive dilation-type response. Post-shearing the specimen was intact, with no separation across clear dilated shear bands. Furthermore, the grain-size distribution conducted post-shearing on the specimen confirmed no particle breakage.

Figure 4.12 Particle crushing along failure planes from CD100-20 MPa test

Table 4.1 Deviatoric load-collapse for CD100- 300MPa at various shearing rates

Shearing rate (%/min)	Total load collapse (kPa)	Data collection Interval (sec)	Collapse rate (kPa/sec)	Axial strain %
0.0009	578	1200	0.48	1.62-1.64
0.005	1148	1200	0.96	1.5-1.6
0.009	1123	1200	0.94	1.62-1.8
0.05	611	30	20.4	1.56-1.58
0.09	312	60	5.2	1.72-1.8

It was observed that there was a sudden drop in load during post-peak softening, irrespective of the shearing rate used when the specimens were tested at s = 300 MPa and $\sigma_3 - u_a$ = 100 kPa. The maximum drop in load was recorded in Table 4.1. It was noted that the data collection interval of 20 minutes was not sufficient to capture the "load-collapse" phenomenon with accuracy. A close observation of the stress-strain plot, with continuous data collection, was frozen, and the software window screen was saved, as shown in Figure 4.11. It clearly shows that for *s* = 300 MPa and $\sigma_3 - u_a$ = 100 kPa, there was a sudden collapse in deviator stress from ~ 1600 kPa to ~ 900 kPa at axial strain of ~ 1.6%.

This may be an instance when particle breakage occurred, leading to a sharp drop in shear capacity with continued shearing. The above observation also underlines

the importance of considering the contribution of the particle crushing phenomenon during post peak softening, especially, to adequately model elasto-plastic behavior during shearing in high suction range. It also emphasizes the need to reduce the data collection interval so that such "load collapse phenomenon" can be captured. Such phenomenon was not observed when $\sigma_3 - u_a$ was increased to 200 and 300 kPa at *s* = 300MPa.

Also, the decrease in load during post-peak-softening for all other tests was more gradual than sudden. When the data collection interval was reduced to 30 sec, there was no such collapse of load observed when suction was reduced to *s* = 20 MPa at all confining pressures applied in this program. This means that such a phenomenon is expected only when suction is highest (*s* = 300 MPa) and external confinement is lowest ($\sigma_3 - u_a$ = 100 kPa), i.e., during a test with maximum dilation. Figure 4.12 clearly shows visible particle crushing/breakage along the interfaces of failure planes from the post CD100-20 MPa test.

4.5.2 Comparison with Previous Strain Rate Studies

Figure 4.13 illustartes the comparison between shearing strain rate and deviator stress at peak, and critical state failure identified from the test data. The relationship is highly non-linear for peak stress failure as compared to the one for critical state failure. In order to facilitate comparison, 0.0009%/min was used as the control shear strain rate. At peak failure condition, clearly, there was a gradual increase in peak deviator response (+4%) with an increase in shear rate from 0.0009%/min to 0.0045%/min, with a sudden large increase (~ +20%) at 0.009%/min. However, there was a gradual reduction (-3%) when shear strain rate was 0.04%/min, and drastic reduction (~ -17%) with further increase of shearing strain to 0.9 %/min. To sum up the test results, the amount of peak strength increase for an initial ten-fold strain rate increase is ~20%, and the peak strength decrease for the second ten-fold strain rate increase is ~17%.

On the other hand, at critical state failure, if 0.0009%/min was taken as the control shearing strain, then there was a small decrease in deviator stress, i.e., -2.5% and -7% with an increase in shearing rate at 0.005%/min and 0.009%/min respectively. However, there was comparatively large decrease, i.e., ~ -13% at 0.04%/min and about ~ -19% at fastest shearing rate of 0.09%/min.

This experimental study led to the very interesting observation that, in general, with an increase in shear strain rate, the peak response initially tends to increase gradually, but after reaching an ultimate, rate it decreases sharply and later stabilizes. However, the critical response tends to decrease initially at a negligible rate, but with a large increase in shear rate, it decreases by an appreciable value.

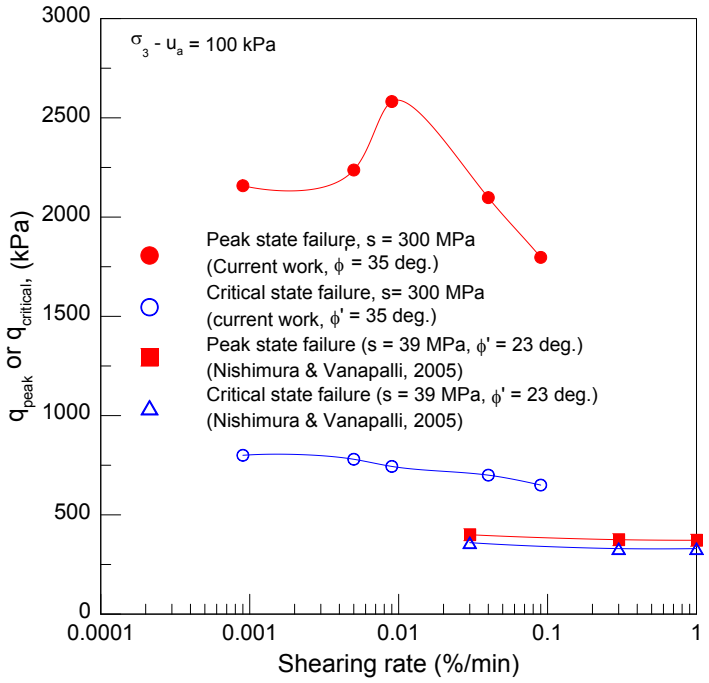

Figure 4.13 Comparison of the peak and critical state failure deviatoric response with increasing shearing strain rates for CD100-300MPa tests

Figure 4.10b shows the volumetric response during the shearing stage. All the specimens showed initial compression, followed by a stress-induced, dilatancy-type

response. In general, the soil specimen had a tendency to dilate less with an increase in shearing rate. There was a negligible change in the final value of volumetric strain at critical state failure, when sheared at rates of 0.0045%/min, 0.009%/min, 0.04%/min and 0.09%/min. However, at all times, the specimens dilated most at the lowest shearing rate of 0.0009%/min, thus indirectly indicating that the shearing rate was slow enough to allow the specimen to dilate freely before failure. On the other hand, other rates were faster, and the specimen failed before undergoing dilation to its full capacity that would truly represent its response owing to high suction-induced increase in soil stiffness.

Based on the shearing rates studies, the shearing rate of 0.0009%/min was chosen for all further CDRH tests. This shear strain rate was slow enough to allow maximum dilation of the specimen along with least influence on peak and critical state failure. This rate was about 10 times slower than the one used for the matric suction range of up to *s* = 500 kPa (axis-translation technique).

Nishimura and Vanapalli, 2005 studied the shearing rate effect on peak and critical strength of a non-plastic silty soil (ϕ' = 23 deg.) tested at constant high suction value of *s* = 39 MPa under $\sigma_3 - u_a$ = 100 kPa). The specimens were prepared by static compaction. The test results suggested that there is some impact of shearing rate on stress-strain behavior characteristics of the tested unsaturated soil specimens. According to their studies, the peak deviator stress decreased by 6%, with an initial ten-fold increase in shearing rate from 0.03%/min to 0.3%/min. A further increase in the shearing rate, from 0.3%/min to 1%/min, caused the peak deviator stress at failure to decrease by 7%.

Figure 4.13 shows the test results from the current work, along with, for comparison purposes, those from Nishimura and Vanapalli, (2005). Clearly, the values of peak, critical strength, and post-peak softening results are less when compared with the

current work, owing to the low friction angle and low suction value. Also, the effect of shearing rate is much pronounced in the current research work than in the previous work.

Both the studies showed a decreasing trend in peak and critical stress, with increasing shearing rate beyond 0.03%/min. The previous work seems to have been done with shearing strain rates above 0.03%/min only. However, the current studies were done at a shearing strain rate range well below 0.03%/min, and the test results showed first a dramatic increase in peak deviator and then a decrease with further decrease in shearing strain rate. The critical state failure criterion, $q = Mp$ seems to be independent of the strain rate since the critical state strength was not much changed, indicating that the critical state friction angle is independent of the strain rate.

Few studies have been done on shear rate in matric suction range using the axis-translation technique. Such testing techniques are costly and require complicated modifications (addition of RH-technique) to the conventional triaxial device to accommodate the unsaturated soil testing at high total suction. They are also time consuming due to long duration periods required for reaching suction-equilibrium because of the slow shear rates employed during testing. The current work will be helpful to future researchers in the assessment of appropriate shear rate in the high suction range.

The slope of the stress path in the current work seems to be independent of the shearing rate since the measured slopes of the stress path were M = 2.99, 2.99, 3, 2.99 and 3 at 0.09%/min, 0.05%/min, 0.009%/min, 0.005%/min and 0.0009%/min, respectively. These studies further explain the importance of considering the strain rate effect on strength and volume change behavior (especially the peak strength), while dealing with unsaturated “intermediate soils” that tend to show high post-peak strain softening.

4.6 Soil Dilatancy at High Total Suction

Dilative type of volumetric soil behavior at critical state has been scantily analyzed. The dilative behavior of granular soils influences its shear strength response. Figure 4.14 shows the effect of an increase in net confining stress, σ_3 - u_a on dilation angles using Method I. The general trend is that the dilation angle is suppressed with increase in external confinement.

Table 4.2 Experimental values of dilation angles (degrees)

σ_3-u_a (kPa)	s (kPa)	Method I	Method II	Method III	Method IV
100	50	7.1	9.1	17.8	7.2
	250	10.3	9.7	23	10.5
	500	12.9	10.8	30	13.2
	750	15.4	11.9	40	16
	20,000	4.5	5.1	30.6	4.5
	300,000	8.9	7	59	9
200	50	5.9	8.7	14	5.9
	250	5.6	8.5	12.8	5.7
	500	7.2	8.98	19.4	7.3
	750	9.9	8.85	30.4	10
	20,000	6.2	7.5	47	7.9
	300,000	5.6	5	43	5.6
300	50	3.5	7.2	10	3.5
	250	2.8	7.4	10.5	3.7
	500	5.8	9	22	5.8
	750	4.6	6.5	17.2	4.7
	20,000	5.3	7	22	6.2
	300,000	1	2.4	35.5	1

Table 4.2 documents the angles of dilations through analysis of experimental data, using Equations 1 and 2, along with direct measurement of peak dilation angles, using Method 3 from both the axis-translation technique, as well as the total suction triaxial tests.

At a net confining stress of σ_3 - u_a = 300 kPa the dilation angle by Method I was reduced to almost 1 deg. There was also an increase in dilation with increase in suction

for σ_3 - u_a = 100 kPa (lowest confinement). However, at σ_3 - u_a = 200 kPa and σ_3 - u_a = 300 kPa (highest confinement), the dilation angle decreased with an increase in suction

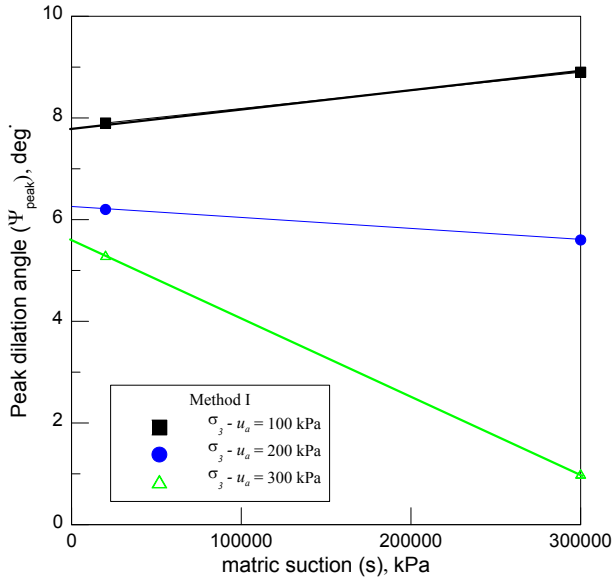

Figure 4.14 Effect of net confining stress, σ_3 - u_a on dilation angles using Method I

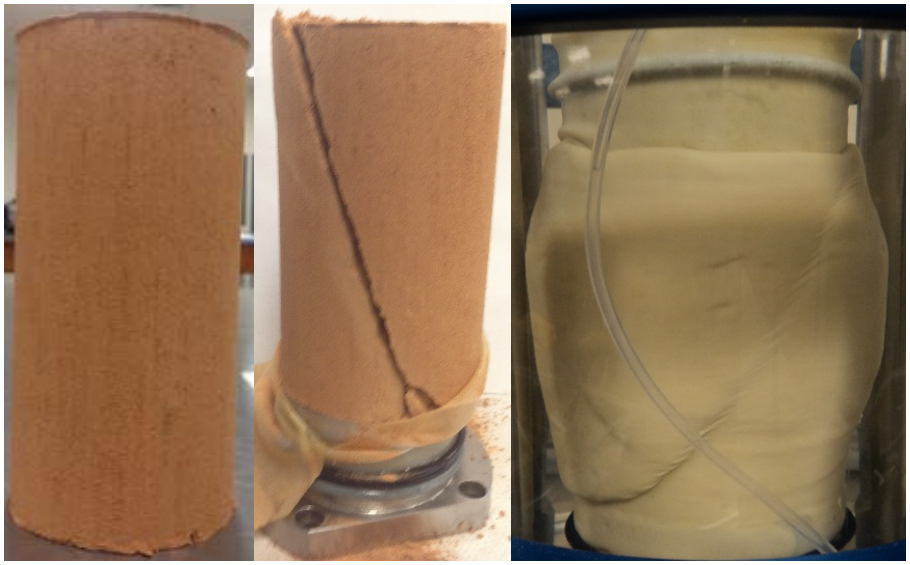

(a) (b) (c)

Figure 4.15 a) Desiccated specimen before test, b) Brittle type failure after CDRH300-300MPa test, c) Bulging type ductile failure after CD300-500 test

. In addition to several factors including soil type, density, grain size distribution, confining pressure, matric suction, and shape of particles, the dilation angles also depend upon whether the soil particles were crushed or not before they overrode the other particles. Post-shearing the sieve analysis revealed that there was particle breakage during shearing.

The high total suction imposed caused an increase in strength and stiffness of the specimen; consequently, the particles were crushed before getting a chance to ride over each other while shearing, thereby suppressing dilation behavior as compared to that occurring at lower matric suction. The dilation angle from Methods I, II and IV are almost same and yield less value, as compared to Method III that gives high values of directly measured peak dilation angles.

4.7 Stress-Strain Studies at High Total Suction

This section explains the interpretation of test results from a series of CD tests in high suction range, i.e., CD100-20MPa; CD200-20MPa; CD300-20MPa as well as CD100-300MPa; CD200-300MPa and CD300-300MPa.

4.7.1 Effect of High Total Suction at Constant Confining Pressure

The results of deviatoric stress and volumetric strain response against axial strain, obtained from the saturated CD triaxial test as well as the CDRH triaxial shear tests under total suction of 20 MPa and 300 MPa but at constant net confining pressure of 100, 200 and 300 kPa, are presented in Figure 4.16a, b, Figure 4.17a, b and Figure 4.18a, b. The specimen sign convention and designation used are the same as those explained in Section 4.3.1.

Figure 4.16a clearly indicates an increase in initial and overall stiffness (i.e. initial and subsequent tangent modulus), as well as the brittleness with increase in total suction. The peak deviatoric stress increased with an increase in total suction. The peak

failure was followed by large strain-softening for *s* = 20 MPa until it reached a critical state.

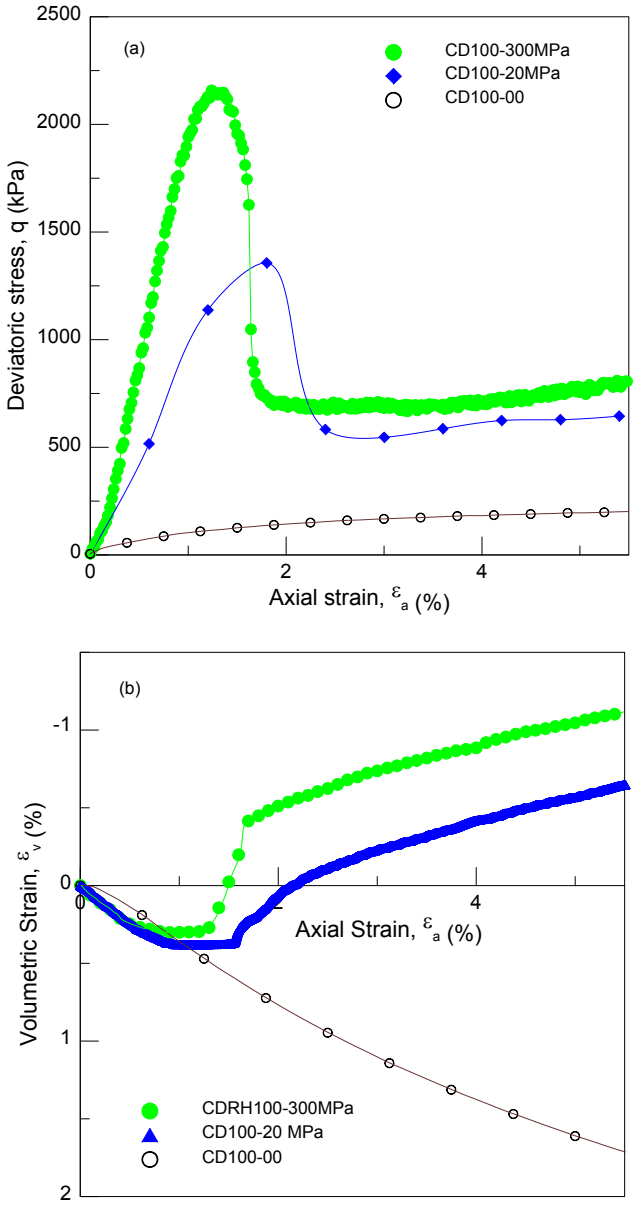

Figure 4.16 (a) Deviatoric stress against axial strain curves, (b) Volumetric strain against axial strain curves at same net confining pressures ($\sigma_3 - u_a$) of 100 kPa; at *s* = 0, 20 MPa and 300 MPa

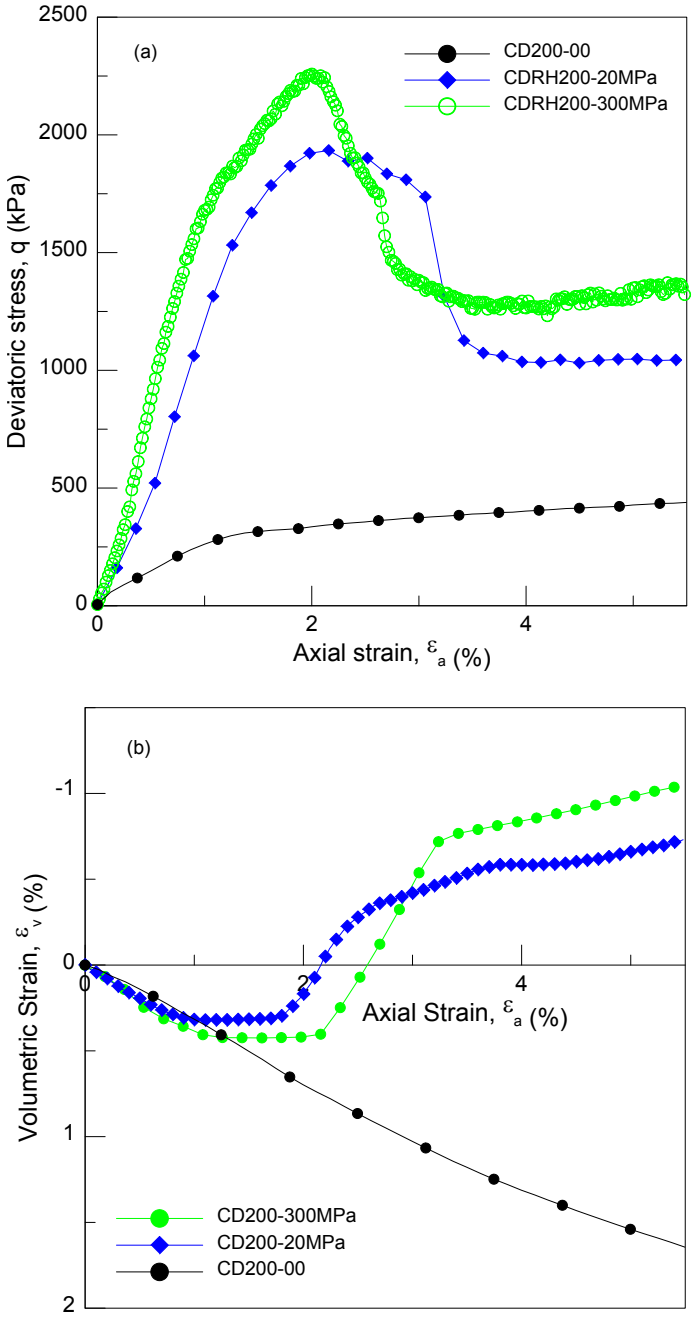

Figure 4.17 (a) Deviatoric stress against axial strain curves, (b) Volumetric strain against axial strain curves at same net confining pressures ($\sigma_3 - u_a$) of 200 kPa; at *s* = 0, 20 MPa and 300 MPa

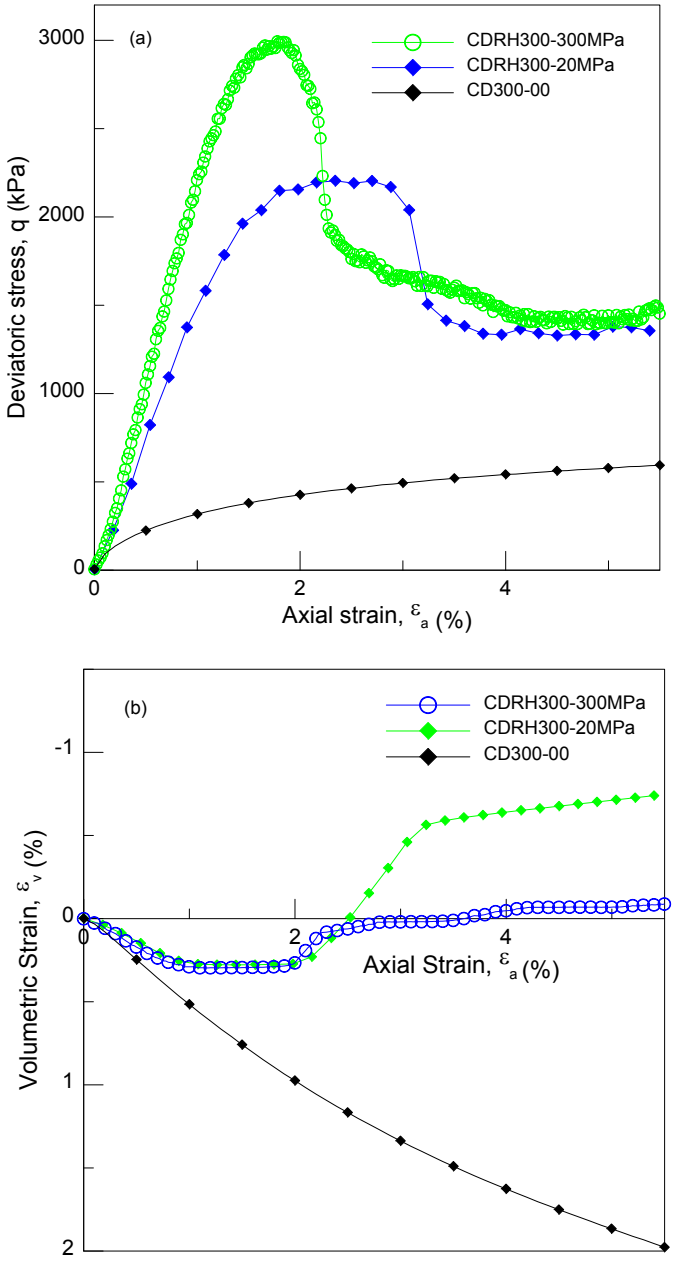

Figure 4.18 (a) Deviatoric stress against axial strain curves, (b) Volumetric strain against axial strain curves at same net confining pressures ($\sigma_3 - u_a$) of 300 kPa; at *s* = 0, 20 MPa and 300 MPa

The strain-hardening type response as seen in saturated soil was replaced by the strain-softening type response with the introduction of high total suction in all specimens. The strain-softening was more pronounced with an increase in total suction. The specimen failed at lower axial strain, as it took less axial strain to reach a critical state with an increase in total suction.

The critical state deviatoric stress increased by about three times, while the peak strength increased by about 5.5 times when the total suction was increased to 20 MPa as compared to its saturated counterpart. The critical state deviator stress increased by about 1.14 times, while the peak strength increased by 1.6 times when the total suction was increased from 20 MPa to 300 MPa. Clearly the stress-strain plot indicates that the elasto-plastic behavior of test soil in high suction range is different compared to specimens tested at a lower suction range.

Figure 4.16 b clearly manifests the change in shear-induced volumetric response from initial compressive to dilational type when the soil saturation state changed from saturated to unsaturated state with the introduction of total suction of magnitude 20 and 300 MPa. All the specimens showed initial compression, followed by a stress-induced dilatancy-type response that increased with an increase in the suction induced. Such types of stress-strain and volumetric response are typical of dense or overconsolidated soils.

The shearing was continued until the material softened back to critical state, at which point the material was expected to exhibit only shear deformations (plastic flow), with no further change in shear strength or volume. All the specimens showed brittle type failure, without any bulging. The variation of deviator stress with axial strain is compared in Figures 4.16a, 4.17a and 4.18a at same confining pressures, but with varying total suction, s = 0 kPa, 20 MPa and 300 MPa.

The stress condition was such that the increase in confining pressure from 100 to 300 kPa, with high total suction up to 20 MPa and 300 MPa would cause higher particle crushing. Hence, even though the suction is high (s = 300 MPa), and it is expected to dilate more, due to high stress condition involved, there would be more particle crushing and, hence, less dilation. Therefore, the importance of particle crushing and confining pressure needs to be considered while modeling soils in high suction range. Usually, particle crushing is expected when high confining pressures are involved, that does not occur in normal practice. However, if suction is very high, then particle crushing may happen even under medium confining pressures.

4.7.2 Effect of Confining Pressure at Constant Total Suction

The results of deviatoric stress and volumetric strain response against axial strain, obtained from the RH-triaxial shear tests under three net confining stresses of 100, 200 and 300 kPa but at the same total suction of 20 and 300 MPa, are presented in Figures 4.19a and 4.19b. The specimen sign convention and designation used were the same as explained earlier.

The water contents at total suction of 20 MPa and 300 MPa were about 1.0% and 0.3%, respectively. The exchange of moisture content was mostly in the vapor phase. Figure 4.19a clearly indicates an increase in initial and overall stiffness (i.e. initial and subsequent tangent modulus), as well as brittleness, with an increase in confinement. The peak deviatoric stress increased with increase in confining pressure.

Figure 4.19b shows the dilational-type shear-induced volumetric response. The specimens showed initial compression followed by stress-induced dilatancy-type response. However, increase in the confinement pressure caused higher compression of the specimens, and, hence, suppressed the amount of dilation. It is manifested in Figure 4.17b, where dilation was suppressed with increased confining pressure from 100 to 300

kPa, as expected. Such types of stress-strain and volumetric response are typical of dense or overconsolidated soils, especially silty sands.

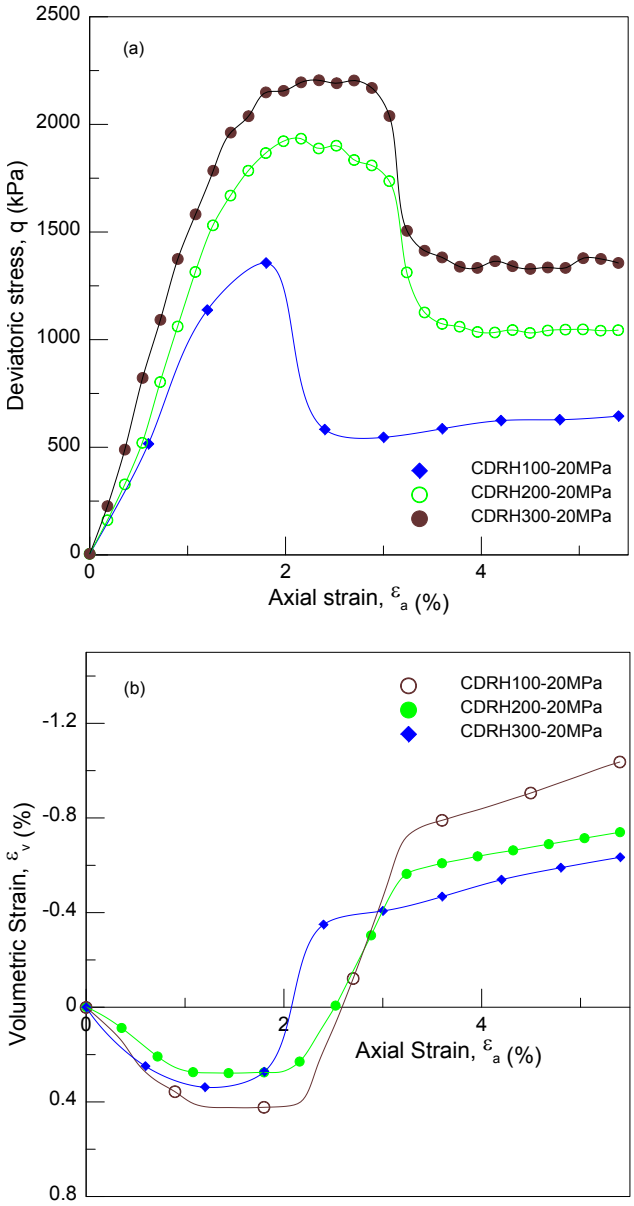

Figure 4.19 (a) Deviatoric stress against axial strain curves, (b) Volumetric strain against axial strain curves at $\sigma_3 - u_a$ = 100, 200 and 300 kPa at *s* = 20 MPa

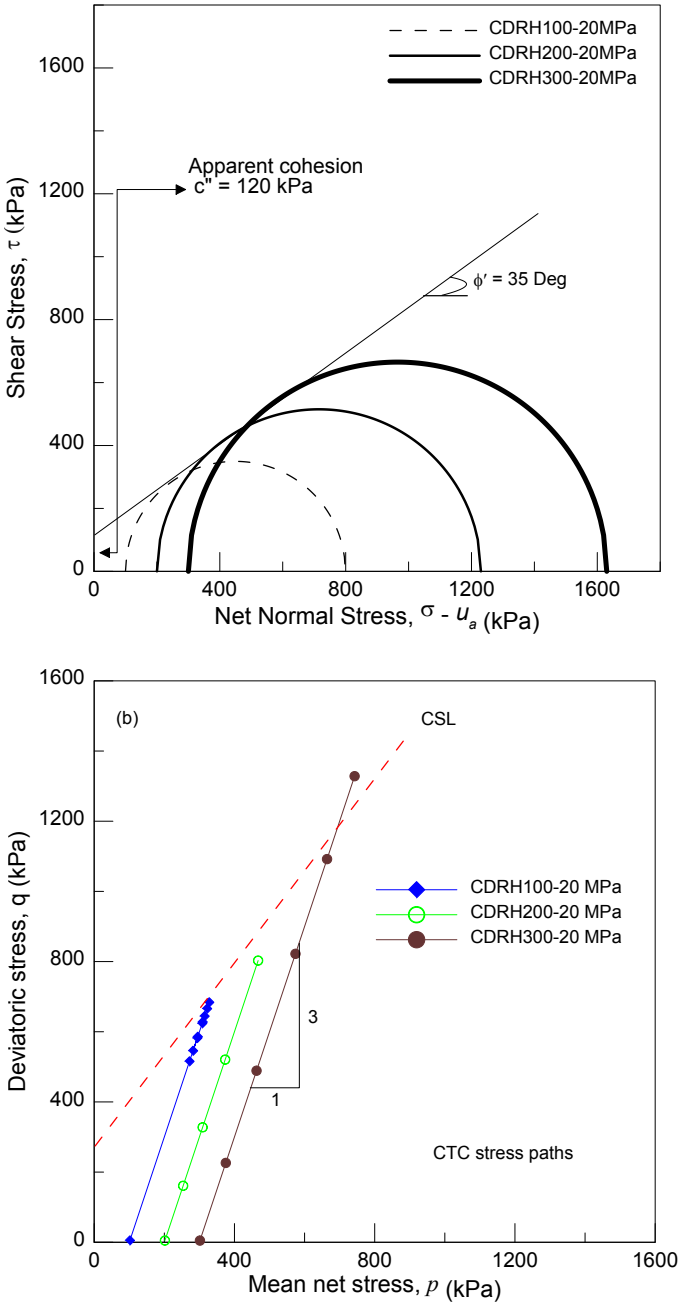

Figure 4.20 a) Mohr's stress circle at three effective confining pressures 100, 200 and 300 kPa and at *s* = 20 MPa, b) Conventional triaxial stress path in p-q space at *s* = 20 MPa

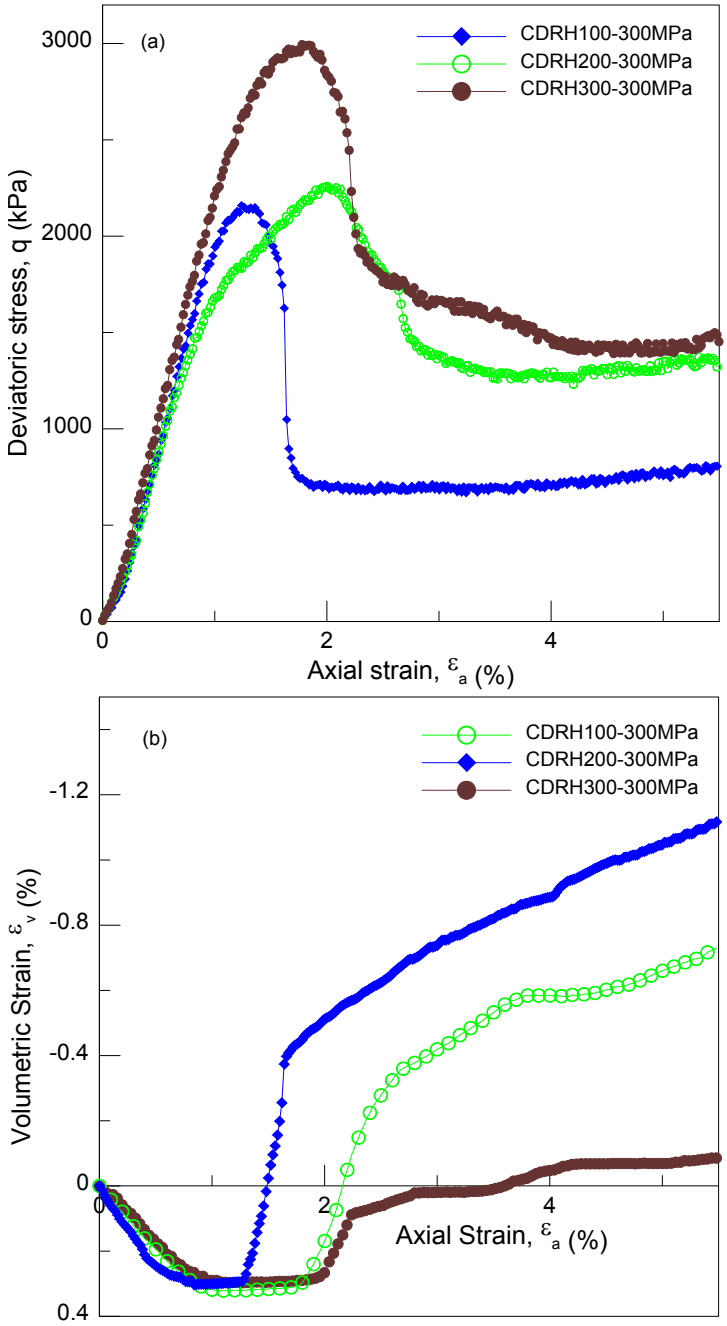

Figure 4.21 (a) Deviatoric stress against axial strain curves, (b) volumetric strain against axial strain curves at $\sigma_3 - u_a$ = 100, 200 and 300 kPa at *s* = 300 MPa

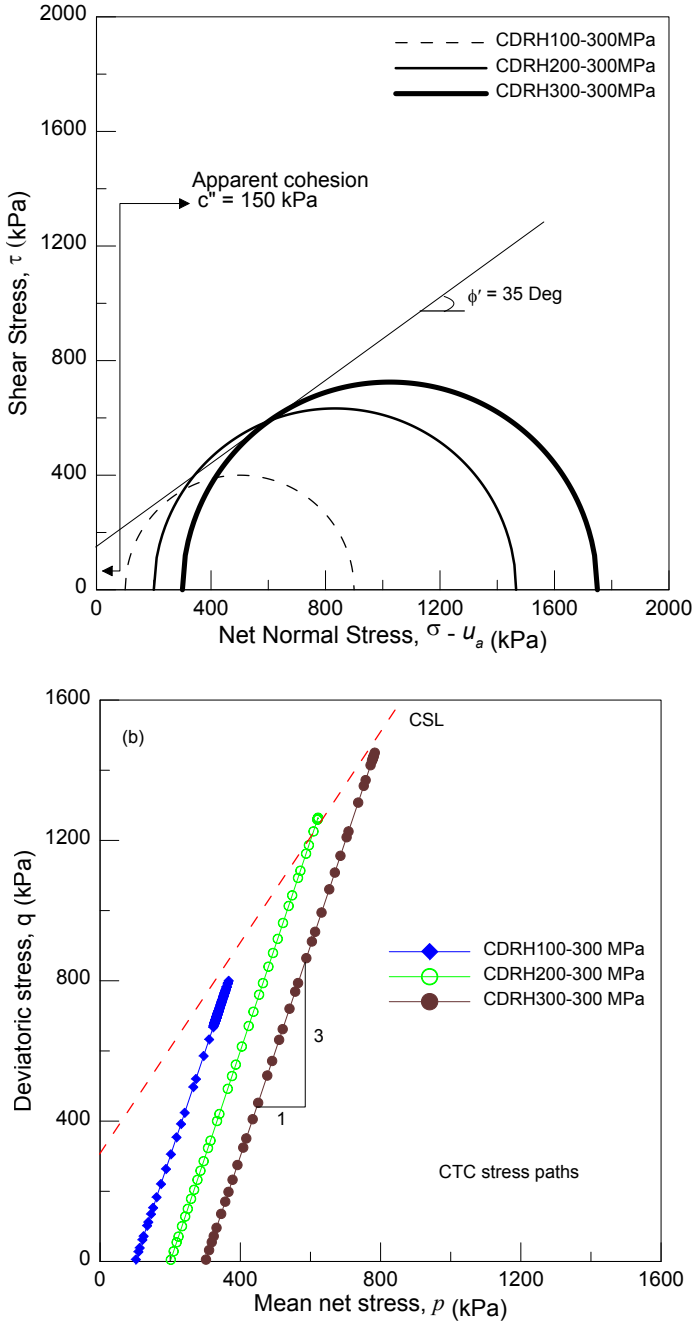

Figure 4.22 a) Mohr's stress circle at three effective confining pressures 100, 200 and 300 kPa and at *s* = 300 MPa, b) Conventional triaxial stress path in *p*-*q* space at *s* = 300 MPa

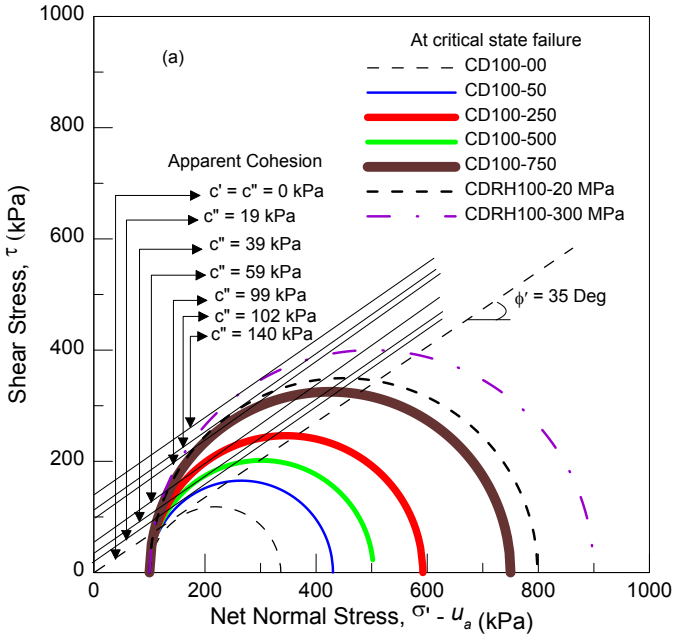

Figure 4.23 Mohr's circle at *s* = 0, 50, 250, 500, 750 kPa, 20 and 300 MPa at σ_3-u_a = 100 kPa

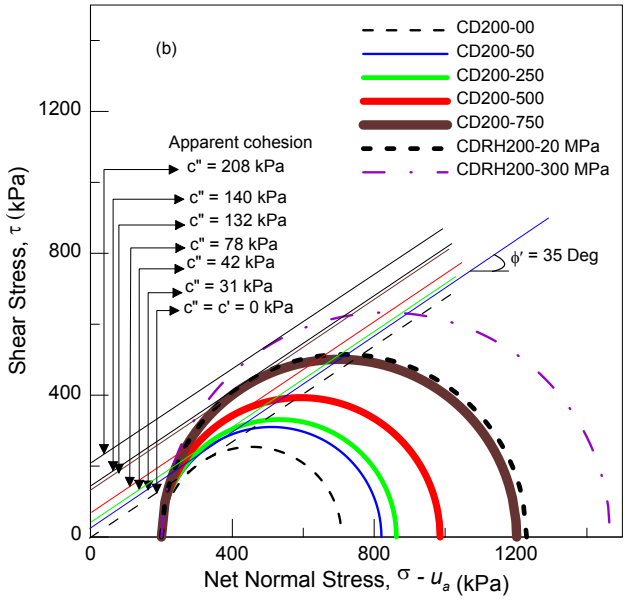

Figure 4.24 Mohr's stress circle at *s* = 0, 50, 250, 500, 750 kPa, 20 and 300 MPa at σ_3-u_a = 200 kPa

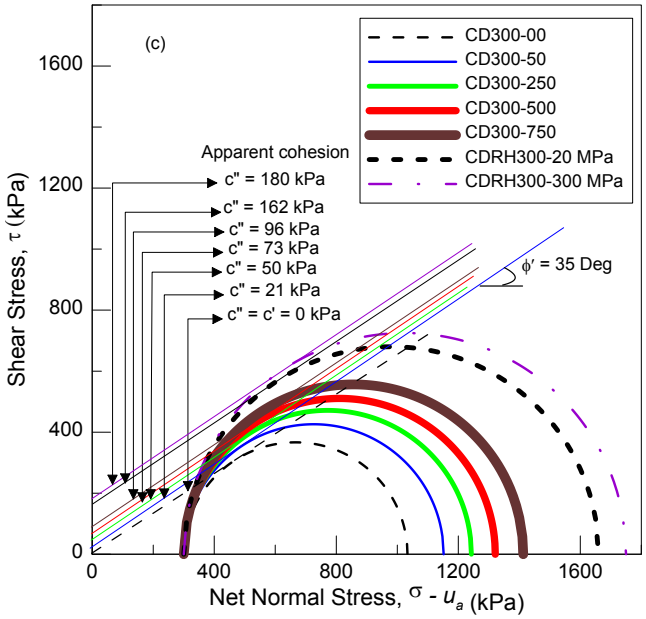

Figure 4.25 Mohr's stress circle at *s* = 0, 50, 250, 500, 750 kPa, 20 and 300 MPa at σ_3-u_a = 300 kPa

Figures 4.20a and 4.22a show three Mohr's circles plotted at different confining pressures for varying matric suction of 20 and 300 MPa. Each Mohr-Coulomb failure envelope was plotted based on three tests performed at three different net confining pressures (i.e., 100, 200 and 300 kPa), but at same total suction (i.e., 20MPa), at critical state failure condition.

A tangent drawn to these three Mohr's circles will intersect the y-axis, yielding the apparent cohesion intercept, c''. The tangent makes approximately an angle of 35 deg. with a horizontal axis, indicating that the saturated effective friction angle does not change with either matric or total suction. It confirms the assumption made in the classic Barcelona basic model that the critical state line slope is independent of soil suction applied. Figures 4.20b and 4.22b show the stress path followed by specimens tested at

100, 200 and 300 kPa of mean net pressure in p'-q space, along with the critical state line at 20 and 300 MPa, respectively.

Figures 4.23, Figure 4.24 and Figure 4.25 depict the Mohr's stress circles, at effective confining pressures of 100, 200 and 300 kPa, with an increase in matric suction at 50, 250, 500 and 750 kPa, as well as high total suction of 20 and 300 MPa. The values of increase in apparent cohesion (c''), and the corresponding angle of internal friction, with respect to soil suction (ϕ^b), is interpreted from Figures 4.23, 4.24 and 4.25 and tabulated in Table 4.3.

Table 4.3 Apparent cohesion and angle of friction with respect to soil suction at (σ_3 - u_a) = 100, 200 and 300 kPa and soil suction *s* = 50, 250, 500,750 kPa, 20 and 300 MPa

Net confining pressure, kPa (σ_3 - u_a)	Soil suction, kPa (*s*)	Apparent cohesion, kPa (c'')	Angle of friction with respect to suction, deg. (ϕ^b)
100	50	19	20.8
	250	39	8.9
	500	59	6.7
	750	99	7.5
	20000	102	0.29
	300000	140	0.03
200	50	31	31.8
	250	42	9.5
	500	78	8.9
	750	132	10
	20000	140	0.4
	300000	208	0.397
300	50	21	22.8
	250	50	11.3
	500	73	8.3
	750	96	7.3
	20000	162	0.46
	300000	180	0.03

It is observed from Table 4.2 that there is a gradual nonlinear (hyperbolic) reduction in ϕ^b from 50 kPa to 750 kPa of matric soil suction, while there is a sharp reduction in ϕ^b in high suction range from 20 MPa to 300 MPa.

(a) (b) (c)

(d) (e) (f)

Figure 4.26 Type of specimen failure at different suction states a) CD300-50 test, b) CD300-250, c) CD300-500, d) CD300-750, e) CDRH300-20MPa, f) CDRH300-300MPa

The decrease in ϕ^b from total suction of 20 MPa to 300 MPa is negligible, indicating less shear strength increase due to the increase in total suction from 20 MPa to 300 MPa.

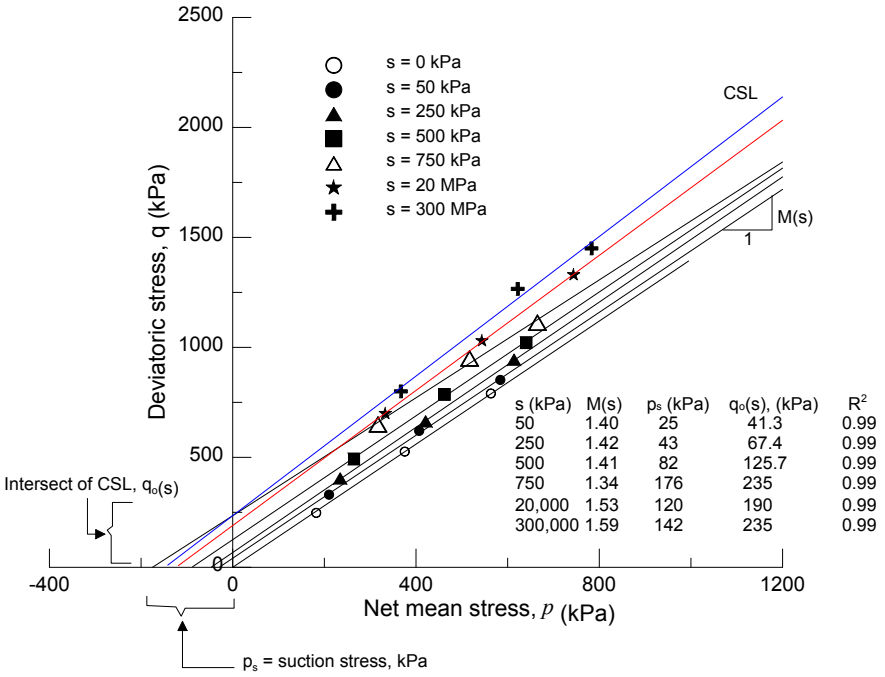

Figure 4.27 Suction stress, p_s and suction independent slope, $M(s)$ determined from best fit critical state lines for *s* = 50, 250, 500, 750, 20000 and 300000 kPa

The elasto-plastic behavior of the unsaturated soil with high soil suction is different than the soil specimens tested at low suction values. The bulging type of failure, with more than one failure shear band, is replaced by a more brittle type, with a distinct single failure shear band, as the soil suction is increased from low-to-medium matric suction, to extremely high total soil suction of 20 MPa to 300 MPa (Figures 4.26 a,b,c,d, e and f).

Figure 4.27 shows the triaxial test results of saturated, as well as unsaturated soil, obtained from the axis-translation technique and Auto-RH equipment combination, with triaxial device in p-q space. The variation of slope of critical state lines (M), suction

stress (p_s) and intercept ($q_{o(s)}$) for the entire range of suction from s = 0 to s = 300 MPa is also tabulated in Figure 4.27.

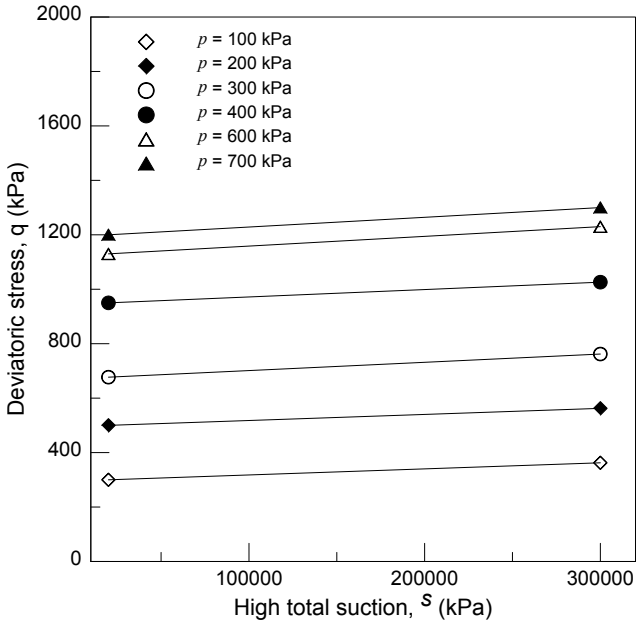

Figure 4.28 Variation of deviatoric stress with high total suction at different values of p

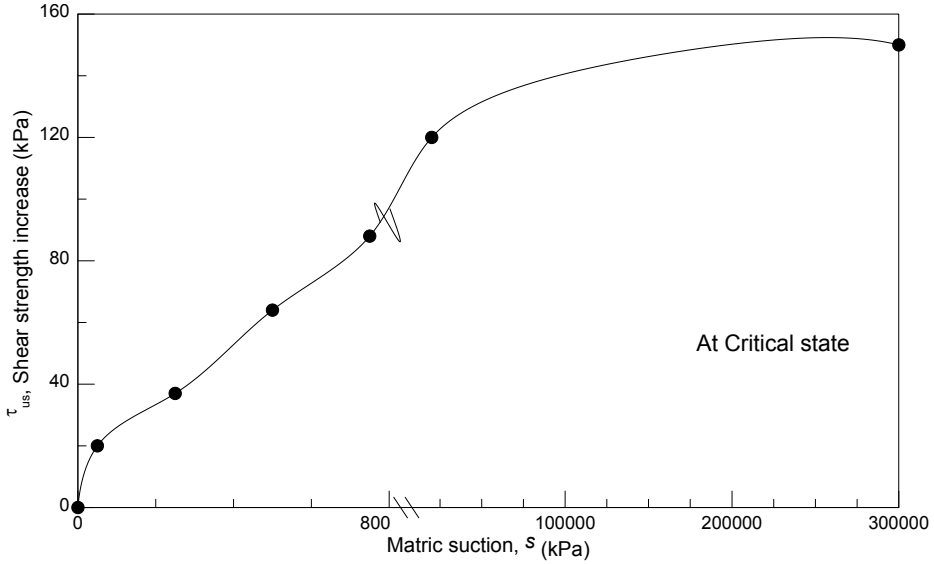

Figure 4.29 Increase in shear strength due to increase in matric suction, s

Figure 4.27 indicates that there is a little influence on the increase in deviator stress with an increase in high total suction from *s* = 20,000 to 300,000 kPa at different values of mean net stress p = 100 kPa to 700 kPa.

Figure 4.28 indicates that there is a slight increase in strength of soil when the high total suction is increased from 20,000 to 300,000 kPa, as compared with the large increase in strength when suction is increased from saturated condition, *s* = 0 kPa to *s* = 750 kPa as shown in Figure 3.43 (Chapter 3). Figure 4.29 shows an increase in shear strength, with increase in matric suction for the range *s* = 0 kPa to 300,000 kPa.

4.8 Practical Applications and Implications

There are practical implications encountered while combining the RH-equipment with an additional setup, such as custom-made chambers that are specifically designed for producing total suction characteristic curves or for using it for a suction-controlled direct shear test, triaxial test, or ring shear test to measure strength and volume change behavior, or suction-controlled consolidation test of unsaturated soils in high suction range. Such implications should be evaluated as accurately as possible and addressed to improve adequate functioning of the combined set up.

Using the axis-translation technique in modified triaxial equipment to achieve high soil suction states requires high air pressures that may lead to hazardous situations. The current assembly does not need high air pressures to impose high soil suction in specimens. Thus, the resulting combination makes it a convenient and safer technique to achieve and control high soil suction states in the soil specimens throughout the various stages involved.

The RH technique seems to be more appropriate than the axis-translation technique for testing unsaturated soils in high suction range. Ng et al., 2007 concluded that the different calibration methods may lead to varying calibrated relationships

between the osmotic pressures and the concentration of PEG solutions. However, the RH-apparatus does not need any semi-permeable membranes or solutions or salt solutions, thus avoiding complex calibration techniques. Delage et al., 1998 extended the maximum value of the applied osmotic pressure to be above 10 Mpa, using an osmotic technique. RH-equipment has the capability to achieve high total suctions above 10 MPa and as large as 600 MPa. However, the time required to achieve it may be much longer, depending upon the specimen sizes involved.

As compared to oedometer and direct shear tests, the soil specimens can be tested along a wide variety of stress paths in the triaxial test thereby simulating different field conditions encountered in geotechnical practice.

4.9 Summary

The Auto-RH equipment was configured with the SWCC chamber, as well as the triaxial equipment. The methodology followed in conducting suction-controlled CD triaxial tests at high suction was explained. Independent shear rate studies were performed and based upon an analysis of stress-strain and volumetric response, an appropriate shear rate of 0.0009%/min was selected to test specimens at high suction.

Suction-controlled isotropic consolidation tests at high suction, *s* = 20 and 300 MPa, indicated a reduction in yield stress ($p_o(s)$), and an increase in volumetric stiffness (λ_s), with increase in total suction. This, confirmed that there cannot be an infinite increase in strength of soil with an increase in suction; it tends to stabilize or decrease (as is in this case), with considerable increase in total suction.

A second series of the experimental program (six tests) was conducted at three different net confining pressures ($\sigma_3 - u_a$ = 100, 200 and 300 kPa) and at two high levels of total suction (i.e. *s* = 20 and 300 MPa). Test results indicated an increase in shear strength, initial stiffness, apparent cohesion and apparent tensile strength with an

increase in total suction, from 20 MPa to 300 Mpa, at the same net confining pressure of 100, 200 and 300 kPa, and vice-versa. However, with an increase in net confining pressure from 100 to 300 kPa, there was a reduction in the rate of increase in shear strength.

The effect of suction and net confining pressure on dilatancy of specimens while shearing was studied. In general, the dilation angle was suppressed with an increase in external confinement (under suction-controlled drained shearing conditions), while the measured dilatancy was enhanced with an increase in suction (at constant net confining stress). The relationship between maximum dilatancy and suction is highly non-linear.

The results of these studies suggest that the angle of friction (ϕ') remains unaffected at high suction. Therefore, the Fredlund et al. (1978) equation can be used to quantify shear strength of unsaturated soils over the entire soil suction range. The angle of friction with respect to soil suction (ϕ^b) decreased with an increase in soil suction, and remained almost constant at higher total suctions of 20 and 300 MPa.

Chapter 5

Modeling Soil Response

5.1 Introduction

Despite significant contributions from various researchers during the past few decades, the understanding of and capability to model the complex behavior of unsaturated soils is still developing (Kodikara, 2012). It has become a challenge to soil modelers to accommodate all possible ranges of unsaturated soil responses. These include post-peak softening, accompanied by stress-induced dilatancy -that is exhibited typically by dense soils. Other challenges include strain-hardening type responses, accompanied by volumetric compressive behavior, which is typical of loose soils, swelling and collapse under wetting, as well as shrinkage and cracking while drying. The verification of proposed constitutive relations must be conducted for a wide range of soils in order to ensure uniqueness and subsequent confidence on the part of researchers and practicing geotechnical engineers (Fredlund et al., 2012).

Soil models are intended to predict soil response and typically consist of stress-strain constitutive laws that are calibrated or best-fitted to experimental findings obtained from laboratory tests on representative soil specimens. Soil specimens can be idealized to be made of discrete particles, and the forces and displacements within these particles may be represented by continuous stress-strain response patterns. Therefore, the use of overall (macro) behavior of soil specimens during testing may be analyzed to obtain the best-fitting parameters essential for soil modeling (Helwany, 2007).

Various features of mechanical behavior of fully saturated soil have been explained quite successfully, using critical state-based models (Roscoe and Burland, 1968; Schofield and Wroth, 1968; Gens and Potts, 1988; Wood, 1990; Wood, 2004; Matsuoka and Sun, 2006; Yu, 2006). The pioneering work by Alonso et al. (1990)

postulated a unified elasto-plastic constitutive framework for unsaturated soils by extending the modified cam clay model (Schofield and Wroth, 1968) from saturated to unsaturated form, using suction as an independent component in stress space, while introducing the concept of the loading-collapse yield surface. Since then, various theoretical critical state-based frameworks have been developed to describe the constitutive behavior of unsaturated soils (Toll, 1990; Josa et al., 1992; Wheeler and Sivakumar, 1992, 1995; Cui and Delage, 1996; Karube, 1996; Bolzon et al., 1996; Vaunat et al., 2000; Georgiadis et al., 2005; Yu, 2006).

Ideally, a constitutive model should be able to simulate unsaturated soil behavior over entire ranges of possible suction and external stress states, while allowing arbitrary stress and hydraulic paths within these ranges. Numerical predictions with these models require proper selection of relevant parameters from a suitable and thorough experimental program. Most of these unsaturated material parameters, including those that define the critical state, are suction dependent hence making suction-controlled laboratory testing a requirement to calibrate them (Russell and Khalili, 2006). This chapter describes the procedure followed to determine these parameters and calibration methods for compacted silty sand soil at low-to-medium suction range (0-750 kPa).

5.2 Barcelona Basic Model

During last two decades or so, several elasto-plastic constitutive models for unsaturated soils have been proposed. However, the critical-based framework originally proposed by Alonso et al. (1990) remains to date, the most widely cited and used model. It is now generally referred to as the Barcelona Basic Model (BBM). The BBM has proven reasonably successful in capturing some of the important features of unsaturated soil behavior, such as an increase in strength and stiffness with increase in suction, as well as the possibility of collapse upon wetting. It is intended for partially saturated soils that

are slightly or moderately expansive, such as partially saturated sands, silts, clayey sands, sandy clays and clays of low plasticity.

5.3 Calibration of Barcelona Basic Model

Adequate capacity of the BBM to reproduce experimental results accurately requires the determination of several model parameters associated with isotropic stress states and changes in suction, as well as those associated with changes in deviatoric shear stress and shear strength (Alonso et al., 1990).

For suction-controlled triaxial testing under axisymmetric stress conditions ($\sigma_2 = \sigma_3$), key variables are defined in this paragraph. The BBM model expresses the isotropic stress state in (p, s) stress space. It defines net mean stress, p as the excess of mean stress, σ_m over air pressure, and matric suction s as the difference between pore-air and pore-water pressures. Hence, $p = (1/3)\ (\sigma_1 + 2\ \sigma_3) - u_a$; $\sigma_m = (\sigma_1 + 2\ \sigma_3)/3$; $s = (u_a - u_w)$; $q = (\sigma_1 - \sigma_3)$, deviator stress; $\varepsilon_{vp} = (\varepsilon_1 + 2\varepsilon_3)$, total volumetric strain; $\varepsilon_q = (2/3)(\varepsilon_1 - \varepsilon_3)$, total shear strain and $v = 1 + e$, specific volume.

5.3.1 Yield Functions

The BBM is formulated in the (p,q,s) stress space. The term "yield" refers to the onset of inelastic behavior while the set of mathematical formulations for yielding are referred to as the "yield criterion" (Selvadurai and Davis, 2002). The BBM postulates two distinct yield functions, based on the effect of applied external pressure or suction in partially saturated soils. The first postulated yield function represents an ellipse-shape yield surface in p-q plane, beyond which plastic compression occurs on account of increased stress or decreased suction, as shown in Figure 5.1. The model assumes that only elastic strains will be accumulated when the soil state lies inside a state boundary hypersurface f_1, as given by Equation 5.1, and plastic strains once the state boundary hypersurface is reached. Plastic behavior is captured and related to the expansion of

yield surface in the *(p,q,s)* space as the soil state traverses the state boundary hypersurface (see Figure 5.1).

$$f_1 = f(p,q,s) = q^2 - M^2(p + p_s)[p_o(s) - p] = 0 \tag{5.1}$$

where M = suction-independent slope of the critical state line in the p-q plane.

$$p_s = ks \tag{5.2}$$

k = slope of the apparent tensile strength line in p-s plane.

s = soil suction.

The second postulated yield function represents the suction increase (SI) yield locus that encloses an elastic region in the (p,s) plane and is related to the plastic compression that occurs with an increase in suction beyond a value s_o, as given below:

$$f_2 = f(s, s_o) = s - s_o = 0 \tag{5.3}$$

where s_o is the maximum past suction ever experienced by the soil.

5.3.2 Loading Collapse (LC) Yield Curve

The yield surface in (p, q, s) space grows in size with an increase in matric suction, *s*, due to the assumption of a monotonic decrease of the volumetric stiffness parameter $\lambda(s)$ with increasing matric suction, expressed as follows:

$$\lambda(s) = \lambda(0)\left[(1-r)e^{(-\beta s)} + \mathrm{r}\right] \tag{5.4}$$

Where, $r = \frac{\lambda(s\to\infty)}{\lambda(0)}$;

β = parameter controlling the rate of increase of soil stiffness with matric suction.

The yield surface of the specimen at a constant matric suction, *s*, may be described by an ellipse that will exhibit an isotropic consolidation stress, $p_o(s)$, that will lie on the loading collapse (LC) yield curve. The LC yield curve in a p-s plane takes the following form (Alonso et al., 1990):

$$\frac{p_o(s)}{p^c} = \left[\frac{p_o(0)}{p^c}\right]^{\frac{\lambda(0)-\kappa}{\lambda(s)-\kappa}} \tag{5.5}$$

where, $p_o(s)$ = generic yield stress which depend on matric suction, s

$p_o(0)$ = preconsolidation stress under saturated condition (s = 0)

p^c = reference/preconsolidation stress at which the LC becomes a straight line (i.e. $p_o(s) = p^c$)

$\lambda(0)$ = compressibility coefficient for the saturated state along virgin loading

$\lambda(s)$ = soil stiffness parameter that varies with matric suction, s

κ = elastic rebound index with respect to net mean stress

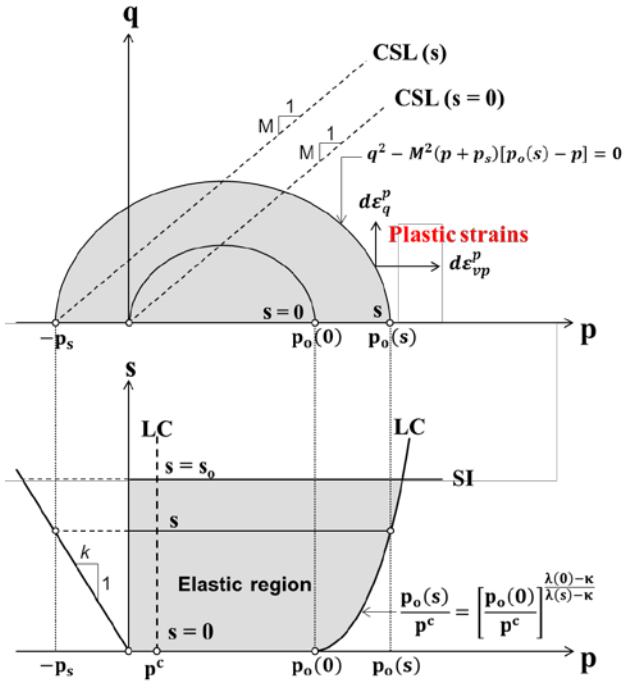

Figure 5.1 General critical state-based framework of Barcelona Basic Model (BBM)

The failure condition is identified at critical state (i.e. p_f, q_f) in order to define the proposed function for the yield locus, which takes an ellipse form. The model assumes a linear increase in cohesion with suction such that the ellipse will intersect the p axis at a point for which p' = $-p_s(s) = -ks$. The major axis of the ellipse will span the segment $-p_s(s)$ to $p_o(s)$ and will be given by Equation 5.1, as shown in Figure 5.1.

5.3.3 Calibration of BBM Parameters under Isotropic Loading

Following the suction equalization stage, the suction-controlled isotropic consolidation stage was performed in the same way as that in Method I described in Chapter 3. Figure 5.2 shows the test results from isotropic consolidation of compacted silty sand under controlled-suction conditions at *s* = 50, 250, 500 and 750 kPa.

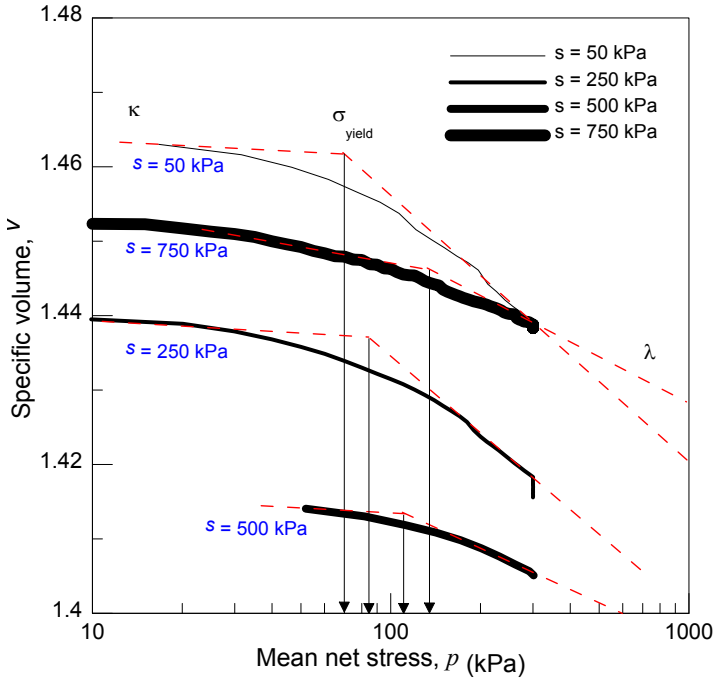

Figure 5.2 Suction-controlled isotropic consolidation at *s* = 50, 250, 500 and 750 kPa

In all cases, yielding was observed during isotropic compression. As expected, yield stresses are significantly influenced by the level of induced suction, with a continuous increase in mean net stress eventually causing the specimen to yield at some point. In general, the yield stress increased with an increase in matric suction, and resulted in a maximum value for highest matric suction *s* = 750 kPa. The values of yield stresses were estimated by the method of intersection of the two linear segments of the consolidation curve, as proposed by Cui and Delage (1996) and Sharma (1998). Figure 5.2 illustrates the graphical determination of the preconsolidation pressure at all induced

and controlled suction states. From ramped consolidation tests conducted under constant-suction states, *s* = 50, 250, 500, and 750 kPa, approximate values for the corresponding preconsolidation pressures, p_o(50) = 72 kPa, p_o(250) = 83 kPa, p_o(500) = 120 kPa, and p_o(750) = 140 kPa, were obtained. This pattern corroborates the existence of an initial LC yield locus induced by the static compaction method used to prepare the specimens, as explained in section 3.2.2 of Chapter 3 .

Figure 5.10 shows the initial LC curve experimentally assessed in this current work, along with previously reported LC curves for different soils and compaction methods (i.e., Wheeler and Sivakumar, 1995; Hoyos, 1998; Laikram, 2007; Hoyos et al., 2012). The target densities/compactive efforts used in the present work are considerably different than the ones used in all other previous works included in Figure 5.10. The compactive effort used in the current research in preparing the specimens clearly manifested as the maximum among all these, as clearly seen from the largest values of compaction-induced pre- consolidation pressure p_o(*s*). Figure 5.2 also illustrates the graphical determination of volumetric stiffness parameter λ(*s*) from ramped consolidation, under constant-suction state, varying from 50 to 750 kPa. The best-fit values of the elastic rebound index for compacted silty sand soil were found to be κ = 0.0008, 0.0012, 0.0014 and 0.0026, for matric suction values *s* = 50, 250, 500 and 750 kPa, respectively. An average value, κ = 0.0015, was adopted.

Likewise, the slopes of the normal compression lines were found to be λ(50) = 0.01381, λ(250) = 0.012146, λ(500) = 0.005097, and λ(750) = 0.0061339, for matric suction values *s* = 50, 250, 500 and 750 kPa, respectively. This pattern is consistent with the BBM formulation, which postulates a monotonic decrease in $\lambda(s)$ with increasing suction.

5.3.4 Loading-Collapse (LC) Yield Curve Parameters

The least square method was used to solve the overdetermined system in Equation (5.4), allowing for the determination of constitutive parameters $\lambda(0)$, r, and β. Using experimental values, $\lambda(50)$ = 0.01381, $\lambda(250)$ = 0.012146, $\lambda(500)$ = 0.005097, and $\lambda(750)$ = 0.0061339, best-fit values for these three unknowns were found to be $\lambda(0)$ = 0.02, r = 0.26, and β = 2.0 MPa^{-1}, with a coefficient of determination, R^2 = 0.85. Figure 5.3 and Figure 5.4 show the experimental values of stiffness parameter $\lambda(s)$, along with parametric predictions using Equation (5.4), for different values of r and β, respectively. Good agreement is observed between experimental and predicted values of $\lambda(s)$ for this partial set of calibrated parameters.

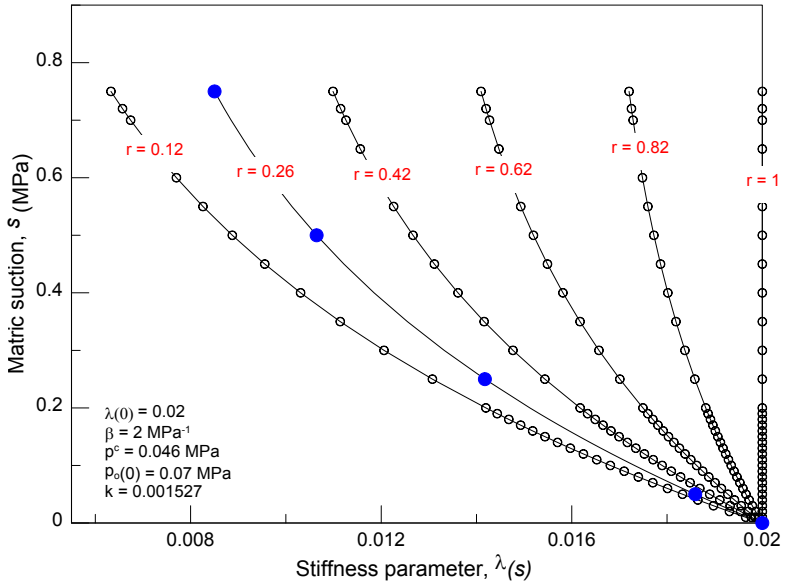

Figure 5.3 Experimental stiffness parameter, $\lambda(s)$, for test soil and predicted curves for various values of r using equation (5.4)

The same method was used to solve the overdetermined system in Equation (5.5), allowing for the assessment of parameters p^c and $p_o(0)$. Using experimental values, $p_o(50)$ = 72 kPa, $p_o(250)$ = 83 kPa, $p_o(500)$ = 120 kPa, and $p_o(750)$ = 140 kPa, best-fit

values for these two unknowns were found to be p^c = 46 kPa and $p_o(0)$ = 70 kPa, with a coefficient of determination, R^2 = 0.99. A parametric performance of the LC yield locus for this partial set of calibrated parameters is shown in Figure 5.5.

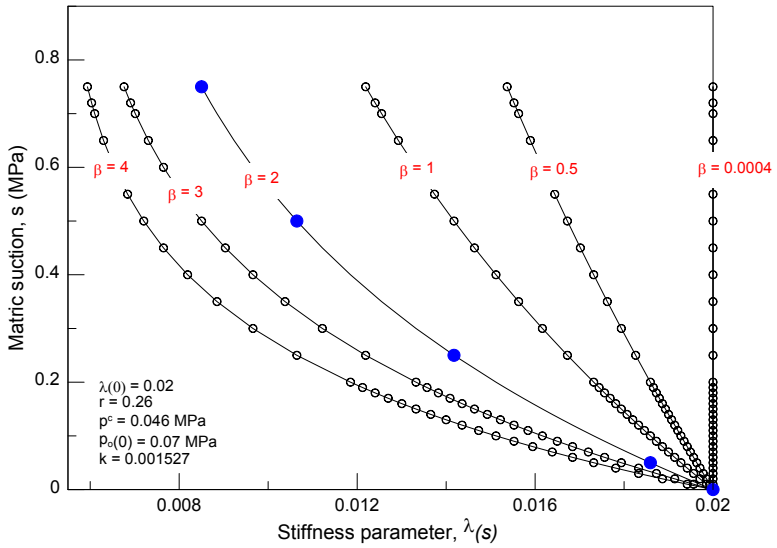

Figure 5.4 Experimental stiffness parameter, $\lambda(s)$, for test soil and predicted curves for various values of β using equation (5.4)

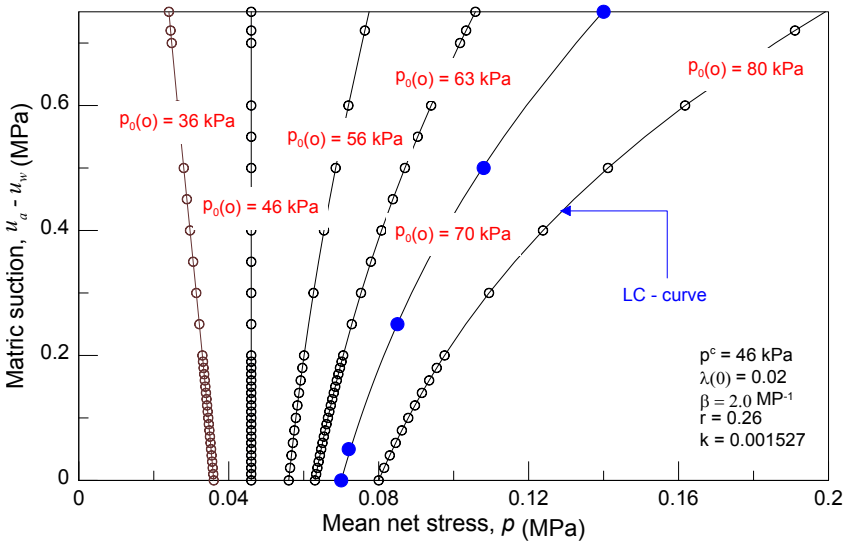

Figure 5.5 Experimental yield stress value along the best fit LC curve and typical curves predicted for different values of $p_o(0)$

The experimental data points from compacted silty sand used in this research show a very close agreement with the LC curve predicted for $p_o(0)$ = 70 kPa.

5.4 Constitutive Behavior under Shear Loading

In this work, the specimens were loaded axially at a constant shearing-rate, and under constant suction (drained) conditions, along conventional triaxial compression (CTC) stress paths. The deviator stress, q, is the difference between the major and minor principal stress and is the measure of strength of soil. A close examination of the experimental q-ε_{axial} plots in Chapter 3 (Figures 3.29, 3.30, 3.31 and 3.32) indicates that as the specimen was compressed, the deviatoric stress gradually increased until it reached a peak, and thereafter, it softened until a residual/critical value was reached. These curves also showed an increase in strength with suction.

5.4.1 Critical State Condition

According to Schofield and Wroth (1968), at a critical state soils behave as a frictional fluid so that yielding occurs at constant volume and constant stresses. This means that the plastic volumetric strain increment would be zero at critical state, since elastic strain increments are expected to be zero due to the constant stress condition at this critical state (Yu, 2006). Continuous loading, while shearing, causes plastic hardening expansion of the yield surface, until the stress state reaches the top of the current yield surface plotted on the p-q stress plane. At this point, the plastic strain increment vector is normal to the tangent at the apex of the ellipse, i.e., parallel to q axis, and a perfect critical state is reached (Wood, 1990). Thus, when the stress state is at the top of the current yield locus, it is assumed that an indefinitely plastic shearing can occur without changes in volume or stress. In other words, plastic shearing could continue indefinitely without further expansion or contraction of the yield surface, leading to a condition of perfect plasticity that is commonly referred to as a critical state.

Each stress state along the shearing stress path may be represented by yield surface that grows in size with an increase in stress ratio (q/p) because of plastic hardening. The locus obtained by joining the apex of these yield surfaces is identified as the critical state line (CSL) and is expressed as follows:

$$q_{cs} = Mp_{cs} \tag{5.6}$$

The subscript "cs" denotes the critical state condition.

5.4.2 Calibration of Model Parameters under Axisymmetric Shearing

Figure 5.6 shows the best-fit critical state lines obtained from the CD triaxial tests as plotted in p-q space for matric suction values, s = 0, 50, 250, 500 and 750 kPa.

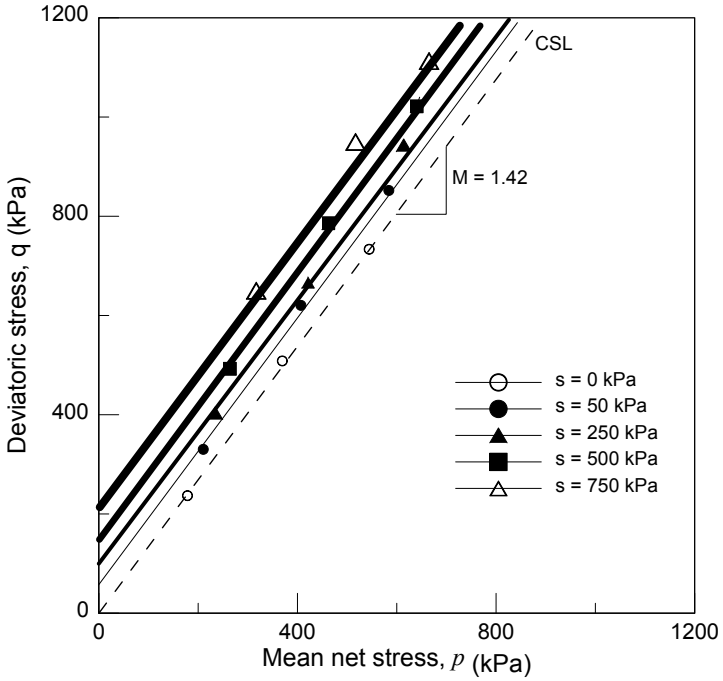

Figure 5.6 Critical state lines in p-q plane generated from suction-controlled CD triaxial tests via axis-translation

It can be readily noticed from Figure 5.6 that the slope of the critical state lines remains virtually constant despite the introduction of suction. Thus, it establishes a unique relationship between deviator and net mean stresses for suction-controlled CD

triaxial tests. However, a noticeable an upward shift in the position of critical state line is observed with the introduction of matric suction, as compared to its saturated counterpart. The intersection of the critical state line with the p-axis on the negative axis, gives the magnitude of the additional tensile strength offered by the soil due to matric suction, as discussed later in this chapter.

5.4.3 Wetting Induced Loading Collapse or Swelling

Compressive type of external pressure, applied at the top and bottom boundaries of saturated and unsaturated soil specimens under drained conditions, creates both shear and normal forces at each grain contact point, thus causing denser packing of the soil grains. Thus, volume change occurs due to rolling and sliding of soil grains under external forces. Similar volume changes can occur in unsaturated soils due to the suction effect, where the interparticle forces are derived from high curvature menisci at the grain contact points. The surface tension forces created across the menisci induce only normal forces between the particles, thereby bonding them together. These normal forces increase with an increase in applied suction. Thus, suction provides the soil matrix with an additional internal confinement, i.e., increase in effective stress at grain point contact, inhibiting sliding and hence increasing its relative stability against deformation. Wetting a soil under such partially saturated state removes these additional interparticle bonds, and, if the stress level is high, the soil may collapse to the equivalent condition it would have experienced under saturated conditions (Jennings and Burland, 1962).

In actual field conditions, wetting (suction decrease) and drying (suction increase) of soil deposits take place under the influence of external confining pressures that might be isotropic or anisotropic. If the wetting phenomenon takes place under light external confinement, the soil may experience slight expansion due to voids imbibing

water; or may undergo large volumetric contractions, termed as “collapse,” due to removal of additional effective stress under large external confinements.

Figure 5.5 showed the loading-collapse (LC) curve assessed for compacted silty sand from suction-controlled isotropic consolidation tests performed prior to shearing. Figure 5.6 showed that the matric suction had a noticeable influence on the final position of the critical state line. Also, the slope $M(s)$ of all critical state lines remained reasonably constant, in clear agreement with the original BBM formulation. Additional key constitutive parameters postulated by the Barcelona Basic Model, including the slope (k) of the apparent tensile strength (ATS) locus in p:s plane and the slope (M) of the critical state lines, can now be calibrated and used for prediction of peak deviator stress at matric suction states varying from 50 to 750 kPa.

Figure 5.7 shows the LC and ATS locus in (p, s) space obtained from this experimental work. Within the range of stresses applied, i.e., matric suction, s = 50 to 750 kPa, and initial net mean stress, p = 100 to 300 kPa, a three dimensional plain-surface plane can be expressed by Equation 5.7 in order to fit all of the experimental values of deviatoric-stress at critical state.

$$q = Mp + Mks = 1.42\,p + 0.316\,s \qquad (5.7)$$

The plane yields best-fit values, M = 1.42, for the slope of critical state lines and, k = 0.223, for the rate of increase in apparent tensile strength with suction. Predicted values of peak deviator stress are reasonably close to those experimentally obtained from suction-controlled CTC tests, yielding a coefficient of determination, R^2 = 0.97, as shown in Figure 5.8. Figure 5.5 showed the influence of varying $p(o)$ on the loading-collapse curve, hence the referenced pre-consolidation stress (p^c), at which the loading-collapse (LC) curve becomes a perfectly straight line, was calibrated as equal to 46 kPa.

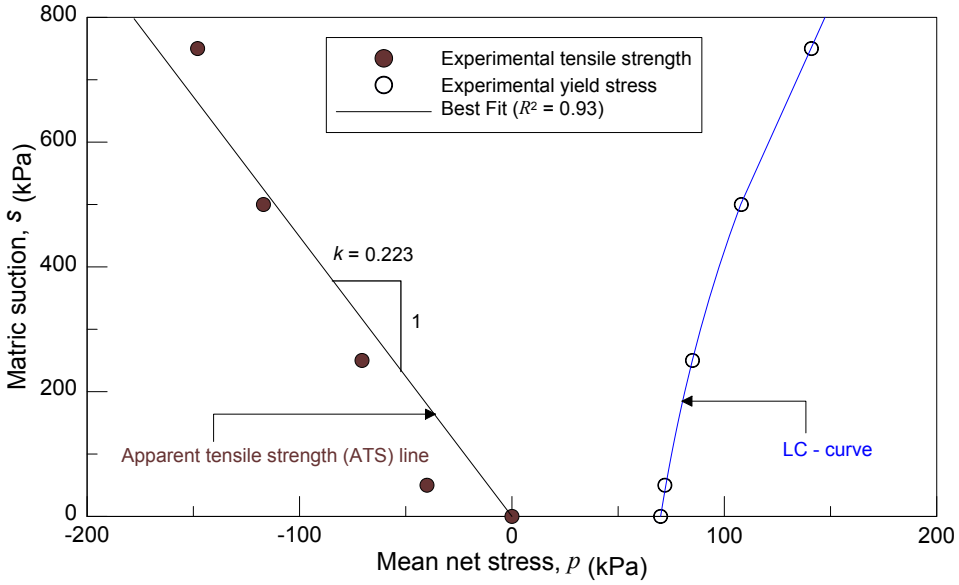

Figure 5.7 Apparent tensile strength (ATS) and loading-collapse (LC) loci experimentally assessed from suction-controlled isotropic loading

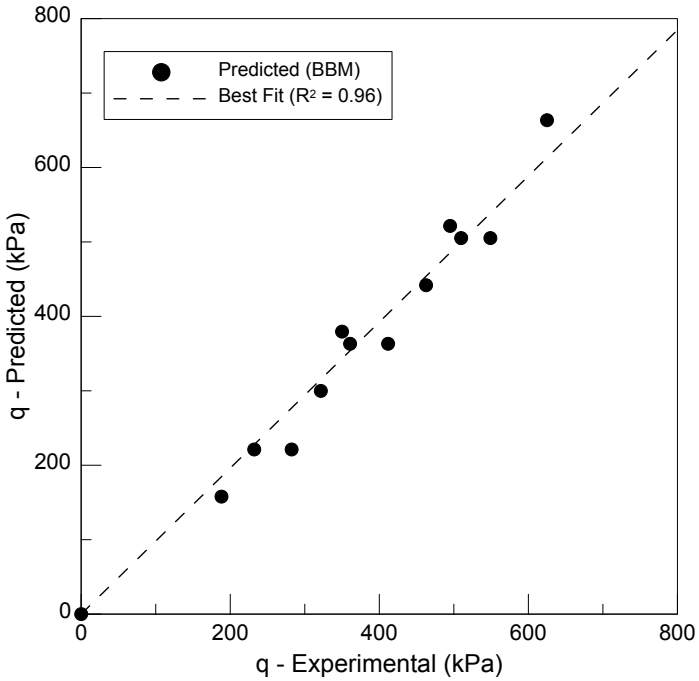

Figure 5.8 Comparison of predicted and experimental values of peak deviator stress as postulated by the BBM framework

Finally, as a consequence of the non-associative flow rule postulated in BBM by Equation (5.31), no plastic shear strain is expected to occur during initial shearing when the soil is under lightly overconsolidated condition. Hence, the elastic shear modulus can be estimated from the initial portion of the deviatoric-stress versus total shear strain curve as G = 25,000 kPa.

Post-consolidation states under isotropic loading follow the normal consolidation line (NCL) in v-p plane (Alonso et al., 1990). As the specimen gets sheared, the stress state moves from its initial position on the NCL and eventually reaches the critical state line. All the specimens showed contraction followed by dilation (Figures 3.29, 3.30, 3.31 and 3.32 in Chapter 3) as did the volumetric change paths in p-v space. Figure 5.9 shows the experimentally assessed critical state lines in p-v plane for matric suction values, s = 0, 250, and 750 kPa. The slope of the CSL is observed to decrease with increasing suction, as postulated by the BBM.

The following set of figures illustrates the overall response of compacted silty sand used in this work as compared to other previous work. Figure 5.10, as mentioned before, shows a comparison of the LC locii assessed from current and previous studies (Wheeler and Sivakumar, 1995; Hoyos et al., 1998; Laikram, 2007; Hoyos et al., 2012). Figure 5.11 illustrates the graphical determination of suction stress "$p_s(s)$" from experimental CSLs. Figure 5.12 shows a comparison of the slopes of CSLs, $M(s)$ assessed from current and previous studies (Wheeler and Sivakumar, 1995; Hoyos et al., 1998; Laikram, 2007; Hoyos et al., 2012). Figure 5.13 shows a comparison of the variation in suction stress, p_s, with an increase in suction as determined from current and previous studies (Wheeler and Sivakumar, 1995; Hoyos et al., 1998; Laikram, 2007; Hoyos et al., 2012). Finally, Figure 5.14 shows a comparison of the variation in the CSL

intercept, μ(s), with an increase in suction as assessed from current and previous studies (Wheeler and Sivakumar, 1995; Hoyos et al., 1998; Laikram, 2007; Hoyos et al., 2012).

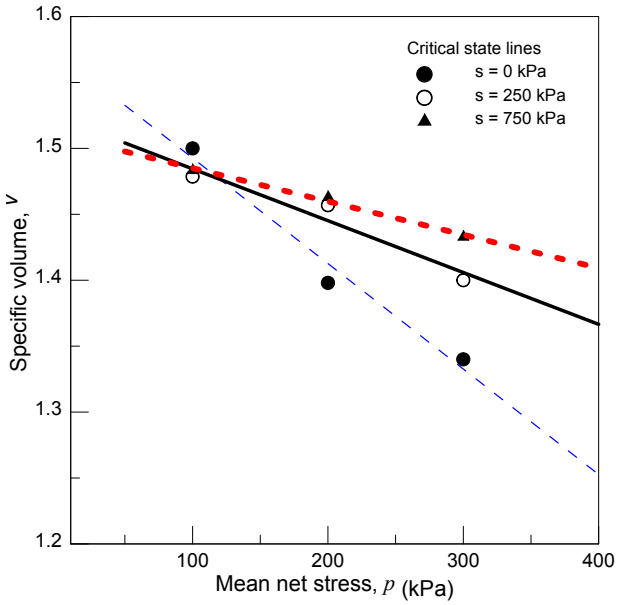

Figure 5.9 Critical state lines at failure in p-v plane

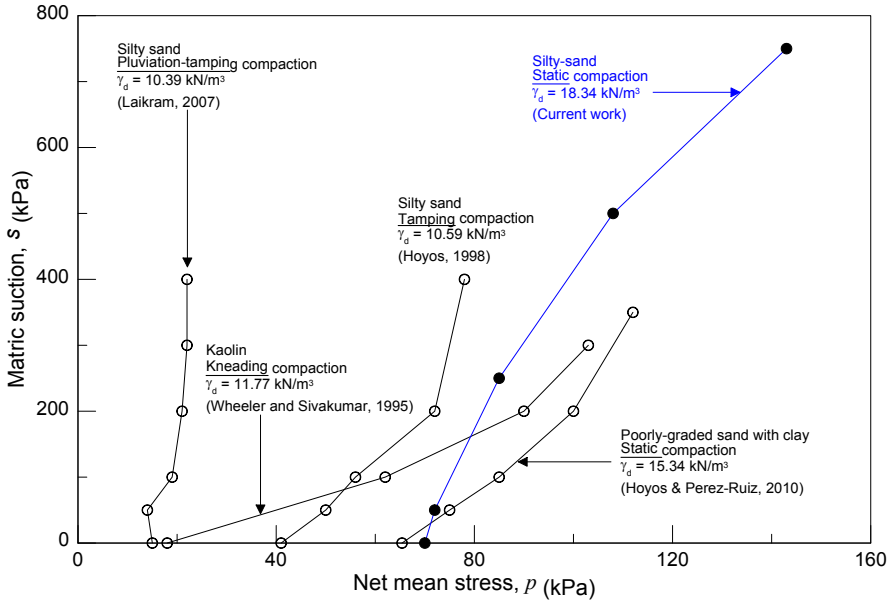

Figure 5.10 Current and previously reported LC curves for different soil compaction conditions

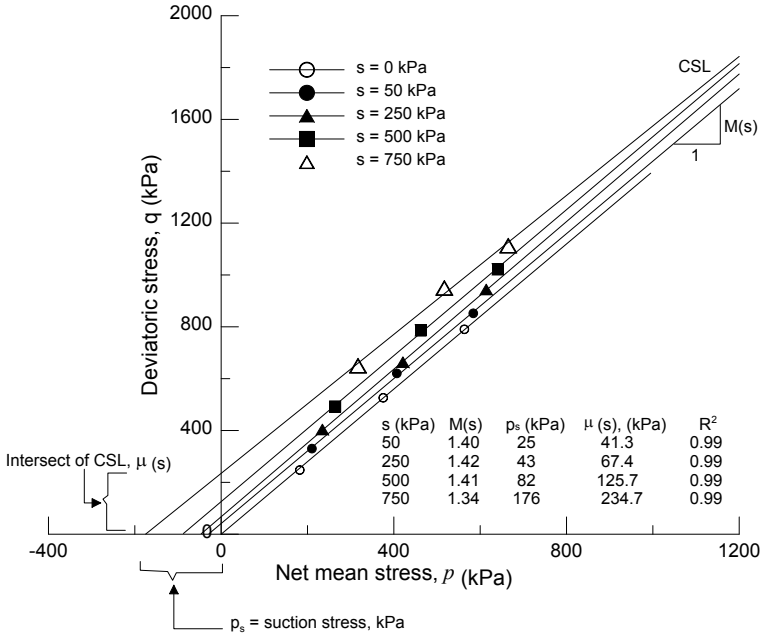

Figure 5.11 Suction stress, $p_s(s)$ and suction independent slope, $M(s)$ determined from best fit critical state lines

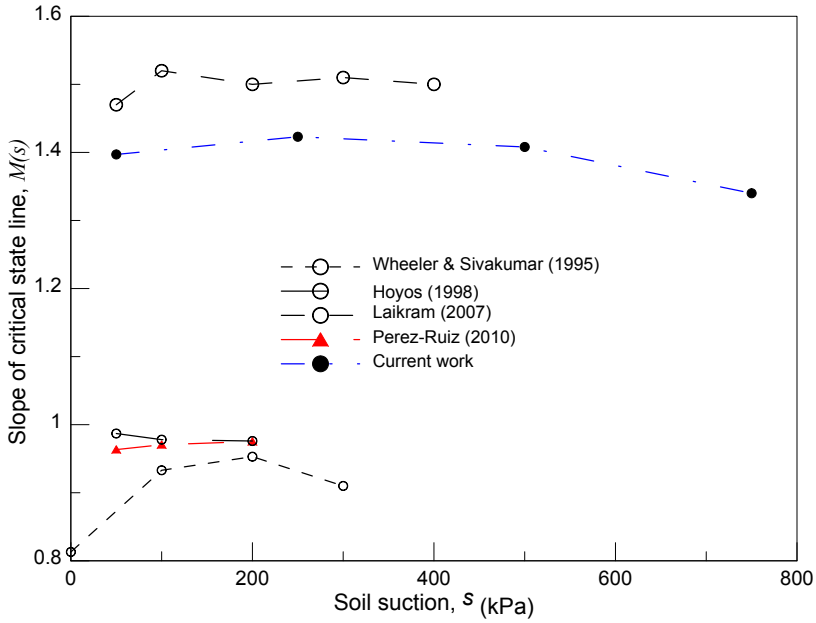

Figure 5.12 Comparison of variation in the slope of critical state line, $M(s)$ with soil suction with previous work

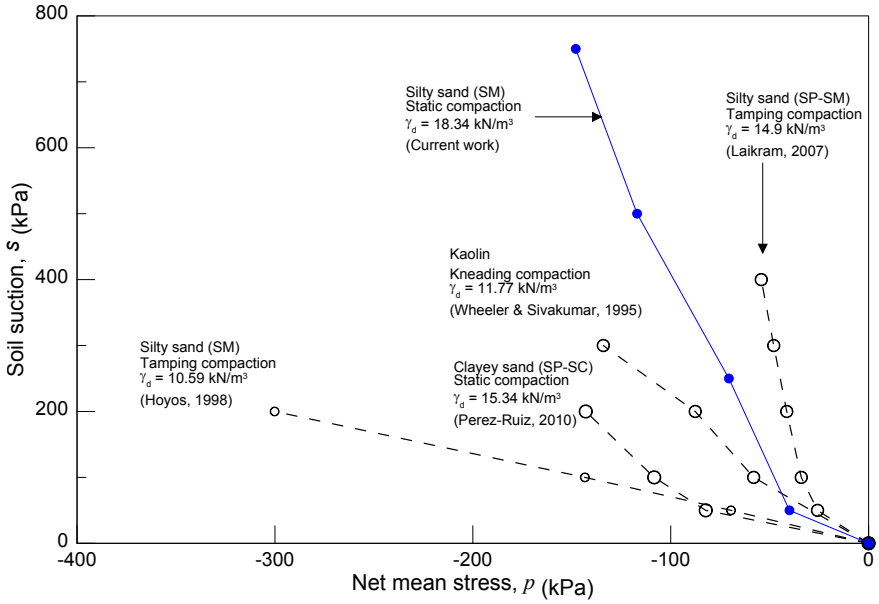

Figure 5.13 Comparison of variation in cohesion, p_s, due to the increase in suction, s present work with previous work

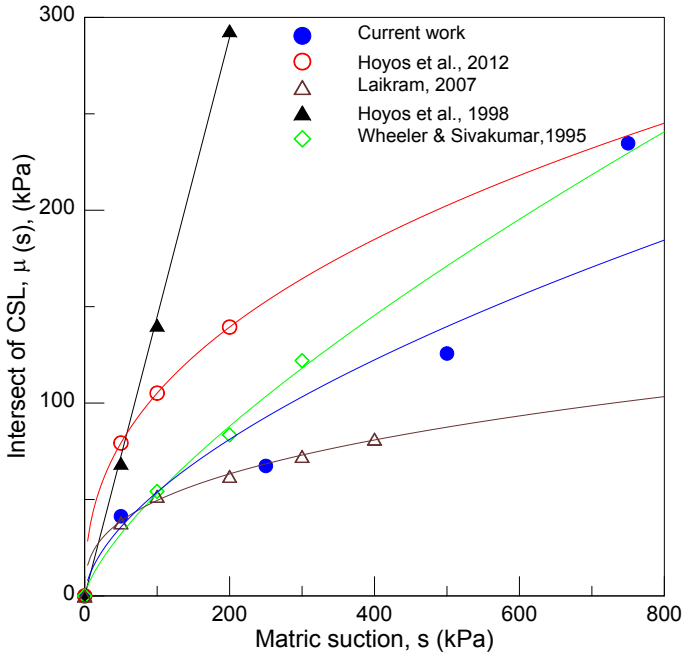

Figure 5.14 Variation of intersect of CSL $q_o(s)$ against matric suction, s

5.5 Numerical Predictions in p-q Stress Space

The response of soil under applied loads is dependent on preconsolidation or stress state history of the soil. Soil specimens whose initial net yield stress, $p_o(s) = p_o^A(s)$, exceeds the initial mean stress, p_{ini}, is said to be lightly overconsolidated, as illustrated in Figure 5.15. Likewise, soil specimens for which the initial mean stress, p_{ini}, applied during the equalization stage exceeds the initial net yield stress, $p_o(s)$, are said to be normally consolidated, as illustrated in Figure 5.16.

The size of the initial yield surface of lightly overconsolidated soils is controlled by the initial yield stress (p_{ini}), $p_o^A(s)$, and p_s. The initial yield stress that lies on the loading collapse (LC) yield curve is calculated by Equation (5.5).

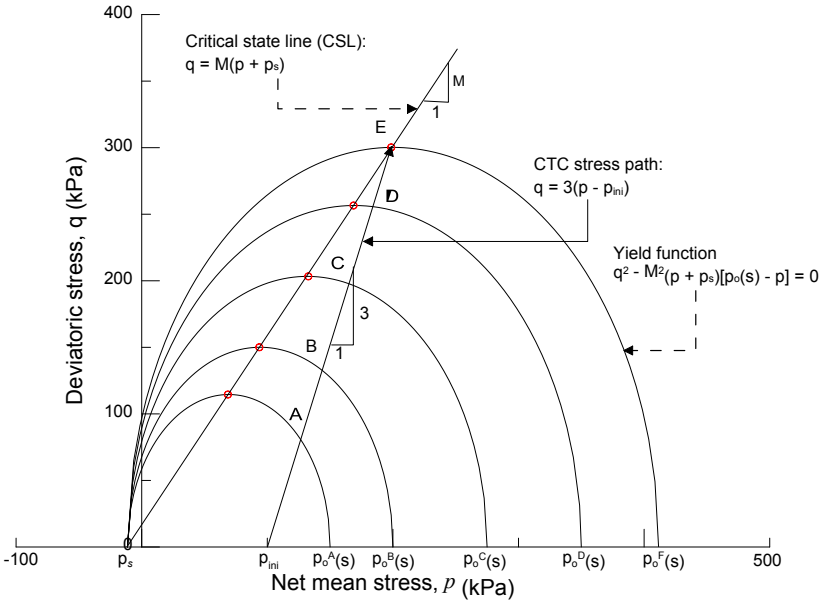

Figure 5.15 Shear-induced expansion of initial yield surface for suction-controlled drained CTC test performed on lightly overconsolidated soil

The initial LC yield curve and the apparent tensile strength increase in cohesion, p_s, were presented in Figure 5.7. For this condition, it is assumed that any loading increment inducing a stress state that lies inside the initial yield surface results in elastic

(recoverable) deformations only, and hence there is no change in the size of the current yield surface.

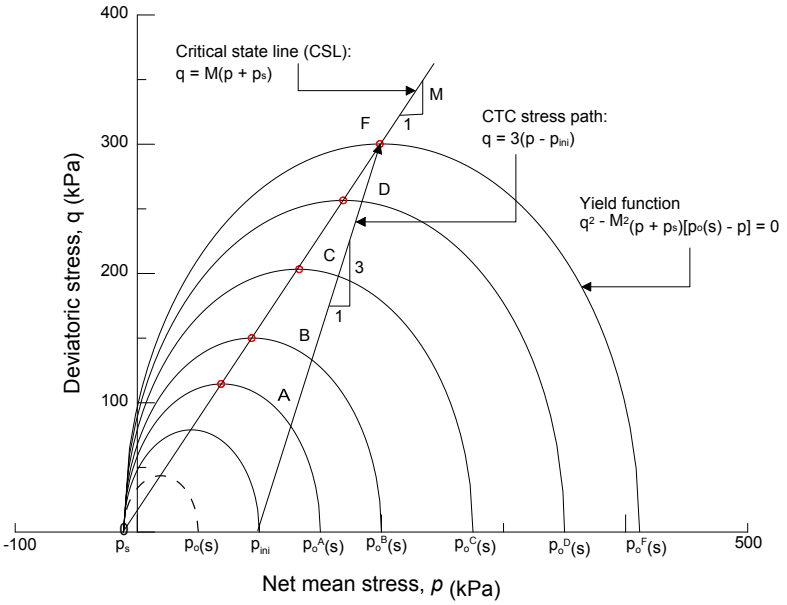

Figure 5.16 Shear-induced expansion of initial yield surface for suction-controlled drained CTC test performed on a normally consolidated soil

On the other hand, if the loading increment induces a stress state that goes beyond the initial yield surface, the latter will expand to the newly induced stress state, resulting in plastic deformations. As depicted in Figure 5.15, the yield surface will expand to the next yield stress, $p_o^B(s)$, which controls the size of the new yield surface in the p-q stress plane. The new LC yield curve can be recalculated using equation (5.5). Explicit integration is then used to compute the constitutive relations that simulate the incremental stress-strain behavior of unsaturated soils under varying stress, as explained in the next section.

Figures 5.17, 5.18, 5.19, and 5.20 show the predicted yield surface and the experimental stress state at failure resulting from the series of drained conventional triaxial compression (CTC) tests conducted on silty sand specimens at constant matric

suction, *s* = 50 kPa, 250 kPa, 500 kPa and 750 kPa, respectively. The experimentally calibrated values of BBM parameters used to predict silty sand response are summarized in Table 5.1.

Table 5.1 Best-Fit BBM parameters calibrated from experimental program

Parameter	Best-fit value	Units
$\lambda(0)$	0.02	-
κ	0.0015	-
β	2.0	MPa^{-1}
r	0.26	-
p^c	0.046	MPa
G	25	MPa
M	1.42	-
k	0.223	-
$P_o(0)$	0.070	MPa

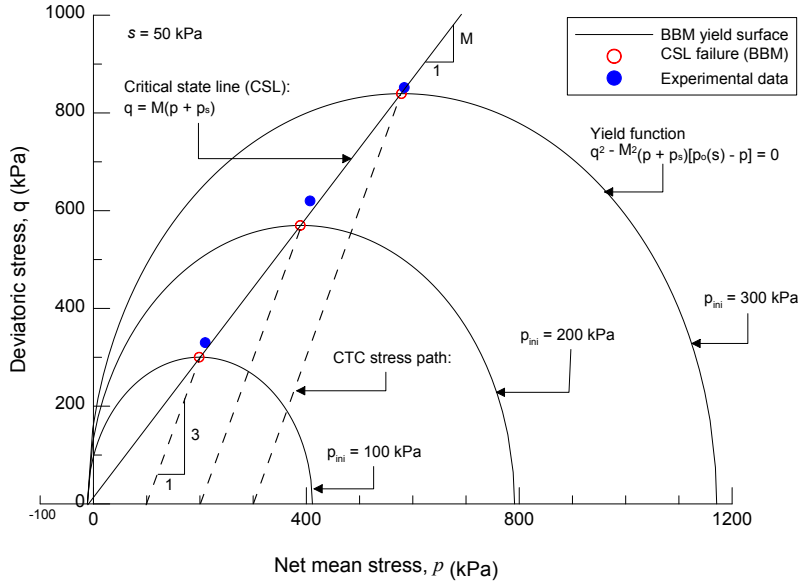

Figure 5.17 BBM prediction of yield surface for drained CTC tests conducted at constant matric suction, *s* = 50 kPa and initial net mean stresses, p_{ini} = 100, 200, and 300 kPa

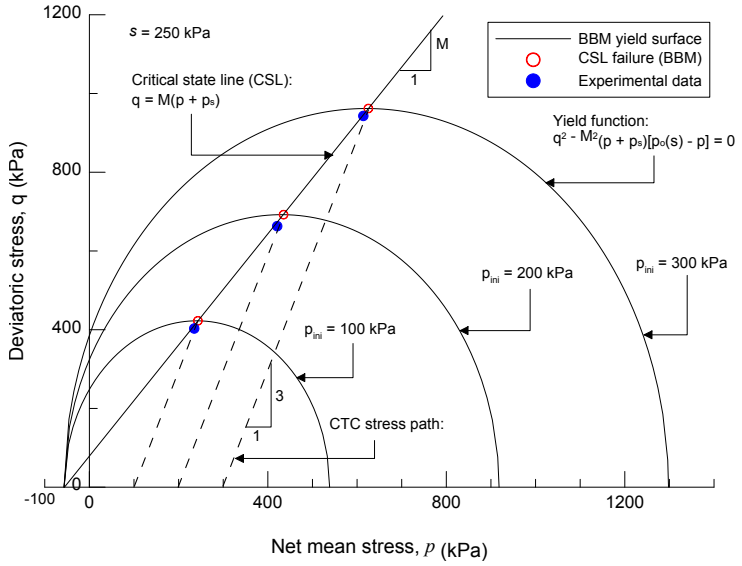

Figure 5.18 BBM prediction of yield surface for drained CTC tests conducted at constant matric suction, s = 250 kPa and initial net mean stresses, p_{ini} = 100, 200, and 300 kPa

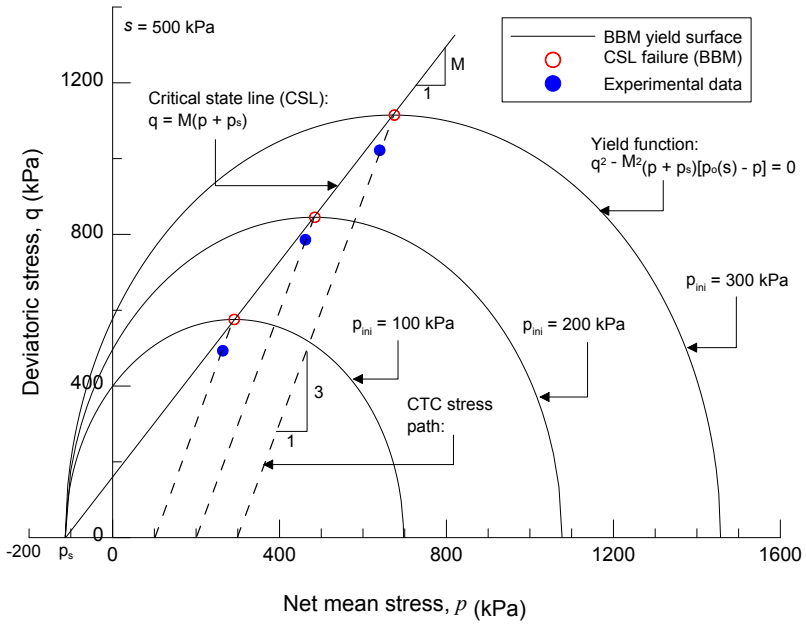

Figure 5.19 BBM prediction of yield surface for drained CTC tests conducted at constant matric suction, s = 500 kPa and initial net mean stresses, p_{ini} = 100, 200, and 300 kPa

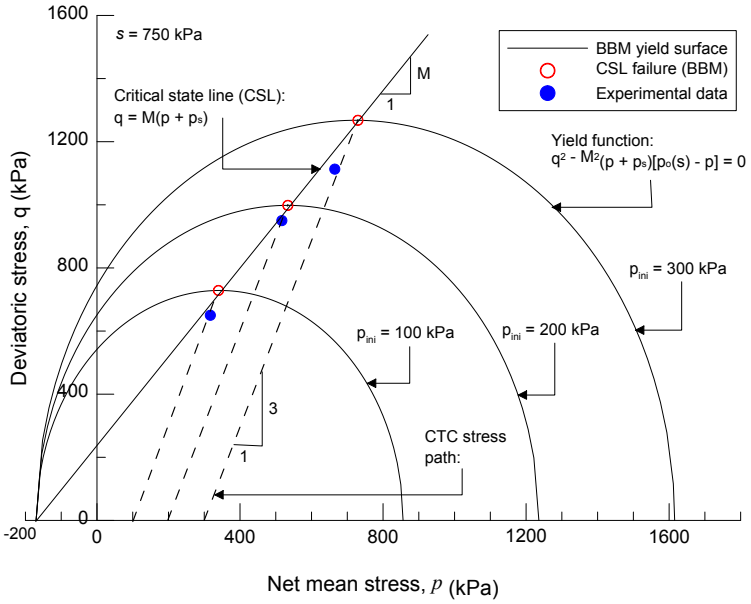

Figure 5.20 BBM prediction of yield surface for drained CTC tests conducted at constant matric suction, s = 750 kPa and initial net mean stresses, p_{ini} = 100, 200, and 300 kPa

5.6 Implementation of Barcelona Basic Model

The original BBM framework assumes that any change in net mean stress, p, within the elastic region will induce purely elastic (recoverable) changes in volume, implying a linear relationship between specific volume, v, and logarithm of mean stress, ln (p), represented by the elastic unloading-reloading line (url) of the soil (Alonso et al., 1990). The elastic volumetric strain increment is calculated as follows:

$$d\varepsilon_{vp}^{e} = -\frac{dv}{v} = \frac{\kappa}{v}\frac{dp}{p} \tag{5.8}$$

Also, the elastic shear strain increments induced by changes in deviator stress, q, can be computed through the shear modulus G, as follows:

$$d\varepsilon_{q}^{e} = \frac{2}{3}(d\varepsilon_{1}^{e} - d\varepsilon_{3}^{e}) = \frac{1}{3G}dq \tag{5.9}$$

The elliptical yield surface is assumed to expand at constant shape, with its size being controlled by the yield stress, $p_o(s)$. The yield surface expansion and soil hardening

are linked with the normal compression of the soil. The relationship between specific volume, $v = 1+e$, and logarithm of net mean stress, ln(p), during isotropic normal compression along the iso-ncl is described by:

$$v = N(s) - \lambda(s) ln \frac{p}{p^c} \tag{5.10}$$

The plastic component of volumetric strain is then calculated as:

$$d\varepsilon_{vp}^{p} = \frac{\lambda(s) - \kappa}{v} \frac{dp_o(s)}{p_o(s)} \tag{5.11}$$

The BBM is a general framework applicable to all stress paths that might be traced in the p-q stress plane, particularly the triaxial compression (TC) and conventional triaxial compression (CTC) tests.

5.6.1 Conventional Triaxial Compression Test

The type of test performed in this research followed the conventional triaxial compression (CTC) stress path. The soil specimen was subjected to constant matric suction and to constant confining net mean pressure, p_{ini}. The specimen failed by monotonic increase of the net axial pressure, σ_1, while keeping the isotropic confining pressure, σ_3 - u_a constant. Therefore, the stress path followed by the stress state in p-q space had a slope of 1H:3V. Hence, the deviatoric stress, $q = (\sigma_1 - \sigma_3)$ is calculated as

$$q = 3(p - p_{ini}) \tag{5.12}$$

Thus, the stress increment $dq = 3dp$ was applied until the critical state line (CSL) was intercepted by the suction-controlled stress path. Upon reaching this point, unlimited plastic shear strain develops, with no additional plastic volumetric strain, and thus the loading could not continue further, causing the stress path to stop at critical state.

It was also evidently clear that the elliptical size of the yield surface was controlled largely by an increase in suction-induced cohesion, p_s and did not depend upon the yield stress, $p_o(s)$. Thus, the LC yield curve, which according to Alonso et al.,

(1990) “plays an important role in the development of the model,” was used only to calculate the yield stress on the initial yield surface for lightly overconsolidated soil, but indeed had nothing to do with the calculation of the expanded yield surface and the stress state at failure (Perez-Ruiz, 2009).

5.6.2 Numerical Predictions by Barcelona Basic Model

The current work concentrated on silty sand’s response along isotropic ($\sigma_1 = \sigma_2 = \sigma_3$) and axisymmetric ($\sigma_2 = \sigma_3$) stress paths. The description of the comprehensive experimental test program undertaken was presented in Chapter 3. Explicit integration of key constitutive relationships has been used in this work to simulate soil response through BBM predictions of a drained (constant-*s*) conventional triaxial compression (CTC) test, as illustrated in Figure 5.21.

The soil was initially in lightly over consolidated conditions, i.e., $p_{ini} \leq p_o(s)$, where matric suction, *s*, was maintained constant throughout the entire test. Once the values of $\lambda(0)$, κ, β, r, p^c, G, M, k, $p_o(0)$, and $s = u_a - u_w$ were obtained, the explicit step-by-step integration procedure of the constitutive relations, as explained by Hoyos (1998) and Macari et al. (2003), can be summarized as follows (Figure 5.21).

Step 1: Compute $\lambda(s)$ using Equation (5.4),

Step 2. An initial yield surface at point “B” describes the boundary of the region where any stress combination may generate purely elastic or recoverable strains. Following the drained CTC stress path from an initial point A within this surface, at each point along it, i.e., B, C, D, and E, a new yield surface can be fully identified, and the specific volume, $v = 1 + e$, corresponding to the unloading-reloading line (url) in the p-v compression plane, can be calculated. Each new yield surface expands up to a corresponding net yield stress, $p_o^B(s)$, $p_o^C(s)$,…….. $p_o^E(s)$, which can be associated with the respective elastic unloading-reloading line, url_B, url_C,…… url_E, ending on its respective

net mean stress, on the isotropic normal compression line (ncl). Compute $p_o^B(s)$ using Equation (5.13) as follows:

$$p_o^B(s) = p^c \left[\frac{p_o(0)}{p^c}\right]^{\frac{\lambda(0)-\kappa}{\lambda(s)-\kappa}} \tag{5.13}$$

Step 3. For lightly overconsolidated conditions, as illustrated in Figure 5.15, the intersection of the CTC stress path and the initial yield surface can be calculated by replacing Equation (5.12) in Equation (5.1) and solving the quadratic equation, $a(p_B)^2 + bp_B + c = 0$ by p_B.

The deviatoric stress at point B can be calculated by replacing in Equation (5.12) the value of the net mean stress, p_B. This point is used to start the loading increment while solving the model. Thus, coordinates of point B on the initial yield locus can be computed as follows:

$$q_B = \frac{-b+\sqrt{b^2-4ac}}{2a} \tag{5.14}$$

$$p_B = p_{ini} + \frac{1}{3} q_B \tag{5.15}$$

where,

$$a = 1 + \left(\frac{1}{9}\right) M^2,$$

$$b = \left(\frac{1}{3}\right) M^2 [2P_{ini} - p_o^B(s) + p_s], and$$

$$c = M^2 [p_{ini} + p_s][p_{ini} - p_o^B(s)] \tag{5.16}$$

Note: In contrast to lightly overconsolidated conditions, in normally consolidated specimens, the initial yield surface of the specimen is exceeded during the equalization stage, and hence the yield surface, at the onset of the shearing stage, is controlled by the initial yield stress, $p_o(s) = p_{ini}$, and the p_s. The intersection of the CTC stress path and the

initial yield surface coincides with the tip of the yield surface, at $q = 0$ and $p = p_{ini}$. This is exactly the point where the CTC stress path (NC-condition) begins.

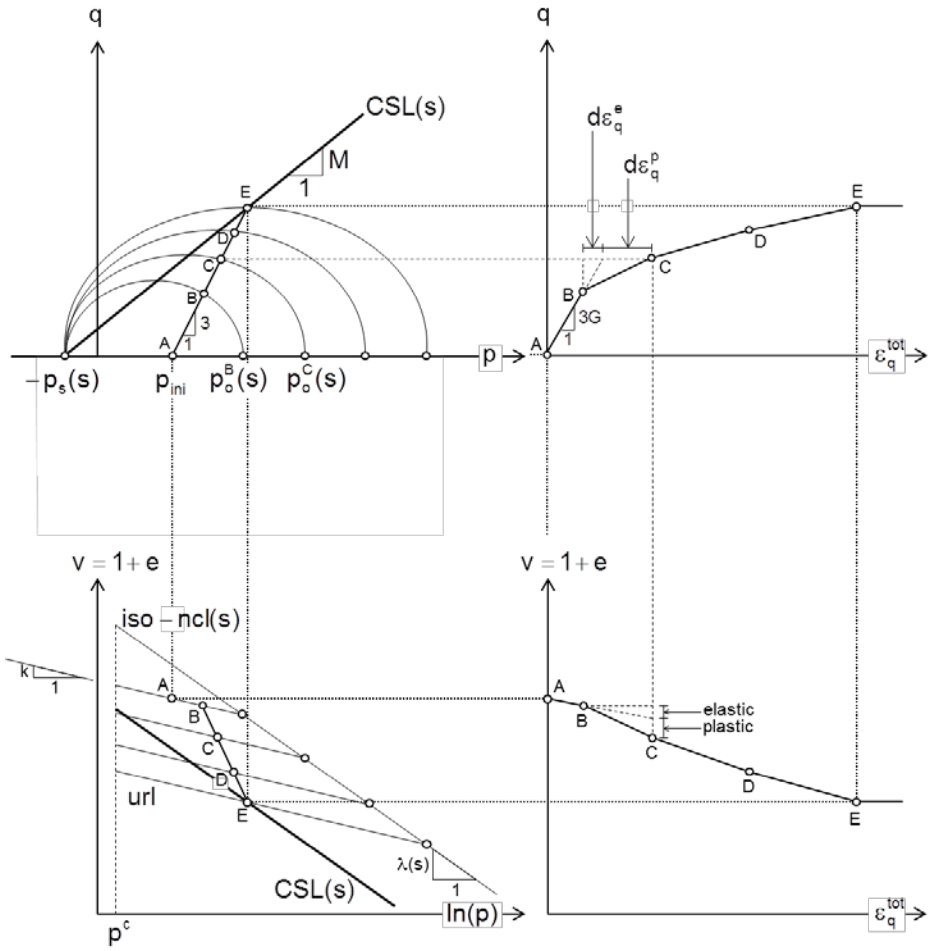

Figure 5.21 Schematic of explicit integration of BBM predictions for a constant-suction CTC test (from Hoyos, 1998; and Macari et al., 2003)

Step 4: As shown in Figure 5.21, for a drained CTC test performed on a lightly overconsolidated soil sample at initial mean pressure, p_{ini}, and constant matric suction, s, the initial specific volume, v_{ini}, lie on the url defined by the yield surface associated with the initial net yield stress, $p_o^B(s)$. The drained compression experienced by the specimen from point A (p_{ini}) to point B represents changes in stress, lying inside the initial yield

surface, and consequently generates purely elastic deformations. The projection of point A (p_{ini}) and point B lie on the unloading-reloading line url_B associated with the initial net yield stress $p_o^B(s)$. The specific volume v_B defined for the projection of point B on the url_B corresponding to p_B is calculated as follows:

$$v_B = v_{ini} - \kappa \ln\left[\frac{p_B}{p_{ini}}\right] \tag{5.17}$$

Step 5. The elastic shear strain increment (deformation) between points A and B, also known as elastic shear strain increments, can be computed for path AB as follows :

$$d\varepsilon_q^e = \frac{1}{3G} q_B \tag{5.18}$$

Step 6. Compute coordinates of the ultimate point E on the CSL as follows:

$$q_E = \left[\frac{3M}{3-M}\right](p_{ini} + p_s) \tag{5.19}$$

$$p_E = p_{ini} + \frac{1}{3} q_E \tag{5.20}$$

The yield surface at failure can be determined by replacing $p_o(s)$ and p_s in Equation (5.1) and then solving either by deviatoric stress q or net mean stress p.

Step 7. Divided interval from q_B to q_E into equal deviatoric stress increments dq along BE.

Step 8. The projection of point $p_o^B(s)$ lies on the intersection of the unloading-reloading line url_B, and the isotropic normal compression line (iso-ncl), i.e., the specific volume v_o^B on the iso-nc line, corresponding to $p_o^B(s)$, can be computed as follows:

$$v_o^B = v_{ini} - \kappa \ln\left[\frac{p_o^B(s)}{p_{ini}}\right] \tag{5.21}$$

Step 9. Consider the first increment BC resulting from step 7. Compute coordinates of point C:

$$q_C = q_B + dq \tag{5.22}$$

$$p_C = p_B + \frac{1}{3}dq \tag{5.23}$$

Step 10. Compute p_o^c(s) for the expanded yield locus through the intermediate point C:

$$p_o^C(s) = p_C + \frac{(q_C)^2}{M^2(p_C + p_s)} \tag{5.24}$$

Step 11. Once the specific volume on the isotropic-ncl, v_o^B, corresponding to the initial net yield stress p_o^B(s) was calculated, it was possible to calculate the specific volume on the iso-ncl associated to any net yield stress, p_o(s) i.e. $p_o^C(s)$, $p_o^D(s)$, and $p_o^E(s)$. The specific volume v_o^C on the iso-nc line corresponding to p_o^c(s) is computed as below

$$v_o^C = v_o^B - \lambda(s)\ln\left[\frac{p_o^C(s)}{p_o^B(s)}\right] \tag{5.25}$$

Step 12. The specific volume, v_o^C, also corresponds to the ending of the elastic unloading-reloading line (i.e. url_C), as illustrated in Figure 5.21. Thus the specific volume v_C at point C on the ir-line corresponding to p_C is given as follows:

$$v_C = v_o^C + \kappa\ln\left[\frac{p_o^C(s)}{p_C}\right] \tag{5.26}$$

Step 13. Following the drained CTC stress path, the changes in volume between two consecutive yield surfaces (e.g., B and C in Figure 5.21), will have recoverable elastic deformations resulting from the change in net mean stress, p, and irrecoverable plastic deformations resulting from the expansion of the yield surface. Plastic deformations are represented by the change in volume or vertical distance between the correspondent unloading-reloading (e.g. url_B and url_C) in the compression plane.

The elastic volumetric and shear strain increments, $d\varepsilon_{vp}^{\ e}$ and $d\varepsilon_q^{\ e}$, between points B and C for path BC can be computed as follows

$$d\varepsilon_{vp}^e = \frac{\kappa}{v}\frac{dp}{p} = \frac{\kappa}{v_B}\left[\frac{p_C - p_B}{p_B}\right] \tag{5.27}$$

$$d\varepsilon_q^e = \frac{1}{3G}[q_C - q_B] = \frac{1}{3G}dq \tag{5.28}$$

Step 14. The total volumetric strain increment between points B and C i.e. $d\varepsilon_{vp}^{tot}$, for path BC is calculated as follows:

$$d\varepsilon_{vp}^{tot} = \frac{-dv_{BC}}{v_B} = \frac{v_B - v_C}{v_B} \tag{5.29}$$

Step 15. The plastic volumetric strain increment $d\varepsilon_{vp}^{p}$, for path BC are calculated as below:

$$d\varepsilon_{vp}^{p} = d\varepsilon_{vp}^{tot} - d\varepsilon_{vp}^{e} \tag{5.30}$$

Step 16. Finally, considering the assumption of a non-associative flow rule for the direction of plastic shear strain increments, $d\varepsilon_q^p$, the plastic shear strain increments for path BC can be calculated using the following equation:

$$d\varepsilon_q^p = \frac{2\alpha q_C}{M^2[2p_C + p_s - p_o^C(s)]}d\varepsilon_{vp}^p \tag{5.31}$$

The constant α is defined as follows:

$$\alpha = \frac{M(M-9)(M-3)}{9(6-M)}\left[\frac{1}{1-\frac{\kappa}{\lambda(0)}}\right] \tag{5.32}$$

Step 17. Compute the total shear strain increment $d\varepsilon_q^{tot} = d\varepsilon_q^{e} + d\varepsilon_q^{p}$, for path BC.

Step 18. Repeat steps 8-17 for point D, and for all subsequent or intermediate points along path DE.

Step 19. Finally, plot *q-p, v-p, q-* ε_q^{tot}, and *v-* $d\varepsilon_q^{tot}$, as depicted in Figure 5.21.

The same procedure summarized above can be used to predict soil response for a drained CTC test performed on a normally consolidated soil specimen at initial mean pressure, p_{ini}, and constant matric suction, *s*. The same procedure can also be extended to other shear stress paths involving constant net mean stress p, such as triaxial compression (TC) tests.

5.7 Comparison of BBM Predicted Soil Response and Experimental Results

Figures 5.22 through 5.33 show the comparison between experimental and predicted deviator stress vs. shear strain response resulting from fully drained (constant suction) CTC tests conducted on triaxial specimens of compacted silty sand at different values of matric suction, *s* = 50 kPa, *s* = 250 kPa, *s* = 500 kPa, and *s* = 750 kPa; with initial values of net mean stress, p_{ini} = 100 kPa, p_{ini} = 200 kPa, and p_{ini} = 300 kPa, respectively.

Numerical predictions were implemented by using the explicit integration technique summarized in the previous section. As expected, no close or thorough agreement is observed between experimental and predicted soil response, given the largely "brittle" and "dilatant" nature of the test soil before it reaches critical state.

In effect, although predictions of deviator stress at critical state (end values) are reasonably close to those experimentally observed, as shown in Figure 5.8, BBM predictions considerably deviate from the stress-strain response of silty sand at lowest suction (s = 50 kPa) and lowest confining pressure ($\sigma_3 - u_a$ = 100 kPa), at which the soil exhibit largest post-peak softening, accompanied by significant dilation. Similarly, at highest matric suction (s = 750 kPa), irrespective of applied confining pressure, BBM predictions are not quite suitable for capturing the large magnitude of post-peak softening observed for statically compacted silty sand.

From a qualitative standpoint, however, relatively better BBM predictions are observed for confining pressure, $\sigma_3 - u_a$ = 200 and 300 kPa, at s = 250 and 500 kPa. In general, the post-peak softening was not adequately simulated with BBM predictions; however, reasonably good predictions are observed mostly during initial shearing stage (up to about 1-2% shear strain), and at large values of shear strain, i.e., at critical state (Figure 5.8).

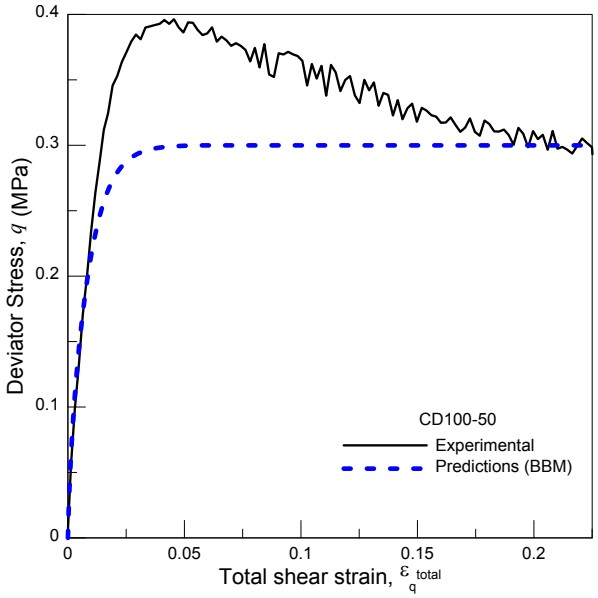

Figure 5.22 Predicted and experimental test results for CD100-50 test

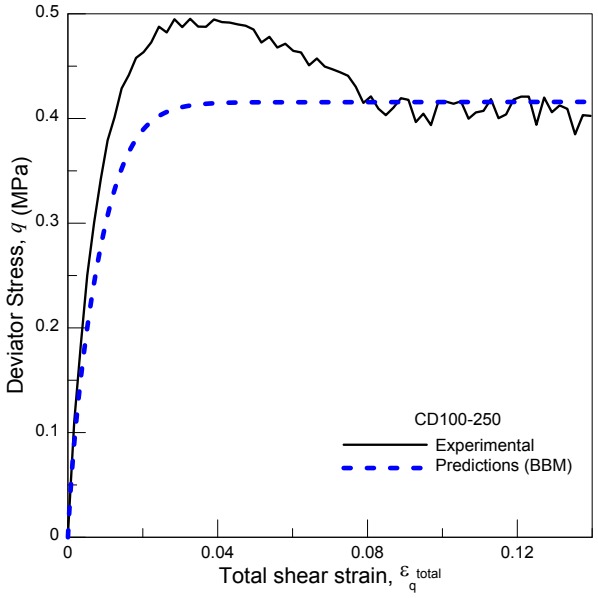

Figure 5.23 Predicted and experimental test results for CD100-250 test

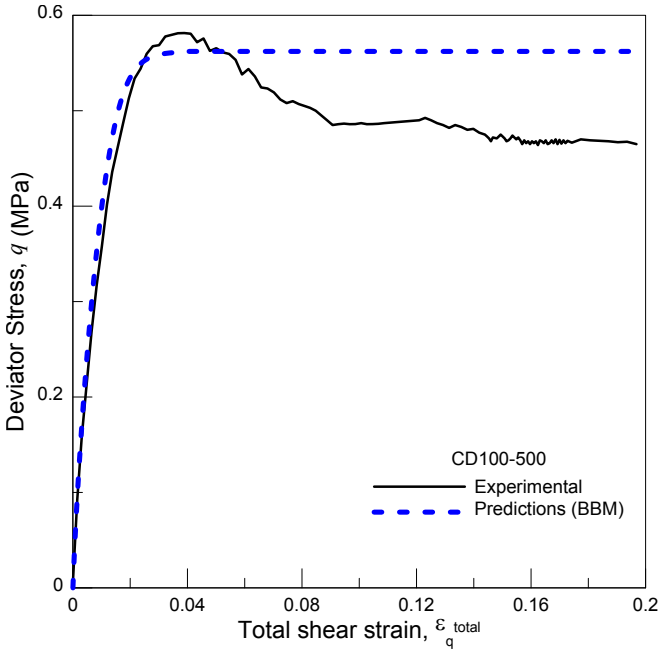

Figure 5.24 Predicted and experimental test results for CD100-500 test

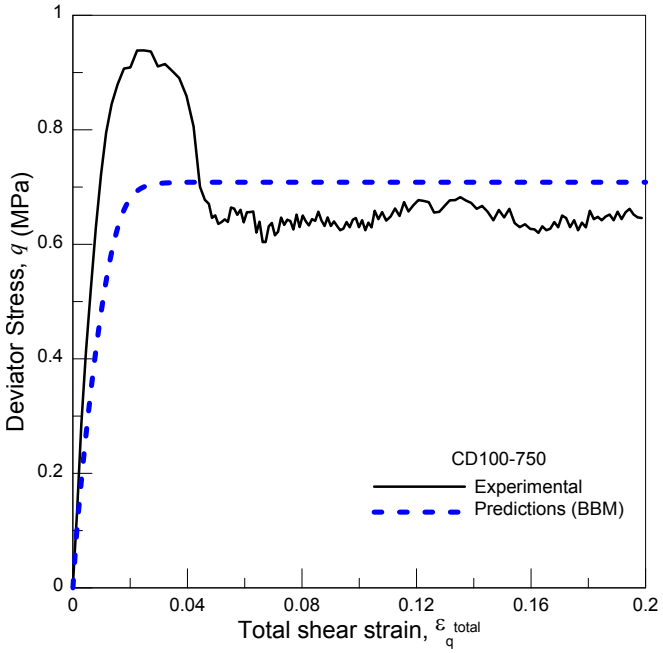

Figure 5.25 Predicted and experimental test results for CD100-750 test

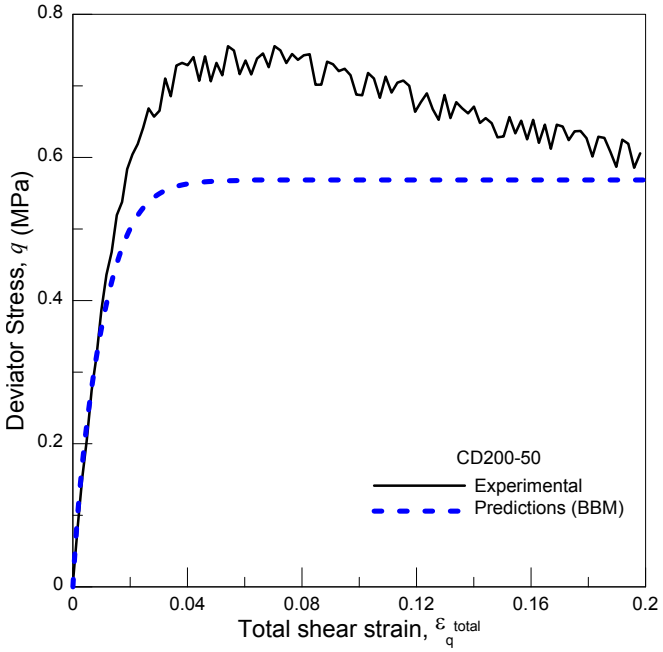

Figure 5.26 Predicted and experimental test results for CD200-50 test

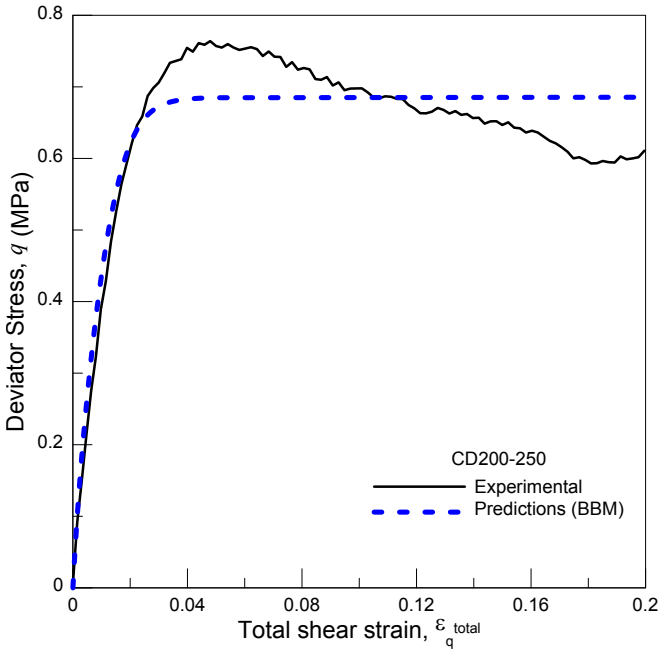

Figure 5.27 Predicted and experimental test results for CD200-250 test

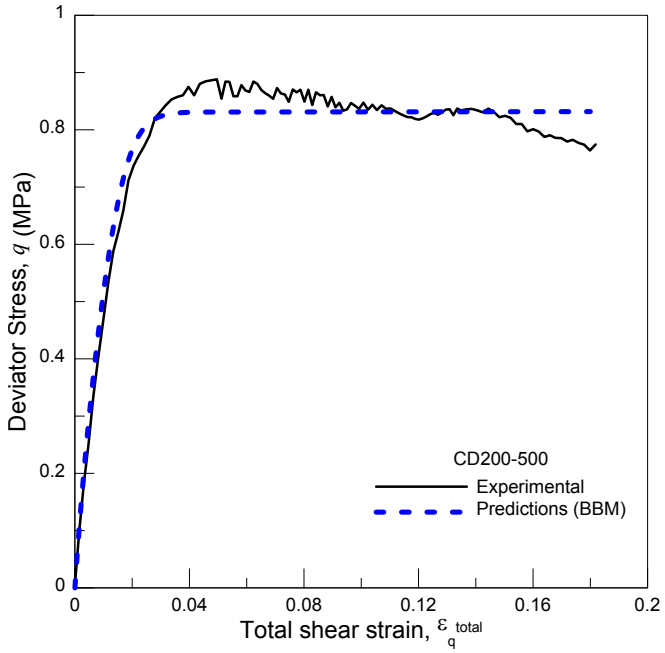

Figure 5.28 Predicted and experimental test results for CD200-500 test

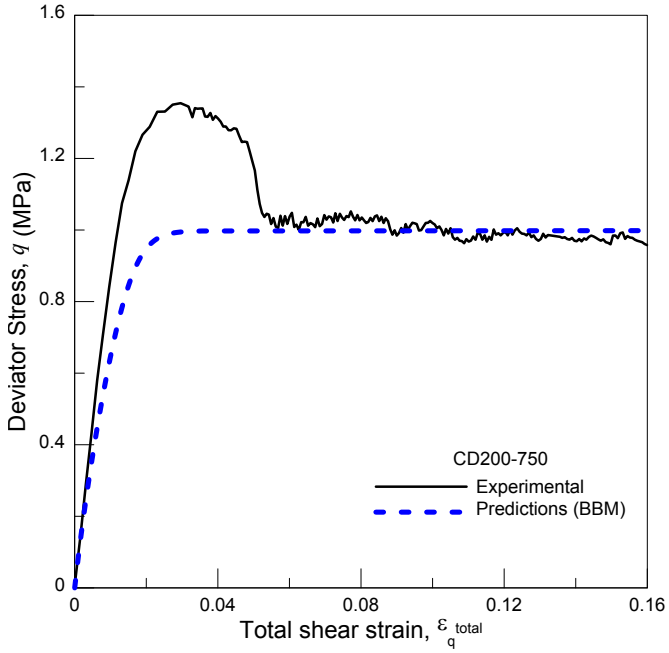

Figure 5.29 Predicted and experimental test results for CD200-750 test

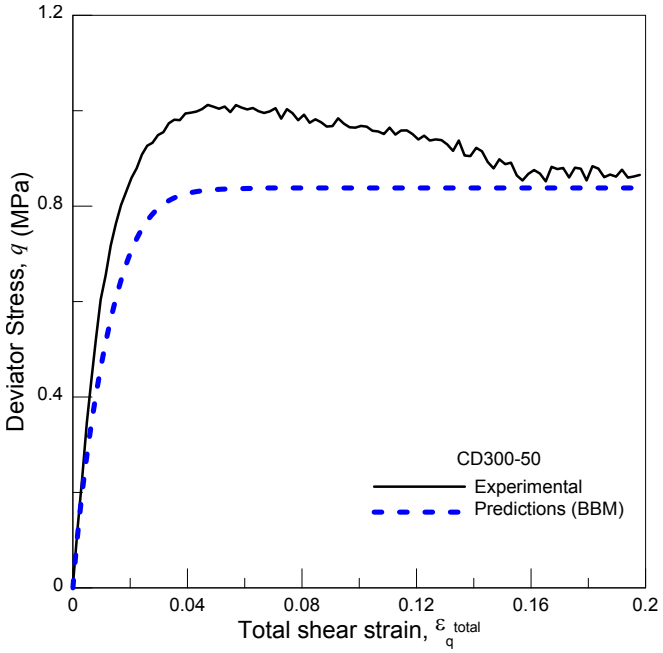

Figure 5.30 Predicted and experimental test results for CD300-50 test

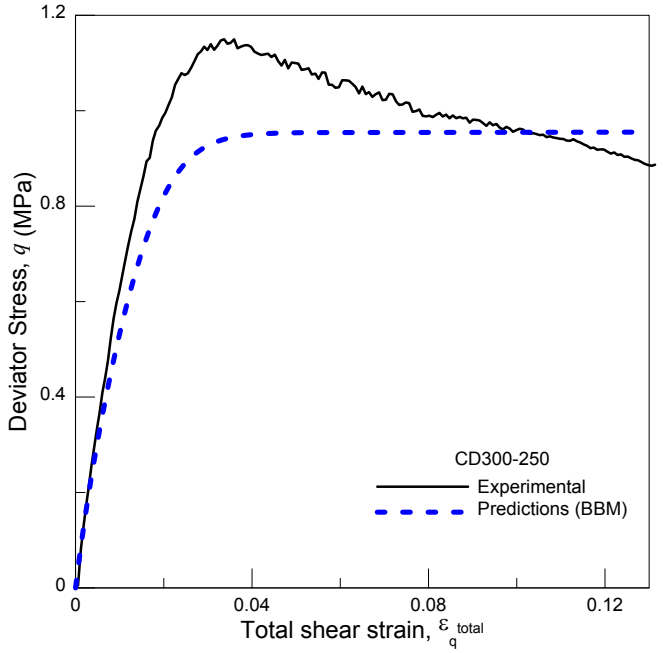

Figure 5.31 Predicted and experimental test results for CD300-250 test

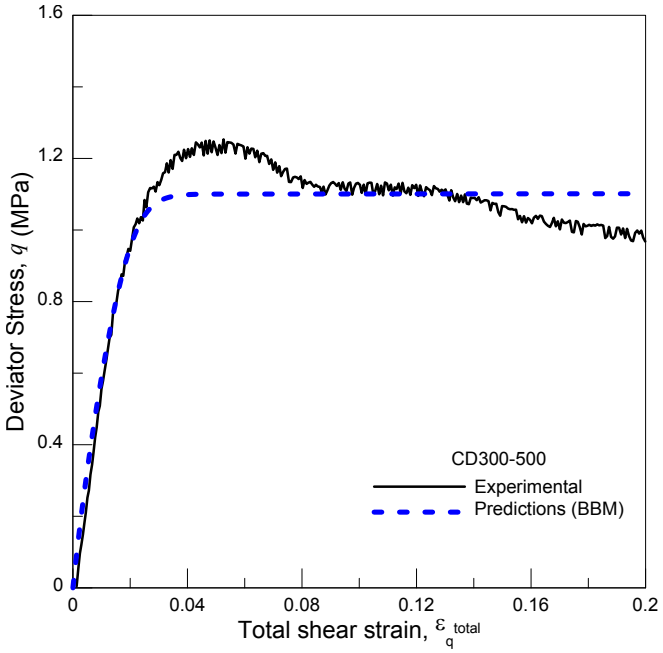

Figure 5.32 Predicted and experimental test results for CD300-500 test

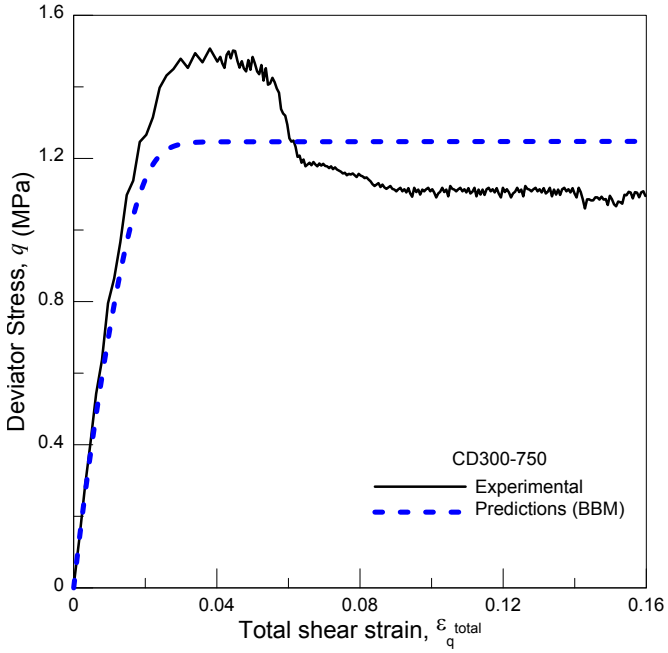

Figure 5.33 Predicted and experimental test results for CD300-750 test

5.8 Simulating Strain-Hardening: Basic Concepts

Hardening type of behavior normally occurs, while inducing shearing on lightly overconsolidated as well as normally consolidated soils. Let us consider a normally consolidated or lightly overconsolidated soil specimen that is isotropically consolidated, under controlled suction condition, to a net mean stress, p_c' (preconsolidation stress) and then unloaded slightly to p_o' (current pressure) such that OCR = p_c'/p_o' < 2, as shown in Figure 5.34. Post consolidation, the specimen is sheared following a drained CTC stress path, under suction-controlled condition, until it reaches critical state failure, as depicted in Figure 5.34. The strain-hardening response normally results in a unique and stable stress-strain response (Pietruszczak et al., 2010).

In this case, the preconsolidation stress, p_c' will control the initial yield surface. During shearing, if the stress path reaches the initial yield surface to the right of the point, at which the CSL intersects the yield surface, hardening behavior, accompanied by compression, will occur. This side of the yield surface is the wet side (sub-critical), as indicated in Figure 5.34. The soil specimen will sustain only elastic strains within the initial yield surface. However, when the stress state of the soil reaches the initial yield surface, the specimen will sustain elastic, as well as plastic, strains.

Further shearing causes the yield surface to expand (hardening), accumulating further plastic strains, until the stress state of the specimen lies on the critical state line at point F, where critical state-type failure occurs. The soil will continue to distort, without changes in shear stress or volume. Note that when the material is strain-hardening, the yield surface at failure stress (critical state) becomes a failure surface, as illustrated in Figure 5.34.

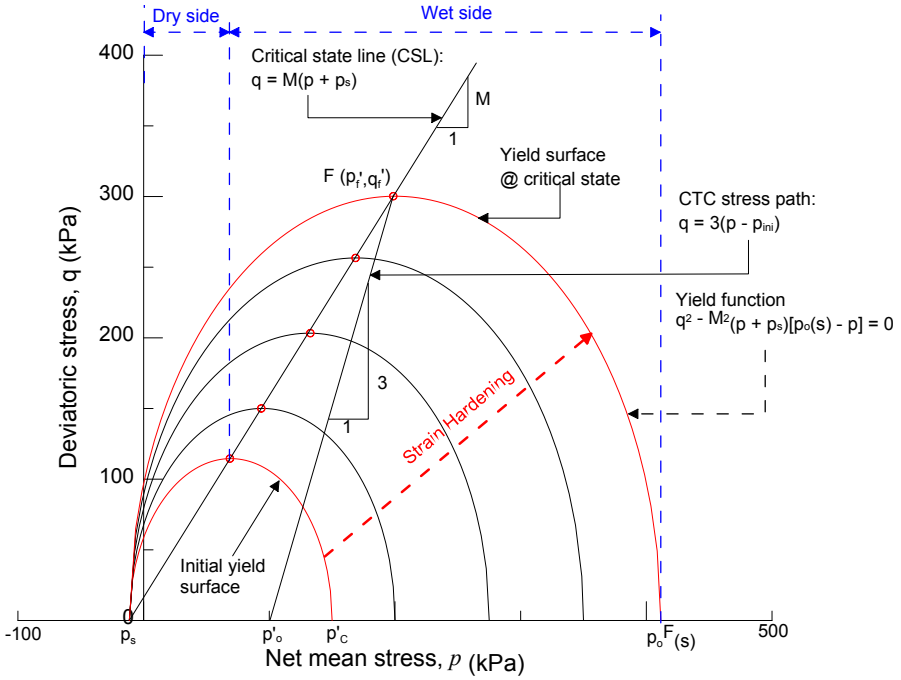

Figure 5.34 Strain-hardening behavior explained using possible BBM yield surface in unsaturated soil (modified from Helwany, 2007)

5.9 Simulating Suction-Controlled Post-Peak Strain Softening: A Future Research Need

A post-peak softening type of response is often observed while shearing a soil specimen that is heavily overconsolidated (OCR>2). Consider a heavily overconsolidated soil specimen that is isotropically consolidated under controlled suction condition to a net mean stress, p_c' (preconsolidation stress) and then unloaded to p_o' (current pressure) so that OCR = p_c'/p_o' >> 2, as shown in Figure 5.35.

Post consolidation, the specimen is sheared, following a drained CTC stress path (1H:3V), under suction- controlled condition. The stress path traverses the possible peak yield surface, to the left of the point F, at which the CSL intersects the yield surface at "peak" strength state, inducing volumetric dilatancy (expansion). This side of the yield surface is the dry side (super-critical), as depicted in Figure 5.35. It should be noted that the term "softening" implies an unstable response, i.e., stress decreases monotonically

as a function of strain, and is often associated with a deformation mode, which is inhomogeneous on a macroscale due to the formation of shear bands (Pietruszczak et al., 2010).

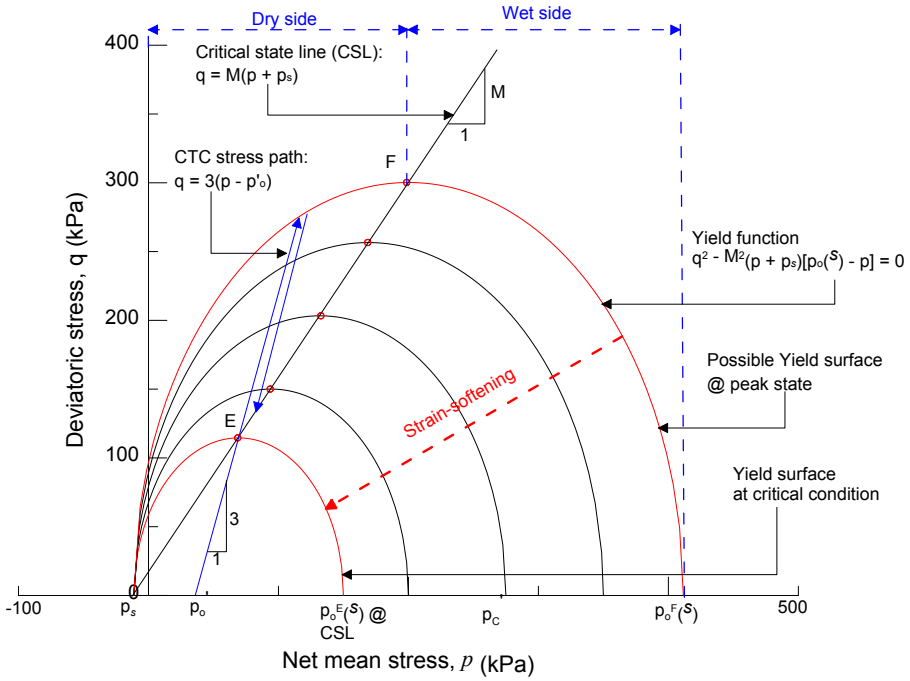

Figure 5.35 Possible evolution of yield surface during strain softening in unsaturated soil (modified from Helwany, 2007)

It should be noted that the stress path traverses the critical state line before reaching the possible peak yield surface, without causing failure. When the stress path reaches the possible peak yield surface (i.e., post-peak), the yield surface will contract (i.e., dilation will be preceded by softening), causing further plastic strains, until the stress state lies back on the critical state line at point E, where critical state failure occurs. It should be noted that when the material is exhibiting softening, the yield surface corresponding to “peak” strength is the outermost yield locus. The experimental program conducted in this research work indicates that the magnitude of post-peak softening of

statically compacted silty sand tends to increase with an increase in the matric suction imposed on the soil specimens.

Continued loading causes the yield surface to move outward (or increase in size) from the current point for hardening materials, while moving inward (or shrink in size) for softening materials. The relative position of current stress with respect to the CSL governs whether the material sustains plastic dilatancy or contractancy. The original BBM framework does not contemplate a stress state that fails to overcome the CSL during plastic loading since the peak stress is always assumed to be reached at critical state. Therefore, it is not suitable for reproducing the transition from initial contractancy to dilatancy (and hence the post-peak strain-softening), which is commonly observed in sands or otherwise dense materials (Figures 3.29, 3.30, 3.31, and 3.32 in Chapter 3).

5.10 Summary

Main features of the Barcelona Basic Model (BBM) formulation are summarized (Alonso et al. 1990). An assessement of the parametric performance of the loading-collapse (LC) locus for compacted silty sand in the $p{:}s$ plane is included. Essential constitutive parameters postulated by the BBM, including the slope of the apparent tensile strength (ATS) locus in p:s plane (k) and the slope of the critical state lines (M), were calibrated for compacted silty sand and then used for prediction of peak deviator stress at matric suction states varying from 50 to 750 kPa. Within the range of stresses applied, i.e., matric suction, s = 50 to 750 kPa, and initial net mean stress, p = 100 to 300 kPa, a three dimensional plain-surface plane, expressed by Equation 5.7, fitted all the experimental values of deviatoric stress at critical state, with a coefficient of determination, R^2 = 0.97.

BBM predictions of stress-strain response of compacted silty sand were made by using the experimentally calibrated parameters, and compared with experimental results.

As expected, given the evidently “brittle” and “dilatant” nature of the test soil, no good agreement was observed between the experimental and BBM predicted stress-strain responses. The post-peak softening of the test soil was not adequately captured. BBM simulations, however, hold reasonably good mostly during the early shearing stage, up to about 1-2% shear strain, and at higher values of shear strain (i.e. at critical state).

Chapter 6

Conclusions and Recommendations

6.1 Introduction

In this research, a series of tests, consisting of 3 consolidated drained triaxial tests on fully saturated soil, were conducted, along with two series of conventional triaxial compression tests (12 tests using axis-translation technique in matric suction range between 50 to 750 kPa and 6 tests using the relative humidity technique in a high total suction range between 20 MPa and 300 MPa), on the unsaturated compacted silty sand to cover a wider range of soil suction states. Eight more experimental tests were done, including 3 tests to examine the effect of different shearing rates, at matric suction of 500 kPa and $\sigma_3 - u_a$ = 300 kPa, and 5 tests at different shearing rates at high total suction of 300 MPa and $\sigma_3 - u_a$ = 100 kPa. Thus, minimum of 29 triaxial tests, including saturated as well as unsaturated soil tests, were performed as part of this research.

Experimental results from these comprehensive series of tests were analyzed to provide (1) evidence of suction-induced increases in yield stress/preconsolidation pressure and tensile strength of unsaturated soil; 2) dependence of apparent cohesion, ϕ^b and shear strength at failure on suction; 3) increase in stiffness, with an increase in suction and 4) uniqueness of the critical state line for saturated, as well as unsaturated, soil in p-q space; 5) prediction of shear strength using properties of the soil water characteristic curve and comparing it with experimental results; 6) effect of suction, as well as confining pressure on dilation angles or rate of dilation, and 7) interpretation of stress-strain curves to explain particle breakage/crushing. Major conclusions from the first series of tests are discussed below.

6.2 Conclusions

1) The stress-strain response for saturated soil showed a strain-hardening type of soil-response during drained shearing. The Mohr's stress circles, drawn at three confining pressures, indicated the strength parameters as c' = 0 kPa and ϕ' = 35 deg. The stresses drawn at critical state failure in p'-q space yielded the critical state line slope M = 1.42.
2) Three CD triaxial tests were conducted on unsaturated silty sand specimens prepared by the static compaction method at a speed of 0.014%/min, 0.0086%/min and 0.0029%/min to assess the suitable shearing rate. Comparison of stress strain plots showed significant influence of shearing rates on peak deviatoric stress, as compared to the critical state deviator stress. To sum up the test results, the shearing rate of 0.014%/min was found to be insufficient in producing completely drained conditions at matric suction of 500 kPa and net effective confining pressure of 300 kPa. The theoretical shear speed found by using a modified approach by Geiser et al., 2006, based on the extension of the classic Gibson and Henkel, 1954 method, seems to be at least 10 times slower than the one found by trial and error experimental speed. Thus, the shear speed, 0.0086%/min was chosen for all the CD tests, using the axis-translation technique on unsaturated soils in this research.
3) The stress-strain curves for suction-controlled tests indicated that the peak deviator stress increased considerably with an increase in matric suction at the same confining pressure. The deviator stress at critical state also increased with increase in matric suction; however, the rate of increase was comparatively less than for peak deviator stress. All the specimens showed the post-peak softening

type of response. The amount of post-peak softening increased with an increase in matric suction at the same confining pressure.

4) The stress-strain curves for suction-controlled tests indicate that the peak deviator stress increased considerably with an increase in confining pressure at the same matric suction. The deviator stress at critical state also increased with an increase in confining pressure; however, the rate of increase was comparatively less than for peak deviator stress. All the specimens showed the suction-induced post-peak softening type of response. The amount of post-peak softening increased with an increase in confining pressure at the same matric suction.
5) Close observation of stress-strain plots, showing the effect of matric suction at different confining pressure and vice-versa on strength behavior, clearly indicated that the effect of confining pressure was much greater than that of an equivalent increase in matric suction.
6) One can also observe that increase in matric suction from s = 50 kPa to s = 500 kPa caused an increase in the rate of shear strength when $\sigma_3 - u_a$ was increased from 100 to $\sigma_3 - u_a$ = 200, but at s = 750 kPa and for $\sigma_3 - u_a$ = 200 to $\sigma_3 - u_a$ = 300, the rate of increase in strength was suppressed because at a high level of confinement there will be bond breakage during continued shearing resulting in the lower rate of increase in suction-induced strength.
7) The volumetric response against the axial strain clearly indicated the change in shear-induced volumetric response from compressive to dilational type when the soil saturation state changed from saturated to unsaturated state, with the introduction of matric suction. All the suction-induced specimens showed initial compression followed by a stress-induced dilatancy-type response. Initial

shearing caused volumetric reduction, but as the particles moved into a better configuration, the enhanced interlocking between particles caused the soil to dilate, as the shearing progressed. The amount of dilatancy was suppressed with an increase in the confining pressure from 100 to 300 kPa as expected. Such type of stress-strain and volumetric response also confirmed the dense or overconsolidated stress history the specimens underwent during their preparation.

8) In particular, it was observed that the effect of confining stress was more dominant when the specimen was sheared under high confining stress of 300 kPa, resulting in suppressed dilation; while the effect of matric suction was more dominant at a low confining stress of 100 kPa, resulting in maximum value of dilation. Increase in suction also contributed to better interlocking between particles; as a result dilative response was augmented at low stress levels.

9) It was also observed that an increase in matric suction caused an increase in the rate of shear strength for s = 50 kPa to s = 500 kPa at $\sigma_3 - u_a$ = 100 to $\sigma_3 - u_a$ = 200, but at s = 750 kPa the rate of increase in strength from $\sigma_3 - u_a$ = 200 to $\sigma_3 - u_a$ = 300 was suppressed because at a high level of confinement there will be bond breakage during continued shearing resulting in the lower rate of increase in suction-induced strength. Thus, bond breakage may not be dominated at low stress levels, but may have a dominating influence at high stress levels thereby limiting to the increase in shear strength response at high suction and high stress levels.

10) Mohr-Coulomb failure envelopes were plotted, based on three tests each at different net confining pressures (i.e., 100, 200 and 300 kPa), but at the same matric suction (i.e., 50, 250, 500 and 750 kPa) at critical state failure conditions.

A tangent drawn to these three Mohr's circles intersected the y-axis, yielding the apparent cohesion intercept, c'' that increased with an increase in the matric suction level. A tangent to three Mohr's circles, at the same matric suction but varying confining pressures, made an angle of approximately 35 deg., with a horizontal line indicating that the saturated effective friction angle does not change with suction. This also confirms the assumption made in the classical Barcelona basic model that the critical state line slope is independent of matric suction applied.

11) The saturated, as well as unsaturated test results from all tests at critical state failure plotted in the p-q plane, indicated that the slope of the critical state line ($M_{critical}$ = 1.42) was minimally changed with the introduction of suction. Thus, it establishes a unique relationship between the deviator stresses and net mean stress for CD triaxial tests. However, clearly an upward shift in the critical state line was visible with the introduction of matric suction, as compared to its saturated counterpart.

12) The loading-collapse (LC) curve was assessed from suction-controlled isotropic consolidation tests performed prior to shearing. The matric suction had a noticeable influence on the final position of the critical state line. Also, the slope $M(s)$ of all critical state lines remained reasonably constant, in clear agreement with the BBM formulation. Key constitutive parameters, postulated by the Barcelona Basic Model (Alonso et al. 1990), including the slope of the apparent tensile strength (ATS) locus in p:s plane (k) and the slope of the critical state lines (M), were calibrated, using experimental results, for prediction of peak deviator stress at matric suction states varying from 50 to 750 kPa. Within the range of stresses applied, i.e., matric suction, s = 50 to 750 kPa, and initial net mean

stress, p = 100 to 300 kPa, the three-dimensional, plain-surface plane, expressed by Equation (5.11), fitted all the experimental values of deviatoric-stress at critical state, with R^2 = 0.96. The plane yielded best-fit values, *M* = 1.42, for the slope of critical state lines, and *k* = 0.217 for the rate of increase in apparent tensile strength with suction. Predicted values of peak deviator stress were reasonably close to those experimentally obtained from suction-controlled CTC tests, yielding a coefficient of determination, R^2 = 0.97.

13) The effect of matric suction on small and large strain stiffness modulus obtained from stress-strain curves was also studied. Clearly, there was an increase in both the small and large strain stiffness modulus, with an increase in suction at all confining pressures. The large strain stiffness modulus ($E_{critical}$) increased almost linearly and showed a small increase in its value with the increase in matric suction, thus indicating less influence of matric suction on large strain modulus ($E_{critical}$). However, a small strain modulus ($E_{1\%}$) showed a significant increase in its value due to the increase in matric suction from *s* = 50 to 750 kPa.

14) The effect of confining pressure on the large and small stiffness modulus was also examined. The plot suggests that the large strain modulus ($E_{critical}$), in general, increased with an increase in external confinement ($\sigma_3 - u_a$) at all values of matric suction with appreciable magnitudes. It also suggests that small strain modulus ($E_{1\%}$), in general, increased with an increase in external confinement ($\sigma_3 - u_a$) at all values of matric suction; however, the rate of increase in small strain modulus tended to become less at *s* = 750 kPa, with an increase in confining pressures from $\sigma_3 - u_a$ = 100 to 300 kPa.

15) The shear strength variation due to the cohesion intercept variation with suction was studied, using the hyperbolic equation proposed by Vilar 2006 and Reis et

al., 2010 that considers an increase in matric suction contributing to an increase in shear strength by increase in cohesion. A reasonable best-fit was obtained for matric suction varying from 50 to 750 kPa range of experimental test results.

16) A hyperbolic equation proposed by Houston et al. (2008) was used to best-fit the angle of friction with respect to the matric suction, with the variation of matric suction in the range of 50 to 750 kPa. A reasonable best-fit was obtained for the experimental data.

17) The prediction of shear strength properties, using at least five different models, based on key model parameters from the soil-water characteristic curve, are presented and compared with experimental values assessed from suction-controlled CD triaxial tests. Vanapalli 1996, Fredlund and Vanapalli 1996, Khallili and Khabbaz 1997 and Hossain and Yin 2010 models were able to predict the shear strength in close agreement with measured shear strength at wider range of soil suction from 50 kPa to 20 MPa. Oberg's and Sallfors 1997 procedure yielded better predictions up to 750 kPa matric suction, while the predictions were not in agreement at high total suction of 20 MPa.

18) The peak deviatoric stress value was greatly affected by the increase in suction. This is clearly reflected by an increase in ϕ_{peak} value when Mohr's stress circles are drawn at peak failure. The angle of internal friction at peak failure (ϕ_{peak}) was obtained as 39 degrees as compared to in $\phi_{critical}$ value of 35 degrees at critical state. The peak failure lines in the p-q space did not change their slope much, but shifted upwards with increase in suction.

19) A hysteresis effect is needed to be taken into account when there is a reversal of suction during testing. It is worth mentioning here that all the specimens during triaxial testing followed the drying path only: all specimens were dried from initial

matric suction of 10 kPa to a final value of 50, 250, 500 or 750 kPa. Hence, within the matric suction range of testing, it is assumed that the specimen did not undergo any hysteretic effect. Similarly, when the specimens were tested in high total suction range using RH-equipment, it always followed a drying path. Beyond the residual suction, there was not supposed to be a hysteresis effect; hence, its influence on altering strength and deformation behavior can be easily neglected. The high suction was beyond the residual suction (more than 15 MPa). Therefore, the hysteretic behavior is not considered to impact the current analysis.

20) The peak strength is greatly influenced by the suction effect, as well as by rate of loading. Peak strength is attained at lower axial strains, as compared to its saturated counterpart, meaning that the critical strength will also be achieved faster due to immediate softening after the peak is achieved. Thus, at lower axial strains, the critical strength is achieved when suction is increased. Critical strength is affected to some extent by rate of loading while using the axis-translation technique. However, it is least affected using the RH-triaxial technique.

21) Conclusions from CDRH studies: Strain rate studies were performed on five identical specimens with same initial conditions, equalized for desired high total suction (300 MPa), and isotropically consolidated under suction-controlled condition, $\sigma_3 - u_a$ = 100 kPa at wide range of shearing rates (i.e. 0.0009%/min, 0.005%/min, 0.009%/min, 0.05%/min and 0.9%/min). In contrast to previous work, the test results showed first an increase and then a dramatic reduction in deviatoric stress, with further increase in shearing rate. Based on the analysis of

stress-strain and volumetric response, the shearing rate of 0.0009%/min was chosen as an appropriate shear rate for high suction range studies.

22) The deviatoric "load-collapse" phenomenon was captured in the stress-strain plot during shearing for CD100-20MPa tests, irrespective of the shearing rate, by reducing the data collection interval. Such a phenomenon was not observed when the confining pressure, $\sigma_3 - u_a$ was increased to 200 and 300 kPa at *s* = 300MPa. Also, even though the data collection interval was reduced to 30 sec, there was no such "collapse of load" captured when suction was reduced to *s* = 20 MPa at all confining pressures applied in this program. The decrease in load during post-peak-softening for all the other tests was more "gradual" than sudden, meaning that such phenomenon is expected only when suction is highest, and confinement is lowest, i.e., during the test with maximum dilation.

23) The effect of suction and net confining pressure on dilatancy of specimens during shearing was also studied. The peak strength was reached following a full mobilization of dilatancy. Four methods were used to evaluate the rate or angle of dilations. In general, the dilation angle was suppressed with an increase in external confinement (under suction-controlled drained shearing conditions) while the measured dilatancy was enhanced with an increase in suction at constant net confining stress. The relationship between maximum dilatancy and suction is non-linear.

24) The amount of dilation observed in specimens using the relative humidity technique, was less as compared than those obtained from the axis translation technique, even though the matric suction imposed, using the latter technique, was less than the high total suction imposed using the former technique. One possible explanation is that the effective stress is large because of the high

suction of soil and, hence, while shearing the particles, may be crushed even before they over-ride. Such conclusion is also corroborated by the visible crushing observed after the test, as well as the grain size distribution conducted on specimens further confirmed by the particle breakage due to shearing. This resulted in the specimens tested using the vapor-equilibrium technique to dilate less than one using axis-translation technique.

25) Further, continuous incremental ratio $d\varepsilon^{v}_{p}/\, d\varepsilon^{v}_{s}$ obtained during suction-controlled CD triaxial tests can be used to incorporate the dependency of appropriate flow rule (associated/non-associated) on suction (Cui and Delage, 1996). Such data will be helpful to future soil modelers in predicting response of dilating soils, using existing or new models.

26) There was an increase in shear strength and initial stiffness with an increase in total suction from 20 MPa to 300 MPa at the same confining pressures of 100, 200 and 300 kPa. However, with an increase in confining pressure from 100 to 300 kPa, there was a decrease in the rate of increase in shear strength. The stress-strain response showed a distinct peak, followed by critical state. The peak deviator stress and critical stress were attained at lower axial strains as compared to specimens tested at lower suction states. The critical state condition developed rapidly after achieving peak failure. The volumetric change during shear showed initial compression followed by dilation. The rate and amount of dilation were suppressed with increase in confinement at the same total suction. Clearly, the elasto-plastic behavior of test soil in high suction range is different from that of test specimens with low suction conditions.

27) The shear strength and initial stiffness increased with an increase in confining pressure at same total suction. The stress-strain response showed a distinct

peak followed by critical state. The amount of strain-softening increased with an increase in confining pressure. The volumetric change during shear showed initial compression followed by dilation. The rate and amount of dilation increases with an increased in total suction.

28) A clear single shear failure plane was observed for all the specimens tested in high suction range. All specimens showed brittle type of failure, with no bulging. On the other hand, the specimens tested, using the axis-translation technique, failed by bulging with multiple failure shear bands. Thus, a clear transition from multiple shear bands with bulging type failure to a distinct single failure shear band with brittle type failure was observed due to an increase of soil suction from the matric suction range to a high value of total suction.

29) The slope of the failure envelope obtained from the Mohr-Coulomb stress circles drawn at critical state failure under a net confining stress of 100, 200 and 300 kPa and total suction of 20 Mpa, as well as 300 MPa, indicates that the friction angle ϕ' was same (35 deg.) as that for its saturated counterpart. These results are consistent with the Fredlund et al. (1978) shear strength equation. It suggests that the Fredlund et al. (1978) equation can be used for interpreting shear strength behavior of unsaturated soils over the entire soil suction range.

30) The cohesion intercepts and apparent tensile strength increased with an increase in total suction, as well as confining pressure. The angle of friction, with respect to soil suction ϕ^b, decreased with an increase in soil suction and remained almost constant at high total suction of 20 and 300 MPa.

31) Analysis of test results indicated that there was a gradual nonlinear (hyperbolic) decrease in ϕ^b, from 50 kPa to 750 kPa, of matric soil suction. On the other hand, there was a sharp reduction in ϕ^b, from 750 kPa matric suction to the one in high

suction range from 20 Mpa to 300 MPa. The reduction in ϕ, from the total suction of 20 MPa to 300 MPa, was negligible, indicating less shear strength increase due to increase of total suction from 20 MPa to 300 MPa.

32) Experimental data related with the strength and volumetric compressibility in the high suction range could help with the accurate calibration of model parameters, leading to the development of constitutive models.

33) Simulations of deviator stress-shear strain were conducted, using the BBM theory, and compared with experimental results obtained using the axis-translation technique. As expected, the post-peak softening was not simulated, and the BBM response held good throughout most of the initial shearing, up to about 1-2% shear strain, and at considerable value of shear strain, i.e., at critical state.

6.3 Future Recommendations

1) Often, the climatic changes are the primary reasons for reversal of suction in the field. Thus, the soil, in reality, is most likely subjected to hysteretic effects that also affect the hydro-mechanical response. The current study was done without considering the hysteretic behavior. It is recommended to carry such studies in the future to find the extent of any such impact on the response of soil.

2) The current research was completed performing the consolidated drained triaxial tests only. However, the fully undrained/constant water content tests are useful in slope stability analysis or short term analysis and are recommended to be performed to complete or complement such studies in the future.

3) Wetting-induced collapse is an important property of unsaturated soil. Current research studies include experimental determination of the loading-collapse curve; however, it has not been verified via actual experiments. It is

recommended such studies be performed in the future to check/verify the loading-collapse curve and get further insight into the accuracy of experimentally-determined loading-collapse locus.

4) Effect of compaction procedure: Compacting the soil with different compaction procedures results in variations in the initial fabric so that the soil materials are required to be modelled as different soils. Such changes in soil fabric are of fundamental importance to the subsequent soil performance for different compaction methods, and the relevant soil constants in any constitutive model depends on the method of compaction (Estabragh et al., 2004). It is recommended that studies be conducted on specimens prepared using different compaction methods and that the effects on the loading-collapse yield curve, strength-deformation and stiffness behavior be examined.
5) The specimens in this study were compacted at +2% wet of the optimum. It is suggested that, in future studies, specimens be compacted to the dry side of optimum and at optimum moisture content. Such studies will facilitate understanding of the shear-induced effect of suction and confining pressure on fabric, generated by the static compaction method at different initial moisture content and densities.
6) Volume change measurements encountered during all stages were estimated using a double-cell wall along with automatic volume change device. It is recommended that the volume change measurements be checked with additional techniques, such as LVDT's or strain gauges mounted directly on specimens along the radial direction, remote laser techniques, automatic digital image capturing system or any other image processing techniques.

7) Modeling typical responses such as strain-induced post peak softening and volumetric behavior showing dilative transition from initial compression, are a challenge to soil modelers. Popular models, such as the BBM and Cambridge models, fail to mimic the smooth transition from compressive to dilation response, as well as the post-peak softening. The stress path in BBM fails to cross the critical state line, consequently cannot simulate the peak and post-peak softening thereafter. Thus, BBM is limited to predicting strain-hardening and compressive type volumetric responses. It is recommended that a more suitable model, such as a bounding surface (BS) plasticity model, be used in the future to simulate shear-induced responses like the one encountered in current research.

6.4 Novelty of Studies

The following are some of the novelties associated with the current work:

1) Limited studies, such as the current work, report on silty sands, especially the intermediate type, with (55% sand, 37% silt and 8% clay portion) over a wider range of soil suction states (50 to 300000 kPa). Measurement of the volume changes during isotropic consolidation were made to obtain essential parameters to establish the elasto-plastic constitutive model for the unsaturated soil.
2) Total volume changes of specimens were monitored using a double-walled triaxial cell, along with a frictionless automatic volume change device and back pressure volume controllers. It is one of the best and most accurate ways to recording the total volume change in specimens. The water volume change was monitored via back water pressure and volume controller. The subtraction of total and water volume change gives the air volume change. Thus, a complete control of air and water volume change is possible during any stage of triaxial testing.

3) The new triaxial device has the capability to raise the house air pressure up to 1500 kPa, thus enabling testing of unsaturated soils, using the axis-translation technique, up to 1500 kPa.

4) The RH-triaxial studies done by Nishimura et al., 2003 measured the relative humidity of the air before it flew into the specimen (influent stream of air), by a sensor and adjusted it to the required relative humidity. As such, the actual relative humidity inside the specimen was assumed to be same as the adjusted one. However, in the current research, the RH of the effluent stream of air that came out of the specimen was measured using a calibrated RH/Temp probe giving an indirect indication of the RH inside the specimen. Also, separate tests were performed to determine the time required for the specimen to equilibrate with the RH of the supplied stream of saturated/dry air. It was confirmed during suction equalization stage, that the specimen was allowed to equilibrate to desired total suction for more than the estimated time.

5) During the RH-triaxial studies done by Nishimura et al., 2003, the influent stream was supplied under air pressure, using flow meter; therefore, while testing, the confining pore-pressure had to be adjusted simultaneously to maintain a constant net normal stress. However, in the current research, the influent stream flowed under atmospheric pressure, and as such, required no adjustment of air pressure. It also truly represented the field conditions, where there was vapor exchange in the ground via air flowing under atmospheric conditions. The peak and critical state was achieved in between 1-5% axial strain for the range of total suction chosen, and, hence, the specimens did not need to be sheared up to considerable axial strains, thus, saving the overall testing time and, to some extent, justifying the slow shearing rate.

References

Adams, B. A., Wulfshon, D., and Fredlund D. (1996). “Air volume change measurement in unsaturated soil testing using a digital pressure-volume controller.” Geotechnical Testing Journal, 19(1), 12-21.

Ali, S. R., Pyrah, I. C., and Anderson, W. F. (1995). “A novel technique for evaluation of membrane penetration.” Geotechnique, Technical note, 45(3), 545-548.

Alonso, E. E., Gens, A., and Josa, A. (1990). “A constitutive model for partially saturated soils.” Geotechnique, 40 (3), 405-430.

Alonso, E. E., Lloret, A., Gens, A., and Yang, D. Q. (1995). “Experimental behavior of highly expansive double-structure clay.” In Unsaturated Soils: Proceedings of the Ist International Conference on Unsaturated Soils, Paris, 6-8 Sept, E. E. Alonso and P. Delage, A. A. Balkema, Rotterdam (eds), Netherlands, 1, 11-16.

Anandarajah, A. and Chen, J. (1994). “Double-layer repulsive force between two inclined platy particles according to Guoy-Chapman theory.” Journal of Colloid Interface Science, 168, 111-117.

ASTM Standard D2487-00. (2003). “Standard classification of soils for engineering purposes (unified soil classification system).” Annual Book of ASTM Standards, Soil and Rock (I), 4(8), ASTM International, West Conshohocken, PA.

ASTM Standard D4318-05. (2003). “Standard test method for liquid limit, plastic limit, and plasticity index of soils.” Annual Book of ASTM Standards, Soil and Rock (I), 4(8), ASTM International, West Conshohocken, PA.

ASTM Standard D5298-03, (2003). “Test methods for determination of the soil water characteristic curve for desorption using a hanging column, pressure extractor, chilled mirror hygrometer, and/or centrifuge.” Annual book of ASTM Standards, 4(8), ASTM International, West Conshohocken, PA.

ASTM Standard D698-00a (2003). “Standard test methods for laboratory compaction characteristics of soil using standard effort (12,400 ft-lbf/ft^3 (600 kN/m^3)).” Annual Book of ASTM Standards, Soil and Rock (I), 4(8), ASTM International, West Conshohocken, PA.

ASTM Standard D6836-02. (2003). “Standard test method for liquid limit, plastic limit, and plasticity index of soils.” Annual Book of ASTM Standards, Soil and Rock (I), 4(8), ASTM International, West Conshohocken, PA.

ASTM Standard D7181-11 (2011). “Standard test method for consolidated drained triaxial compression test for soils.” Annual Book of ASTM Standards, Soil and Rock (I), 4(8), ASTM International, West Conshohocken, PA.

ASTM Standard D854-06 (2003). “Standard test methods for specific gravity of soil solids by water pycnometer.” Annual Book of ASTM Standards, Soil and Rock (I), 4(8), ASTM International, West Conshohocken, PA.

Baldi, G., and Nova, R. (1984). “Membrane penetration tests in triaxial testing.” Journal of Geotechnical Engineering, 110(1), 403-420.

Bao, C. G., Gong, B. and Zhan, L. (1998). “Properties of unsaturated soils and slope stability of expansive soil.” Keynote lecture, UNSAT 98, 2nd International Conference on Unsaturated Soils, Beijing.

Bardet, J. P. (1997). “Experimental soil mechanics.” Prentice Hall, Inc, Upper Saddle River, NJ.

Barrera, M. (2002). “Estudio experimental del comportamiento hidro-mecanico de suelos colapsables.” Ph.D. Thesis, Universitat Politecnica de Catalunya, Barcelona, Spain.

Bear, J. (1979). Hydraulic of groundwater. McGraw-Hill, New York, 190-224.

Billiam, J. (1972). “Some aspects of the behavior of granular materials at high pressures.” Stress-Strain Behavior of Soils, R.H.G. Parry Ed., G.T.Foulis and Co. London, UK, 3-58.

Bishop, A. W. and Henkel, D. J. (1957). “The measurement of soil properties in the triaxial test.” Edward Arnold, Ltd, London.

Bishop, A. W., Alpan, I., Blight, G. E., and Donald, I. B. (1960). “Factors controlling the strength of partially saturated cohesive soils.” In: Research Conference on Shear Strength of Cohesive Soils held in Boulder, CO, 503-532.

Bishop, A. W., and Donald, I. B. (1961). “The experimental study of partly saturated soil in triaxial apparatus.” In Proceedings of the 5th International Conference in Soil Mechanics and Foundation Engineering, Paris, 13-21.

Bishop, A. W. and Green, G. E. (1965). “The influence of end restraints on the compressive strengths of cohesionless soil.” Geotechnique, 15(3), 243-266.

Bishop, A. W. and Henkel, D. J. (1962). “The measurement of soil properties in the triaxial test.” 2nd Edition, London, UK, Edward and Arnold Publishers.

Blatz, J. A., and Graham, J. (2000). “A method for controlled suctions in triaxial testing.” Geotechnique, 50(4), 465-470.

Blatz, J. A., Graham, J. and Chandler, N. A. (2002). “Influence of suction on the strength and stiffness of compacted sand-bentonite.” Canadian Geotechnical Journal, 39, 1005-1015.

Blatz, J. A., Cui, Y-J., and Oldecop, L. (2008). Vapour equilibrium and osmotic technique for suction control.” Geotechnical and Geological Engineering, 26, 661-673.

Bocking, K. A. and Fredlund, D. G. (1980). “Limitations of the axis-translation technique.” Proceedings of the 4th International Conference on Expansive Soils, Denver, CO, June 16-18, D. Snethen, Ed., ASCE, NY, 1, 117-135.

Bolton, M. D. (1986). “The strength and dilatancy of sands.” Geotechnique, 36(1), 65-78.

Bolzon, G., Schrefler, B. A. and Zienkiewicz, O. C. (1996). “Elastoplastic soil constitutive laws generalized to partially saturated states.” Geotechnique, 46(2), 279-289.

Boso, M., Tarantino, A., and Mongiovi, L. (2005). “A direct shear box improved with the osmotic technique.” Proceedings of advanced experimental unsaturated soil mechanics, Trento, 85-91.

Cabarkapa, Z., and Cuccovillo, T. (2006). “Automated triaxial apparatus for testing unsaturated soils.” Geotechnical Testing Journal, 29(1), 21-29.

Chavez, C., Romero, E., and Alonso, E. E. (2005). “Volume change measurement of partially saturated rockfill in triaxial tests.” International symposium on advanced experimental unsaturated soil mechanics, EXPERUS 2005, Trnto, 1, 93-98.

Chen, J., Lin, C., and Lee, W. (2003). “Dilative behavior of granular materials.” International Journal of offshore and polar engineering, 13(4), 301-307.

Clayton, C. R. I., and Khatrush, A. S. (1986). “A new device for measuring local axial strains on triaxial specimens” Geotechnique, 36(4), 593-597.

Clayton, C. R. I., Khatrush, A. S., Bica, A. V. D., and Siddique, A. (1989). “The use of hall effect semiconductors in geotechnical instrumentation.” Geotechnical Testing Journal, 12(1), 69-76.

Cole, D. M. (1978). “A technique for measuring radial deformation during repeated load triaxial testing.” Canadian Geotechnical Journal, 15, 426-429.

Crooney, D., Coleman, J. D. and Bridge, P.M. (1952). “The suction of moisture held in soil and other porous materials”. Road Research Tech. Paper No. 24, Road Research Laboratory, London: HMSO.

Cui, Y. J. and Delage, P. (1996). “Yielding and plastic behaviour of an unsaturated compacted silt.” Geotechnique, 46(2), 291-311.

Datcheva, M. and Schanz, T. (2003). “Anisotropic bounding surface plasticity with rotational hardening for unsaturated frictional material.” Journal de Physiqye iv, 105, 305-550.

Davis, R. O. and Selvadurai, A. P. S. (2002). “Plasticity and geomechanics.” Cambridge University Press, UK.

Delage, P., Suraj De Silva, G. P. R., and De Laure, E. (1987). “Un nouvel appareil triaxial pour les sols non satures.” Proc. 9th European Conference on SMFE, Dublin, 25-28.

Delage, P., Howat, M. D., and Cui, Y. J. (1998). “The relationship between suction and swelling properties in a heavily compacted unsaturated clay.” Engineering Geology, 50, 31-48.

Delage, P., Suraj De Silva, G. P. R., and Vicol, T. (1992). “Suction controlled testing of non saturated soils with an osmotic consolidometer.” Proc. 7th International Conference on Expansive Soils, Dallas, 206-211.

Dineen, K., and Burland, J. B. (1995). “A new approach to osmtically controlled oedometer testing.” Proc. Ist International Conference on Unsaturated Soils, Paris, 2, 459-465.

Fawcett, R. G. and Collis, G. N (1967). “A filter-paper method for determining the moisture characteristics of soil.” Australian Journal of Experimental Agriculture and Animal Husbandry, 7, 162-167.

Fredlund, D. G. (1975). “A diffused air volume indicator for unsaturated soils.” Canadian Geotechnical Journal, 12(4), 533-539.

Fredlund, D. G., and Morgenstern, N. R. (1977). “Stress state variables for unsaturated soils.” Journal of Geotechnical Engineering Division, American Society of Civil Engineers, 103(5), 447-466.

Fredlund, D. G., and Rahardjo, H. (1977). “Soil mechanics for unsaturated soils.”New york, Wiley.

Fredlund, D. G., and Rahardjo, H. (1985). “Theoretical context for understanding unsaturated residual soil behavior.” In Proceedings, Ist International Conference on Geomechanics in Tropical Lateritic and Saprolitic Soils, Feb., Sao Paulo, Brazil, 1, 295-305.

Fredlund, D. G., and Xing, A. (1994). “Equations for the soil-water characteristic curve.” Canadian Geotechnical Journal, 31(4), 521-532.

Fredlund, D. G., Xing, A., Fredlund, M. D., and Barbour, S. L. (1996). “The relationship of the unsaturated soil shear strength to the soil-water characteristic curve.” Canadian Geotechnical Journal, 33, 440-448.

Gachet, P., Klubertanz, G., Vulliet, L. and Laloui, L. (2003). “Interfacial behavior of unsaturated soil with small-scale models and use of image processing techniques.” Geotechnical Testing Journal, 26(1), 12-21..

Gallage, C. P. K., and Uchimura, T. (2006). “Effects of wetting and drying on the unsaturated shear strength of a sity sand under low suction.” Proceedings of 4th International Conference on Unsaturated Soils, ASCE, Arizona, GSP147, 1247-1258.

Gallipoli, D., Gens, A., Sharma, R., and Vaunat, J. (2003). “An elasto-plastic model for unsaturated soil incorporating the effects of suction and degree of saturation on mechanical behavior.” Geotechnique, 53, 123-135.

Gan, J. K. M., Fredlund, D. G. and Rahardjo, H. (1988). “Determination of shear strength parameter for unsaturated soil using direct shear test.” Canadian Geotechnical Journal, 25(3), 500-510.

Garga, V. K., and Zhang, H. (1997). “Volume changes in undrained triaxial tests on sands.” Canadian Geotechnical Journal, 34, 762-772.

GCTS. (2008). “CATS Triaxial Test Manual users guide and manual.” Geotechnical Consulting & Testing Systems. Tempe, Arizona. 177 p.

GCTS. (2009). “SCON-2000 Digital system controller users guide and reference manual.” Geotechnical Consulting & Testing Systems. Tempe, Arizona. 96 p.

Geiser, F. (1999). “Comportement mecanique d’un limon non sature: etude experimentale et modelisation constitutive, Ph.D. Thesis, Ecole Polytechnique Federale de Lausanne, EPFL, Switzerland.

Gens, A., and Potts, D. M. (1988). Critical state models in computational geomechanics.” Engineering Computations, 5(3), 178-197.

Georgiadis, K., Potts, D. M., and Zdravkovic, L. (2005). “Three-dimensional constituitive model for partially and fully saturated soils.” International Journal of Geomechanics, 5(3), 244-255.

Gibson, R. E. and Henkel, D. J. (1954). “Influence of duration of tests at constant rate of strain on measured drained strength.” Geotechnique, 4(1), 6-15.

Gitirana Jr., G. F. N., and Fredlund, D. G. (2004). “Soil-water characteristic curve equation with independent properties.” Journal of Geotechnical and Geoenvironmental Engineering, ASCE, 130(2), 209-212.

Gulhati, S. K., and Satija, B. S. (1981). “Shear Strength of Partially Saturated Soils.” 10th International Conference on Soil Mechanics and Foundation Engineering, 1, 609-612.

Hamblin, A. P. (1981). “Filter paper method for routine measurement of field water potential.” Journal of Hydrology, 53, 355-360.

Head, K. H. (1998/1986). “Effective stress tests, Volume 3, Manual of soil laboratory testing (2nd ed.).” John Wiley and Sons.

Helwany, S. (2007). “Applied soil mechanics with abaqus applications.” John Wiley and Sons, Inc., Hoboken, New Jersey.

Hilf, J. W. (1956). “An investigation of pore-water in compacted cohesive soils.” PhD. Dissertation, Technical Memo. No. 654, U. S. Department of the Interior, Bureau of Reclaimation, Design and Construction Division, Denver, CO.

Hird, C. C., and Haji, A. R. (1995). “A simulation of tube sampling effects on the stiffness of clays.” Geotechnical testing Journal, 18(1), 3-14.

Ho, D. Y. F. and Fredlund, D. G. (1982). “A multistage triaxial test for unsaturated soils.” ASTM Geotechnical Testing Journal, 5(1/2), 18-25.

Hossain, M. A., and Yin, J. (2010). “Shear strength and dilative characteristics of an unsaturated compacted completely decomposed granite soil.” Canadian Geotechnical Journal, 47, 1112-1126.

Houlsby, G. T. (1991). “How the dilatancy of soils affects their behavior.” Proc. 10th Eur. Conf. on SMFE, Florence, 4, 1189-1202.

Houlsby, G. T. (1997). “The work input to an unsaturated granular material.” Geotechnique, 47, 193-196.

Houston, S. L., Houston, W. N., and Wagner, A. M. (1994). Laboratory filter paper suction measurements.” Geotechnical Testing Journal, 17(2), 185-194.

Hoyos, L. R., Diego, D. Perez-Ruiz., and Puppala, A. J. (2012). “Modeling unsaturated soil response under suction-controlled true triaxial stress paths.” International Journal of Geomechanics, 12(3), 292-308.

Hoyos, L. R., Laloui, L., and Vassallo, R. (2008). “Mechanical testing in unsaturated soils.” Geotechnical Geology Engineering, 26, 675-689.

Hoyos, L. R., Thudi, H. R., and Puppala, A. J. (2007). “Soil-water retention properties of cement treated clay.” Problematic Soils and Rocks and In Situ Characterization, 1-8.

Hoyos, L. R. (1998). “Experimental and computational modeling of unsaturated soil behavior under true triaxial stress states.” Ph.D. dissertation, Georgia Institute of Technology, Atlanta.

Lowe, J. and Johnson, T. C. (1960). “Use of back pressure to increase degree of saturation of triaxial test specimens.” ASCE Research Conference on Shear Strength of Cohesive Soils, Boulder, Colorado, USA, 819-836.

Ishikawa, T., Zhang, Y., Segawa, H., Miura, S., and Tokoro, T. (2012). “Developement of medium-size triaxial apparatus for unsaturated granular base course material.” Advances in Transportation Geotechnics II: 2nd International Conference on Transportation Geotechnics (ICTG), Japan, 534-540.

Jennings, J. E. and Burland, J. B. (1962). “Limitations to the use of effective stresses in partly saturated soils.” Geotechnique, 2, 125-144.

Josa, A., Balmaceda, A., Gens, A., and Alonso, E. E. (1992). “An elastoplastic model for partially saturated soils exhibiting a maximum of collapse.” Proceedings, 3rd International Conference on Computational Plasticity, Barcelona, 1, 815-826.

Josa, A., Alonso, E. E., Lloret, A., and Gens, A. (1987). “Stress-strain behavior of partially saturated soils.” In: Proceedings of the 9th European Conference on Soil Mechanics and Foundation Engineering, Dublin, 2, 561-564.

Kassif, G. and Ben Shalom, A. (1971). “Experimental relationship between swell pressure and suction.” Geotechnique, 21(3), 245-255.

Katti, R. K. (2000). “Coulombian cohesion approach to engineering of expansive soil deposits: Field performance.” In Advances in Unsaturated Soils, GSP No 99 (eds, C. Shackleford, S. L. Houston and N. Y. Chang), Reston: ASCE, 467-486.

Khalili, N., Habte, M. and Valliapan, S. (2005). “A bounding surface plasticity model for cyclic analysis of sands.” International Journal of Numerical methods in Engineering, 63(14), 1939-1960.

Khalili, N. and Khabbaz, M. H. (1998). “A unique relationship for the determination of the shear strength of unsaturated soils.” Geotechnique, 48(5), 681-687.

Khan, A. H., and Hoag, D. L. (1979). “A non-contacting transducer for measurement of lateral strains.” Canadian Geotechnical Journal, 16, 409-411.

Khattab, S. A. A., and Al-Taie, L. Kh. I. (2006). “Soil-water characteristic curves (SWCC) for lime treated expansive soil from mosul city.” In Miller G., Zapata, C., Houston, S. L., and Fredlund, D. G. (eds), Fourth International Conference on Unsaturated Soils, Carefree, Arizona on April 2-5; 1671-1682.

Kirkpatrick, W. M., and Younger, J. S. (1970). “Strain conditions in compression cylinder.” Journal of Soil Mechanics and Foundation Division, 96(SM5), 1683-1695.

Kodikara, J. (2012). “New framework for volumetric constitutive behavior of compacted unsaturated soils.” Canadian Geotechnical Journal, 49, 1227-1243.

Kohgo, Y., Nakano, M., and Miyazaki, T. (1993). “Theoretical aspects of constitutive modelling for unsaturated soils.” Soils and Foundations, 33(4), 49-63.

Kolymbas, D. and Wu, W. (1989). “A device for lateral strain measurements in triaxial tests with unsaturated specimens.” Geotechnical Testing Journal, 12(3), 227-229.

Kosugi, K. (1997). “A new model to analyze water retention characteristics of forest soils based on soil pore radius distribution.” Journal of Forest Research, 2(1), 1-8.

Kramer, S. L., Sivaneswaran, N., and Davis, R. O. (1990). “Analysis of membrane penetration in triaxial test.” Journal of Engineering Mechanics, 116(4), 773-789.

Lade, P. V., and Yamamuro, J. A. (1997). “Effects of nonplastic fines on static liquefaction of sands.” Canadian Geotechnical Engineering Journal, 34(6), 918-928.

Lagerwerff, J. V., Ogata, G. and Eagle, H. E. (1961). “Control of osmotic pressure of culture solutions with polyethylene glycol.” Science, 133, 1486-1487.

Laikram, A. (2007). “Modeling unsaturated soil response under suction-controlled multi-axial stress states.” Ph.D dissertation, Univ. of Texas at Arlington, Arlington, TX.

Laloui, L., Peron, H., Geiser, F., Rifa, I. A., and Vulliet, L. (2006). “Advances in volume measurement in unsaturated triaxial tests.” Soils and Foundations, 46(3), 341-349.

Lappala, E. G., Healy, R. W., and Weeks, E. P. (1987). Documentation of the computer program to solve the equations of fluid flow in variably saturated porous media, Water-Resources and Investigation Reports, 83-4099, US Geological Survey, Denver, Colorado.

Laudahn, A., Sosna, K., and Bohac, J. (2005). “A simple method for air-volume change measurement in triaxial tests.” Geotechnical testing Journal, 28(3), 313-318.

Leong, E. C. and Rahardjo, H. (2002). “Soil-water characteristic curves of compacted soils.” Proceedings of the 3rd International Conference on Unsaturated Soils, Juca de Campos and F. A. M. Marinho, eds, Recife, Brazil, 271-276.

Lee, K. L. (1978). “End restraint effects on undrained static triaxial strength of sand.” Journal of Geotechnical Engineering Division, ASCE, 104(GT6), 687-704.

Likos, W. J. and Lu, N. (2002). “Filter paper technique for measuring total suction.” Transportation Research Record: Journal of the Transportation research Board, 1786, 120-128.

Likos, W. J. and Lu, N. (2003). “Automated humidity system for measuring total suction characteristics of clay.” Geotechnical testing Journal, 26(2), 1-12.

Likos, W. J. (2012). “User Manual automated relative humidity control system.”

Lowe, J. and Johnson, T. C. (1960). “Use of back pressure to increase degree of saturation of triaxial test specimens.” Proceedings, Research Conference on Shear Strength of Cohesive Soils, American Society of Civil Engineers, 819-836.

Lo Presti, D. C. F., Pallara, O. and Puci, I. (1995). “A modified commercial triaxial testing system for small strain measurements, preliminary results on Pisa clay.” Geotechnical Testing Journal, 18(1), 15-31.

Lu, N., and Likos, W. J. (2004). Unsaturated Soil Mechanics. John Wiley and Sons, Inc. New Jersey.

Maatouk, A. (1993). “Application des concepts d’etat limite et d’ etat critique a un sol partiellement sature effondrable.” Ph.D. Thesis, Universite de laval, Montreal, Canada.

Maatouk, A., Leroueil, S., and Rochelle, P. L. A. (1995). “Yielding and critical state of a collapsible unsaturated silty soil.” Geotechnique, 45(3), 465-477.

Malaya, C. and Sreedeep, S. (2012). “Critical review on the parameters influencing soil-water characteristic curve.” Journal of Irrigation and Drainage Engineering, 138(1), 55-62.

Mahalinga-Iyer, U. and Williams, D. J. (1985). “Unsaturated strength behavior of compacted lateritic soils.” Geotechnique, 45(2), 317-320.

Manosuthkij, T., Puppala, A. J., Nazarian, S., Saride, S., and Hoyos, L.R. (2008). "Comparisons between field and laboratory suction measurements of expansive clays." Journal of the Transportation Research Board, TRR No. 2053, 39-46.

Marinho, F. A. M. and Oliveira, O. M. (2005). "The filter paper method revisited." Geotechnical Testing Journal, 29(3), 1-9.

Marinho, F. A. M. (2005). "Nature of soil-water characteristic curve for plastic soils." Journal of Geotechnical and Geoenvironmental Engineering, 131(5), 654-661.

Marinho, F. A. M., Stuermer, M. (2000). "The influence of the compaction energy on the SWCC of a residual soil." Advances in Unsaturated Soils, Geotechnical Special Publication No. 99, C. Shackleford, S. L. Houston, N-Y. Chang, Eds., ASCE, Reston, VA, 125-141.

McQueen, I. S. and Miller, R. F. (1968). "Calibration of a wide-range gravimetric method for measuring moisture stress." Soil Science, 106(3), 225-231.

Matsuoka, H., and Sun, D. A. (2006). "The SMP concept-based 3D constituitive models for geomaterials." Taylor and Francis Group, London, UK.

Mitchell, J. k. (1986). "Fundamentals of soil behavior." 3rd edition, Wiley, Hoboken, N. J.

Miller, C. J., Yesiller, N., Yaldo, K., and Meraayyan, S. (2002). "Impact of soil type and compaction conditions on soil water characteristic." Journal of Geotechnical and Geoenvironmental Engineering, 128(9), 733-742.

Molenkamp, F. and Luger, H. T. (1981). "Modelling and minimization of membrane penetration effects in tests on granular soils." Geotechnique, 31(4), 471-486.

Morvan, M., Wong, H., and Branque, D. (2011). "Incorporating porosity-dependent hysteretic water retention behavior into a new constitutive model of unsaturated soils." Canadian Geotechnical Journal, 48, 1855-1869.

Murray, E. J. and Sivakumar, V. (2010). “Unsaturated soils: A fundamental interpretation of soil behavior.” Wiley-Blackwell, A John Wiley & Sons, Ltd, Publication.

Navarro, V., and Alonso, E. E. (2000). “Modeling swelling soils for disposal barriers.” Computers and Geotechnics, 27, 19-43.

Ng, C. W. W., Zhan, L. T, and Cui, Y. J. (2002). “ A new simple system for measuring volume changes in unsaturated soils.” Canadian geotechnical Journal, 39, 757-764.

Ng, C. W. W., and Zhou, R. Z. B. (2005). “Effects of soil suction on diltancy of an unsaturated soil.” Proceedings of the 16th International Conference on Soil Mechanics and Geotechnical Engineering in Harmony with the Global Environment, 2, 559-562.

Ng, C. W. W., Cui, Y., Chen, R. and Delage, P. (2007). “The axis-translation and osmotic techniques in shear testing of unsaturated soils: a comparison.” Soils and Foundation, 47(4), 675-684.

Nishimura, T., Toyota, H. and Koseki, J. (2010). “Evaluation of apparent cohesion of an unsaturated soil.” Unsaturated soils - Experimental studies in unsaturated soils and expansive soils, Buzzi, Fityus & Sheng (eds), Taylor and Francis group, London, 109-114.

Nishimura, T., Toyota, H., Vanapalli, S. K. and Won, O. T. (2008). “Determination of the shear strength behavior of an unsaturated soil in the high suction range using vapor pressure technique.” Proc. Of the Ist European Conference on Unsaturated Soils. Unsaturated Soils: Advances in Geo-Engineering, Toll et al. (eds) CRC Press: Taylor and Francis Group, 441-447.

Nishimura, T. and Vanapalli, S. K. (2005). “Volume change and shear strength behavior of an unsaturated soil with high soil suction.” 16th International Conference on Soil Mechanics and Geotechnical Engineering. 563-566.

Nishimura, T. and Fredlund, D. G. (2003). “A new triaxial apparatus for high total suction using relative humidity control.” 12th Asian Regional Conference on Soil Mechanics and Geotechnical Engineering, Leung et al. (eds), World Scientific Publishing.

Oberg, A. and Sallfors, G. (1997). “Determination of shear strength parameters of unsaturated silts and sands based on the water retention curve.” Geotechnical Testing Journal, 20(1), 40-48.

Oka, F., Kodaka, T., Suzuki, H., Kim, Y. S., Nishimatsu, N. and Kimoto, S. (2010). “Experimental study on the behavior of unsaturated compacted silt under triaxial compression.” Soils and Foundations, Japanese Geotechnical Society, 50(1), 27-44.

Padilla, J. M., Perera, Y. Y., Houston, W. N. and Fredlund D. G. (2005). “A new soil-water characteristic curve device.” Advanced Experimental Unsaturated Soil Mechanics – Tarantino, Romero & Cui (eds), Taylor and Francis Group, London, 15-22.

Perera, Y. Y., Zapata, Z. E., Houston, W. N., and Houston, S. L. (2004). “Long-term moisture conditions under highway pavements.” Proceedings of Geo-Trans 2004, GSP No 126, Geotechnical Engineering for Transportation Projects, Los Angeles, California, USA, July 27-3, (1), 1132-1143.

Perez-Ruiz, D. D. (2009). “A refined true triaxial apparatus for testing unsaturated soils under suction-controlled stress paths.” Ph.D. dissertation, Univ. of Texas at Arlington, Arlington, TX.

Pietruszczak, S. (2010). “Fundamentals of plasticity in geomechanics.” Taylor and Francis Group, CRC Press, London, UK.

Puppala, A. J., Konnamas, P. and Vanapalli, S. K. (2006). “Soil-water characteristic curves of stabilized expansive soils.” Journal of Geotechnical and Geoenvironmental Engineering, 132(6), 736-751.

Puppala, A. J., Saride, S., and Chomtid, S. (2009). “Experimental and Modeling studies of permanent strains of subgrade soils.” ASCE, Journal of Geotechnical and Geoenvironmental Engineering, 135(10), 1379-1389.

Puppala, A. J., Manosuthkij, T., Nazarian, S., Hoyos, L. R., and Chittoori, B. (2012). “In situ matric suction and moisture content measurements in expansive clay during seasonal fluctuations.” Geotechnical Testing Journal, 35(1), 1-9.

Rahardjo, H., Satyanaga, A., D’ Amore G. A. R., and Leong, E. (2012). “Soil-water characteristic curves of gap-graded soils.” Engineering Geology, 125, 102-107.

Rahardjo, H., Lim, T. T., Chang, M. F., and Fredlund, D. G. (1995). “Shear strength characteristics of a residual soil.” Canadian Geotechnical Journal, 32, 60-77.

Rampino, C., Mancuso, C., and Vinale, F. (1999). Laboratory testing on an unsaturaed soil: equipment, procedures, and first experimental results. Canadian Geotechnical Journal, 36, 1-12.

Richards, B. G. (1965). “Measurement of the free energy of soil moisture by the psychrometric technique using thermistors, in moisture equilibria and moisture changes in soils beneath covered areas.” A Symposium in Sydney, Australia, Edited by G. D. Aitchison, Butterworths and Co. Ltd, 35-46.

Rifai, A., Laloui, L., and Vulliet, L. (2002). “Volume measurements in unsaturated triaxial test using liquid variation and image processing.” In: Proceedings of the 3rd International Conference on Unsaturated soils, Recife, Brazil, 2, 441-445.

Rojas, J. C., Mancuso, C. and Vinale, F. (2008). “A modified triaxial apparatus to reduce testing time: Equipment and preliminary results.” Unsaturated Soils: Advances In Geo-Engineering, Toll et al. (eds), Taylor and Francis Group, London.

Roscoe, K. H., and Burland, J. B. (1968). “On the generalized stress-strain behavior of “Wet” Clay, In Engineering Plasticity.” J. Heyman and F. Leckie (Ed.), Cambridge University Press, Cambridge, 535-609.

Rowe, P. W. (1962). “The stress-dilatancy relation for static equilibrium of an assembly of particles in contact.” Proceedings of Royal Society. A., 269, 500-527.

Russel, A. R. and Khalili, N. (2006). “A unified bounding surface plasticity model for unsaturated.” International Journal of Numerical and analytical methods in Geomechanics, 30(3), 181-212

Salgado, R. (2006). “The engineering of foundations.” McGraw-Hill publishing company.

Sawangsuriya, A., Edil, T. B., Bosscher, P. J. (2008). “Modulus-suction-moisture relationship for compacted soils.” Canadian Geotechnical Journal, 45, 973-983.

Schofield, A., and Wroth, C. P. (1968). “Critical state soil mechanics.” McGraw-Hill, London.

Schofield, R. K. (1935). “The pF of the water in soil.” Transactions, 3rd International Congress of Soil Science, T. Murby, London, 37-48

Scott, R. and Ko, H. K. (1970). “Stress deformation and strength characteristics.”In: State of the art volume.” 7th International Conference on Soil Mechanics and Foundation Engineering held in Mexico City, Mexico, 1969, 1-47.

Sharma, R. S. (1998). “Mechanical behavior of unsaturated highly expansive clays.” Ph.D. Thesis, University of Oxford, UK.

Sillers, W. S. and Fredlund, D. G. (2001). “Statistical assessment of soil-water characteristic curve models for geotechnical engineering.” Canadian Geotechnical Journal, 38, 1297-1313.

Sivakumar, V. (1993). “A critical state framework for unsaturated soils.” Ph.D. Thesis, University of Sheffield, UK.

Sreedeep, S. and Singh, D. N. (2006). Nonlinear curve-fitting procedures for developing soil-water characteristic curves.” Geotechnical Testing Journal, 29(5), 1-10.

Tang, G.X., Graham, J. and Wan, A. W. L. (1998). “On yielding behavior of an unsaturated sand-bentonite mixture.” In Proceedings of the 2nd International Conference on Unsaturated Soils, Beijing, 1, 149-154.

Tang A-M., Cui, Y-J. (2005). “Controlling suction by the vapor equilibrium technique at different temperatures and its application in determining the water retention properties of MX80 clay.” Canadian Geotechnical Journal, 42, 287-296.

Tarantino, A. and Mongiovi, L. (2000a). “Experimental investigations on the stress variables governing unsaturated soil behavior at medium to high degrees,” Proc. Experimental Evidence and Theoretical Approaches in Unsaturated Soils, Trento, 3-19.

Terzaghi, K. (1936). “The shear resistance of saturated soils.” Proceedings of Ist International Conference Soil Mechanics and Foundation Engineering, Cambridge, MA, 1, 54-56.

Tindall, J. A. and Kundel, J. R. (1999). “Unsaturated zone hydrology for scientists and engineers.” Prentice Hall, Inc., New Jersy.

Toll, D. G., and Ong. B. H. (2003). “Critical-state parameters for an unsaturated residual sandy clay.” Geotechnique, 53(1), 93-103.

Toll, D. G. (2000). “The influence of fabric on the shear behavior of unsaturated compacted soils.” In Advances in unsaturated soils (eds C Shackelford, S. L. Houston and N-Y Chang), Reston: American Society of Civil Engineers, Geotechnical Special Publication No 99, 222-234.

Toll, D. G. (1990). “A framework for unsaturated soil behaviour.” Geotechnique, 40(1), 31-44.

Vaid. Y. P. and Sasitharan, S. (1992). The strength and dilatancy of sands.” Canadian Geotechnical Engineering Journal, 29, 522-526.

Van der Raat, Fredlund, D. G., Clifton, A. W., Klassen, M. J. K., and Jubien, W. E. (1987). “Soil suction measurements at several sites in western Canada.” Transportation Research Record: Transportation Research Board, Washington, DC, 24-35.

Van Olphen, H. (1991). “Clay colloid chemistry.” 2nd edition, Krieger, Boca Raton, Fla.

Vanapalli, S. K., Sillers, W. S. and Fredlund, M. D. (1998). “”The meaning and relevance of residual state to unsaturated soils.” 51st Canadian Geotechnical Conference, Edmonton, Alberta, October 4-7, 1-8.

Vanapalli, S. K., Fredlund, D. G., and Pufahl, D. E. (1999). “The influence of soil structure and stress history on the soil-water characteristics of a compacted till.” Geotechnique, 49(2), 143-159.

Vanapalli, S. K., Fredlund, D. G., Pufahl, D. E. and Clifton, A. W. (1996). “Model for the prediction of shear strength with respect to soil suction.” Canadian Geotechnical Journal, 33, 379-392.

Vanapalli, S. K., and Fredlund, D. G. (2000). “Comparison of different procedures to predict unsaturated soil shear strength.” Advances in Unsaturated Geotechnics, 195-209.

Vaunat, J, Romero, E., and Jommi, C. (2000). “An elasto-plastic hydro-mechanical model for unsaturated soils.” Experimental evidence and theoretic approaches in unsaturated soils (Eds. Tarantino, A. and Mancuso, C), 121-138, Rotterdam: Balkema.

Vesic, A. S., and Clough, G. W. (1968). “Behavior of granular materials under high stresses.” Journal of Soil Mechanics and Foundations Division, ASCE, Technical note, 107(GT7), 1003-1008.

Vicol, T. (1990). “Comportement hydraulique et mechanique d’un limon non sature. Apllication a la modelisation.” Theses de doctorat de l’ENPC, Paris, 257.

Wang, Q., Pufahl, D. E. and Fredlund, D. G. (2001). “A study of critical state on an unsaturated silty soil.” Canadian Geotechnical Journal, 39, 213-218.

Wheeler, S. J. (1988). “The undrained shear strength of soils containing large gas bubbles.” Geotechnique, 38(3), 399-413.

Wheeler, S. J., and Sivakumar, V. (1995). “An elasto plastic critical state framework for unsaturated soil.” Geotechnique, 45(1), 35-53.

Wood, D. M. (1990). “Soil behavior and critical state soil mechanics.” Cambridge University Press, New York.

Wood, D. M. (2004). “Geotechnical modelling.” Spon Press, New York.

Yang, C., Cui, Y. J., Pereiro, J. M. and Huang, M. S. (2008). “A constitutive model for unsaturated cemented soils under cyclic loading.” Comput. Geotech., 35(6), 853-859.

Yu, H. S. (2006). “Plasticity and geotechnics.” Springer, New York.

Zhang, L., and Chen, Q. (2005). “Predicting bimodal soil-water characteristic curves.” Journal of Geotechnical and Geoenvironmental Engineering, 131(5), 666-670.

Zhang, L. L., Fredlund, D. G., Zhang, L. M., and Tang, W. H. (2004). “Numerical study of soil conditions under which matric suction can be maintained.” Canadian Geotechnical Journal, 41, 569-582.

Biographical Information

Ujwalkumar Dashrath Patil was born in Nandurbar district of Maharashtra state in India. He received his B.S. degree from North Maharashtra University, India. He completed his first Masters degree in Geotechnical Engineering from Pune University in India. Then onwards he worked as a Lecturer in civil engineering at an Institute affiliated to North Maharashtra University for about seven years.

In August 2007, he came to United States and completed his second degree in Geotechnical engineering fron San Diego State University, California (USA) under guidance of Dr. Julio R. Valdes in December 2008. Then onwards he worked with Kleinfelder, Inc as a civil engineer from August 2008 till January 2011.

He was admitted to The University of Texas at Arlington as a graduate doctoral student with teaching and research assistantship from 2011 till August 2014, under the guidance of his advisor Dr. Anand J. Puppala and co-advisor Dr. Laureano R. Hoyos. Mr. Ujwalkumar D. Patil has successfully completed all requirements for the Degree of Doctor of Philosophy in Civil Engineering on July 15, 2014 and he will receive the degree in summer, 2014 Commencement ceremony.